THE KOLBEL ENGELHARDT SYNTHESIS; CATALYSIS BY SUPPORTED COBALT AND COPPER SYSTEMS

Marcus

BY GERARD ROE

BEING A THESIS SUBMITTED AS REQUIREMENT FOR

THE DEGREE OF

MASTER OF SCIENCE

AT THE UNIVERSITY OF TASMANIA

JANUARY, 1989

DECLARATION

To the best of my knowledge, this thesis contains no copy or paraphrase of material previously published or written except when due reference is included in the text.

GERARD ROE

ACKNOWLEDGEMENTS

I would like to thank all those who helped me in doing the work towards this thesis:

Professor Frank P. Larkins - for his ideas and encouragement as my supervisor.

Dr. Michael Ridd - for his useful discussions and assistance with experimental work.

Mr. Supachai Supaluknari, Ms. Elzbieta Chelkowska, Dr. Ashraf Khan and Mr. Ridzuan Nordin - other members of the research group who always gave useful advice and particularly computational aid.

Messrs. Marshall Hughes, Peter Dove and John Davis - the technical men who kept the apparatus functioning.

Messrs. Owen Taplin, Martin Read, Craig Williams, Andrew Mitchell and Miss Luz Montes for their great friendship.

Ms. Sandra Petrie - for her patience and efficiency as my typist.

My parents, Professor Michael Roe and Dr. Margot Roe - for their ceaseless support.

ABSTRACT

A suite of alumina (Al_2O_3) and silica ($SiO_2$40Å) supported Co and Cu catalysts, physical mixes of the single metal catalysts, and mixed metal hybrid catalysts were investigated by temperature programmed reduction (TPR) and assessed in terms of their Kolbel Engelhardt (KE) activities. By comparison of the results from the different preparations it was shown that mixed non-stoichiometric Co/Cu oxides occurred on the calcined hybrids, which were reduced to interactive Co^o and Cu^o particles. This metal species distribution was associated with the production of high aromatic yields relative to aliphatic analogues. The most interesting sample was a Co/Cu on silica supported catalyst with Co and Cu to support ratios both of 10 on a weight percent basis (Co/Cu/$SiO_2$40Å; 10:10:100).

This sample was screened in a series of CO/H_2O feeds of varying CO:H_2O ratios. There were two regimes of feed composition, defined as the CO rich regime and the H_2O rich regime. The performance of Co/Cu/$SiO_2$40Å; 10:10:100 was entirely different in each. Within the CO rich regime carbon deposition *via* the Boudouard reaction was the predominant cause of CO conversion at high temperature (300°C, 325°C), whereas in the H_2O rich regime substantial excess H_2 was produced. The most favourable product distributions were given at a CO:H_2O feed ratio of 1:1.

The Co/Cu/$SiO_2$40Å; 10:10:100 catalyst and the physical mix analogue, Co/$SiO_2$40Å; 10:100 + Cu/$SiO_2$40Å; 10:100, were characterised in detail using techniques including X-ray diffraction (XRD), electron probe microanalysis, and thermogravimetry. On the calcined hybrid sample Cu occurred as Cu^{2+} surface networks and Co as Co_3O_4. These species were reduced totally during the activation procedure. The interaction between Co and Cu, suggested by TPR and screening evidence, was caused by the close proximity of the two metals rather than the formation of mixed metal stoichiometric oxides or alloys.

Mechanistic studies using infrared (IR) spectroscopy indicated that CO adsorbed to Co/Cu/$SiO_2$40Å; 10:10:100 on Cu^o particles and at Co^o/Cu^o crystallite interfaces. When water was introduced a formate type species and polyene were observed. The formate species was probably a water gas shift reaction (WGSR) intermediate, and the polyene a common intermediate to the formation of coke and aromatic products. Reactivity experiments involving ethene conversion and coke stripping with H_2O and H_2 confirmed the role of polyene as an intermediate.

CONTENTS

1 INTRODUCTION

1.1 Development of the Kolbel Engelhardt Synthesis

The oil crisis of 1973, coupled with an increasing awareness of the diminishing global reserves of oil has, despite current low prices, resulted in a continuing interest in the conversion of coal to oil. One method of producing oil from coal is to proceed via an indirect route in which coal is initially reacted with steam to produce a mixture of carbon monoxide (CO) and hydrogen (H_2). This process is called the water gas reaction and may be represented as

$$COAL + H_2O \rightarrow xCO + yH_2$$

The proportion of CO to H_2 depends upon a variety of factors including the coal used and the gasification technique employed.

Having gasified the coal using the water gas reaction the resultant mixture of CO and H_2 must be converted to liquids suitable for use as a fuel. This may be accomplished by reacting CO and H_2 over iron (Fe), cobalt (Co) or nickel (Ni) catalysts at elevated temperatures. In Germany prior to World War II, and more recently in South Africa, where the threat of a cut in supply of fuel from crude oil made the establishment of large scale synthetic fuel plants a strategic necessity, a great deal of research effort was devoted to this process known as the Fischer Tropsch (FT) synthesis.

In early FT synthesis work during the 1930s it was observed that the stoichiometry of the process over Fe catalysts was different to that over Co and Ni systems. Specifically the reactions were

$$CO + 2H_2 \xrightarrow{Co, Ni} -CH_2- + H_2O \qquad \text{eqn .1.1.1}$$

$$2CO + H_2 \xrightarrow{Fe} -CH_2- + CO_2 \qquad \text{eqn. 1.1.2}$$

Fischer and Koch (1930) had proposed a surface carbide mechanism in which it was proposed that carbon dioxide (CO_2) was produced by reaction of adsorbed oxygen atoms with CO, and H_2O by reaction of the same species with H_2

i.e.

$$CO \rightarrow C_{ads} + O_{ads} \qquad \text{eqn. 1.1.3}$$

$$CO + O_{ads} \rightarrow CO_2 \qquad \text{eqn. 1.1.4}$$

$$O_{ads} + H_2 \rightarrow H_2O \qquad \text{eqn. 1.1.5}$$

The sum of the equations 1.3 and 1.4 is known as the Boudouard reaction.

$$2CO \rightarrow C_{ads} + CO_2 \qquad \text{eqn. 1.1.6}$$

Although the Fischer school had considered the water gas shift reaction (WGSR)

$$CO + H_2O \rightleftarrows CO_2 + H_2 \qquad \text{eqn. 1.1.7}$$

its role in CO_2 production was not deemed important and hence was not systematically investigated.

Kolbel and Engelhardt (1950, 1951) pioneered work in this area. It was shown that the FT synthesis over Co exhibited the stoichiometry of eqn. 1.1.2 if the WGSR was promoted. In contrast, the stoichiometry over Fe was that of eqn. 1.1.1 if intermediate water was removed from the reactor, so hindering the WGSR. The conclusion was that eqn. 1.1.2 was the sum of eqn. 1.1.1, the Fischer Tropsch reaction (FTR), and the WGSR.

Further extension of these ideas led to development of a new method of hydrocarbon synthesis from CO and steam, the Kolbel Engelhardt (KE) synthesis (Kolbel and Engelhardt, 1950, 1951, 1952; Kolbel and Vorwerk, 1957; Kolbel and Bhattacharyya, 1958; Kolbel and Gaube, 1961). The overall equation is

$$3CO + H_2O \rightarrow CH_2 + 2CO_2 \qquad \text{eqn. 1.1.8}$$

which can be formally represented as the FTR summed with multiple applications of the WGSR.

Industrially obtained synthesis gas is often H_2 deficient (Anderson, 1984). Before being used as a FT feed such gas mixtures must be enriched with H_2, so as to give a CO:H_2 ratio of 1:2 consistent with FT stoichiometry (refer to eqn. 1.1.1). The supplementary H_2 is obtained on an industrial scale using the WGSR. The process of external "shifting" is expensive financially and complex engineering-wise.

The KE synthesis provides a simpler route to hydrocarbon formation. Synthesis gas need only be enriched with water for use as a KE feed, and H_2 is then produced *in situ*. Active KE catalysts could also utilise H_2 deficient feeds directly, because the H_2O produced by the FTR could be converted to H_2 by the WGSR. The stoichiometry of eqn. 1.1.2 would then apply. Despite these potential advantages, the KE synthesis has been largely ignored.

1.2 Outline of the Current Study

Bifunctional catalyst systems, containing active WGSR and FTR components, should be active towards the KE synthesis. Such systems were investigated in this thesis.

Supported Co catalysts are generally FT active (Vannice, 1975). In a study involving a suite of supported catalysts (Roe, 1986; Roe *et al.*, 1988), it was shown that Co supported on a high surface area silica (617.0 m^2/g, designated $SiO_2$40Å) and a high surface area alumina (148.3m^2/g, designated Al_2O_3) gave the most favourable product distributions in a FT feed. Catalyst systems supported on these oxides were, therefore, further investigated.

Copper is the most active low temperature WGSR metal (Newson, 1980; Andrew, 1980; Grenoble *et al.*, 1981). In the work reported in this thesis, a suite of Cu catalysts were prepared, using both Al_2O_3 and $SiO_2$40Å as supports with metal to support ratios on a weight basis of 10:100, 5:100 and 1:100.

Copper was also used to dope Co systems. Three hybrid catalysts of this type were prepared using each support. The weight ratios of Co, Cu and support were respectively 10:10:100, 10:5:100 and 10:1:100.

The single metal Co and Cu catalysts, physical mixes of the two and the hybrid Co/Cu catalysts were all characterised using temperature programmed reduction (TPR) and assessed in terms of their KE activities.

The most interesting catalyst proved to be Co/Cu/$SiO_2$40Å; 10:10:100, and this catalyst was examined in more detail. It was screened using KE feeds of varying CO/H_2O compositions. The nature of the catalyst under the optimal conditions was then evaluated. The techniques used included X-ray diffraction (XRD), electron probe microanalysis and thermogravimetry. The mechanism of the KE synthesis was also investigated using the same catalyst system.

The ultimate aim of the study was elucidation of the mechanism, with a view to predicting optimal catalysts and conditions for the KE synthesis.

2 LITERATURE REVIEW

2.1 Screening of KE Catalysts

The first main body of research pertaining to the Kolbel Engelhardt synthesis was performed in the 1950s. Kolbel and his co-workers hoped to utilise CO rich gases produced by the steel industry (Kolbel and Ralek, 1984) as a feed. Interest in the process waned during the 1960s and 1970s. Research work focussed on the improvement of the Fischer Tropsch synthesis during this time.

Recently, a number of "second generation" coal gasifiers have been developed which are more thermally efficient and therefore economical than older models (Kolbel and Ralek, 1984). The modern gasifiers yield gas which is hydrogen lean compared to that produced by the older devices. Interest in the KE synthesis has resurged in a bid to overcome the disadvantage of H_2 deficiency.

A variety of supported metal catalysts have been screened. (Kolbel and Ralek, 1984; Chaffee *et al.*, 1984; Chaffee and Loeh, 1985, 1986; Ekstrom and Lapszcewicz, 1985; Tominaga *et al.*, 1984, 1986). The active metals used include Fe, Co, and Ni.

The hydrocarbon distributions reported have all fitted the kinetic polymerisation model proposed by Schulz (1935) and Florey (1936). The probability of chain growth (α) typically decreased with temperature and increased slightly with increased contact times (*i.e.* decreased flow rates). There was also a decrease in the yields of olefins relative to paraffins with increased reaction time. FT catalysts typically behave in the same way.

Some general features of the KE synthesis were unique. The methane yield of the KE synthesis was very low compared to that given by the FT synthesis. Oxygenates were produced in relatively higher concentrations. Olefinic hydrocarbons were predominantly formed whereas paraffinic compounds are produced preferentially under FT conditions (Kolbel and Ralek, 1984).

Ekstrom and Lapszcewicz (1985) probed these general differences in a series of controlled experiments using $CO/H_2/H_2O$ feed of varying composition. A $Co/MgO/ThO_2$/kieselguhr catalyst was used in this study. At a synthesis temperature of 208°C the hydrocarbon yield using a FT feed was greater by a factor of 15 than under KE conditions. Such low conversion of CO/H_2O feeds may explain the general lack of interest in the KE synthesis.

An interesting feature of KE product distributions was reported by Chaffee and Loeh (1985). They found that a high concentration of aromatics were formed relative to aliphatic hydrocarbons of corresponding carbon numbers by a SiO_2 supported Ni catalyst under KE conditions. The $CO:H_2O$ ratio was 4.3:1, and the overall figure of CO conversion to hydrocarbons was 9%. The effects of changes in feed composition, temperature and space velocity on the production of aromatics were later investigated (Chaffee and Loeh, 1986) using the same catalyst. Aromatic production was favoured by increased temperatures, space velocities and CO partial pressures. A detailed analysis of the hydrocarbon fraction with carbon number eight (C8s) was carried out. At maximum, aromatics were found to constitute approximately 60% of all the C8 products.

Tominaga *et al.* (1984, 1986) are the only workers to have documented a study of a bifunctional catalyst system. A FT active Co/SiO_2 catalyst was physically mixed with a Cu-Cr oxide catalyst active towards the WGSR. The catalyst mix proved an active KE catalyst. The yield of hydrocarbons on a % carbon basis was 4.4%. The mix produced similar overall yields of hydrocarbons in $CO/H_2/H_2O$ and CO/H_2 feeds, although the average molecular weight of hydrocarbon products was greater under KE conditions. The products of maximum yield were C5s under FT conditions and C10s under KE conditions.

2.2 Mechanisms

2.2.1 The Kolbel Engelhardt Mechanism

There are two pathways by which the KE synthesis may proceed. The first pathway involves sequential coupling of the WGSR and the FTR, according to the combined reaction equations (see section 1.1). The second possibility is that CO and H_2O react directly together to produce hydrocarbons, without the production of internal H_2.

The sequential pathway is almost universally accepted. Most screening results are consistent with this mechanism. The similarity in FT and KE product distributions for example, suggests that the FTR is a "half reaction" of the KE synthesis. The high activity of hybrid catalyst systems supports the idea of WGSR and FTR co-operation.

Further supporting evidence is provided by the kinetic studies of Kolbel *et al.* (Kolbel and Ralek, 1984). Concentration profiles were measured in a fixed bed, and hence integral mode, reactor. Typically profiles appeared as in fig. 2.2.1.

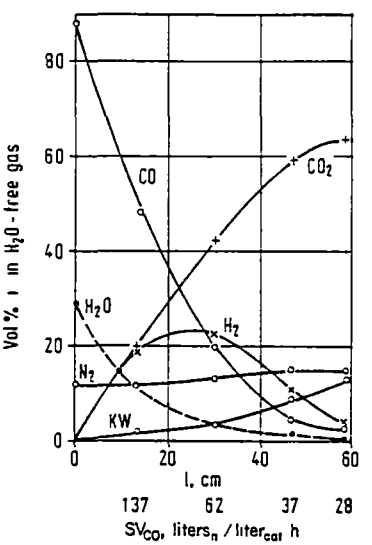

fig. 2.2.1: Course of the KE reaction over Fe at 7 atm and 260°C (Kolbel and Hammer, 1960).

In the above example, hydrocarbons were produced after an induction period during which time significant H_2 conversion occurred. There was a delicate balance between the WGSR and the FTR and eventually a steady state was reached where H_2 consumption equalled its production. Such behaviour is typical of a consecutive reaction.

Few attempts have been made to identify intermediates of the KE synthesis. Miyata *et al.* (1984) approached this problem and found that the rates of formation of hydrocarbons in the reactions of carbided Fe catalysts with both H_2O and H_2 were less than the rates measured under steady state synthesis conditions. They concluded surface carbide was not a reactive intermediate.

Kotanigawa *et al.* (1981) studied Fe catalysts by Fourier transform infrared spectroscopy (FTIR) and X-ray crystallography in an attempt to observe reactive species. They proposed a mechanism which was concerted, and exceptional in that sense. The scheme was

$$CO \rightarrow C_s + O_{ads}$$

$$C_s + H_2O \rightarrow = CH$$

$$= CH + H_2O \rightarrow [CH_2 = CH -]$$

The key reaction in a set of possible equilibria was

$$2Fe_3C + 8H_2O \rightarrow 2Fe_3O_4 + C_2H_4 + 6H_2$$

Studies by Gustafson (1981), Gustafson and Lunsford (1982) and Lunsford and Niwa (1982) employing Ru/zeolite, Rh/zeolite, Rh/SiO_2 and Rh/Al_2O_3 catalysts concentrated on purely the methanation of CO by steam. Conventional kinetic analysis as well as X-ray photoelectron spectroscopy (XPS) and infrared (IR) spectroscopy were used to show that methane production proceeded sequentially and that the pre-deposition of surface carbon was crucial.

In support of the proposed involvement of surface carbide Kuijpers *et al.* (1984) suggested that over a Ni/SiO_2 catalyst quantitative conversion of CO to methane occurred according to eqn. 2.2.1a.

$$4CO + 2H_2O \rightarrow CH_4 + 3CO_2 \qquad \text{eqn. 2.2.1a}$$

Surface carbide which was formed reacted with water in a 1:1 ratio.

$$2C + 2H_2O \rightarrow CH_4 + CO_2 \qquad \text{eqn. 2.2.1b}$$

The possibility that H_2 was produced *via* the WGSR and immediately consumed was not ruled out, but no excess H_2 was produced. Rabo and Elek (1980) observed the same behaviour on Co, Ni and Ru systems.

Although the KE reaction has not been studied in detail, a great deal of research effort has been devoted to the FT synthesis particularly, and the WGSR also. Given that the KE synthesis proceeds sequentially, much of this work may be a useful aid to elucidation of the KE mechanism.

2.2.2 The Fischer Tropsch Synthesis

The definitive treatment of screening data by Anderson (1956) and Rautavuoma (1979) using the Schulz Florey equations demonstrated that FT products are formed by stepwise insertion of one carbon atom species. Experiments using tracer molecules suggest that this species is the methylene grouping, CH_2 (Kummer *et al.*, 1948; Pichler and Schulz, 1976; Ponec and van Barneweld, 1979; Pettit and Brady, 1981). These common features are integral to the three mechanisms most commonly advocated in the literature; the CH_x stepwise polymerisation mechanism, the hydroxycarbene mechanism and the CO insertion mechanism.

(a) The CH_x Stepwise Polymerisation Mechanism

In this model molecules of CO dissociate and the resultant C atoms are hydrogenated and then polymerised to form products.

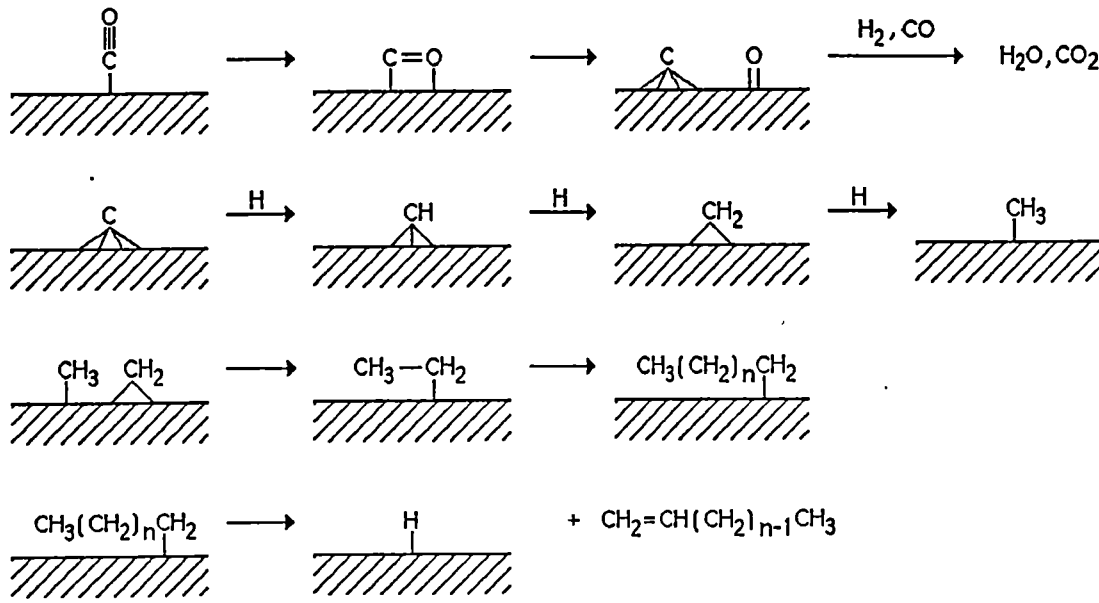

fig. 2.2.2a Reactions of the CH_x stepwise polymerisation mechanism

This is essentially a variant of the carbide intermediate mechanism proposed in the earliest papers of Fischer and Tropsch (1930) and later modified by Rideal and Craxford (1939). They postulated that partly hydrogenated surface or bulk carbide block polymerised rather than doing so in a stepwise manner, a subtle difference. Such a mode of polymerisation in two or three dimensions should give a high proportion of branched hydrocarbons, but hydrocarbons formed by the FT synthesis are mostly linear.

The CH_x stepwise polymerisation mechanism is currently accepted as the mechanism of the FT synthesis. This acceptance largely results from a series of experiments where labelled CO has been used to predeposit a carbide layer *via* the Boudouard reaction. (Araki and Ponec, 1976; Wentreck *et al.*, 1986; Rabo *et al.*, 1978; Sachtler *et al.*, 1979; Biloen *et al.*, 1979).

Araki and Ponec (1976) predeposited ^{13}C on Ni and Fe foils, and then introduced a $^{12}CO/H_2$ feed. Production of $^{13}CH_4$ preceded that of $^{12}CH_4$ and $^{12}CO_2$. They concluded that the following reaction sequence occurred.

$$^{13}C_{ads} + 2H_2 \rightarrow {}^{13}CH_4$$

$$^{12}CO \rightarrow {}^{12}C_{ads} + O_{ads}$$

$$^{12}C_{ads} + 2H_2 \rightarrow {}^{12}CH_4$$

$$O_{ads} + {}^{12}CO \rightarrow {}^{12}CO_2$$

The production of CO_2 without H_2O was consistent with the CH_x polymerisation mechanism alone. In the other mechanisms, H_2 attack is assumed to precede CO bond cleavage. Water is inevitably produced when O is removed from reactive intermediates prior to chain growth. In similar pulse experiments H_2O was produced from the reaction of H_2 with adsorbed O atoms, but the greater reactivity of surface carbide as opposed to adsorbed CO was beyond dispute (Wentreck *et al.*,1976; Rabo *et al.*, 1978).

The main flaw of such experiments is that hydrogenation of the surface carbon produced predominantly methane. Higher hydrocarbons were not produced in a pure H_2 feed. They only appeared when fresh CO was introduced (Wentreck *et al.*, 1976; Biloen *et al.*, 1979). Whether the production of methane by hydrogenation of the predeposited carbide was directly comparable to the mechanism which produced the higher hydrocarbons is, therefore, contentious.

Surface spectroscopy has been used in attempts to directly observe reactive intermediates. XPS studies have shown that facile dissociative chemisorption of CO on transition metal surfaces does occur (Rabo *et al.*, 1978; Roberts, 1980) and that the adsorbate layer is heterogeneous. Studies of an Fe foil under "reaction conditions"

implied the presence of amorphous surface carbon and polymeric CH_x species. The high vacuums necessary within an XPS spectrometer are not typical of FT synthesis conditions.

In situ IR studies provide a more representative pressure regime. Growth of CH_x chains has been observed using this technique on Ni/SiO_2, Fe/SiO_2 and Ru foils. (Blyholder and Neff, 1962, 1963; King, 1980; Tamaru, 1980). These studies were not able to determine whether these species were intermediates or products.

The CH_x stepwise polymerisation theory gave the best agreement with an elegant kinetic model derived by Pettit and Brady (1981). This paper is the most often cited of a myriad of publications on the kinetics of the FT synthesis. Numerous rate laws have been determined, but the results do not present a uniform picture. The order of H_2 partial pressure, for example, varies from O to 2 (Dry, 1981). Any attempt to predict mechanisms by formulating models to fit such results must be viewed with suspicion.

(b) The Hydroxycarbene Mechanism

Here CO is directly hydrogenated to hydroxycarbene species. Chain growth occurs by the elimination of water between neighbouring species.

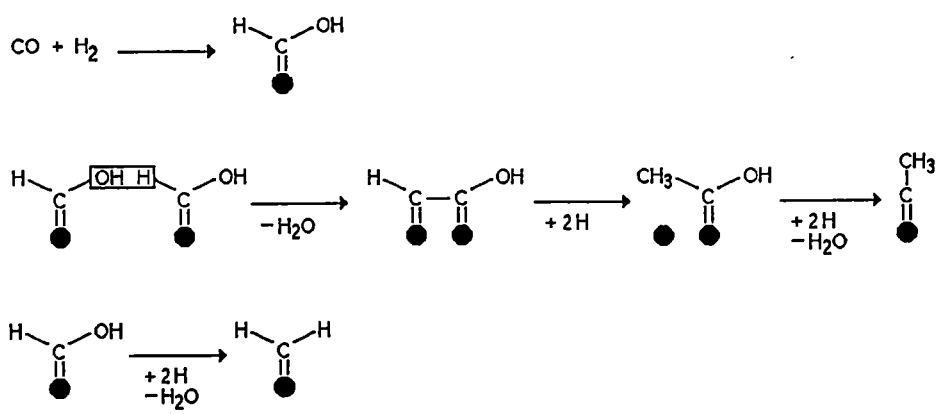

fig. 2.2.2b Some reactions from the hydroxycarbene mechanism.

There is very little convincing experimental evidence to support this mechanism (Ponec, 1984).

(c) The CO Insertion Mechanism

In this proposal CO inserts into either metal-H or metal-C bonds on the catalyst surface. Hence surface carboxyl species form which react further by a series of hydrogenation and CO insertion reactions.

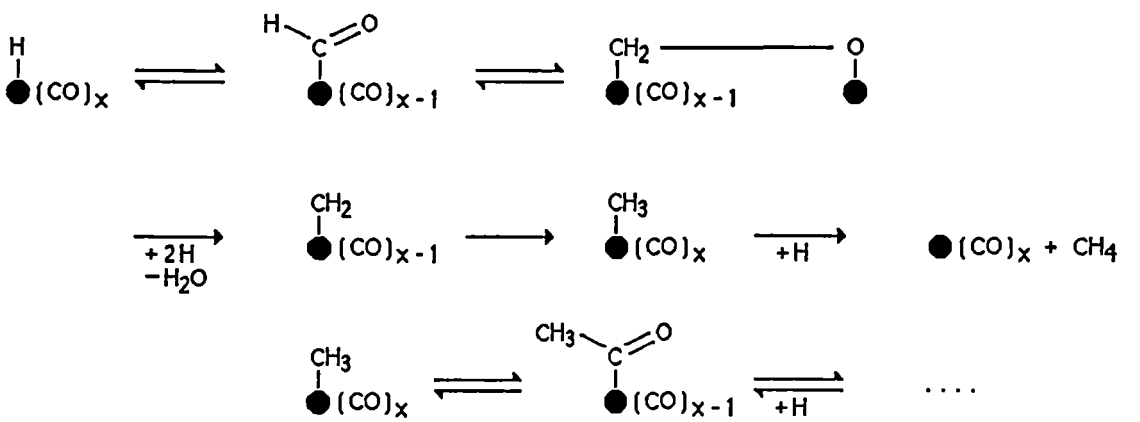

fig. 2.2.2c Various pathways involving CO insertion steps and C-O bond hydrogenolysis.

IR spectroscopy has been used to identify stable carboxyl, carbonyl and carbonate surface species on several catalysts (Blyholder, 1966; Kolbel *et al.*, 1970; Blyholder and Goodsel, 1971; Blyholder *et al.*, 1976). Analogous reactions are known to occur in several homogeneous catalyst systems (Ponec, 1984). The mechanism cannot be excluded and, although not dominant, may well play a role in the formation of oxygenates. Hybridised mechanisms which include CO insertion as a terminating step in the CH_x stepwise polymerisation mechanism are able to account completely for all usual products (Minderman *et al.*, 1982; Cressdy *et al.*, 1982).

2.2.3 The Water Gas Shift Reaction

The active species of low temperature Cu based WGSR catalysts is thought to be Cu^0, because, as with the FT synthesis, catalysts must be reduced in order to activate them (Young and Clark, 1973). Electron spin resonance (ESR) and electrical conductivity measurements have confirmed this idea (Ghosh *et al.*, 1969; Leherte *et al.*, 1976).

Formate ion is almost certainly the key WGSR intermediate. Such species have been observed during *in situ* IR studies of numerous catalysts (Davydov *et al.*, 1977; Amenomiya, 1979; Edwards and Schrader, 1984). Decomposition of a formate type intermediate appeared to be the rate determining step of the forward and reverse WGSR over a CuZnO catalyst studied by Van Herwijnen *et al.*, (1980).

i.e. $H_2O + CO \underset{slow}{\overset{fast}{\rightleftharpoons}} [H_2CO_2] \underset{fast}{\overset{slow}{\rightleftharpoons}} H_2 + CO_2$ eqn. 2.2.1

This was concluded because of the similarity of these rates with those for the analogous decompositions of formic acid over the same catalyst.

A satisfactory mechanism for Cu based catalysts which is consistent with these oft quoted observations has not been published. Grenoble *et al.* (1981) suggested a general model, where CO was activated on metal sites and H_2O on support sites, which accounted for the effect of support on activity. Amenomiya and Pleizier (1982) disputed that such a mechanism applied universally. On K promoted Al_2O_3 catalysts it was proposed that the reaction proceeded as in fig. 2.2.3a

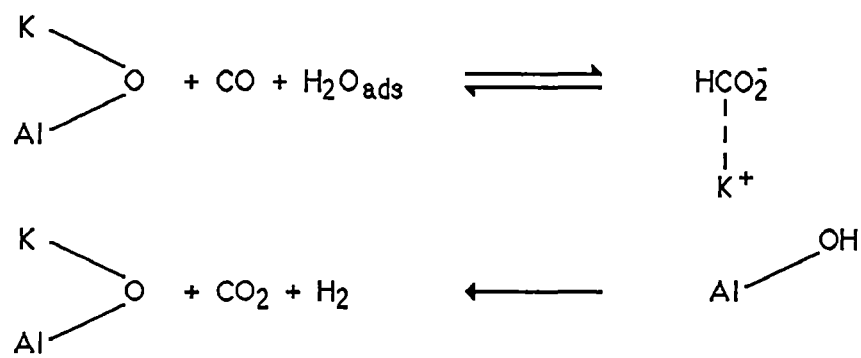

fig. 2.2.3a A proposed mechanism for the WGSR on K promoted alumina.

A comparable mechanism has been postulated earlier for Cu catalysts, with Cu^{1+} instead of Cu^{0} as the active species (Davydov *et al.*, 1977).

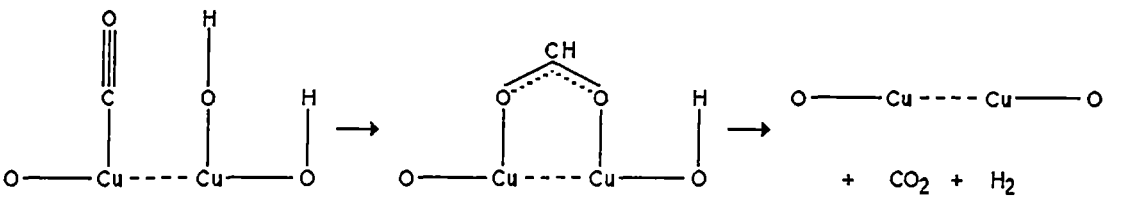

fig. 2.2.3b A possible reaction scheme for the WGSR on Cu catalysts.

2.3 Characterisation of Supported Co and Cu Catalysts by Temperature Programmed Reduction

The TPR method is a simple and quick means of identifying the presence of metal species either on a catalyst surface or in the bulk. When used in conjunction with other techniques, which allow determination of the nature of the various species observed, the value of TPR is augmented. Such techniques include XPS, X-ray diffraction and UV/Vis diffuse reflectance spectroscopy.

The TPR technique was only recently developed, but because of its popularity enough results have already been produced to prompt the writing of several review articles (Hurst *et al.*, 1980; Lemaitre, 1984) and a book (Jones and McNicol, 1986). Most of the commonly used catalytic materials have now been investigated using the method.

On Co/Al_2O_3 catalysts, the bulk oxide, Co_3O_4, as well as Co ions in surface networks and aluminate species have been observed using TPR in association with X-ray diffraction and XPS. The interactive Co ions and aluminate were both reduced at higher temperatures than the bulk oxide (Paryjczak *et al.*, 1980; Castner and Santilli, 1984; Arnoldy and Mouljin, 1985; van't Blik and Prins, 1986).

Two types of interactive Co ions were observed by Arnoldy and Mouljin (1985) and van't Blik and Prins (1986). Arnoldy and Mouljin (1985) suggested the two types were octahedral and tetrahedral Co^{2+}. Van't Blik and Prins (1986) suggested that differing valence states caused the two reduction phases observed. The peaks were attributed to Co^{2+} and Co^{3+} ions bonded in surface sites.

Reduction peaks occurring at and above the reduction temperature of unsupported Co_3O_4 have also been observed on Co/SiO_2 catalysts (Paryjczak *et al.*, 1980; Castner and Santilli, 1984; Martens *et al.*, 1986) and Co/MgO (Sexton *et al.*, 1986). These were assigned to Co_3O_4 and interactive Co^{2+} ions respectively in all but the Co/MgO study. Sexton *et al.* assigned the low temperature peak to the reduction of Co_3O_4 to CoO and the high temperature peak to a CoO to Co^0 conversion.

Supported Cu catalysts behave differently. On Cu/SiO_2 catalysts, low temperature peaks in the range of 250°C to 300°C have been observed. These peaks occurred below the reduction temperatures of bulk cupric oxide, CuO (Robertson *et al.*, 1975; Gentry and Walsh, 1982; Shimokawabe *et al.*, 1983; Delk and Vavere, 1984). Typically CuO reduced at 400°C. The low temperature peaks were generally assigned to dispersed CuO species.

Smaller high temperature peaks have also been observed in two of the studies. Shimokawabe *et al.* (1983) suggested peaks at 400°C and 700°C were due to the stepwise reduction of interactive CuO to Cu^0 *via* Cu^{1+}. Gentry and Walsh (1982) found no evidence for a two stage reduction and assigned the 600°C observed peaks to distinct Cu phases, specificially copper silicates.

On α-Al_2O_3 and β-Al_2O_3 a peak at 300°C again occurred (Gentry and Walsh, 1983). A peak at 600°C was also observed on Cu/α-Al_2O_3 but not on Cu/β-Al_2O_3, which belied the chemical similarity of the two supports. The high temperature reduction was attributed to a Cu-Al surface spinel.

Delk and Vavere (1984) studied Cu/TiO_2 catalysts and observed two reduction phases at 130°C and 220°C. They attributed the low temperature peak to Cu^{2+} in intimate contact with the TiO_2 support, and the other peak to dispersed CuO. The reduction of interactive species preceded that of the oxide, which is a different order than that proposed for Cu/SiO_2 and Cu/Al_2O_3 catalysts.

The thrust of the majority of TPR studies to date has been to investigate the change in distribution of various oxidic metal species present on calcined catalysts as a function of the preparation procedure. In general, high calcination temperatures and low metal loadings encourage the formation of interactive species.

Only in the paper by Castner and Santilli (1981) was an attempt made to correlate TPR profiles with activity. The process in question was CO hydrogenation catalysed by supported Co systems. The authors found that activity was directly proportional to the availability of surface Co^0 after reduction of the calcined catalysts in H_2. The amount of available Co^0 was in turn determined by the proportion of oxidic Co species which reduced at temperatures below 500°C according to the TPR data acquired using the calcined samples.

2.4 Justifications for the Current Study

Few catalysts have been screened for their KE activities. In particular, little work has been performed using bifunctional catalysts. Bimetallic hybrids, as opposed to physical mixes, have been ignored completely. The effect of varying the $CO:H_2O$ feed ratios is also not well researched. Optimal catalysts and optimal conditions must therefore be regarded as unestablished.

Although the KE synthesis is generally accepted to proceed by sequential coupling of the WGSR and FTR, active intermediates have not been positively identified. This knowledge is needed to gain a comprehensive understanding of the KE mechanism.

The logical development and design of optimal catalyst systems requires the identification of active metal species and elucidation of the roles they play. A thorough characterisation of an active KE catalyst, in association with an understanding of the mechanism, should enable this information to be found. No active KE catalysts have previously been characterised in detail.

This thesis was geared to make a contribution to these deficiencies in our knowledge of the KE synthesis.

3 EXPERIMENTAL

3.1 Reagents

The inorganic salts used were cobalt(II) nitrate hexahydrate, $Co(NO_3)_2.6H_2O$) (BDH chemicals, 97.5% minimum assay) and copper (II) nitrate trihydrate, $Cu(NO_3)_2.3H_2O$ (laboratory reagent).

The supports were high purity (99.9%) Al_2O_3 (Strem chemicals, NATL 93-1380) and $SiO_2$40Å (Merck, prod. no. 10181).

The unsupported oxides used were cobaltosic oxide, Co_3O_4 and cupric oxide, CuO (specpure, Johnson Matthey chemicals).

The experimental gases used were chemical pure (99.5%) CO (Matheson), ultra high purity (99.999%) H_2(CIG), and high purity (99.99%) Ar (CIG). The gases used to operate gas chromatographs were high purity (99.99%) O_2 free N_2 (CIG), industrial grade (99.5%) H_2 (CIG), ultra high purity (99.999%) He, industrial grade air (CIG) and compressed air. Calibration mixtures were a 1000 ppm mix of C1 to C6 normal paraffins diluted in N_2 (Alltech) and a special gas mixture of 6% CH_4, 31% CO_2, 38% CO and 25% H_2 (CIG).

3.2 Catalyst Preparation

The single metal catalysts were all prepared by impregnation. The supports were slurried in distilled water, and aqueous solutions containing the appropriate amounts of $Co(NO_3)_2.6H_2O$ or $Cu(NO_3)_2.3H_2O$ were added. The mixtures were evaporated to dryness with constant heating and stirring. Each sample was calcined in air at 400°C for 24 hours. The calcined catalysts were ground and passed through a B55 100 mesh (0.0063 inches) sieve. The fractions less than 100 mesh were used in all experiments. The bimetallic hybrid catalysts were prepared in the same way, except that $Co(NO_3)_2.6H_2O$ and $Cu(NO_3)_2.3H_2O$ were dissolved together and added to the slurried supports. The physical mixes were prepared by combining equal weights of calcined and sifted supported Co and Cu catalysts.

3.3 Screening

3.3.1 Reaction Methodology

Screening was carried out at atmospheric pressure and varying temperatures in a single pass fixed bed microreactor. The apparatus is shown in fig. 3.3.1.

Two sets of screening experiments were carried out. For preliminary Kolbel Engelhardt screening the flow rates of CO and Ar were 2 ml/min and 6 ml/min respectively. The water bath temperature was held at 60°C giving the desired CO:H_2O ratio of 3:1. The sample size was approximately 0.8g for single metal and hybrid catalysts, and 1.6g for physical mixes. All samples were dried *in vacuo* before weighing. The samples were packed between quartz wool plugs. The catalysts were activated by pre-reduction for two hours *in situ* at 400°C in a 5 ml/min H_2 flow. The samples were screened at 250°C, 275°C, 300°C and 325°C.

In the second set of screening experiments the CO:H_2O feed ratio was varied. The flow rate of CO was held constant at 5 ml/min, and no diluent Ar was used. Five separate experiments were performed. For each experiment the CO:H_2O ratio was fixed, and the sample temperature was varied from 250°C to 325°C at 25°C intervals. The CO:H_2O ratios used were 3:1, 2:1, 1:1, 1:2 and 1:3. The water bath was held at 65.3°C, 71.9°C, 81.7°C, 89.0°C and 92.3°C respectively to obtain these ratios. The sample size of Co/Cu/$SiO_2$40Å;10:10:100 was again approximately 0.8g on a dry weight basis. The usual activation procedure (5 ml/min H_2 flow, 400°C, 2 hours) was used.

In all circumstances, activity measurements were not made until product distributions had reached steady state at 250°C. This generally involved a period of two to three hours. After a new temperature was set, steady state was again attained before data acquisition. The catalyst samples were thus held at each temperature for between one and two hours. By the end of each screening experiment, catalysts had been on-stream for at least eight hours.

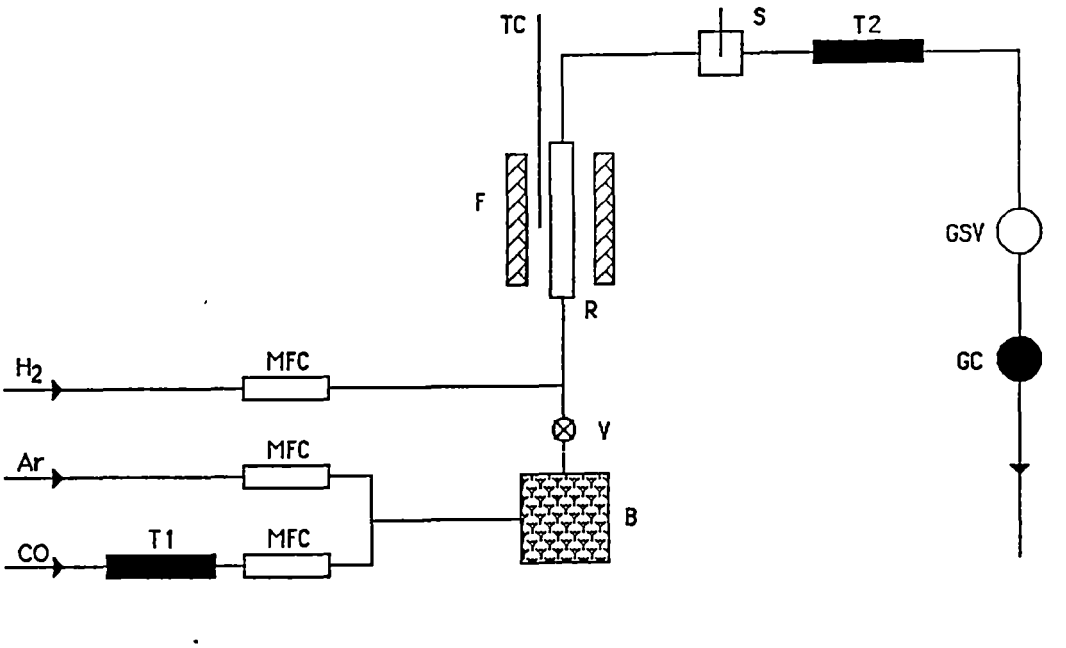

fig. 3.3.1 Schematic diagram of KE screening rig.

MFC - manual mass flow controllers (Porter, model VCO-1000).

B - water filled bubbler immersed in a heated water bath.

V - switching valve (Whitey). This enabled the bubbler to be isolated.

R - pyrex reactor, 150 mm long x 9 mm diameter. Temperature was controlled using a Pye Ether thermoregulator.

TC - external thermocouple.

T1,T2 - cold traps held at -76°C and -40°C respectively.

GSV - gas sampling valves.

GC - gas chromatographs.

S - septum.

The gas line between bubbler and reactor was heated using an air gun.

3.3.2 Product Analysis

For preliminary experiments, C1, C2 and C3 hydrocarbons as well as CO and CO_2 were monitored on-line by gas chromatography. For extensive hydrocarbon analysis, 5 ml gas aliquots were removed through the septum and manually injected into an external gas chromatograph (GC). In the second set of experiments, where CO:H_2O ratios were varied, H_2 concentrations were also measured on line. Technical information regarding the GC characteristics is given below.

(a)	Products	CO, CO_2
	GC model	Varian 920
	Detector type	thermal conductivity
	Column	packed carbosieve
	Carrier gas	H_2
	Flow rates (ml/min)	
	- reference	25
	- sample	25
	Oven temperatures (°C)	
	- injector	150
	- column	80
	- detector	150

(b)	Products	C1-C3 hydrocarbons
	GC model	Shimadzu GCO 4A PTF
	Detector type	flame ionisation
	Column	packed chromosorb
	Carrier gas	N_2
	Flow rates (ml/min)	
	- reference	25
	- sample	25
	Oven temperature (°C)	
	- injector	50
	- column	40
	- detector	50
(c)	Products	gaseous hydrocarbons
	GC model	Hewlett Packard 5880 A series
	Detector type	flame ionisation
	Column	Chrompack
		25mm x0.45 mm (o.d.) 10.32 mm (i.d.)
		liquid phase CP Si.15CB
		film thickness 4.7 μm
	Carrier gas	He
	Head pressure (p.s.i.)	7
	Oven temperatures (°C)	
	- injector	240
	- column	programmed; 30°C for 3 mins,
		ramped to 180°C at 10°C/min,
		held at 180°C for 5 mins
	- detector	240

(d)	Products	H_2
	GC model	Gowmac series 550
	Detector type	thermal conductivity
	Column	packed carbosieve
	Carrier gas	N_2
	Flow rates (ml/min)	
	- reference	25
	- sample	25
	Oven temperatures	
	- injector	50
	- column	25
	- detector	50

A switched electronic integrator (Hewlett Packard 3390A) received signals from the on-line GCs to give a printed record of the relative amounts of gas components detected. Area counts of component peaks obtained were compared to the corresponding area counts of calibration gas mixtures to determine mole percentages of each of the detected species.

The extensive hydrocarbon chromatograms were analysed by the GC series 5880 A terminal. The concentration of each hydrocarbon fraction (*i.e.* C1, C2, ..., C9) was quantified relative to C1 concentrations using the assumption that the integrated peak areas were proportional to the weight of each fraction. The absolute concentrations were obtained by equating the C1 molar percentages measured on-line and externally (further details are given in Appendix 1).

The retention time for each hydrocarbon fraction was determined using gas-chromatography mass-spectrometry (GCMS). The GC was a Hewlett Packard 5890 model, and the mass spectrometer a Hewlett Packard 5970 mass selective detector. The column and column conditions used for GCMS analysis were identical as for flame ionisation analysis.

3.4 Catalyst Characterisation

3.4.1 Temperature Programmed Reduction

The apparatus for the TPR experiments was laboratory built and is depicted in fig. 3.4.1.

All TPR runs were conducted at a heating rate of 0.2°C/s. The runs commenced at room temperature and concluded between 800°C and 900°C. The H_2 and Ar flow rates were 0.48 ml/min and 7.1 ml/min respectively. Consumption of H_2 was calibrated using Co_3O_4.

The sample weight of calcined catalysts depended on loading. For single metal Co catalysts and the hybrid systems, approximately 40mg samples were used. For physical mixes, 80mg, 40mg of each single metal catalyst, were measured out. For Cu catalysts with metal to support weight ratios of 10:100, 5:100 and 1:100, sample sizes were 40mg, 80mg and 400mg respectively. Samples were not pre-treated. The TPR profiles of activated catalysts were acquired using approximately 0.8g samples for single metal and hybrid catalysts and 1.6g samples for physical mixes. The samples were pre-reduced *in situ* for two hours at 400°C, the same activation procedure as was used in the screening experiments (see section 3.3.1). The TPR profiles of activated, air exposed catalysts were obtained using the same sample sizes (40 mg, 80 mg) as for the calcined samples.

The TPR profiles of spent catalysts were obtained using 40 mg (single metal and hybrid catalysts) and 80 mg (physical mixes) samples. These samples were packed separately from a larger weight (0.8g, 1.6g) of catalyst. The combined samples were activated in the usual way and exposed to a 1:1 $CO:H_2O$ feed at 250°C until steady state product distributions were established. The larger proportion of each combined sample was then removed from the reactor and a TPR profile acquired immediately on the remaining weight of catalyst. This procedure minimised exposure of the catalysts to air.

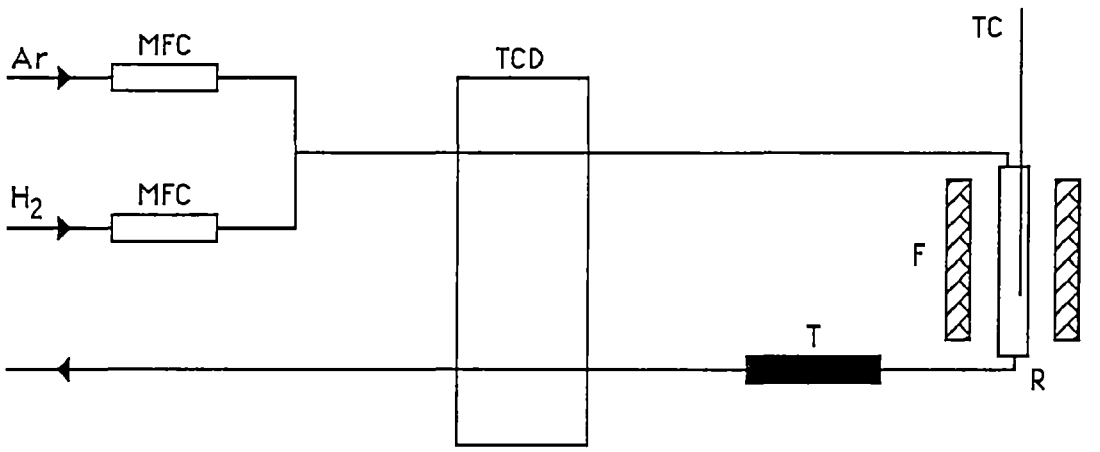

fig. 3.4.1 Schematic diagram of TPR apparatus.

MFC - electronic mass flow controllers (Porter, model 201 SSVC)*.

TCD - thermal conductivity detector (Carle)*.

TC - internal sheathed thermocouple*.

R - quartz reactor, 400 mm long x 9 mm diameter.

F - quartz furnace, 200 mm long x 20 mm diameter.

T - water trap.

* A Pulsar microcomputer was used to read the TCD and TC outputs as well as to control the MFCs and the heating rate of the furnace.

3.4.2 Elemental Analysis

Cobalt and copper loadings were determined by flame atomic absorption spectroscopy using a Varian-AA 1475 spectrometer. Approximately 100 mg (on a dry weight basis) of single metal and hybrid catalysts, or 200 mg or the physical mixes, were digested in concentrated HNO_3. The digested mix was made up to 100.0 ml in 10% (by volume) HNO_3. A 1.0 ml aliquot of this solution was then diluted by a factor of 100.0, again in 10% HNO_3. The absorption of this mix was calibrated against Co and Cu standards containing 0.5 to 5 ppm (by weight) of the respective metals.

3.4.3 X-ray Diffraction

X-ray diffraction patterns were obtained for calcined (400°C in air, 24 hours), activated (400°C, 5 ml/min H_2, 2 hours) and spent (1:1 CO:H_2O feed until steady state, 250°C) catalysts as well as a Co/Cu oxide standard.

The standard was prepared from samples of $Co(NO_3)_2.6H_2O$ and $Cu(NO_3)_2.3H_2O$ containing equivalent weights of Co and Cu respectively. The salts were mixed and dissolved together in distilled water and then the water was dissolved off with constant heating and stirring. The dried mix was calcined in air at 400°C, ground by hand and sifted through a 100 mesh sieve.

A Phillips X-ray diffractometer (model PW1050/25 number DY3145) was used to acquire diffraction patterns. The samples were powdered (less than 100 mesh). Each sample was scanned from a diffraction angle (2θ) of 5° to between 60° and 70°. The radiation source was Cu. The $K\alpha_1$ and $K\alpha_2$ X-rays were unresolved, which gave a weighted mean wavelength of 1.5418 Å. The samples were air exposed prior to and during acquisition of diffraction patterns.

3.4.4 Electron Probe Microanalysis

Electron probe microanalysis was performed with a Jeol XA-50A instrument. The technique was used in order to find the distribution of Co and Cu species rather than to deduce metal loadings. Maps of Co, Cu and Si distributions were acquired on a macroscopic scale where the magnification of the sample region ranged from 120 to 700 times. Between 500 and 1000 counts were accumulated for each element mapped. Calcined, activated and spent catalysts as well as the blank calcined $SiO_2$40Å support were investigated in this way. Powdered samples (<100 mesh) were mounted on adhesive tape and gold coated before analysis. Investigation of the calcined, activated and spent Co/Cu $SiO_2$40Å;10:10:100 was also carried out at a microscopic level (magnification 3000 times). To prepare the samples the catalyst was finely ground in an automated grinder for one hour. The powder was then pressed into a disk, which was subsequently gold coated.

3.4.5 Surface Area Measurement

Nitrogen adsorption isotherms were measured at liquid N_2 temperatures with a conventional glass apparatus. Surface areas were calculated using the BET model (Anderson and Pratt, 1985).

3.4.6 Thermogravimetry

Uptake of CO was measured in a modified Mettler BE22 balance. Pressed samples of approximately 40 mg were first evacuated at room temperature to a pressure of less than $1x10^{-6}$ torr. The samples were then reduced under 400 mbar of H_2 at 400°C for 12 hours. The evacuation procedure was repeated, then the sample was progressively exposed to 100 mbar, 200 mbar and 300 mbar of CO at room temperature. All gases were passed through an acetone/liquid N_2 (-76°C) trap to purify them before use.

3.5 Mechanistic Studies

3.5.1 Infrared (IR) Studies

The apparatus used for IR experiments is depicted in fig. 3.5.1. The IR cell was similar to that designed by Yates *et al.* (1984).

Wafers of 10 mg/cm^3 were prepared by compression at 8 tonne/cm^2 pressure. Activated and air exposed samples of Co containing catalysts (Co/$SiO_2$40Å;10:100 and Co/Cu/$SiO_2$40Å; 10:10:100) were used in the wafers. The Co containing samples had to be diluted with the support (1 part of catalyst to 4 parts of $SiO_2$40Å by weight) to make wafers which were transparent to IR radiation. Suitable wafers were prepared from undiluted calcined Cu/$SiO_2$40Å;10:100.

Two experiments were performed in which CO chemisorption and the KE mechanism were each investigated. The wafers were reduced in the IR cell at 300°C for 12 hours under 3 ml/min H_2 flow before commencement of both experiments.

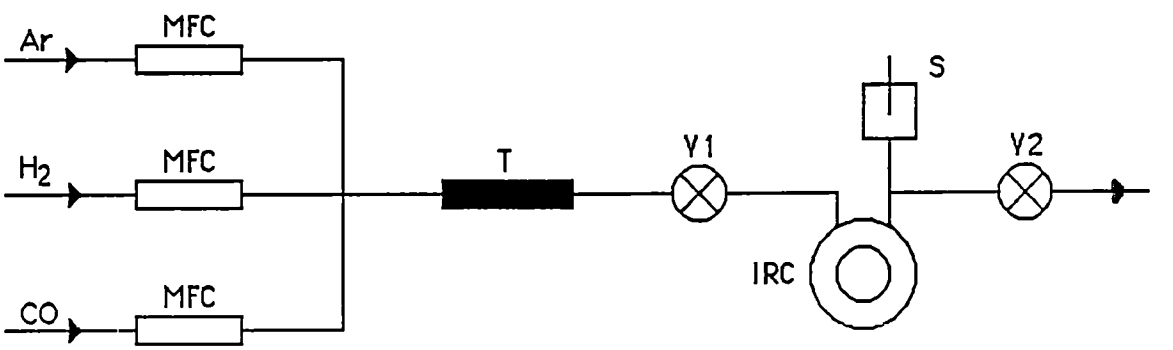

fig. 3.5.1 Schematic diagram of IR rig.

MFC - manual mass flow controller (Porter, model VCO-1000).

T - trap held at -76°C.

V1,V2 - two way valves (Whitey).

IRC - infrared cell.

S - septum.

CO Chemisorption

After activation (300°C, 3 ml/min H_2 flow, 12 hours), the H_2 flow was maintained while the cell was allowed to cool to room temperature. A spectrum of the catalyst was acquired at this stage. The wafer was then exposed to CO (5 ml/min) for approximately one hour. The CO flow was subsequently stopped, and the cell was purged with Ar (20 ml/min) for approximately one hour. Another spectrum was acquired. The sample was then heated in the Ar flow, and further spectra obtained as the temperature was raised.

Kolbel Engelhardt Activity

This experiment was performed only with Co/Cu/$SiO_2$40Å;10:10:100. A fresh wafer was prepared in the normal way. It was pre-treated identically to the wafer used for the CO chemisorption experiment (*i.e.* reduced for 12 hours at 300°C in 3 ml/min H_2, cooled, exposed to CO, purged with Ar and heated). The sample was then exposed to a CO flow (5 ml/min). Liquid H_2O was injected manually into the cell. The volume of the aliquots was 5μl, which is equivalent to approximately 6.8 ml of water vapour. Successive spectra were acquired and the appearance of characteristic CO and H_2O peaks was used to confirm the presence of both gases. However the exact CO:H_2O ratio was not known. The cell was then isolated (*i.e.* valves 1 and 2 were closed - refer to fig. 3.5.1a) and treated at 260°C in the static CO/H_2O atmosphere for approximately 0.5 hours. Further spectra were obtained and referenced against the spectrum given by the catalyst at 260°C in Ar.

3.5.2 Reactivity of Ethene

The same apparatus as for the screening experiments was used (see section 3.3.1). An ethene (0.5 ml/min) and Ar (4.5 ml/min) gas mix was passed through the bubbler, which was held at 81.7°C. A 0.8g (on a dry weight basis) sample of Co/Cu/$SiO_2$40Å;10:10:100 was used. The reaction temperatures studied were 250°C, 275°C, 300°C and 325°C. The sample was activated in the normal way (400°C, 5

ml/min H_2, 2 hours) and stabilised in a 1:1 CO:H_2O feed at 250°C prior to ethene exposure.

Product analysis was also carried out in the same way as for screening experiments (see section 3.3.2). The conversions of ethene to each hydrocarbon fraction were calculated making the assumptions that the hydrocarbons measured represented the sum total of hydrocarbon products, that peak areas were proportional to the weight of the appropriate fractions and that ethene was the only possible source of hydrocarbons in the system.

3.5.3 Reactivity of Coke

The same apparatus was used as for screening experiments. A 0.8g Co/Cu/$SiO_2$40Å;10:10:100 sample (dry weight basis) was activated in the normal way (400°C, 5 ml/min H_2, 2 hours) and allowed to stabilise in a 1:1 CO:H_2O feed at 250°C. The sample was then carbided in a pure CO flow (5 ml/min) at 325°C for one hour. The CO was passed through the line generally used for H_2 (refer to fig. 3.3.1). The levels of CO and CO_2 were measured on-line. The presence of CO_2 indicated that the Boudouard reaction (eqn 1.1.6), and hence carbon deposition, was proceeding. The sample was then exposed to an Ar:H_2O 1:1 feed. The Ar flow was 5 ml/min, and the water bath was held at 81.7°C.

Subsequently, H_2 was introduced to the feed mixture through the line used for CO in screening experiments (refer to fig. 3.3.1). The composition of the feed was 0.2:0.8:1 H_2:Ar:H_2O and the flow rates of H_2 and Ar were 1 ml/min and 4 ml/min respectively.

Product analysis was carried out as for screening experiments. The % conversion of H_2 was deduced from hydrocarbon concentrations by stoichiometric consideration. That the initial H_2 concentration was only 20% was also taken into account.

4 CHARACTERISATION OF Co AND Cu CONTAINING CATALYSTS

4.1 Introduction

In this section of the work, the single metal supported Co catalysts ($Co/SiO_2$40Å;10:100, Co/Al_2O_3;10:100) and supported Cu catalysts ($Cu/SiO_2$40Å;10:100, 5:100 and 1:100, Cu/Al_2O_3;10:100, 5:100 and 1:100), the physical mixes of the single metal catalysts, and the hybrid Co/Cu catalysts ($Co/Cu/SiO_2$40Å;10:10:100, 10:5:100 and 10:1:100, $Co/Cu/Al_2O_3$;10:10:100, 10:5:100 and 10:1:100) were all characterised by TPR, and assessed in terms of their KE activities. From comparison of these results, the nature and the number of active species on each catalyst system was evaluated. The aim was to find a catalyst which was both active towards the KE synthesis, and interesting in terms of the active species present.

4.2 TPR of Calcined Catalysts

4.2.1 Theory of the Method

In the temperature programmed reduction experiment a sample is placed in a reactor and subjected to a linear temperature rise while a reducing gas mixture (usually H_2 diluted in an inert gas) is flowed over it. The inlet gas passes through one arm of a thermal conductivity detector (TCD) prior to entering the reactor (refer to fig. 3.4.1). The effluent gas from the reactor passes through the second arm of the TCD. Since a TCD is sensitive to changes in gas composition between its two arms (Lemaitre, 1984), any consumption of H_2 in the reactor causes an imbalance in gas composition between the inlet and effluent gases, resulting in a signal to be output from the TCD. The magnitude of the TCD signal is directly proportional to the difference in H_2 concentrations between the inlet and outlet gases.

Therefore, if a H_2/Ar mixture is passed over the catalyst bed at a temperature at which no reduction occurs, the inlet and outlet compositions will be identical and no TCD response should be obtained. However, if the temperature is raised such at a reduction occurs H_2 will be consumed in the reactor. This results in a decrease in the effluent H_2 concentration, which in turn causes a response by the TCD. Thus the TCD signal at a particular temperature is proportional to the H_2 consumption at that temperature.

Since a linear heating rate is used in the experiment, temperature is directly proportional to time. The total amount of H_2 consumed by a sample during a run can therefore be determined by integration of the TPR profile (*i.e.* measurement of the area beneath it). This area can be readily calibrated using a sample of known composition which reduces with a known stoichiometry. Thus TPR is a useful quantitative tool.

The temperature at which reduction occurs for a given species depends on the particular kinetics and thermodynamics of the process involved. Different species should then reduce at different temperatures. The number of peaks and their positions in a TPR profile therefore show the number and variety of reducible species on a sample. Hence TPR is also a valuable qualitative tool for catalyst characterisation.

The aluminates described in sections 4.2. and 4.3 are not identical to the bulk compounds. Rather they are aluminate species confined to the surface of the Al_2O_3 support. Hence their thermodynamic properties, including reducabilities, probably differ to bulk analogues.

Furthermore, during the temperature programmed reduction experiment, the sample is not at equilibrium and so thermodynamic data is of questionable relevance. When a reduction proceeds, water is constantly removed and hydrogen is constantly replenished. According to Le Chatelier's Principle, reduction is thus encouraged. A compound may therefore reduce at a lower temperature during a temperature programmed experiment compared to in a closed system. This situation is an example where kinetics and thermodynamics must be differentiated.

Both or either of the above reasons explain why the aluminates reduced at temperatures which, at first glance, seem surprisingly low. Whether or not the explanations are correct does not alter that reduction of the Al_2O_3 support, *via* some pathway, was definitely observed.

4.2.2 Calcined Co Catalysts

Co/Al_2O_3;10:100

The Co/Al_2O_3, 10:100 catalyst gave a complex TPR profile (refer to fig. 4.2.2). There were three main reduction peaks centred at 420°C, 520°C and 620°C respectively. Reduction was not complete even at 800°C, and so the H_2 consumption did not return to zero (*i.e.* baseline) levels.

The first peak at 420°C occurred at a similar position to the peak given by the reduction of bulk Co_3O_4. This suggests that bulk Co_3O_4 was present on the calcined catalyst. This mixed valence oxide is the most thermodynamically stable of the cobalt oxides and would therefore be expected to form preferentially during calcination. Quantitative analysis of the peak areas shows that approximately 25% of the total cobalt loading occurred as bulk oxide.

The reduction peaks at 520°C and 620°C were caused by the reduction of Co^{2+} surface networks. Differing geometric types of Co^{2+} gave rise to the distinct reduction peaks. Using diffuse reflectance spectroscopy, it has been shown that the 520°C peak was associated with octahedral Co^{2+} ions, and the 620°C peak with Co^{2+} ions of tetrahedral geometry (Roe, 1986). The Co^{2+} ions presumably occupied different sites on the surface of the Al_2O_3 support. Measurements of H_2 consumption suggested that Co^{2+} species which interacted with the support in this way reduced with the stoichiometry of CoO. The reduction equation which applied can be regarded as

$$H_2 + CoO\,Al_2O_3 \rightarrow Co + Al_2O_3 + H_2O \qquad \text{eqn. 4.4.2a}$$

The high temperature reduction was characteristic of cobalt aluminate (Arnoldy and Mouljin, 1985). Such a species would be expected to reduce with the stoichiometry of eqn. 4.2.2b.

$$CoAl_2O_4 + 4H_2 \rightarrow Co + 2Al + 4H_2O \qquad \text{eqn. 4.2.2b}$$

Thus a feature which appears to have distinguished Co^{2+} in the well defined lattice of the aluminate from surface networks of Co^{2+} is that the support as well as the oxidic Co was effectively reduced.

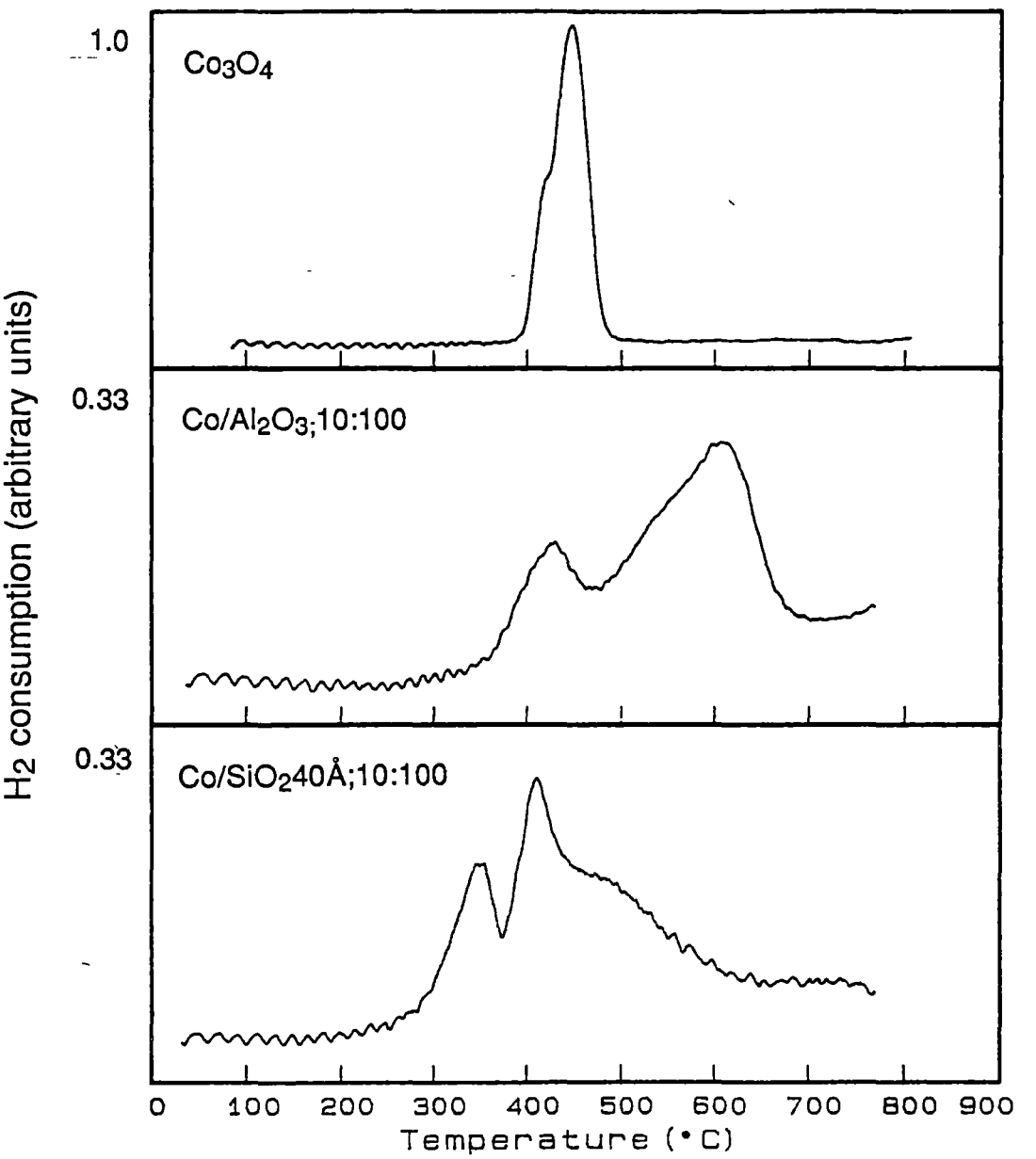

fig. 4.2.2 TPR profiles of calcined Co catalysts and Co_3O_4.

The TPR peak assignments made are the same as reported by van't Blik and Prins (1986). Paryjczak *et al.* (1980), and Castner and Santilli (1981) observed two types of interactive Co^{2+} species, but did not differentiate between octahedral and tetrahedral geometries. Arnoldy and Mouljin (1985) saw two interactive species, but suggested they were of different valencies (2+ and 3+) rather than different geometries.

Co/$SiO_2$40Å;10:100

Four distinct peaks appeared on the profile given by this catalyst (refer to fig. 4.2.2). The peaks at 370°C and 410°C were probably associated with the two stage reduction of Co_3O_4 according to the equations below.

$$Co_3O_4 + H_2 \rightarrow 3CoO + H_2O \qquad \text{eqn. 4.2.2c}$$

$$3CoO + 3H_2 \rightarrow Co + 3H_2O \qquad \text{eqn. 4.2.2d}$$

The area of the second peak was approximately three times the area of the first which is consistent with the above stoichiometry. The shift to lower temperature and the increased separation of the two stages of reduction compared to the behaviour of unsupported Co_3O_4 reflect differing reducibilities of supported and unsupported oxides.

Reduction regimes were also observed at approximately 520°C and 620°C, as on Co/Al_2O_3;10:100. This coincidence suggests that reduction of the same interactive Co^{2+} species was involved. Diffuse reflectance and X-ray photoelectron spectroscopies were used to confirm these assignments (Roe, 1986). Importantly, there appears to be a direct analogy between the behaviour of Co on this $SiO_2$40Å support and that for Al_2O_3.

Similar high temperature reduction peaks have been reported by van't Blik *et al.* (1986) and Paryjczak *et al.* (1980). These peaks were attributed to the reduction of cobalt silicate formed at the Co_3O_4 support interface. This explanation differs slightly with that offered above. Assignment of the high temperature reduction observed for Co/$SiO_2$40Å;10:100 to cobalt silicates was not consistent with quantitative treatment of

the data (Roe, 1986). The inconsistency resulted because silicates would be expected to have reduced with a H_2 to Co ratio of greater than one to one (two to one in the case of cobaltous orthosilicate, Co_2SiO_4, for example) by analogy with aluminates. Interactive Co^{2+} species appear to have reduced with precisely a one to one H_2 to Co stoichiometry.

4.2.3 Calcined Cu Catalysts

Cu/Al_2O_3 Catalysts

The TPR profiles of the Cu/Al_2O_3 catalysts as well as that of unsupported CuO are given in fig. 4.2.3a. All three catalysts gave a peak at 300°C. Similar low temperature peaks have been observed by Gentry and Walsh (1982) who attributed them to bulk, though well dispersed, CuO. In the present study CuO did not reduce until 550°C, and the peak was a broad one. The low temperature peaks observed on all the Cu/Al_2O_3 TPR profiles are completely different, both in terms of shape and position, to the peak given by the reduction of CuO. Assignment of the low temperature peaks to CuO, in the same manner as the 420°C reduction peak on Co supported catalysts was assigned to bulk Co_3O_4, is therefore unreasonable.

Instead, the 300°C peak can be assigned to an oxidic Cu species interacting with the Al_2O_3 support. The Cu ions may well form a surface network, analogous to the Co situation. The formal oxidation state of the surface species was probably +2. The samples were calcined in air and under these circumstances the original Cu^{2+} ions in the nitrate salt used for catalyst preparation (see section 3.2) would have retained their original charge. Such surface species have been observed by EXAFS and XPS (Kakuta *et al.*, 1986; Sermon *et al.*, 1987).

On Cu/Al_2O_3;10:100 and Cu/Al_2O_3;5:100 a second peak at 480°C, just 70°C below the reduction temperature of bulk oxide, occurred. The peak was largest on the catalyst of highest Cu loading. The amount of bulk oxide on a catalyst is likely to increase as the metal loading is raised. This has been shown to apply on Cu/SiO_2

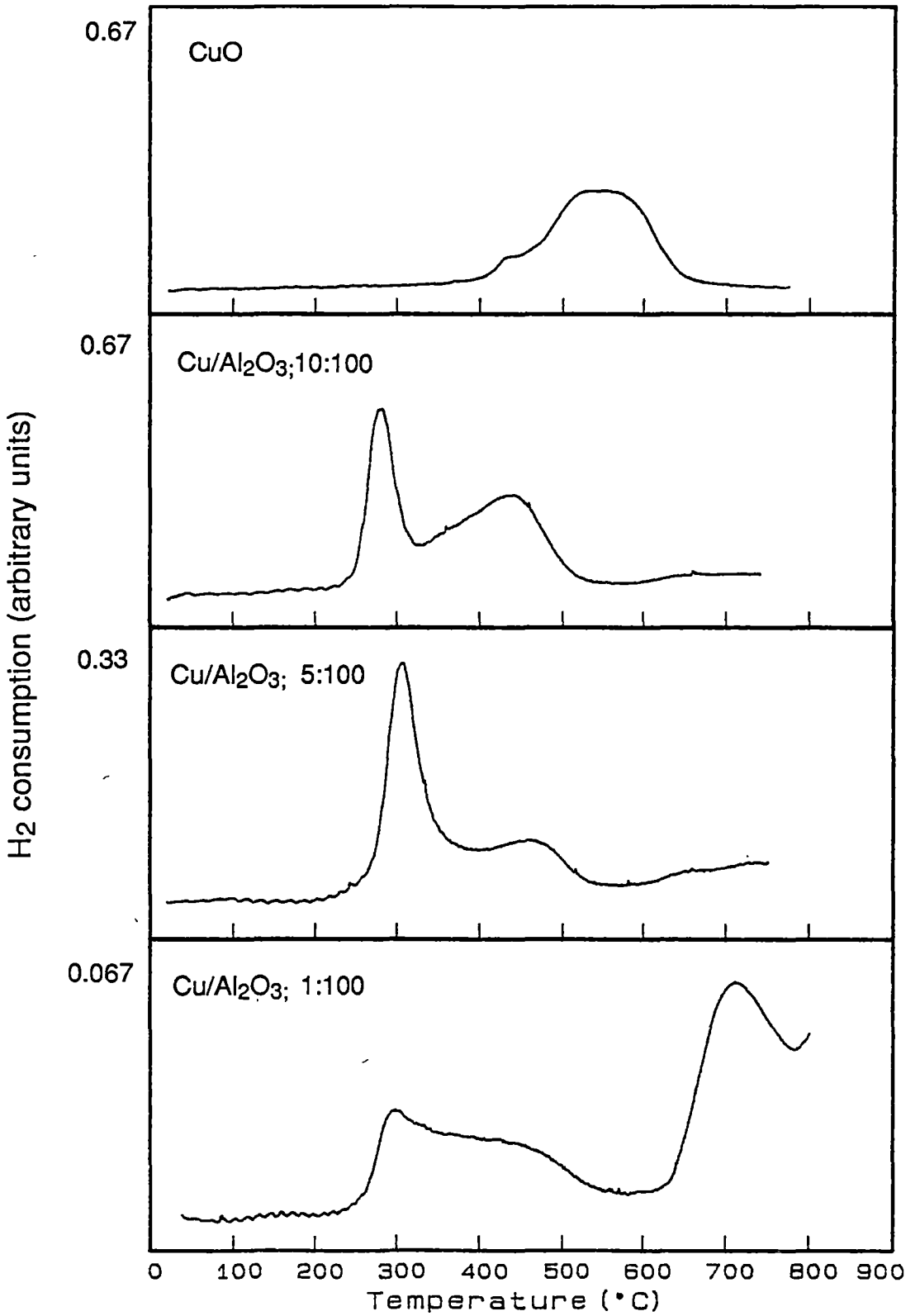

fig. 4.2.3a TPR profiles of calcined Cu/Al_2O_3 catalysts and CuO.

(Shimokawabe *et al.*, 1983) and Co/Al_2O_3 (Arnoldy and Mouljin, 1985) systems. This peak was probably therefore caused by the reduction of bulk CuO. Gentry and Walsh (1982), in contrast, assigned a high temperature peak observed in a study of Cu/Al_2O_3 to a surface spinel.

The TPR profile obtained for Cu/Al_2O_3;1:100 indicates the dramatic effect metal loading can have on species distribution. Rapid low temperature reduction commenced, but the sharp peak observed on the catalysts of higher Cu loading did not eventuate. Instead, there was H_2 consumption over a wide range followed by substantial amounts of H_2 consumption at above 630°C.

The area beneath the TPR profile represents H_2 consumption in excess of that accounted for by the total Cu on the catalyst, assuming the Cu species to be divalent and thus reduced with one to one stoichiometry according to eqn. 4.2.3a.

$$CuO\ Al_2O_3 + H_2 \rightarrow Cu + Al_2O_3 + H_2O \qquad \text{eqn. 4.2.3a}$$

The increased peak area is consistent with that the Al_2O_3 support being reduced. The reduction of copper aluminates (Gentry and Walsh, 1982), according to eqn. 4.2.3b, would give such a disproportionately large peak.

$$Cu\ Al_2O_4 + H_2 \rightarrow Cu + 2Al + 4H_2O \qquad \text{eqn. 4.2.3b}$$

The high temperature peak was almost certainly caused by such a process.

The poor definition of the low temperature peak on Cu/Al_2O_3;1:100 slightly complicates interpretation of the results. The distortion observed was probably a result of reaction of Cu^{2+} ions with the Al_2O_3 support to give the aluminate species. Such migration of Co ions into a well defined Al_2O_3 lattice has been previously reported (Arnoldy and Mouljin, 1985). Prior to the TPR run all the Cu probably occurred as interactive surface species. The $CuAl_2O_4$ was not initially present, seemingly being formed during the TPR run by reaction of the surface networks. A disadvantage of the TPR technique is that it can be a destructive process. These results further justify the recurring idea that the reduction of the interactive species did not entail reduction of the support, in contrast to the situation for well defined compounds involving metal and support moieties (see section 4.2.2).

The lower concentration of Cu ions on Cu/Al_2O_3;1:100 may well have led to the preponderance for aluminate formation. Aluminate formation must necessarily have involved reaction of oxidic Cu with the support. Such a process would be favoured by low Cu loading. When the Cu loading was higher, clustering and reduction of the interactive Cu^{2+} ions to Cu metal would have predominated. Distortion of the appropriate TPR peaks would not be observed in this situation. This interpretation may be extended to rationalise similar behaviour in other systems.

The distribution of Cu species as analysed using TPR evidence is consistent with the colour of the catalysts. The lowest loading catalyst, Cu/Al_2O_3;1:100, was pale green. The interactive Cu^{2+} which gave rise to the 300°C reduction peak must have caused the green colouration given that the entire Cu loading initially occurred as this species on Cu/Al_2O_3;1:100. The intensity of the green colour became greater with Cu loading in parallel with the increase in size of, and hence the number of species responsible for, the 300°C peak. The increase in the concentration of CuO with Cu loading was accompanied by a darkening in colour of the samples. This effect was observed because CuO is black (CRC Handbook, 1974-1975).

Cu/$SiO_2$40Å Catalysts

All three catalysts gave a peak at 300°C, similar in shape and position to the low temperature peaks on the Cu/Al_2O_3 catalysts (refer to fig. 4.2.3b). Another phase of reduction, most prominent on Cu/$SiO_2$40Å;1:100, occurred at 380°C. The profiles are very similar to those observed by Robertson *et al.* (1975), Paryjczak *et al.* (1980), Gentry and Walsh (1982), Shimokawabe *et al.* (1983) and Delk and Vavere (1984).

All these groups attributed the low temperature peak to the reduction of dispersed CuO. The shape and position arguments which contradicted a similar assignment for Cu/Al_2O_3 profiles also apply here. More likely the peak was caused by a surface network, similar in nature to that on Cu/Al_2O_3 samples

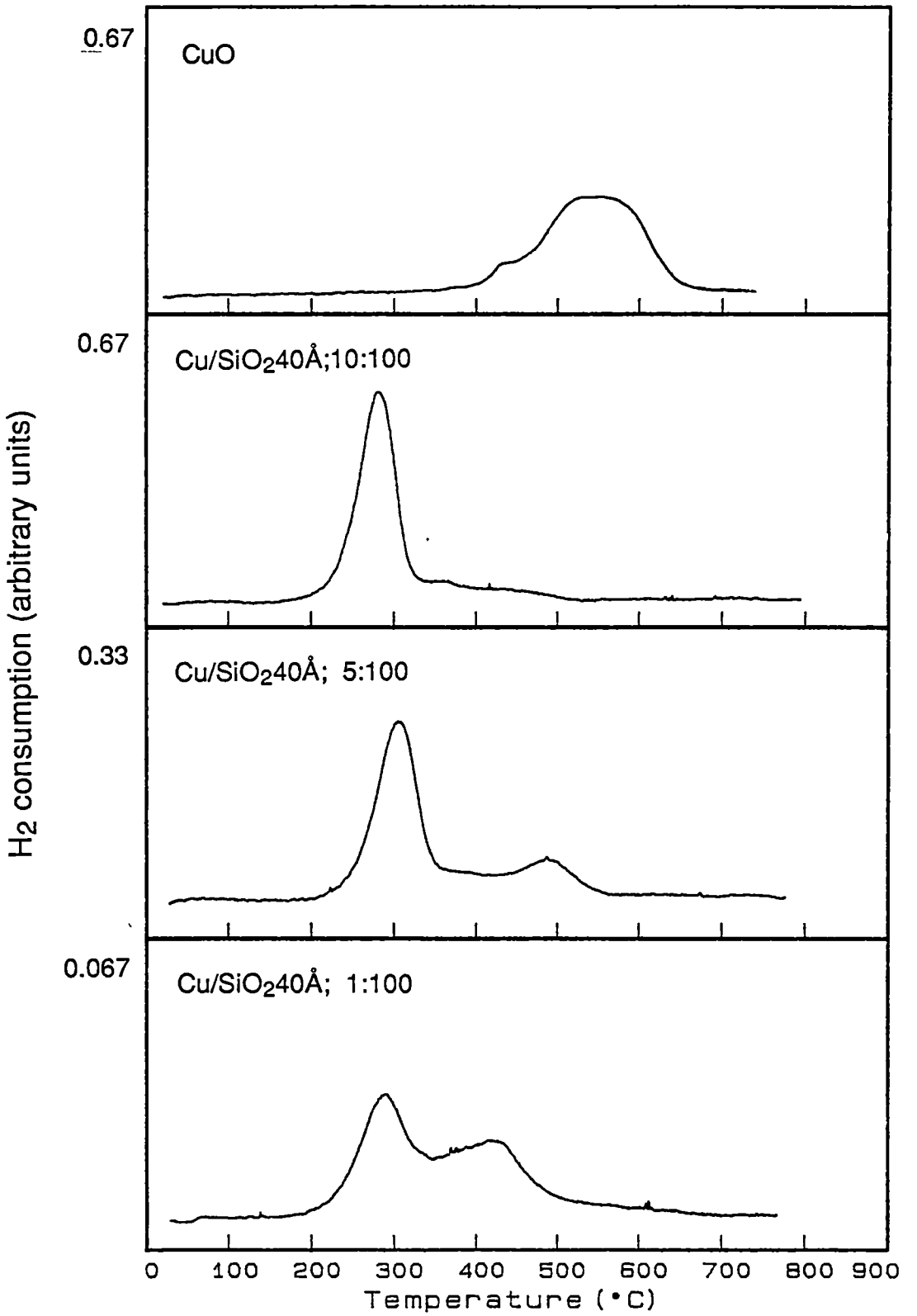

fig 4.2.3b TPR profiles of calcined $Cu/SiO_2$40Å catalysts and CuO.

The colour of the catalysts again confirms this interpretation. The 300°C peak was virtually the only reduction observed for $Cu/SiO_2$40Å;10:100 and $Cu/SiO_2$40Å;5:100 (refer to fig. 4.2.3b) and thus the interactive Cu responsible for that peak must have been the predominant species present. Both these catalysts were green. Had bulk CuO caused the 300°C reduction the two samples would have been black.

The peak at 380°C cannot be compared directly with the high temperature peak on the Al_2O_3 supported catalysts for several reasons. It increased rather than decreased in size relative to the low temperature peak as Cu loading was lowered. From previous work the proportion of interactive Cu species is known to increase with decreased metal loading (Gentry and Walsh, 1982; Shimokawabe *et al.*, 1983). Furthermore the peak appeared at a temperature approximately 200°C, rather than just 80°C, below that for bulk oxide. These two considerations suggest that the reduction was not of bulk CuO, but of another interactive species.

The two species which gave rise to the 300°C and 380°C reduction peaks probably had the same formal oxidation state of +2, using the maintenance of charge arguments postulated in the discussion of the Cu/Al_2O_3 catalysts. The consumption of H_2 was consistent with this valency state. Differing geometry of coordinated Cu^{2+} was the probable cause of the two distinct peaks, similar to the supported Co situation (see section 4.2.2). Differing geometries of surface Cu^{2+} species has been observed in XPS studies (Sermon *et al.*, 1987). No direct evidence has been obtained in the current study which allows the geometries of the two species to be assigned.

4.2.4 Calcined Physical Mixes

Similar amounts of the Co and Cu catalysts constituted the mixes. The proportion of support relative to active metals was doubled as a result. The normalisation factor for weight used in the preparation of profiles was therefore obtained by dividing the total weight of the mix by two. The same treatment was used throughout the current work whenever weight normalisation for the physical mixes was required. This procedure validates comparison of the physical mixes and hybrid catalysts. An alternative approach was to prepare the mixes from Co and Cu catalysts with doubled metal loadings. However the higher metal to support ratios on such single metal catalysts relative to the hybrid system would have complicated interpretation of results.

The reduction profiles given by the physical mixes are direct additives of the profiles given by the appropriate single metal samples (compare figs. 4.2.2 a/b, 4.2.3 a/b and 4.2.4 a/b). Assignment of the TPR peaks is correspondingly straightforward in all cases. For example, in the TPR profile of the physical Co/Al_2O_3;10:100 and Cu/Al_2O_3;5:100 mix, the first peak was due to the reduction of interactive Cu^{2+} and the second to Co_3O_4. The simultaneous reduction of CuO and surface networks of Co^{2+} gave rise to a complex third reduction peak. High temperature reduction of aluminates was also apparent.

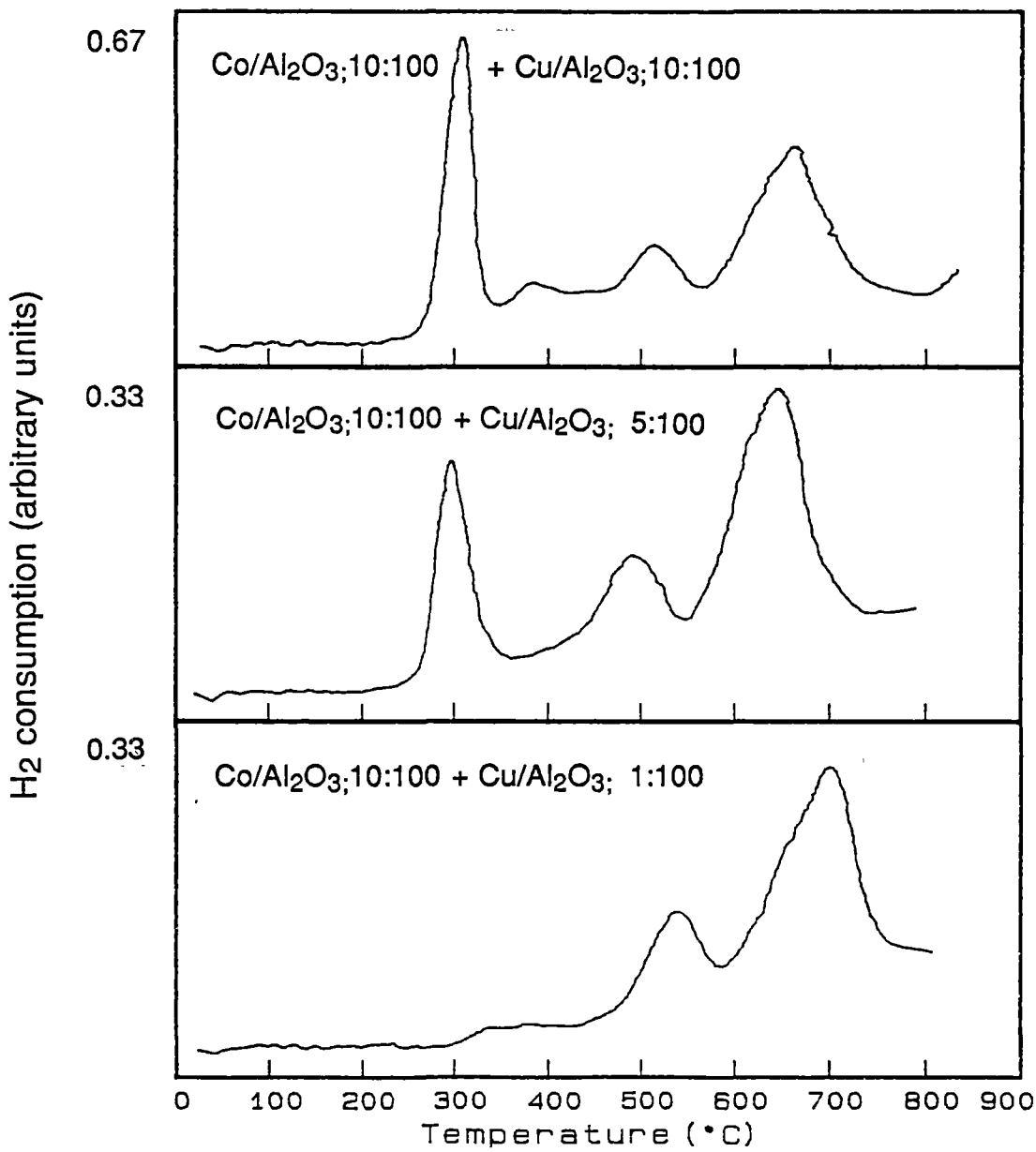

fig 4.2.4a TPR profiles of calcined Al_2O_3 supported physical mixes.

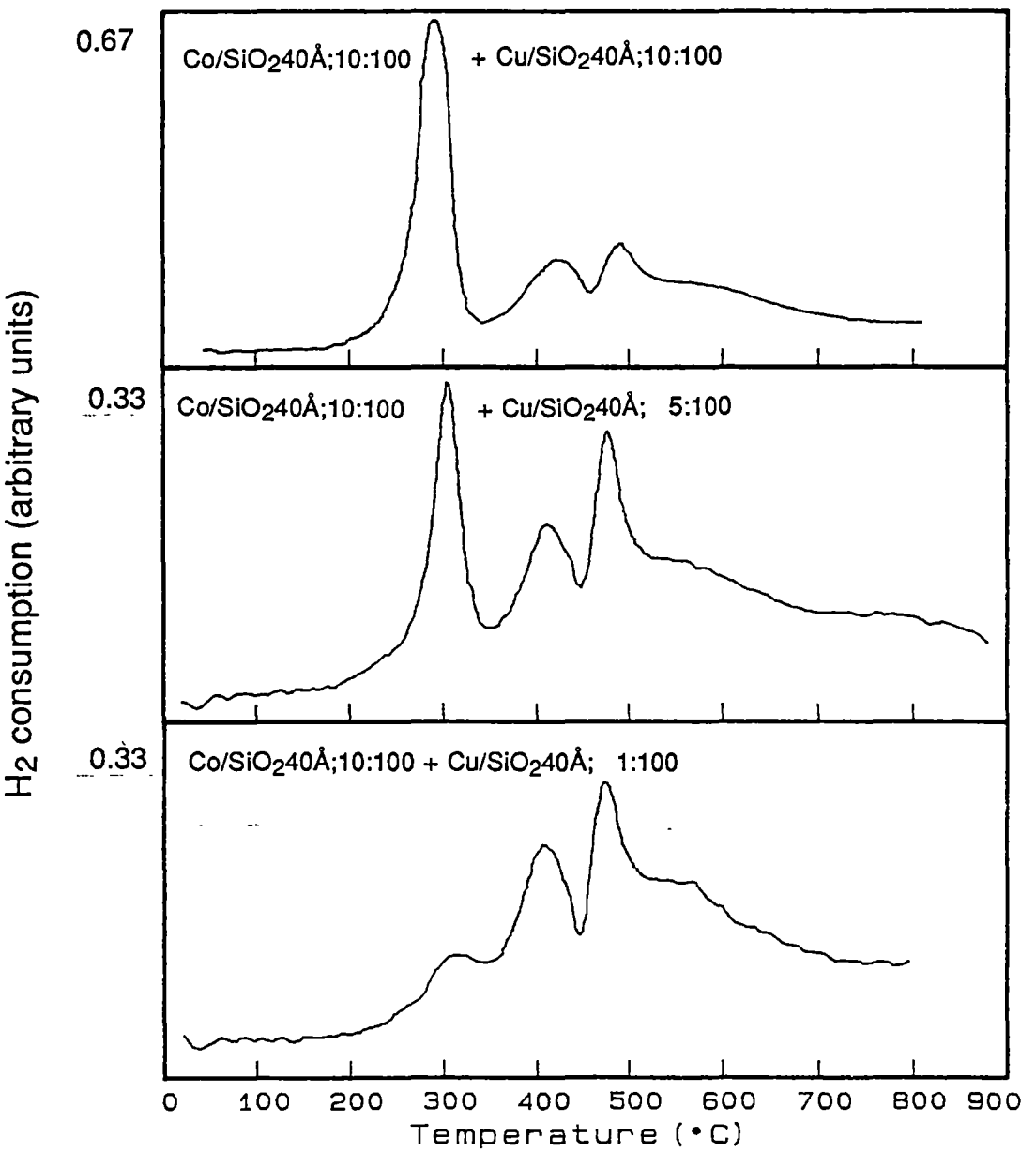

fig.4.2.4b TPR profiles of calcined $SiO_2$40Å supported physical mixes.

4.2.5 Calcined Hybrid Catalysts

Co/Cu/Al_2O_3 Catalysts

The TPR profiles of hybrid catalysts (refer to fig. 4.2.5a) were different to those given by the corresponding physical mixes (compare figs. 4.2.4a and 4.2.5a). There were only two major reduction regimes as opposed to the three distinctly observed for the physical mixes. The first regime consisted of a broad peak which commenced at 300°C and finished at 600°C. The second regime was a well defined peak centred at 620°C. Some high temperature reduction attributed to $CoAl_2O_4$ (see section 4.2.2) was also observed.

The low temperature shoulder of the broad reduction peak was similar in position to that caused by the reduction of interactive surface Cu^{2+}. It was likely associated with a similar species. The remainder of the peak was probably caused by the reduction of Co_3O_4 since it coincided in temperature with the reduction of Co_3O_4 on the physical mix.

In the physical mix profiles, surface Cu^{2+} and bulk Co_3O_4 reduced discretely to give two distinct reduction peaks. These peaks merged in the case of the hybrid catalysts. The slightly altered reducibilities of the appropriate species suggest that a mixed Co/Cu/oxide had formed. A similar interpretation was made by Jenking *et al.* (1977) in a TPR study of Cu/Ni systems.

The hybrid catalysts exhibited no reduction peaks due to octahedral Co^{2+}. However the reduction peak at 620°C due to tetrahedral Co^{2+} was more predominant than for the physical mixes. The overall number of interactive species had not changed, but the ratios of octahedral and tetrahedral species did alter.

Quantitative analysis of the TPR profiles suggested that effectively all of the Cu on the hybrid catalysts occurred in the mixed oxide species. Only 40% of the Co occurred in the oxide. The remainder appeared as tetrahedral Co^{2+} ions and $CoAl_2O_4$.

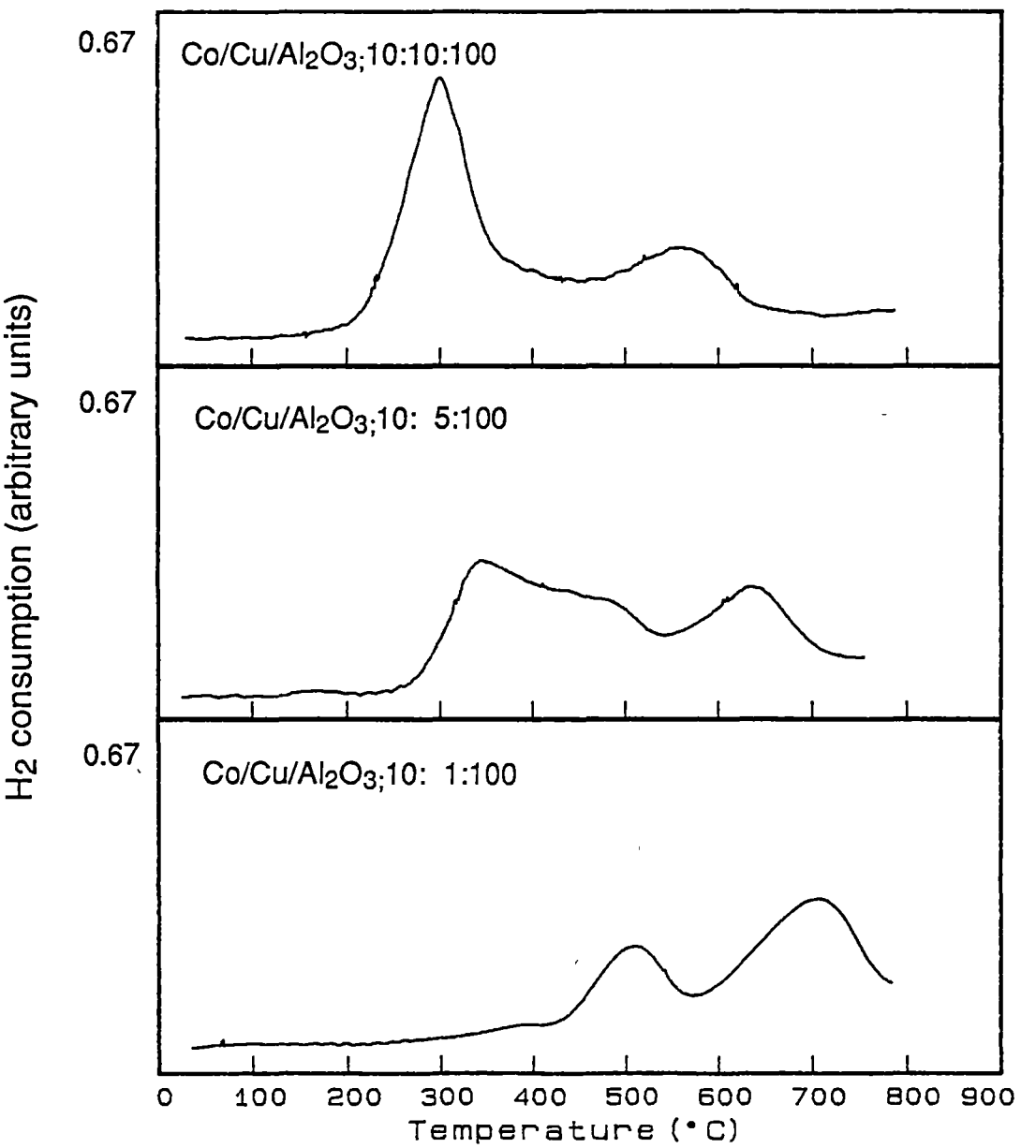

fig. 4.2.5a TPR profiles of calcined Al_2O_3 supported hybrid catalysts.

Co/Cu/$SiO_2$40Å Catalysts

Just one reduction peak was given by each of the catalysts, centred at 400°C (refer to fig. 4.2.5b). The peaks observed for the physical mixes assigned to surface Cu^{2+} and Co_3O_4 (see sections 4.2.2, 4.2.3 and 4.2.4) have merged. This behaviour parallels that exhibited by the Co/Cu/Al_2O_3 catalysts. A mixed Co/Cu oxide again appears to have formed during the preparation procedure. The same positional arguments as applied for the Al_2O_3 supported hybrids suggest that the low temperature shoulder was probably due to Cu^{2+} reduction with the remainder of the peak caused by Co_3O_4 reduction. Measurement of the H_2 consumption represented by the peak shows that virtually all of the metal on the catalyst was found in the mixed Co/Cu oxide.

For the hybrid catalysts some H_2 consumption was observed at 620°C, the temperature at which octahedral Co^{2+} reduced on the physical mixes and Co/$SiO_2$40A;10:100 alone (see sections 4.2.2 and 4.2.4). The peak was smaller than for the physical mixes, which suggests that octahedral Co^{2+} species were fewer on the hybrids. Even on the physical mixes, octahedral Co^{2+} species constituted just 20% of the total Co loading.

The introduction of Cu resulted in the removal of octahedral Co^{2+} species as evidenced by the absence of a 520°C reduction peak (see section 4.2.2). The same effect was observed for the Al_2O_3 supported ~~hydrides~~ hybrids. This coincidence suggests that Co^{2+} and Cu^{2+} competed for support sites with octahedral geometry. Most commonly then, Cu^{2+} probably occurred with this geometry. An indirect assignment of the TPR peaks given by the supported Cu catalysts can thus be made. The peaks at 300°C may be due to reduction of octahedral Cu^{2+}. By elimination the peaks at 380°C, observed only on the $SiO_2$40Å supported catalysts, can be attributed to tetrahedral Cu^{2+} (see section 4.2.3).

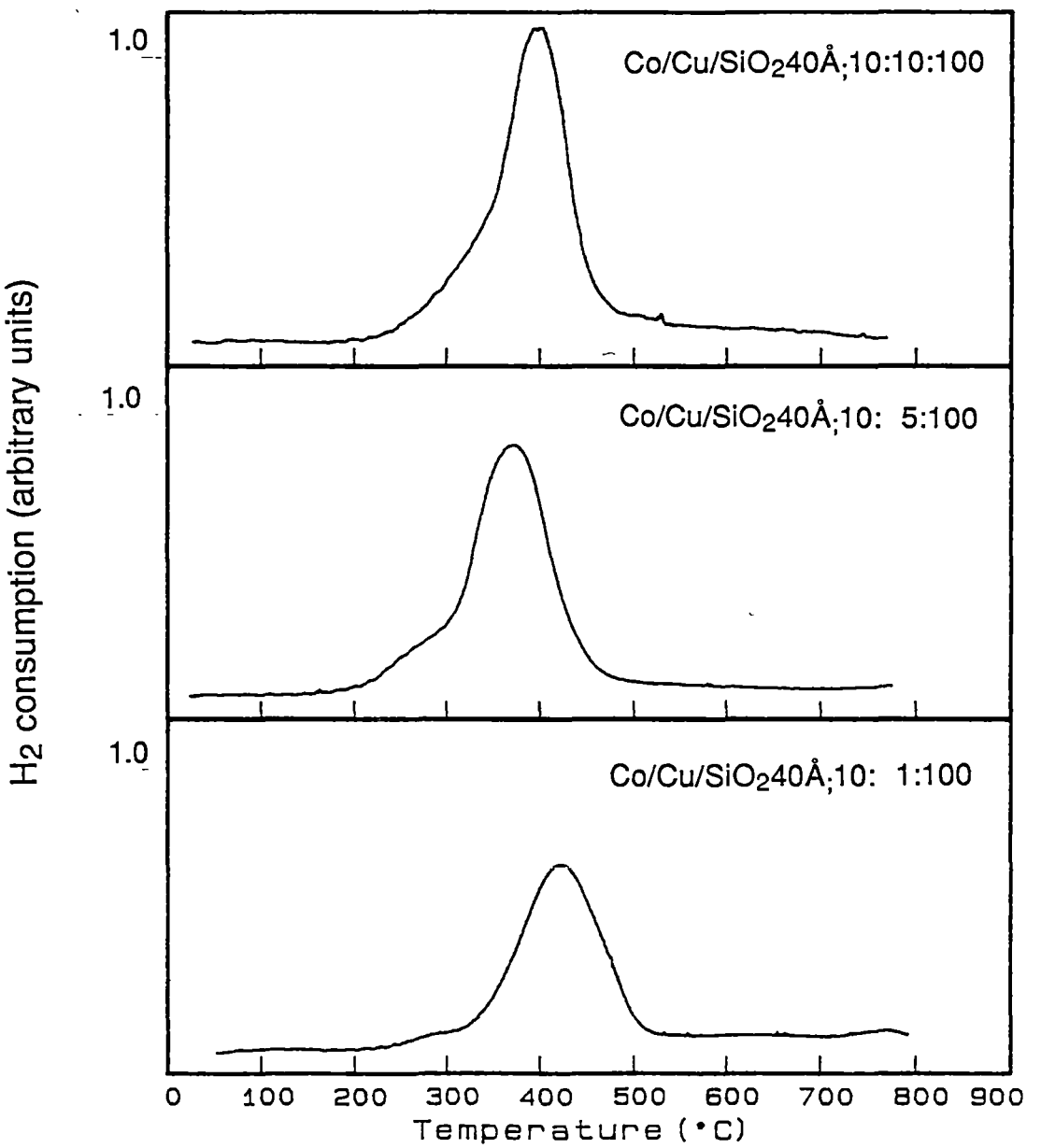

fig. 4.2.5b TPR profiles of calcined $SiO_2$40Å supported hybrid catalysts.

4.3 TPR of Activated Catalysts

4.3.1 Outline

The TPR profiles shown in figs 4.3.2a/b-4.3.5a/b were given by the various catalysts immediately after activation. By comparing these profiles with those given by the calcined catalysts, distributions of metal species on the activated samples were assessed.

In general, activation led to the disappearance of TPR peaks which were positioned below 600°C on the profiles of the calcined samples. New high temperature peaks, attributed to aluminates and silicates, appeared on the activated TPR profiles. The implication of these results was that the oxidic species affected by reduction were not just reduced to the metal, but also reacted with the support.

Any species present immediately after activation may be altered during Kolbel Engelhardt synthesis. Thus caution must be exercised in using these results as an indication to the nature and distribution of the final active species.

4.3.2 Activated Co Catalysts

Co/Al_2O_3;10:100

The peaks in the TPR profile of calcined Co/Al_2O_3;10:100 caused by the reduction of Co_3O_4 and octahedral Co^{2+} ions did not occur in the profile of the activated catalyst (compare figs. 4.2.2 and 4.3.2). A reduction peak at 620°C occurred in both situations, which suggests that tetrahedral Co^{2+} surface species remained intact during the activation process. The amount of $CoAl_2O_4$ on the activated catalyst was greater than on the calcined sample. This was shown by substantial H_2 consumption at high temperature (*circa* 800°C).

The aluminate most likely originated from the reaction of either or both the species affected by the activation process, bulk oxide or octahedral Co^{2+} ions. The formation of cobalt aluminate by heating cobalt oxides and alumina together is a well known process (Pascal, 1963). The transition of a surface network of Co^{2+} ions to a

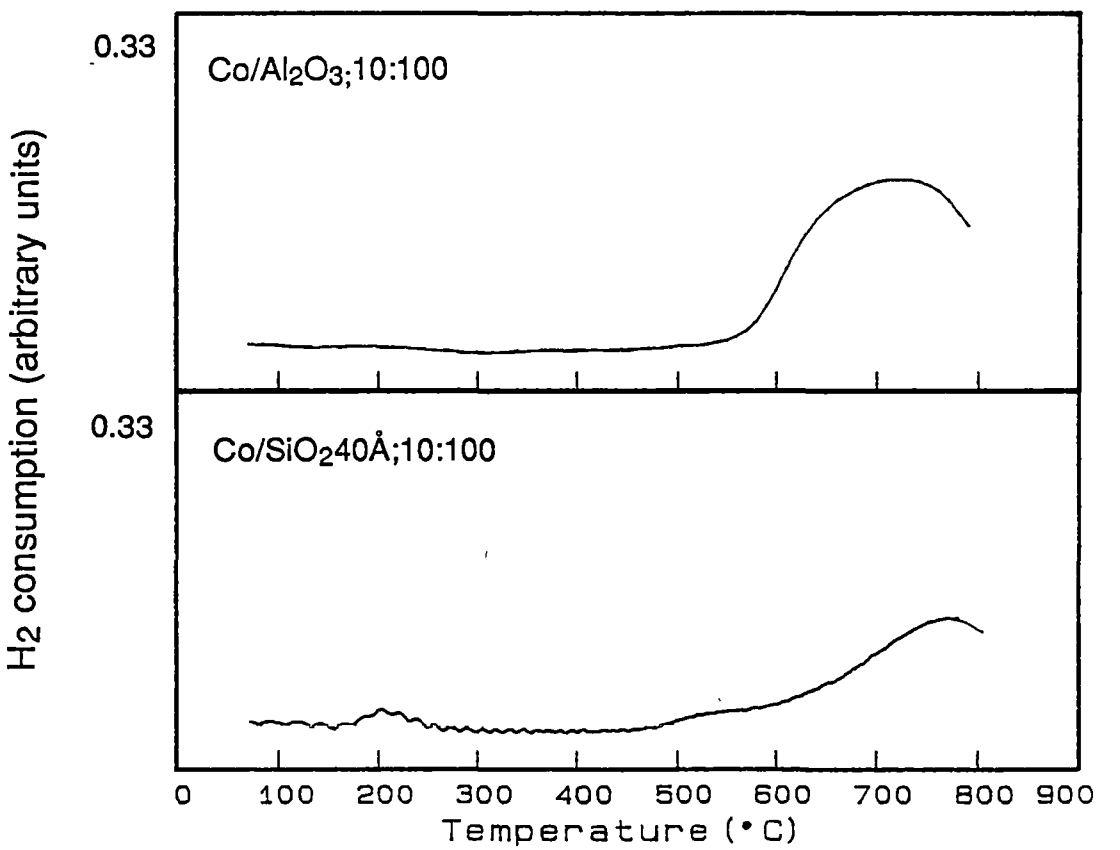

fig. 4.3.2 TPR profiles of activated Co catalysts.

bulk spinel also seems a feasible process for aluminate formation, although it has not been reported in the literature. Analogous behaviour was apparent during the reduction of Cu/Al_2O_3;1:100 (see section 4.2.3).

Bulk oxide and octahedral Co^{2+} accounted for approximately 66% of the total metal loading on calcined Co/Al_2O_3;10:100 (Roe, 1987). Quantitative analysis of the area beneath the $CoAl_2O_4$ peak exhibited by the activated sample suggests that approximately 30% of the Co originally present as bulk oxide and octahedral Co^{2+} was converted to the aluminate. The remainder was almost certainly reduced to a Co^o species not detectable by TPR. Thus only about 50% of the total Co loading was available as Co^o after the activation process.

This Co^o can be regarded as the only potentially active species. Oxidic Co is generally considered inactive. The Co atoms associated with the aluminate spinel as well as the tetrahedral Co^{2+} ions would not have been available for catalysis.

$Co/SiO_2$40Å;10:100

The peaks due to octahedral Co^{2+} and Co_3O_4 on the TPR profile of the calcined sample were not apparent on the profile given by the activated sample (compare figs. 4.2.2 and 4.3.2). The peak assigned to interactive tetrahedral Co^{2+} ions were present on both. These comparisons suggest that Co^o, derived from octahedral Co^{2+} species and Co_3O_4, occurred on the activated catalyst. Tetrahedral Co^{2+} ions remained intact after activation.

4.3.3 Activated Cu Catalysts

Cu/Al_2O_3 Catalysts

After activation of the Cu/Al_2O_3 catalysts the peaks assigned to CuO and interactive surface Cu^{2+} no longer occurred (compare figs. 4.2.3a and 4.3.3a). Small peaks at 820°C appeared, most likely caused by the reduction of $CuAl_2O_4$. The same assignment was made for the high temperature reduction peak on calcined Cu/Al_2O_3;1:100 (see section 4.2.3). The $CuAl_2O_4$ originated from either, or both, of the oxidic species apparent on the calcined samples.

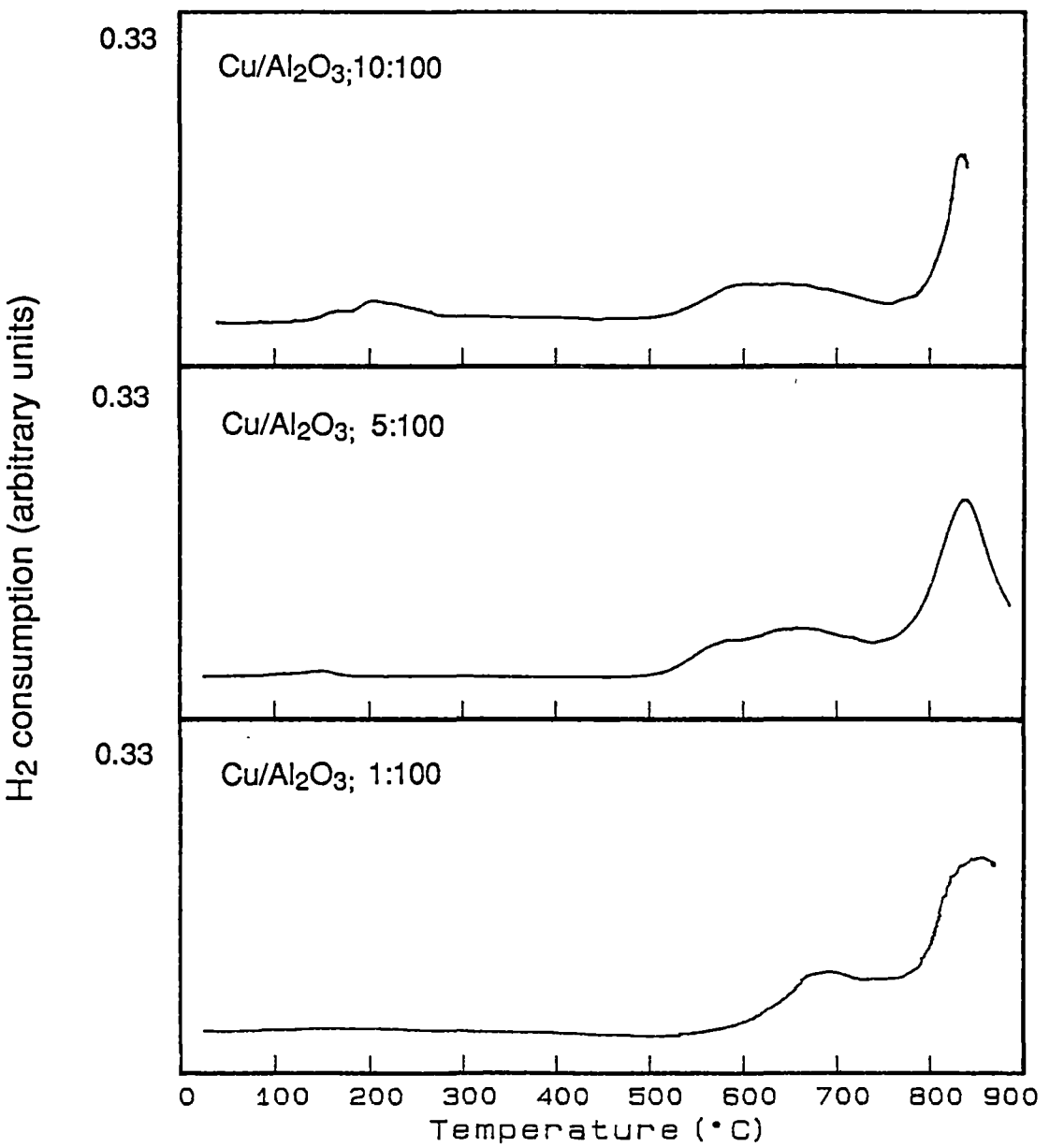

fig 4.3.3a TPR profiles of activated Cu/Al_2O_3 catalysts.

The small size of the aluminate peak relative to the total integrated areas beneath the TPR profiles given by Cu/Al_2O_3;10:100 and Cu/Al_2O_3;5:100 suggests that the conversion of the oxidic species on the salient calcined samples to aluminate on the activated samples was minor. The removal of these species must therefore have been caused predominantly by their reduction to Cu^o. Quantitative treatment suggests that virtually all the Cu present on the higher loading catalysts was so reduced.

The size of the aluminate peak given by activated Cu/Al_2O_3;1:100 was equivalent to that given by the calcined catalyst. The area beneath the distorted low temperature peak observed on the profile of calcined Cu/Al_2O_3;1:100 (see section 4.2.3) therefore represents the difference in H_2 consumption between the two samples. The amount of Cu corresponding to this difference was reduced by activation. Approximately 50% of the total Cu content of the catalyst was reduced according to this approach. This contrasts with the near complete reduction on the higher loading catalysts.

The extent of reduction to Cu^o occasioned by activation, information provided by direct comparison of the TPR profiles of calcined and activated Cu/Al_2O_3 samples, is a possible guide towards catalytic activity. Closer inspection of the profiles given by the activated catalysts yields further information of less practical importance but nevertheless of interest.

The amount of $CuAl_2O_4$ on activated Cu/Al_2O_3;10:100 was 80% of that which occurred on an equivalent weight of Cu/Al_2O_3;1:100. The behaviour demonstrates that decreased Cu loading led to increased metal support interaction. The same trend was observed in the context of calcined catalysts, and the same concentration effect can be used to rationalise the results (see section 4.2.3).

A peak at 620°C preceded the $CuAl_2O_4$ reduction on the profiles of all three catalysts. The area of this peak was 40% of the aluminate peak area in all cases. This relationship suggests that the peak was a precursor of aluminate. After activation the precursor rather than $CuAl_2O_4$ itself may have been the only oxidic species present on the catalyst. The precursor could then be converted to aluminate during the TPR run.

The reduction of similar precursor species on activated Co/Al_2O_3;10:100 would have been observed by the tetrahedral Co^{2+} reduction peak (see section 4.3.2).

The position of the aluminate peak shifted to higher temperature as the Cu loading was decreased. The positions were 820°C, 830°C and 850°C respectively (refer to fig. 4.3.3a). This trend can be described by a concentration effect, as was the increased interaction trend.

The transition of the aluminate precursor to aluminate proper was probably a diffusion controlled process. In solid state reactions, just as for gas phase processes, the rate of diffusion is controlled *inter alia* by concentration (Galway, 1967). The rate of aluminate formation was probably determined by the concentration of Cu ions relative to "free" surface Al_2O_3. Other variables possibly involved, such as ion mobility and thermal gradients, would all have been equal on the set of Cu/Al_2O_3 catalysts.

Activation of Cu/Al_2O_3;10:100 afforded the lowest absolute number of oxidic Cu ions, as shown by the relative combined areas of the precursor and aluminate peaks (refer to fig. 4.3.3). Coverage of the Al_2O_3 supported by Cu^0 would have been greatest for this catalyst simply because activation of this sample gave the highest metal yield. Thus the availability of free Al_2O_3 would have been least. Extension of these arguments show that while the Cu loading decreased, there was an increase in the availability of free Al_2O_3, and the number of oxidic species present after activation. The Al_2O_3 would have diluted the oxidic Cu ions. The diluent effect possibly caused the overall oxidic Cu concentration to decrease with Cu loading.

Assuming that aluminate formation was proportional to this concentration, a corresponding decrease in the rate of the formation reaction would also have resulted. A slowing in the rate of formation would have been associated with a time delay in $CuAl_2O_4$ reduction. Since temperature was ramped linearly with time, the aluminate reduction peak should then shift to higher temperature with decreased Cu loading, as indeed occurred.

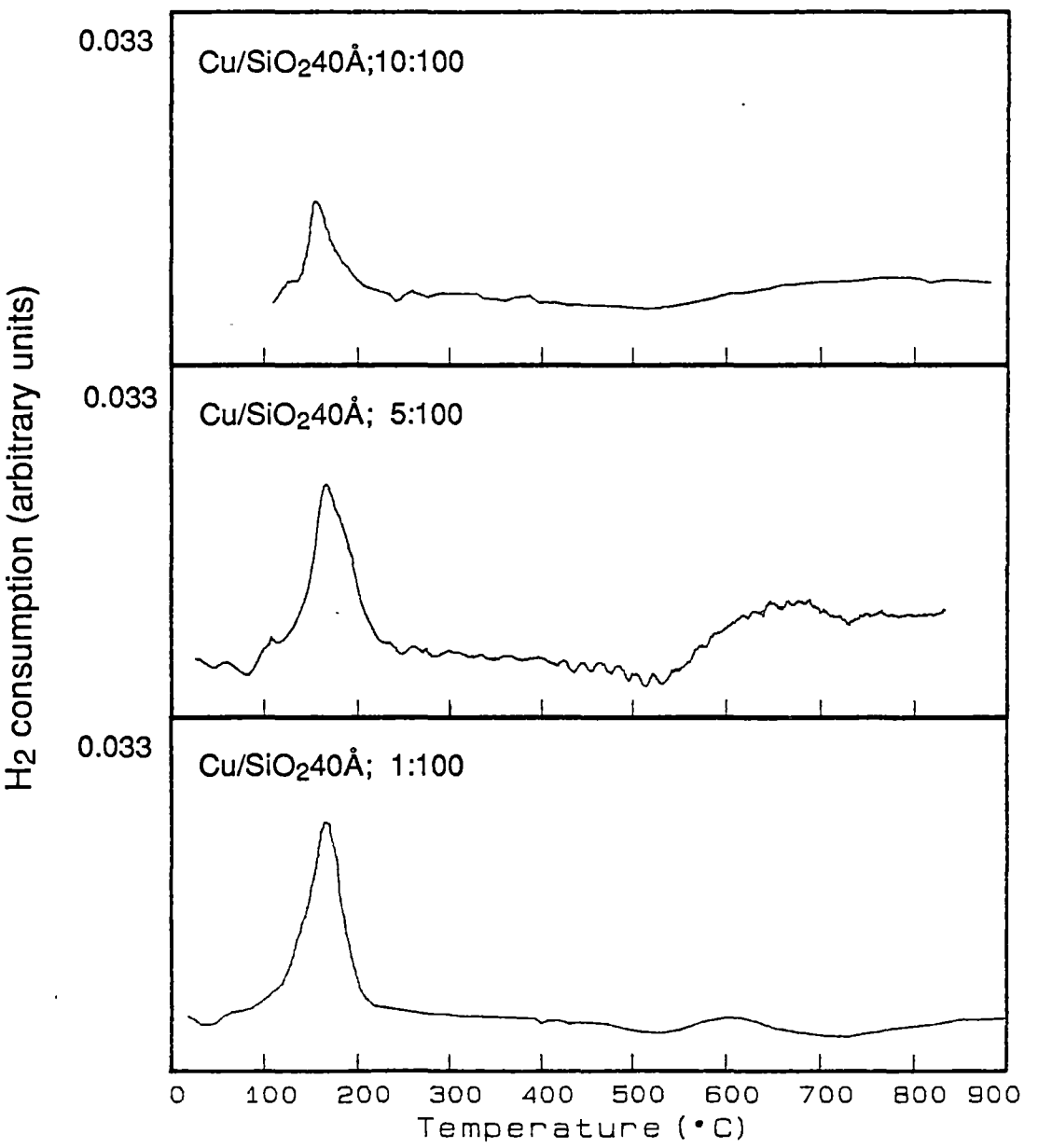

fig. 4.3.3b TPR profiles of activated $Cu/SiO_2$40Å catalysts.

Cu/$SiO_2$40Å Catalysts

Very small low temperature (100°C) peaks were observed on the profiles of the three Cu/$SiO_2$40Å catalysts (refer to fig. 4.3.3b). These peaks were probably caused by oxidic species formed from the reaction of Cu^0 with oxygen impurities in the Ar/H_2 gas stream which was introduced immediately after activation (see section 3.4.1). Otherwise, virtually no H_2 consumption was observed on any of the profiles. This suggests that the oxidic Cu species on the calcined samples were quantitatively reduced to Cu^0 with no reaction between metal and support occurring during the activation process. The $SiO_2$40Å support was thus inert compared to Al_2O_3, which simplifies characterisation of the catalysts.

4.3.4 Activated Physical Mixes

Co/Al_2O_3;10:100 + Cu/Al_2O_3 Mixes

The TPR profiles of the activated physical mixes shown in fig. 4.3.4a were direct additives of the profiles given by the respective single metal catalysts, just as were the TPR profiles of the calcined catalysts (see section 4.2.4).

Broad peaks occurred in the temperature region of 420°C to 820°C. These peaks were multiplets, containing reduction peaks due to tetrahedral Co^{2+}, $CoAl_2O_4$ and $CuAl_2O_4$ in that order. Aluminate precursors would also have contributed to H_2 consumption.

Reduction was declining at 820°C on Co/Al_2O_3;10:100 + Cu/Al_2O_3;10:100 and Co/Al_2O_3;10:100 + Cu/Al_2O_3;5:100. Reduction was still rising on Co/Al_2O_3;10:100. The shift to higher temperature with decreased Cu loading of the $CuAl_2O_4$ peaks caused this difference (see section 4.3.3).

The absence of low temperature reduction peaks observed for the calcined physical mixes (see section 4.2.4) indicates that both Co^0 and Cu^0 were formed during activation by the reduction of the oxidic species responsible for these peaks. Whether or not Co^0 and Cu^0 interacted during the process cannot be determined from TPR data.

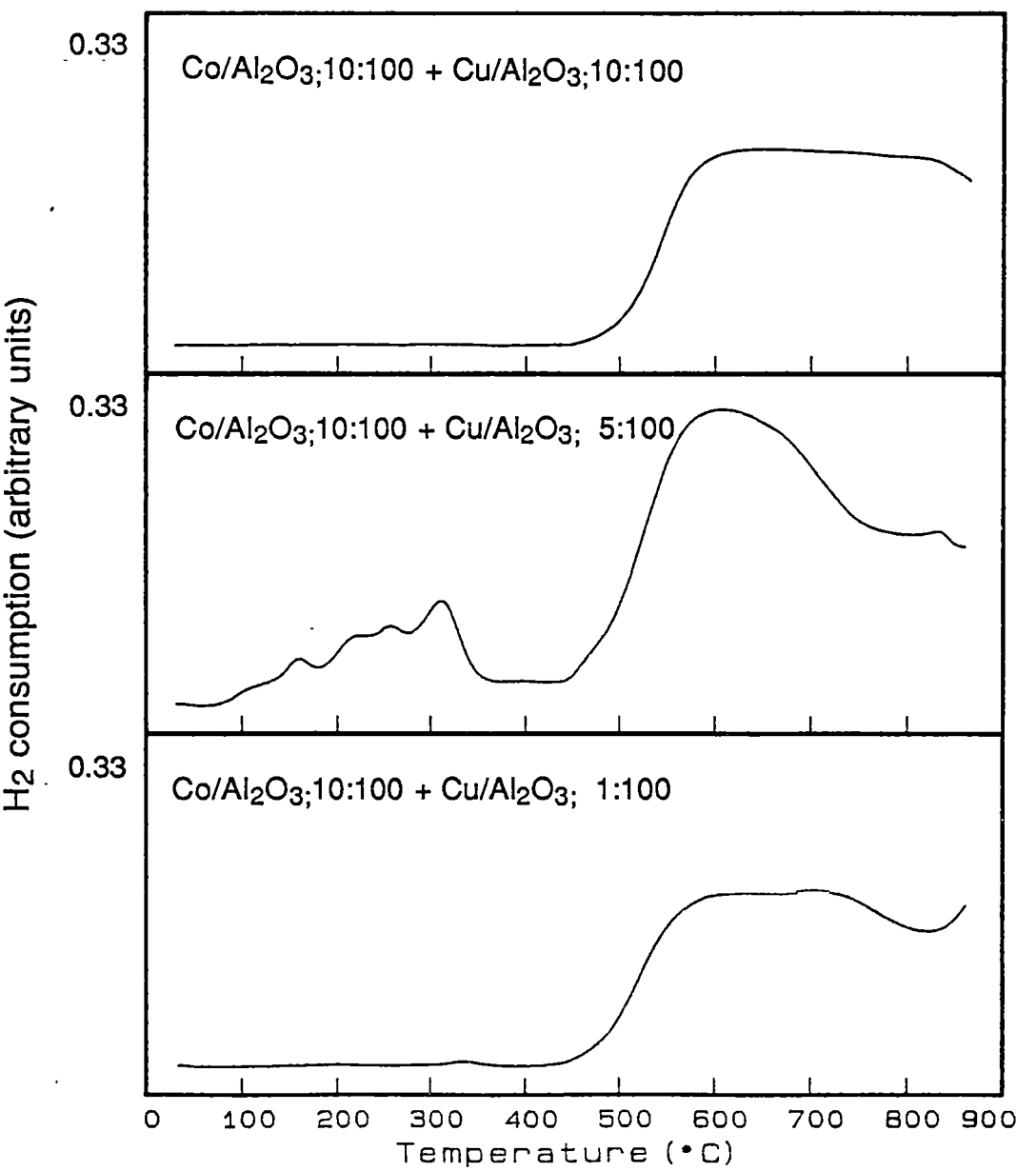

fig. 4.3.4a TPR profiles of activated Al_2O_3 supported physical mixes.

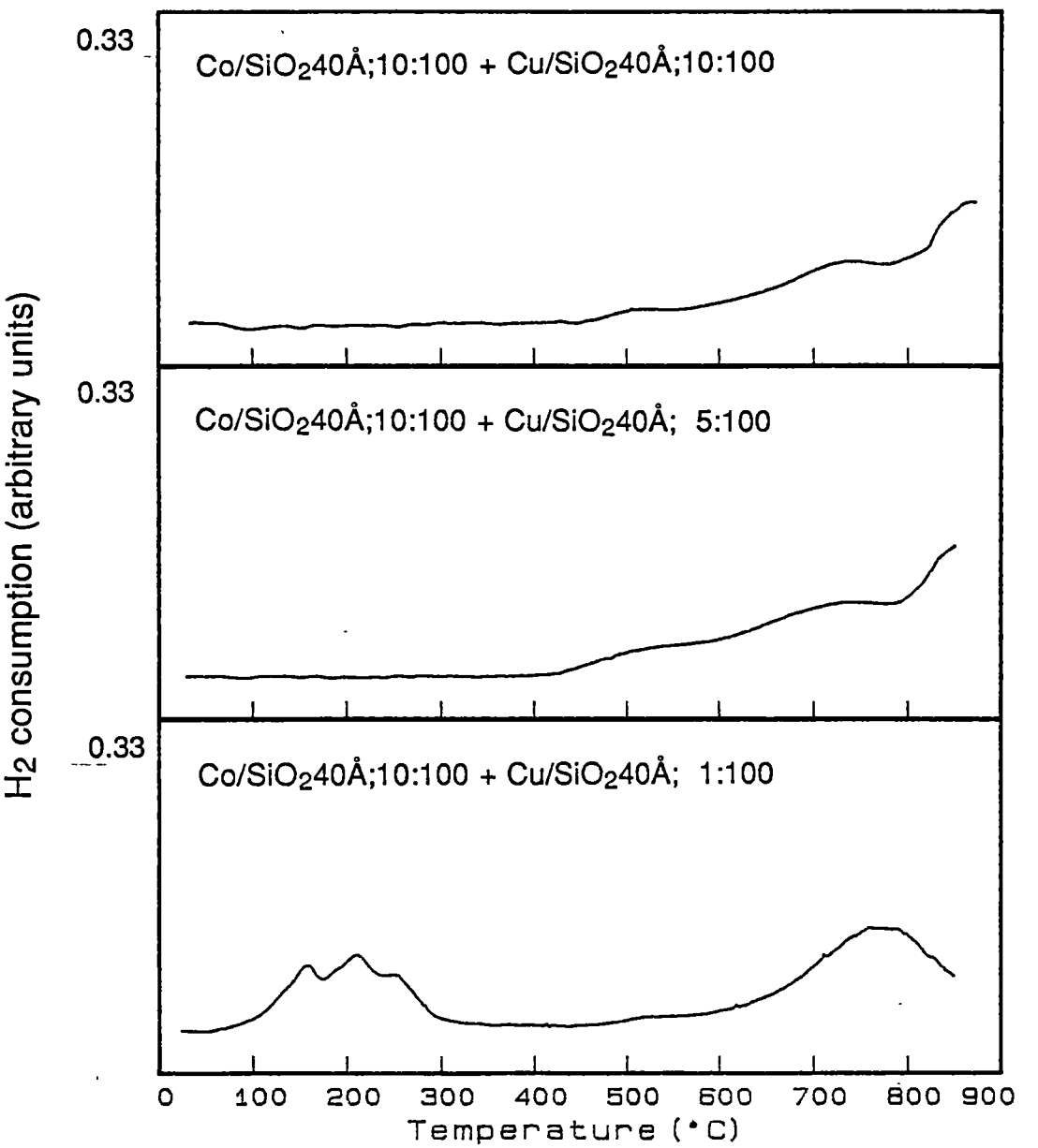

fig. 4.3.4b TPR profiles of activated $SiO_2$40Å supported physical mixes.

Co/$SiO_2$40Å;10:100 + Cu/$SiO_2$40Å

The TPR profiles of the activated Co/$SiO_2$40Å;10:100 on Cu/$SiO_2$40Å physical mixes were again direct additives of the appropriate profiles given by single metal catalysts (compare figs 4.3.2b and 4.3.3b). Thus Co^o and Cu^o must have occurred on the active catalysts, but the nature of species cannot be ascertained.

4.3.5 Activated Hybrid Catalysts

Co/Cu/Al_2O_3 Catalysts

The Co/Cu oxides on the calcined samples were removed by activation (refer to fig. 4.3.5a). The reduction of these mixed metal oxides would be anticipated to have given mixed Co/Cu metal particles. These two metals have limited miscibility - 8% is a figure quoted (Huckel, 1951). A significant amount of alloy would not therefore have formed. However some interaction resulting from the spatial proximity of Co^o and Cu^o may be anticipated.

The position and range of the peaks given by the activated Co/Cu/Al_2O_3 hybrid catalysts were identical to those given by the physical mixes (compare figs. 4.3.4a and 4.3.5a). This suggests that the same oxidic species were present, they being octahedral Co^{2+} and the various aluminate species.

Over Co/Cu/Al_2O_3;10:10:100 and Co/Cu/Al_2O_3;10:5:100 the extent of H_2 consumption between 620°C and 820°C was diminished compared to the appropriate physical mixes (compare figs. 4.3.4a and 4.3.5a). Reduction of $CuAl_2O_4$ occurred in this temperature region (see section 4.3.3). Apparently $CuAl_2O_4$ formation was inhibited by the added presence of Co. The higher overall metal loading explains this inhibition. Interaction between Co and Cu moieties may well have competed with the reaction between Cu and Al_2O_3 to give aluminate. The increased levels of aluminate formation with decreased Cu loading observed on the Cu/Al_2O_3 catalysts is a closely related phenomenon and was similarly rationalised (see section 4.3.3).

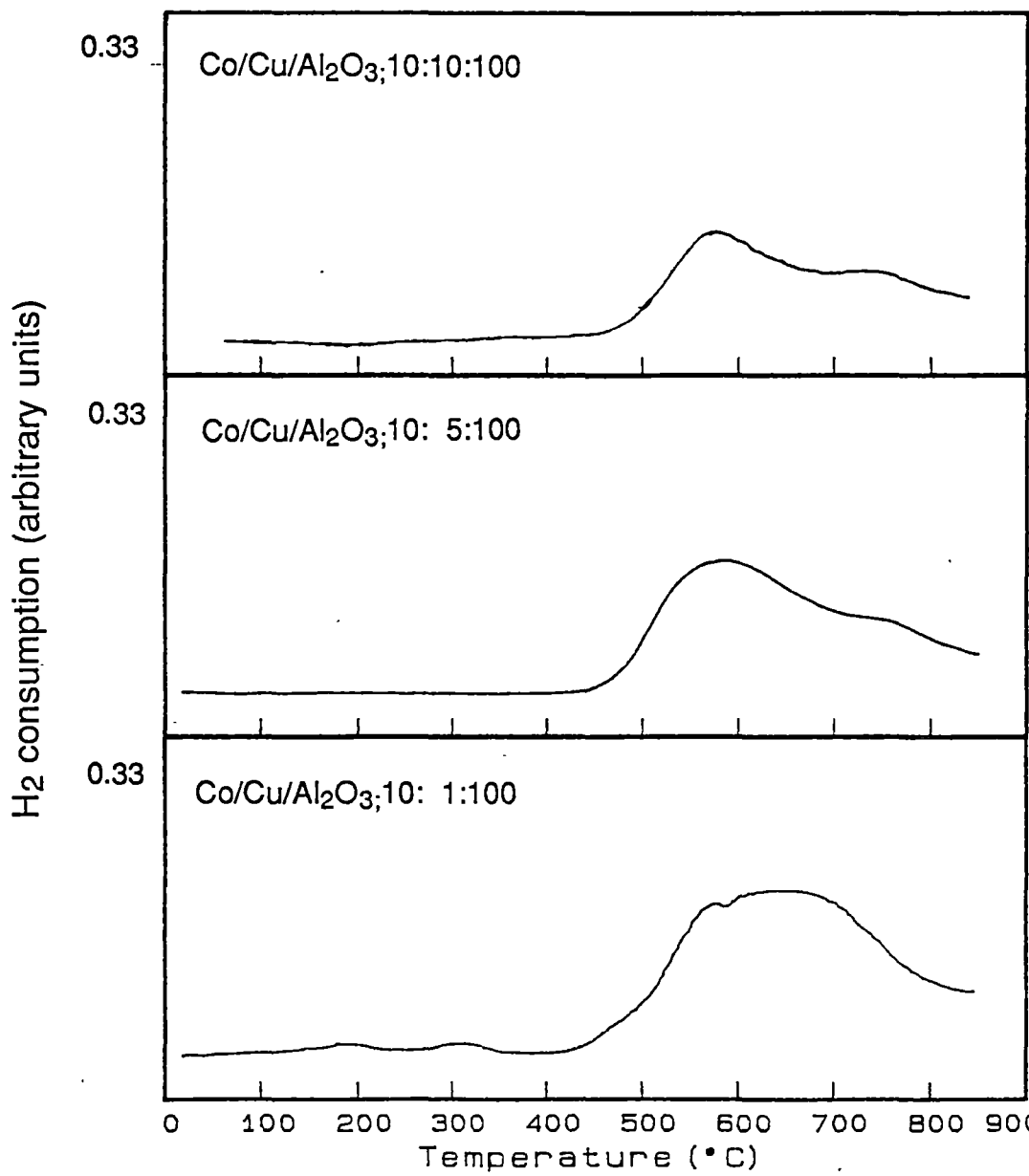

fig. 4.3.5a TPR profiles of activated Al_2O_3 supported hybrid catalysts.

The profile given by $Co/Cu/Al_2O_3$;10:1:100 differed slightly to those given by $Co/Cu/Al_2O_3$;10:10:100 and $Co/Cu/Al_2O_3$;10:5:100. The extent of H_2 consumption at 740°C was more than on hybrid catalysts with higher metal loadings, suggesting that $CuAl_2O_4$ was more abundant on $Co/Cu/Al_2O_3$;10:1:100. This result again reflects the trend of increased interaction with decreased loading (see section 4.3.3).

The temperature of the $CuAl_2O_4$ reduction peak was shifted to lower temperature compared with the peak given by the physical mix of Co/Al_2O_3;10:100 + Cu/Al_2O_3;1:100 and Cu/Al_2O_3;1:100 itself. The presence of Co would have decreased the availability of free Al_2O_3 on the hybrid catalyst. The concentration of oxidic Cu relative to free Al_2O_3 on $Co/Cu/Al_2O_3$;10:1:100 was probably comparable to the concentration on Cu/Al_2O_3;10:100. The rate of formation of $CuAl_2O_4$, and therefore the peak position given by the reduction, would therefore be expected to occur at similar positions on the two samples (see section 4.3.4). Inspection of the profiles verifies this assertion, (compare figs. 4.3.3a and 4.3.5a).

Since only the Co/Cu oxide observed on the calcined samples was affected by activation it was the probable source of the aluminates. The comparative areas of the $CuAl_2O_4$ peak given by the activated sample and the Cu^{2+} shoulder given by the calcined catalyst suggests that, at most, 25% of the Cu in the mixed Co/Cu oxide was converted to $CuAl_2O_4$ on $Co/Cu/Al_2O_3$;10:10:100 and $Co/Cu/Al_2O_3$;10:5:100 (compare figs. 4.2.5a and 4.3.5a). A similar maximum fraction of the Co was converted to $CoAl_2O_4$. At a minimum, therefore, 75% of the Co/Cu/oxide was reduced to metal. These deductions take into account that the amount of H_2 required to reduce a mole of aluminate is four times that required to reduce a mole of interactive Co^{2+} or Cu^{2+} (see sections 4.2.2 and 4.2.3).

Similar analysis suggests that virtually all of the Cu on $Co/Cu/Al_2O_3$;10:1:100 was converted to $CuAl_2O_4$. Approximately 25% of the Co involved in the Co/Cu oxide was converted to $CoAl_2O_4$, similar to the conversions observed for $Co/Cu/Al_2O_3$;10:10:100 and $Co/Cu/Al_2O_3$;10:5:100.

After activation then, the approximate weight percentage of Co^0 on all the hybrid catalysts was 3%. The weight percentages of Cu were around 8%, 4%, and less than 1% in order of decreased Cu loading.

Co/Cu/$SiO_2$40Å Catalysts

Small reduction peaks were observed at low (100°C) and high (800°C) temperatures on the catalysts which had been reduced (400°C, 5 ml/min H_2 flow, 2 hours) prior to the TPR run (refer to fig. 4.3.5b). The former were probably a result of partial reoxidation of metal species, the latter being indicative of interactive species in low concentrations. The high temperature peaks occurred at a similar temperature to the reduction of octahedral Co^{2+} ions. Such interactive surface networks may well have been present prior to activation (see section 4.2.5).

The absence of the Co/Cu/oxide shows that it was reduced during activation. A mixed Co^0/Cu^0 species probably formed. The active mixed metal species on the $SiO_2$40Å and Al_2O_3 supported hybrids were probably similar in nature, since the parent mixed Co/Cu oxides appeared similar judging by TPR evidence (see section 4.2.5).

The quantity of the mixed Co^0/Cu^0 particles and the proportions of Co^0 and Cu^0 would have differed between the two catalyst sets however. Unlike the situation for the Al_2O_3 catalysts, total reduction of oxidic Co and Cu effectively occurred on the $SiO_2$40Å supported hybrids. The actual quantities of reduced metals would thus have been equivalent to the quantity of oxidic species on the calcined samples. A small increase in the weight percentages would be expected to occur after reduction because of the net weight loss of the catalysts due to the removal of oxygen.

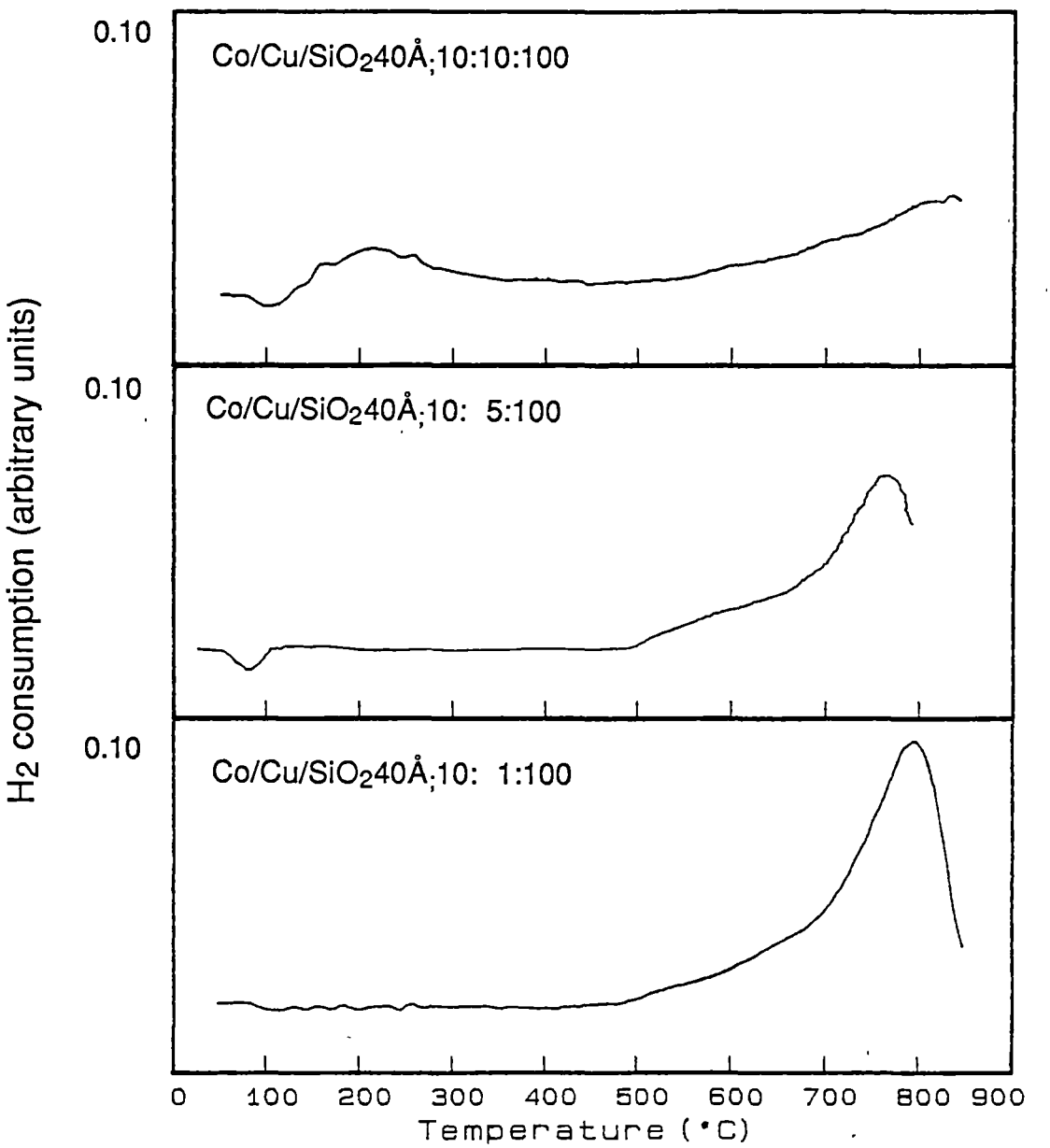

fig. 4.3.5b TPR profiles of activated $SiO_2$40Å supported hybrid catalysts.

4.4 Kolbel Engelhardt Activity

4.4.1 Screening Analysis

In this section of the work, the major products analysed were Cl to C3 hydrocarbons and CO_2. Levels of reactant CO were also measured. A limitation of the analysis was that concentrations of H_2, a likely product, were not assessed.

The supported Co, supported Cu and hybrid Co/Cu catalysts were all screened according to this approach. The activities of $SiO_2$40Å and Al_2O_3 supported physical mixes were similarly assessed. The behaviour of the highest loading physical mixes was compared to that of samples where the appropriate catalysts were separately packed and simultaneously screened. The results are all summarised in tables 4.4.2 - 4.4.5 and figs. 4.4.2 - 4.4.5.

Extensive hydrocarbon analyses, detecting molecules of carbon number 8 and below, were carried out at 250°C and 325°C for the catalysts of highest and lowest activity for each supported suite (*e.g.* Co/$SiO_2$40Å;10:100, Co/Cu/$SiO_2$40Å;10:10:100). The possible range of volatile hydrocarbon production was defined by these upper and lower limiting cases.

Although higher molecular weight products were almost certainly synthesised, such oils and waxes would have accumulated on the catalysts and the surfaces of the screening apparatus. The absence from the effluent of such long chain hydrocarbons explains their non-detection.

Typically in catalytic reactions such as the KE synthesis which obey Schulz Florey kinetics, the CO conversion to oils and waxes is of the same order as, though rather less than, the conversion to lighter products. Numeric errors caused by the non-detection of heavier fractions are therefore negligible.

The level of product analysis performed for the experiments outlined in this section, while not complete, was sufficient to elucidate the relative activities of the various catalyst preparations. More extensive analyses on the most active catalyst are reported in the next chapter.

4.4.2 Activities of Supported Co Catalysts

The benchmark catalyst for this work, provided by the Division of Energy Chemistry C.S.I.R.O., was $Co/SiO_2$40Å;10:100. It was found to be an active FT catalyst (Roe, 1986; Roe *et al.*, 1988). The laboratory prepared Co/Al_2O_3;10:100 catalyst gave similar results in a FT feed ($CO:H_2:H_2O$ = 1:2:0). The two catalysts also proved to give similar activities in a KE feed ($CO:H_2:H_2O$ = 3:0:1) as shown by the results in figs. 4.4.2a-c and table 4.4.2.

The hydrocarbon fraction consisted mainly of ethene and acetylene. Unsaturated C3s were the next most dominant product, followed by methane. Only trace amounts of molecules with carbon number 4 and above were observed. The hydrocarbon concentrations were at least two orders of magnitude lower in the CO/H_2O feed than when a CO/H_2 feed was used (Roe, 1986).

Unsaturated C2 hydrocarbons are regarded as the building blocks of the petrochemical industry because they can be readily polymerised to long chain hydrocarbons. The high selectivity towards unsaturated C2 hydrocarbons is therefore a potentially useful feature of these catalysts. This advantage is offset by the low conversions exhibited.

The amount of CO_2 associated with hydrocarbon production was consistently less than that which was actually measured (refer to table 4.4.2). The discrepancy became marked at higher temperatures (300°C, 325°C).

The non-inclusion of hydrocarbons with carbon numbers 4 and above in the calculation of the CO_2 figures would not have contributed significantly to the discrepancy. The concentrations of heavier hydrocarbons were so low as to be not quantifiable.

There were two possible sources of CO_2 in the reactor other than hydrocarbon synthesis by the KE reaction. They were the WGSR (producing H_2 in excess of that consumed by CO hydrogenation) and the Boudouard reaction (resulting in carbon deposition). These processes must have provided virtually all the CO_2 constituting the difference between actual CO_2 levels and the amount associated with hydrocarbon

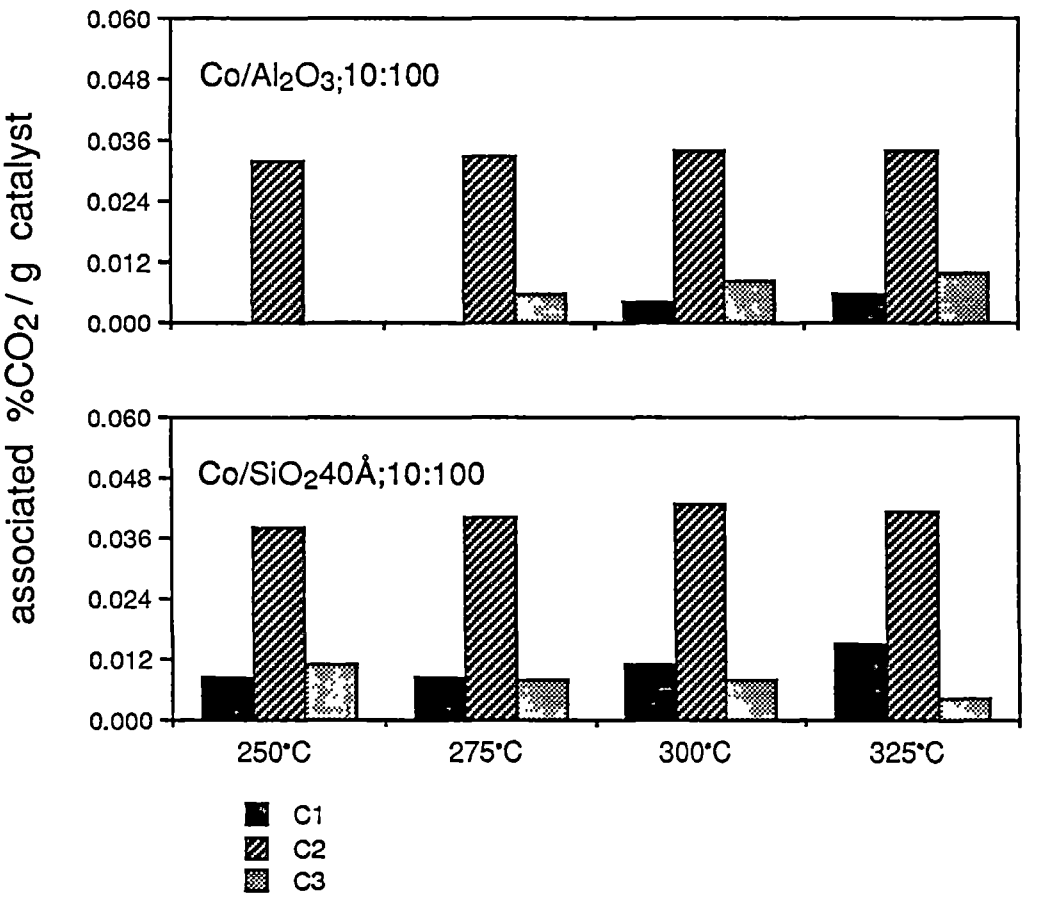

fig. 4.4.2a $\%CO_2$ associated with C1 to C3 hydrocarbons for supported Co catalysts.

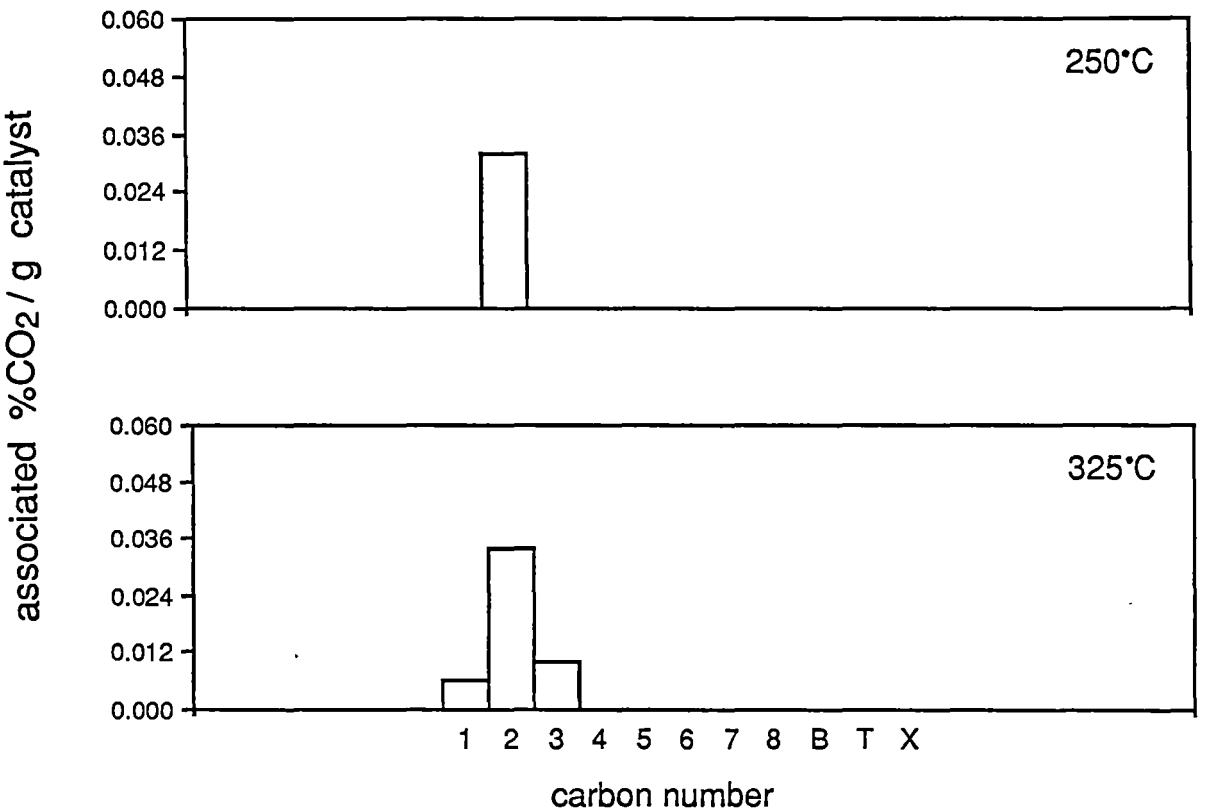

fig. 4.4.2b Extensive FID analyses for Co/Al_2O_3;10:100.

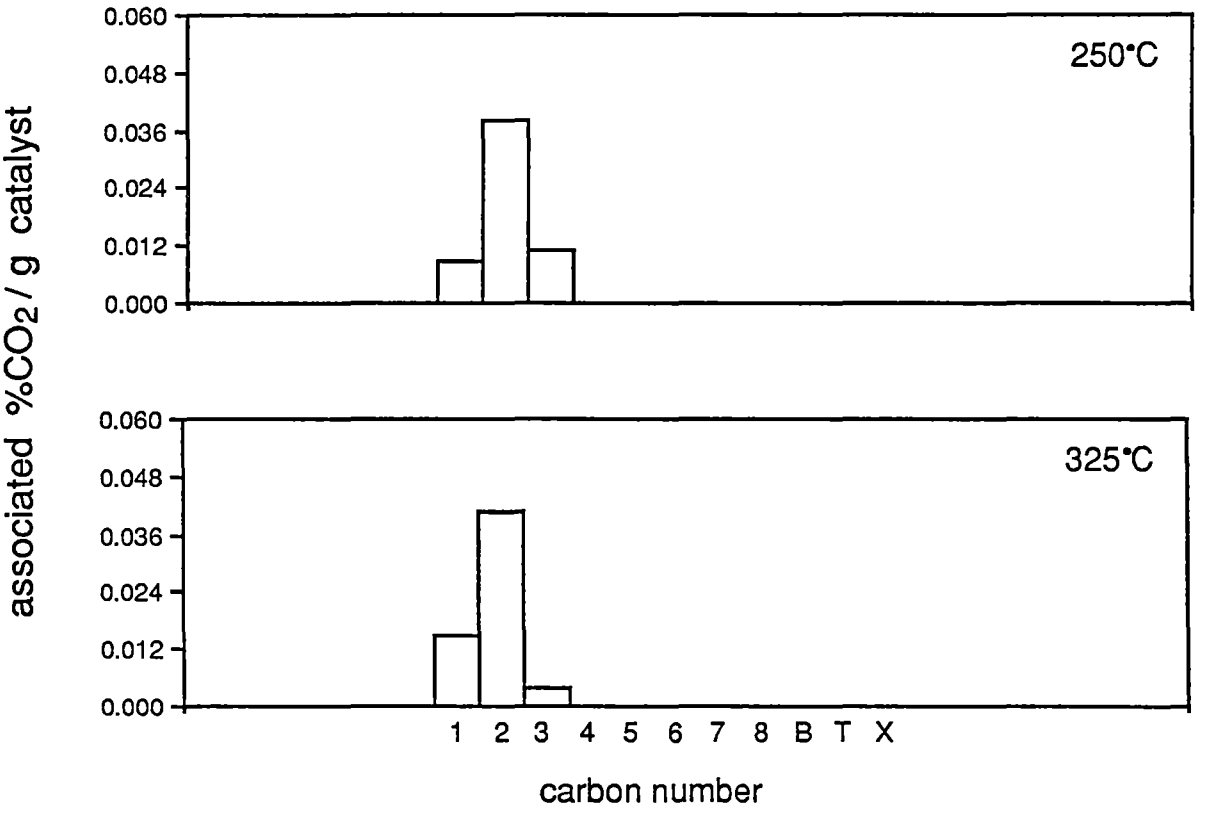

fig. 4.4.2c Extensive FID analyses for $Co/SiO_2$40Å;10:100.

	Co/Al_2O_3;10:100		$Co/SiO_2$40Å;10:100	
T(°C)	actual % CO_2	%CO_2 associated with C1s+C2s+C3s	actual % CO_2	%CO_2 associated with C1s+C2s+C3s
250	t	0.032	0.50	0.058
275	t	0.090	1.6	0.056
300	t	0.047	2.1	0.062
325	2.8	0.050	5.1	0.060

t = trace (<0.30%)

Table 4.4.2 Actual %CO_2 and %CO_2 associated with low molecular weight hydrocarbons for supported Co catalysts.

production. Without measurement of H_2 concentrations it is impossible to assess which reaction was the major contributor.

4.4.3 Activities of Supported Cu Catalysts

Cu/Al_2O_3 Catalysts

All three Cu/Al_2O_3 catalysts were active towards methanation at each temperature studied (refer to fig. 4.4.3a). Small amounts of C2s (0.042% maximum) and C3s (0.013% maximum) were also produced. The trace levels (less than 0.30%) of CO_2 were consistent with the quantitative conversion of CO and H_2O to the hydrocarbon products, without the occurrence of coking or excess H_2 production (see section 4.4.2). The production of methane increased with temperature, but was not affected by Cu loading. The C2 and C3 hydrocarbon yields were not influenced by either of these variables.

$Cu/SiO_2$40Å Catalysts

The set of $Cu/SiO_2$40Å catalysts all produced substantial amounts of CO_2 (approximately 6%), but none synthesised hydrocarbons. Variations of metal loading and temperature had little effect on the extent of CO_2 production (refer to table 4.4.3).

At 250°C the CO_2 production was almost certainly associated with H_2 production by the WGSR. The absence of hydrocarbons shows that the KE synthesis was not the CO_2 source and the Boudouard reaction is unlikely to proceed significantly at this temperature. The WGSR was probably also responsible for CO_2 production at elevated temperatures (275°C, 300°C, 325°C) since little variation in activity occurred as the temperature was raised.

The activities of the Cu/Al_2O_3 and $Cu/SiO_2$40Å catalysts were thus completely different, even though the TPR results showed that Cu^0 was present on both (see section 4.3.3). The contrast in activities suggests that the electronic properties of the Cu^0 formed during activation were different on the two supports. .

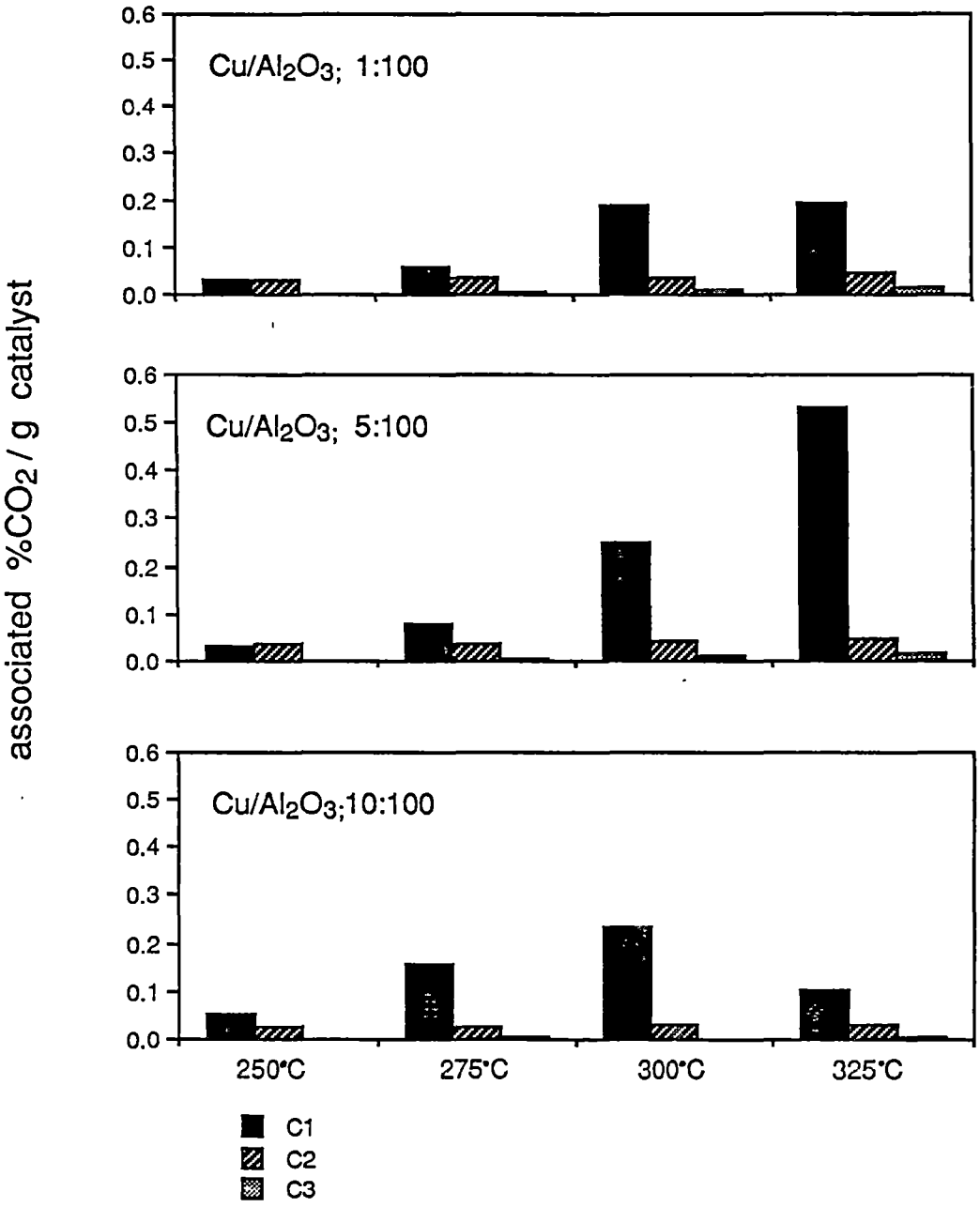

fig. 4.4.3 $\%CO_2$ associated with C1 to C3 hydrocarbons for Cu/Al_2O_3 catalysts.

	$Cu/SiO_2$40Å;1:100	$Cu/SiO_2$40Å;5:100	$Cu/SiO_2$40Å;10:100
T(°C)	actual $\%CO_2$	actual $\%CO_2$	actual % CO_2
250	7.0	6.7	4.5
275	6.3	6.9	4.9
300	6.9	7.2	5.6
325	6.8	7.0	5.9

Table 4.4.3 Actual $\%CO_2$ for $Cu/SiO_2$40Å catalysts.

4.4.4 Activities of Physical Mixes

Co/Al_2O_3;10:100 + Cu/Al_2O_3 Mixes

All the physical mixes of this type gave similar product distributions and feed conversions (refer to fig. 4.4.4a and table 4.4.4a). Methane was the predominant product, with small amounts of C2 and C3 hydrocarbons also being produced. Extensive FID analysis showed only trace amounts of heavier hydrocarbons were present.

The maximum percentage of effluent CO_2 observed was only 7.3%. The amount of CO_2 associated with hydrocarbon product was considerably less than the actual levels measured. Again (see section 4.4.2) this implies that the difference was caused by CO_2 production from the WGSR and/or the Boudouard reaction.

The intimate physical mixes behaved, activity wise, as additives of the single metal catalysts. The Cu/Al_2O_3 catalysts produced significant methane concentrations (associated CO_2 levels > 0.01%) but only traces of CO_2 (< 0.30% at 325°C). The Co/Al_2O_3;10:100 catalyst produced trace methane, but significant concentrations of CO_2. The physical mixes produced significant concentrations of both these products. Both single metal catalysts and the physical mix synthesised observable levels of C2 and C3 hydrocarbons.

An important ramification of this argument is that Co and Cu did not interact during the activation procedure. The TPR results did not establish this categorically (see section 4.3.4).

Comparison of the activities given by a sample where Co/Al_2O_3;10:100 and Cu/Al_2O_3;10:100 were packed sequentially in the reactor and the intimate mix of the same catalysts lendsfurther support to this idea. Interaction between Co and Cu was clearly impossible in the former situation. The conversion given by both samples were virtually identical (compare figs. 4.4.4a and 4.4.4c, tables 4.4.4a and 4.4.4c). The findings thus suggest that no interaction occurred in either situation.

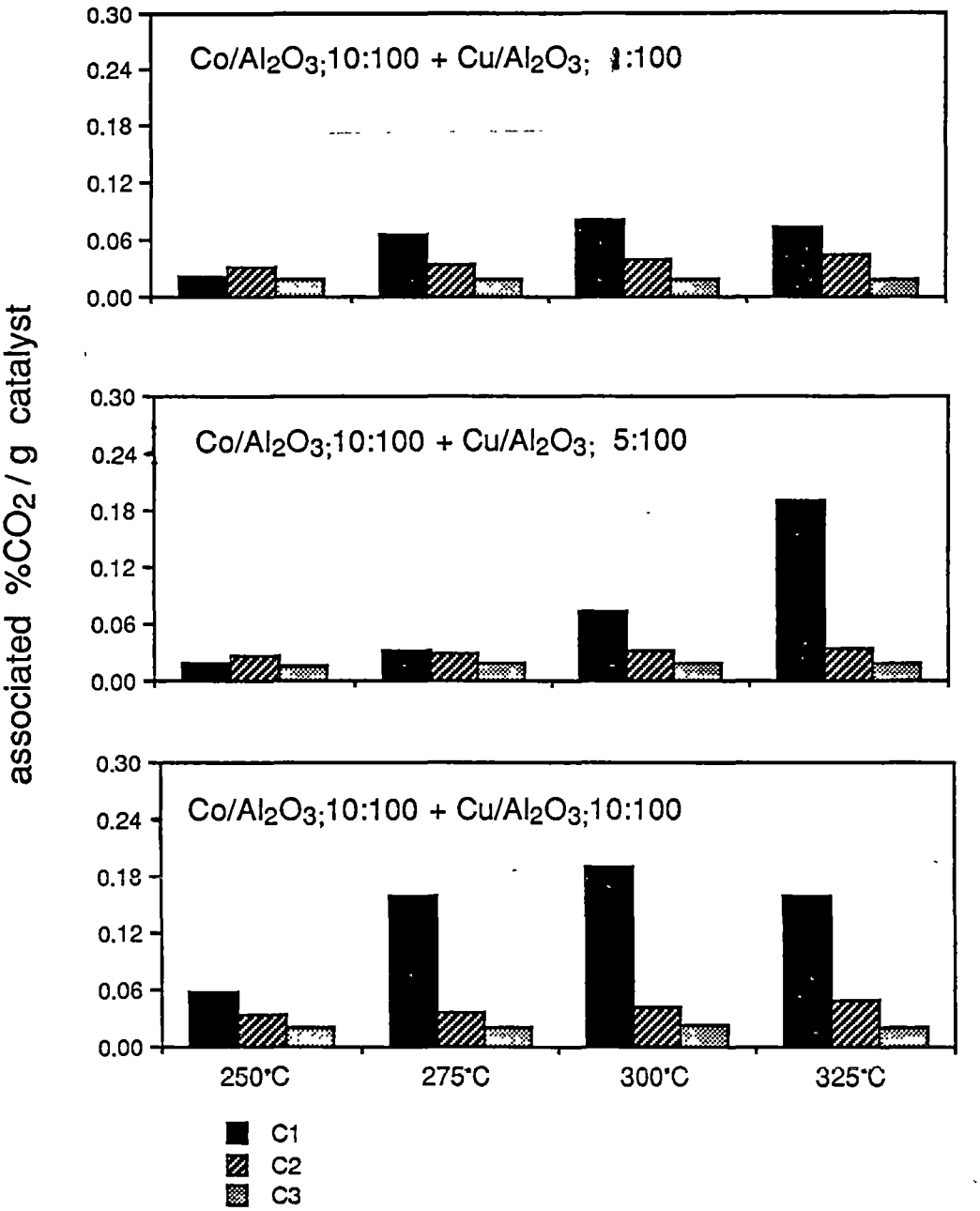

fig. 4.4.4a %CO_2 associated with C1 to C3 hydrocarbons for Al_2O_3 supported physical mixes.

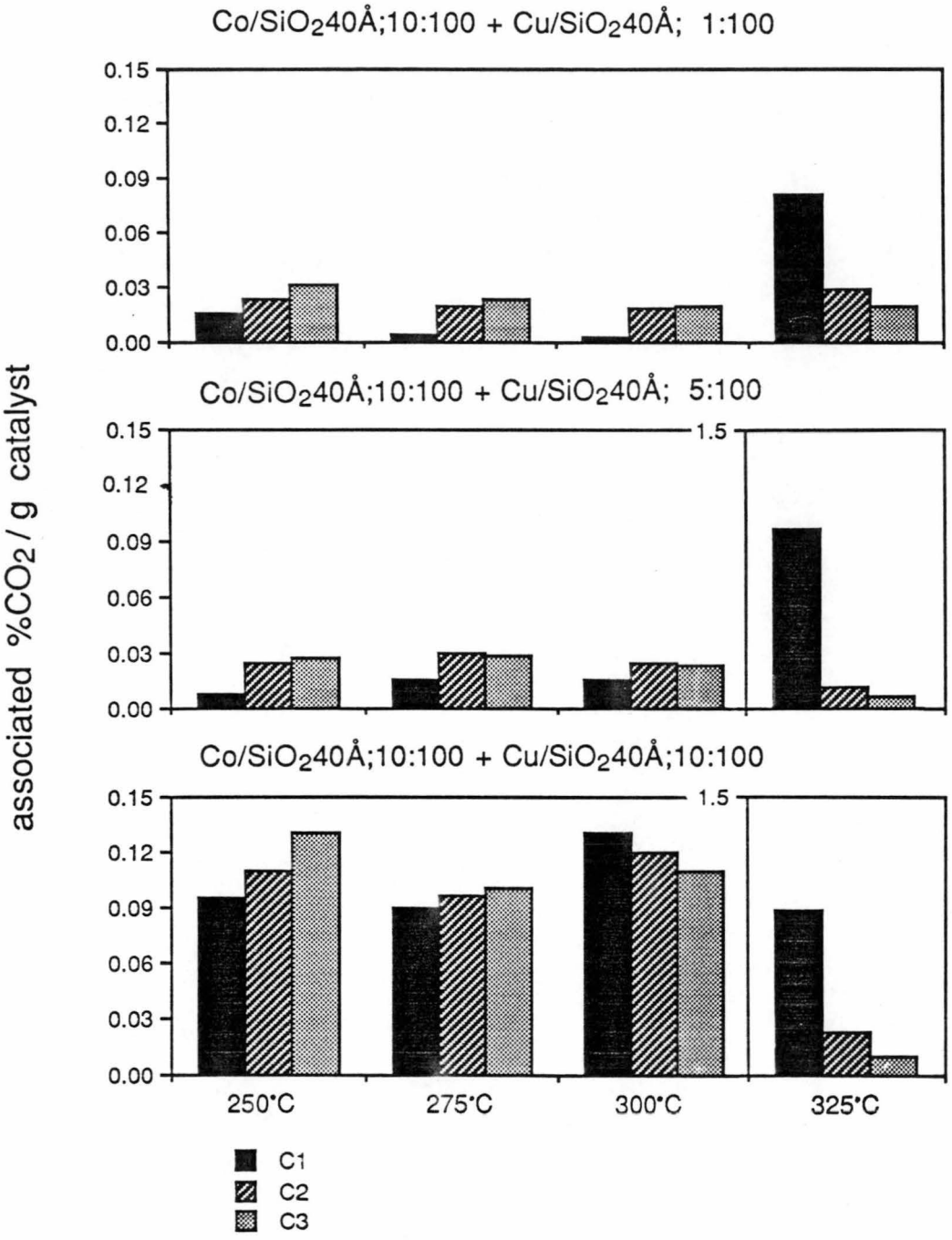

fig. 4.4.4b %CO_2 associated with C1 to C3 hydrocarbons for $SiO_2$40Å supported physical mixes.

	Co/Al_2O_3;10:100 + Cu/Al_2O_3; 1:100		Co/Al_2O_3;10:100 + Cu/Al_2O_3; 5:100		Co/Al_2O_3;10:100 + Cu/Al_2O_3;10:100	
T(°C)	actual % CO_2	% CO_2 associated with C1s+C2s+C3s	actual % CO_2	% CO_2 associated with C1s+C2s+C3s	actual % CO_2	%CO_2 associated with C1s+C2s+C3s
250	t	0.069	t	0.060	t	0.11
275	t	0.12	t	0.077	t	0.22
300	t	0.14	t	0.12	t	0.26
325	6.3	0.14	4.0	0.24	7.3	0.23

t = trace (<0.30%).

Table 4.4.4a Actual %CO_2 and %CO_2 associated with low molecular weight hydrocarbons for Al_2O_3 supported intimate physical mixes.

	$Co/SiO_2$40Å;10:100 + $Cu/SiO_2$40Å; 1:100		$Co/SiO_2$40Å;10:100 + $Cu/SiO_2$40Å; 5:100		$Co/SiO_2$40Å;10:100 + $Cu/SiO_2$40Å;10:100	
T(°C)	actual % CO_2	% CO_2 associated with C1s+C2s+C3s	actual % CO_2	% CO_2 associated with C1s+C2s+C3s	actual % CO_2	%CO_2 associated with C1s+C2s+C3s
250	0.40	0.070	4.3	0.060	8.5	0.34
275	0.66	0.046	5.3	0.075	7.0	0.29
300	1.2	0.039	7.3	0.064	7.7	0.36
325	9.7	0.13	22	1.1	9.8	1.2

t = trace (<0.30%).

Table 4.4.4b Actual %CO_2 and %CO_2 associated with low molecular weight hydrocarbons for $SiO_2$40Å supported intimate physical mixes.

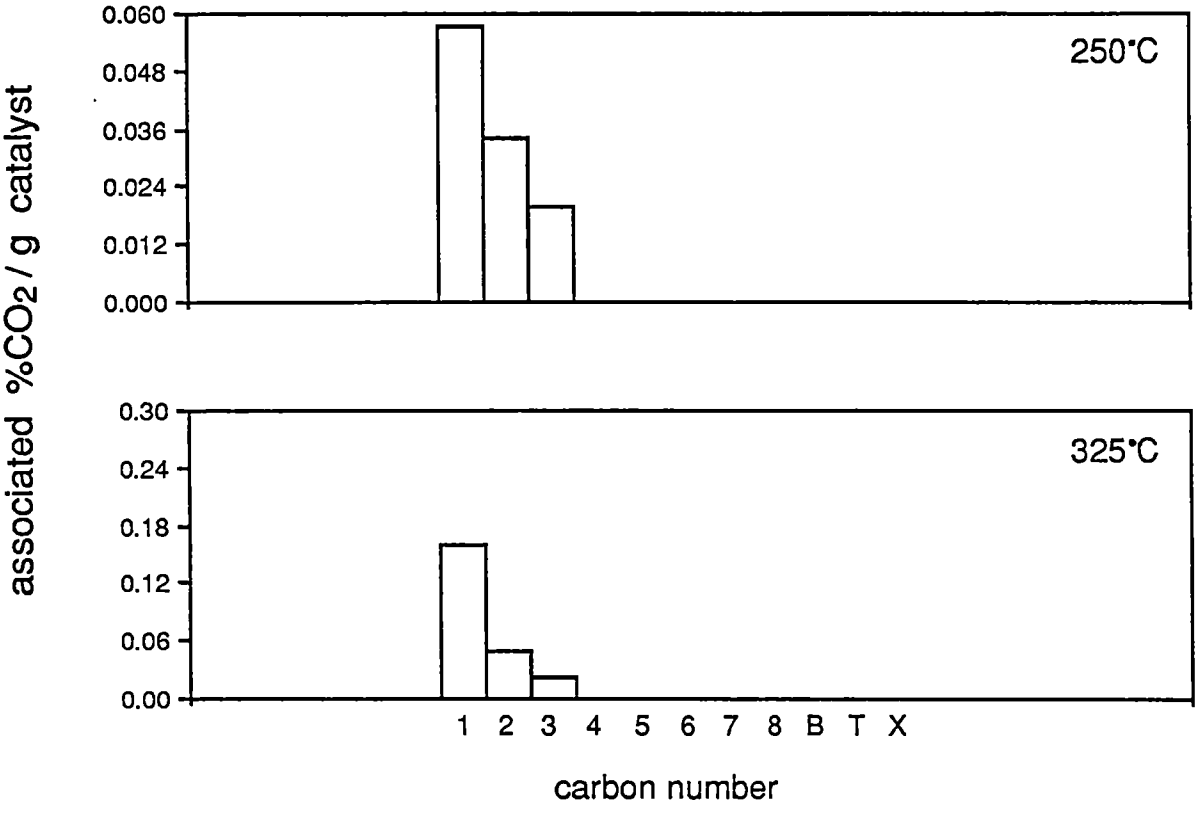

fig. 4.4.4d Extensive FID analyses for Co/Al_2O_3;10:100 + Cu/Al_2O_3; 10:100.

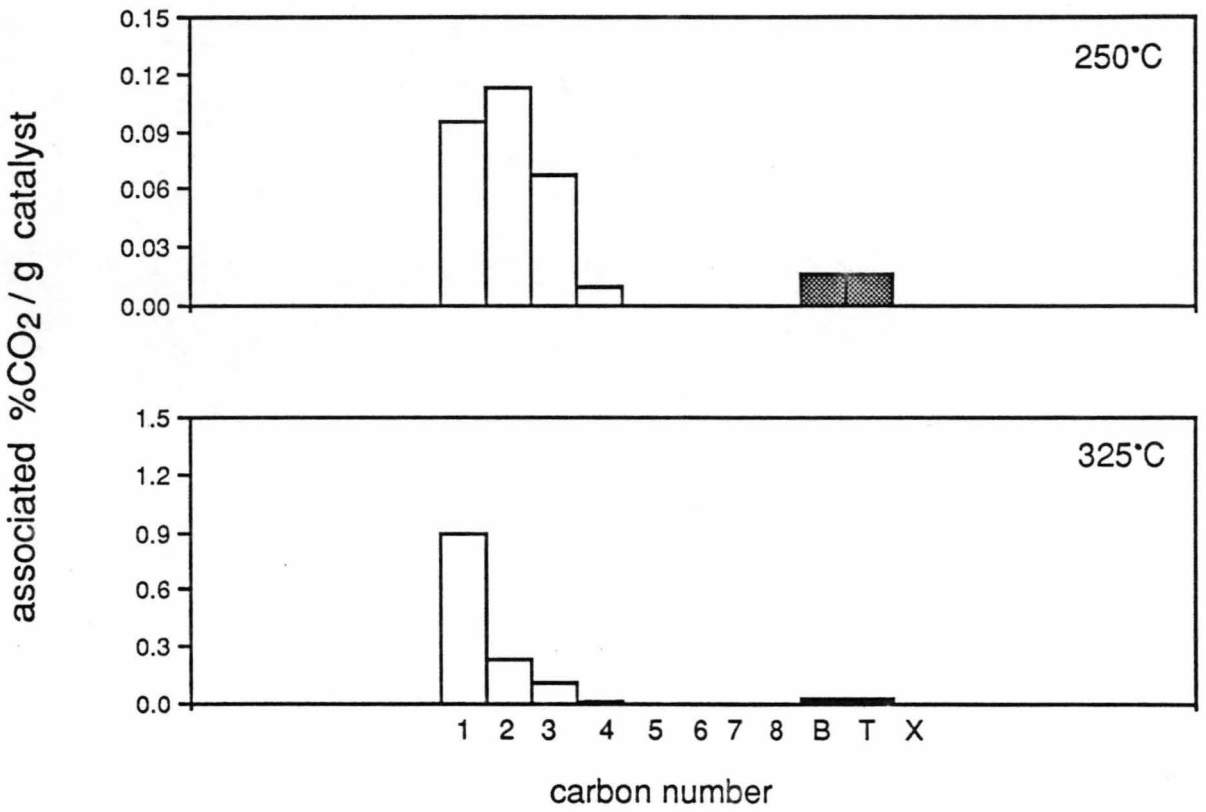

fig. 4.4.4e Extensive FID analyses for $Co/SiO_2$40Å;10:100 + $Cu/SiO_2$40Å;10:100.

$Co/SiO_2$40Å;10:100 + $Cu/SiO_2$40Å Mixes

Overall Activities

This set of catalysts all produced hydrocarbons in greater amounts than either the $Cu/SiO_2$40Å catalysts, which produced no hydrocarbons whatsoever, or the $Co/SiO_2$40Å;10:100 catalyst. The $Cu/SiO_2$40Å;10:100 + $Co/SiO_2$40Å;10:100 mix was the most active. Extensive hydrocarbon analysis showed that C4 hydrocarbons and the aromatic compounds, benzene, toluene and xylene (BTX) as well as C1, C2 and C3 products were synthesised over this composite catalyst (refer to fig. 4.4.4b and table 4.4.4b).

The results imply that the hydrocarbon synthesis proceeded by consecutive coupling of the WGSR and the FTR, as is widely accepted. A logical interpretation of the results is that Cu^o species, active towards the WGSR (see section 4.4.3), produced H_2 which was consumed by a FT process catalysed by supported Co^o.

The Effect of Temperature

At 250°C, 275°C and 320°C, the actual % CO_2 was, at most, 8.3% ($Co/SiO_2$40Å;10:100 + $Cu/SiO_2$40Å;10:100 at 250°C) and methane production was suppressed relative to C2 and C3 hydrocarbon formation. These product distributions suggest that the ambient H_2 partial pressures were low at these temperatures. A gradual increase in activity was observed in this temperature range for all three mixes according to the Arrhenius equation.

The activities at 325°C for all the mixes were substantially higher than at the lower temperatures. This was particularly so with respect to methane production. In moving from 300°C to 325°C, methane levels were raised by a factor of six over the $Co/SiO_2$40Å;10:100 + $Cu/SiO_2$40Å;10:100 combination. The increase was greater when $Cu/SiO_2$40Å;5:100 and $Cu/SiO_2$40Å;1:100 were mixed with the Co catalyst. The factors involved were 64 and 37 respectively. The effect on the production of the other hydrocarbon products and CO_2 was not as marked.

The increase in methane concentrations suggests that H_2 levels jumped. In the H_2 rich environment low molecular weight products have formed preferentially to longer chain products. Excess H_2 from the WGSR may here account for a large fraction of the difference between measured and calculated CO_2 levels. The production of excess H_2 over a supported Ni catalyst was proposed by Chaffee and Loeh (1986) for similar reasons, but was not confirmed by direct measurement of H_2.

An alteration in the WGSR activity of the Cu/$SiO_2$40Å components in the physical mixes would necessarily have caused the marked increase in H_2 production. The Cu/$SiO_2$40Å catalysts when screened individually did not exhibit such behaviour. Such change in product distribution was probably associated with a transformation of the catalyst structure, particularly modification in the distribution and the nature of active Cu^o species. A modification of this type may well be accompanied by a change in the rates of the WGSR reaction, and even a complete switch in mechanism. Marked changes in reaction rates are unlikely to occur independently from structural alteration.

The Effect of Cu Loading

Activity increased with Cu loading for the $SiO_2$40Å supported physical mixes (refer to fig. 4.4.4b and table 4.4.4b). This is probably because the amount of Cu determined the degree of hydrogen production and, correspondingly, the extent of hydrocarbon production on Co^o species by the FTR. The rate of the FTR is known to be proportional to H_2 partial pressure. This kinetic interpretation (Kolbel and Ralek, 1984) applies whether or not the WGSR is rate determining. The WGSR becomes the rate determining step when H_2 consumption by the FTR exceeds its production by the WGSR. The loading of Cu did not affect H_2 production at any one temperature when the Cu/$SiO_2$40Å catalysts were screened individually (see section 4.4.3).

Interaction between Co/$SiO_2$40Å;10:100 and Cu/$SiO_2$40Å Catalysts

At low temperatures and Cu loadings, actual %CO_2 levels were lower for the physical mixes than when the appropriate Cu/$SiO_2$40Å catalysts were screened individually, (*e.g.* Co/$SiO_2$40Å;10:100 + Cu/$SiO_2$40Å;1:100 at 250°C *versus*

$Cu/SiO_2$40Å;1:100 at 250°C - compare to tables 4.4.3b and 4.4.4b). Since the $Cu/SiO_2$40Å catalysts were almost certainly active towards the WGSR, this result implies H_2 production was suppressed by the addition of $Co/SiO_2$40Å;10:100.

Furthermore, at high temperatures and Cu loadings, actual $\%CO_2$ levels were higher for the physical mixes than for the corresponding $Cu/SiO_2$40Å catalysts (*e.g.* $Co/SiO_2$40Å;10:100 + $Cu/SiO_2$40Å; 5:100 at 325°C *versus* $Cu/SiO_2$40Å;5:100 at 325°C - compare tables 4.4.3b and 4.4.4b). Although the Boudouard reaction may well have partially contributed to this difference, the implication here is that the WGSR activity of the $Cu/SiO_2$40Å catalysts was enhanced as a result of physical mixing.

The above mentioned alterations in behaviour of the Cu^0 species occasioned by physically mixing $Cu/SiO_2$40Å catalysts with $Co/SiO_2$40Å;10:100 may be interpreted as evidence for direct interaction between Co^0 and Cu^0 to form new mixed metal species. Since the Co^0 and Cu^0 species must originally have been supported on separate $SiO_2$40Å particles, any interaction of these species implies their migration. Assuming such interaction did occur it must have been caused by the activation process. The TPR results (see section 4.3.4) prove that the actual process of physical mixing did not have this effect.

The interaction explanation contradicts that proffered to rationalise the behaviour of the Al_2O_3 mixes. A more satisfactory explanation is that physical effects caused the interaction between $Co/SiO_2$40Å;10;100 and the $Cu/SiO_2$40Å catalysts.

The hydrocarbons produced by the FT active $Co/SiO_2$40Å;10:100 catalyst may, for example, have covered active sites on the $Cu/SiO_2$40Å shift catalyst. This would have resulted in the inhibition of H_2 production, as seemingly occurred at low temperatures and low Cu loadings.

The synergism observed at higher temperatures can also be rationalised by physical effects. Equilibrium considerations suggest that higher H_2 production would have occurred over the Cu catalysts when they were involved in the intimate mixes rather than screened alone. Immediate consumption of H_2 in the FTR catalysed by $Co/SiO_2$40Å;10:100 would continually have encouraged its production *via* the WGSR by the $Cu/SiO_2$40Å components.

Internal heating may also have contributed to synergism. The FTR reaction is highly exothermic (ΔH = -165kJ/mole). The WGSR is less so (ΔH = -39.8kJ/mole). As hydrocarbon production by Co/$SiO_2$40Å; 10:100 increased, the temperature of the Co catalyst particles would have been raised. The heat would be readily transferred to the Cu/$SiO_2$40Å particles. Thus the active Cu species were probably, on average, at a slightly higher temperature in the intimate mix than when screened alone. Such a difference may well cause a significant variation in the rates of WGSR, consequently H_2 levels and hydrocarbon production. A similar explanation for a jump in methane formation over supported Ru catalysts was postulated by Gustafson (1981).

Separately Packed Co/$SiO_2$40Å; 10:100 and Cu/$SiO_2$40Å;10:100

Product distributions were affected by the order of packing. When the feed gas was passed first over Co/$SiO_2$40Å,10:100 and then Cu/$SiO_2$40Å;10:100, the hydrocarbon distributions were similar to those given by Co/$SiO_2$40Å;10:100. When the Cu catalyst was the first exposed to the feed gas, methane levels were increased relative to the benchmark although C2 and C3 hydrocarbon levels changed little (compare figs. 4.4.2a and 4.4.4c). When the Cu catalyst was second in the bed and hence exposed to the feed after the Co catalyst, the H_2 it produced did not significantly contact the FT active Co/$SiO_2$40Å; 10:100. The hydrocarbon yield was low because hydrogenation of CO by the Co catalyst could not readily proceed. When Cu/$SiO_2$40Å;10:100 was first exposed to the feed gas, Co/$SiO_2$40Å;10:100 could consume the available H_2, and the hydrocarbon yield was raised. The dependence of activity on the order of packing provides further strong evidence for the sequential coupling KE mechanism.

The lesser activity of the separately packed mixes compared to the intimate mix, whether or not the packing order facilitated hydrocarbon production, shows that the proximity between the two catalyst types influenced their mode of interaction. The equilibrium and heating effects proposed to account for the synergism in the Co/$SiO_2$40Å;10:100 + Cu/$SiO_2$40Å;10:100 mix would only operate when the samples were in intimate contact.

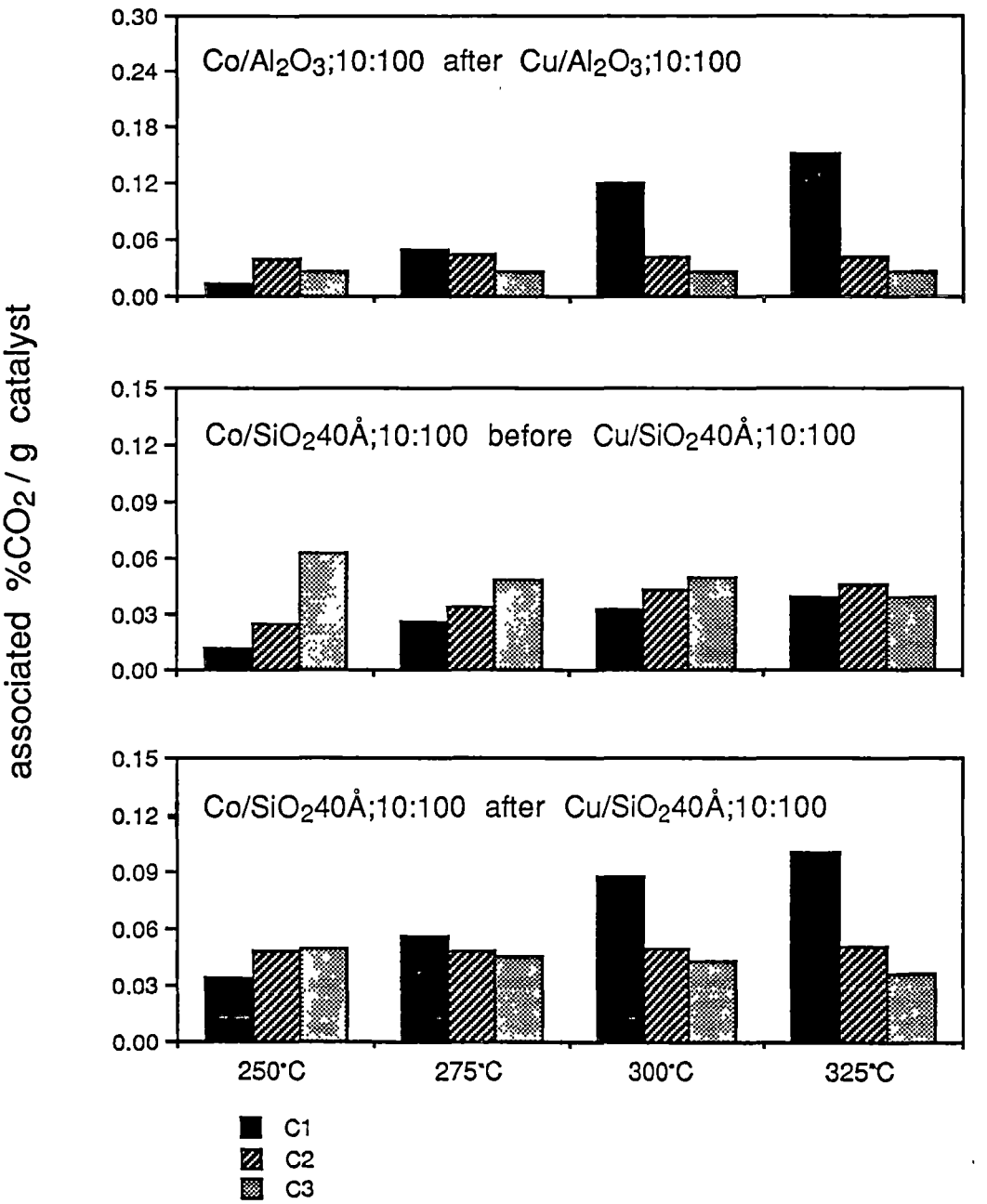

fig. 4.4.4c %CO_2 associated with C1 to C3 hydrocarbons for separately packed samples.

	Co/Al_2O_3;10:100 +Cu/Al_2O_3;10:100 packed separately Cu/Al_2O_3;10:100 first exposed		$Co/SiO_2$40Å;10:100 +$Cu/SiO_2$40Å;10:100 packed separately $Co/SiO_2$40Å;10:100 first exposed		$Co/SiO_2$40Å;10:100 +$Cu/SiO_2$40Å;10:100 packed separately $Cu/SiO_2$40Å;10:100 first exposed	
T(°C)	actual $\%CO_2$	$\%CO_2$ associated with C1s+C2s+C3s	actual $\%CO_2$	$\%CO_2$ associated with C1s+C2s+C3s	actual $\%CO_2$	$\%CO_2$ associated with C1s+C2s+C3s
250	t	0.078	12	0.10	6.2	0.13
275	t	0.12	11	0.11	7.4	0.15
300	t	0.19	12	0.13	7.7	0.18
325	2.2	0.22	11	0.12	7.3	0.19

t = trace (<0.30%)

Table 4.4.4c Actual $\%CO_2$ and $\%CO_2$ associated with low molecular weight hydrocarbons for separately packed physical mixes.

4.4.5 Activities of Hybrid Catalysts

Co/Cu/Al_2O_3 Catalysts

The hybrid Co/Cu/Al_2O_3 catalysts all produced low amounts of methane. At low temperatures and Cu loadings, C2 hydrocarbons were the dominant products. At higher temperatures (300°C, 325°C), for Co/Cu/Al_2O_3;10:100 and Co/Cu/Al_2O_3;10:5:100, the % CO_2 values associated with both C2s and C3s were greater than 0.05% (refer to fig. 4.4.5a).

Extensive FID analysis of the products synthesised by Co/Cu/Al_2O_3;10:10:100 at 325°C revealed the presence of benzene, toluene and xylene. The total % CO_2 associated with aromatics was 0.043%. The benchmark catalyst, Co/$SiO_2$40Å;10:100, was less active on the same basis of hydrocarbon production (see section 4.4.2).

The measured levels of CO_2, although never greater than 10%, always exceeded the calculated CO_2 values (refer to table 4.4.5). This suggests that coking and/or excess H_2 production (see section 4.4.2) occurred to some extent.

The observed trend of increased hydrocarbon production with Cu loading matches the increased availability of Cu^0 suggested by TPR evidence (see section 4.3.5). This implies that the amount of Cu controlled the rate of the WGSR, and therefore the availability of H_2, as was the case for the Co/$SiO_2$40Å;10:100 + Cu/$SiO_2$40Å mixes (see section 4.4.4).

This accordance enables identification of the oxidic species which gave rise to the crucial active species. The low temperature shoulder apparent on all the TRR profiles of Co/Cu/Al_2O_3 catalysts represented the Cu component of the mixed Co/Cu oxide. This species became active towards the WGSR. The Co which contributed to the mixed oxide peak became active towards the FTR.

Given that the KE synthesis proceeds sequentially, an increase in the rate of the FTR instead of the WGSR would also have given a lift in hydrocarbon production. Higher Cu loadings plausibly caused such an increase. In this case, the Cu need not be regarded as WGSR active. However the magnitude of the increase in activity occasioned by the introduction of Cu is inconsistent with this reasoning. Doubling the loading of Co would have approximately doubled the rate of the FTR, and therefore hydrocarbon

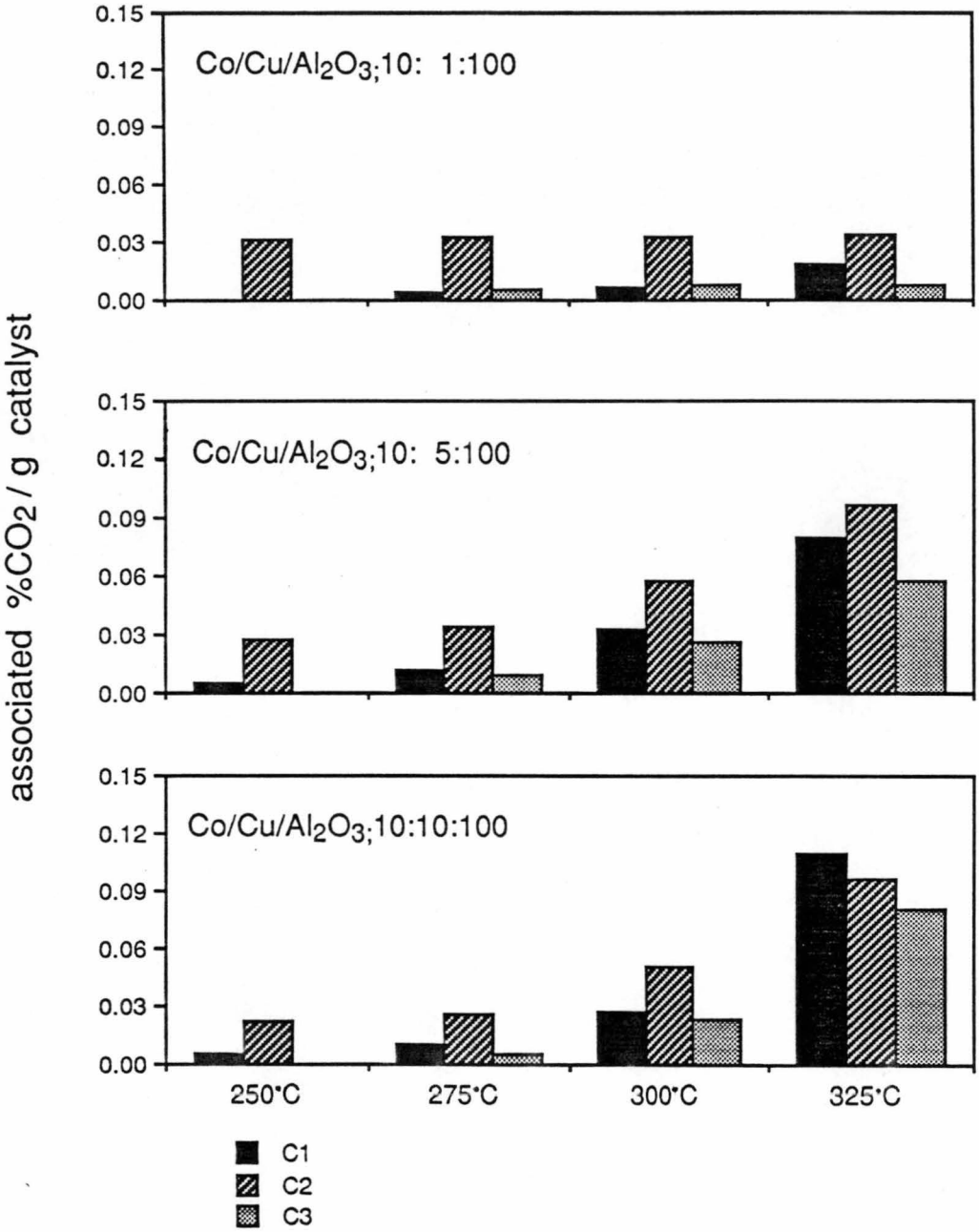

fig. 4.4.5a %CO_2 associated with C1 to C3 hydrocarbons for Al_2O_3 supported hybrid catalysts.

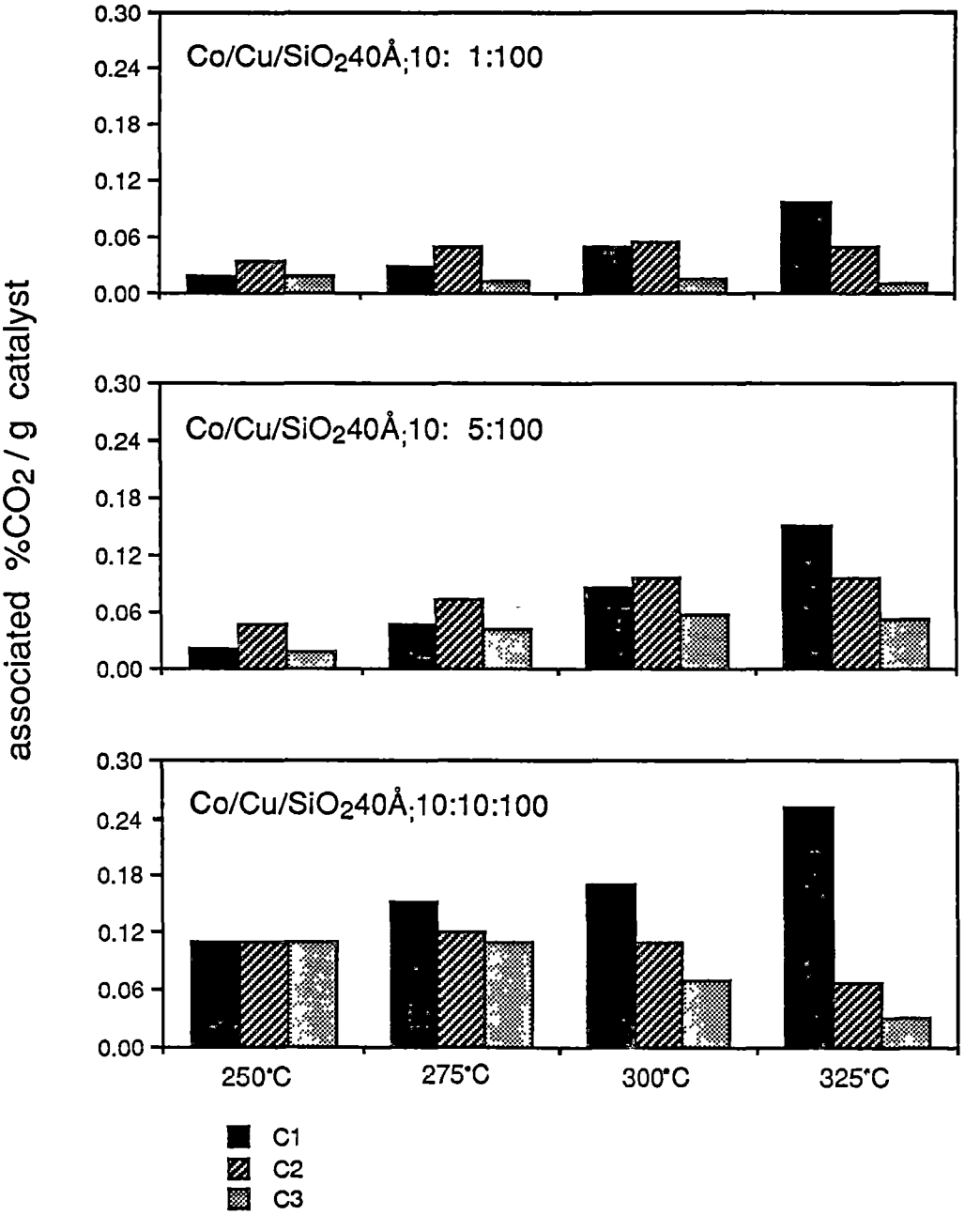

fig. 4.4.5b %CO_2 associated with C1 to C3 hydrocarbons for $SiO_2$40Å supported hybrid catalysts.

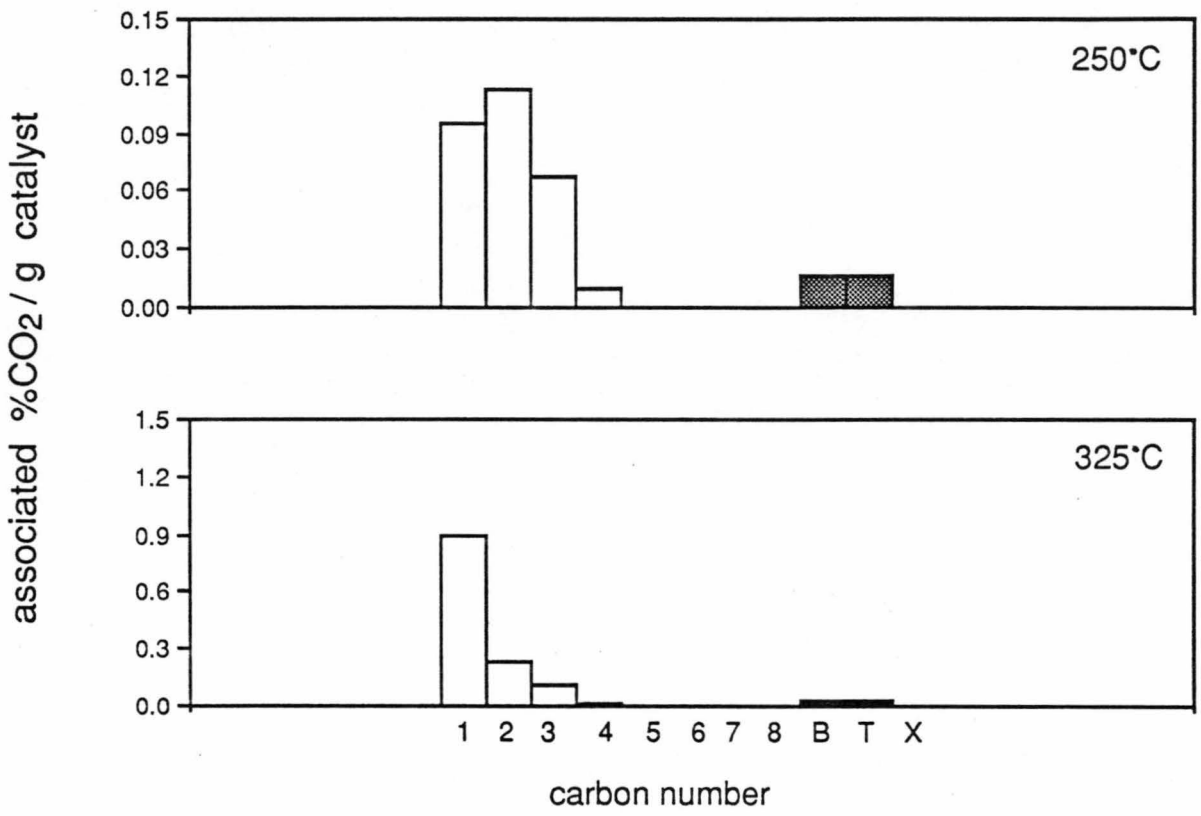

fig. 4.4.4e Extensive FID analyses for $Co/SiO_2$40Å;10:100 + $Cu/SiO_2$40Å;10:100.

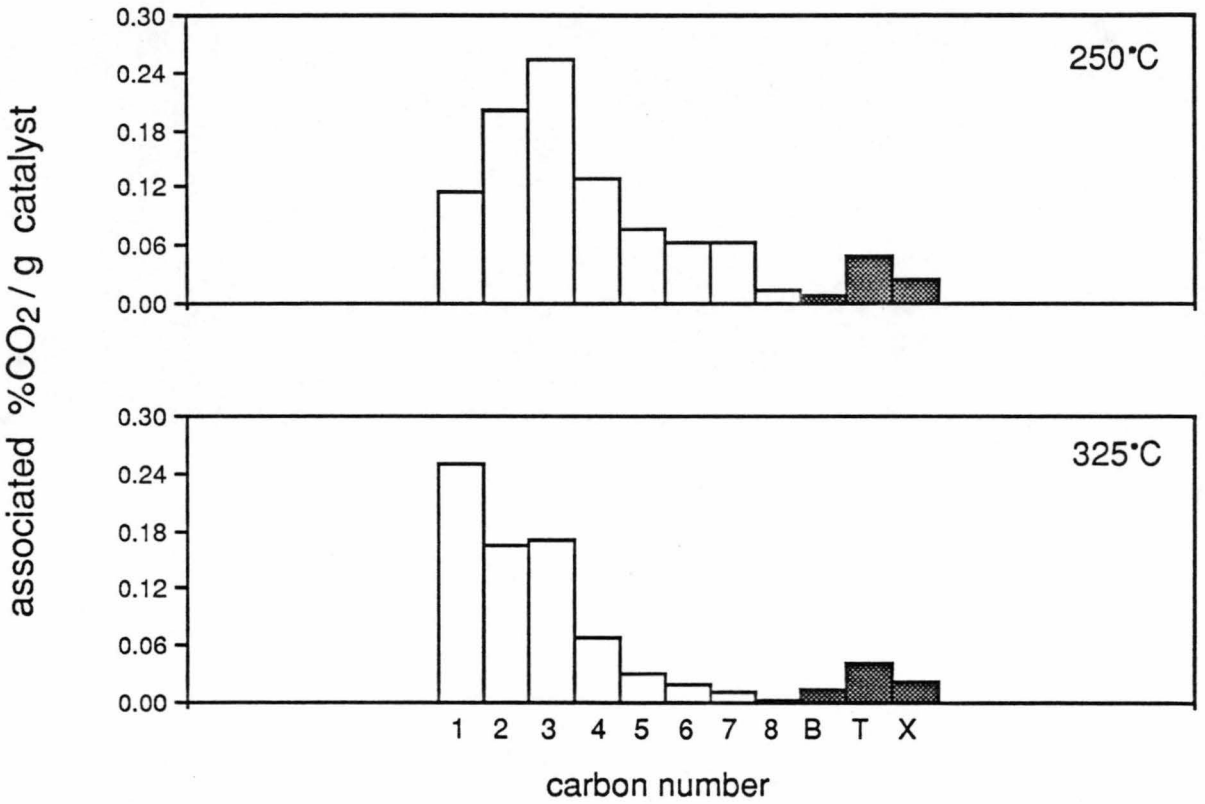

fig. 4.4.5d Extensive FID analyses for Co/Cu/$SiO_2$40Å;10:10:100.

	$Co/Cu/Al_2O_3$;10:1:100		$Co/Cu/Al_2O_3$;10:5:100		$Co/Cu/Al_2O_3$;10:10:100	
T(°C)	actual $\%CO_2$	% CO_2 associated with C1s+C2s+C3s	actual $\%CO_2$	$\%CO_2$ associated with C1s+C2s+C3s	actual $\%CO_2$	% CO_2 associated with C1s+C2s+C3s
250	t	0.031	t	0.032	t	0.028
275	t	0.043	t	0.056	t	0.043
300	t	0.046	t	0.12	t	0.10
325	1.1	0.060	4.3	0.23	4.6	0.29

t = trace (<0.30%)

Table 4.4.5a Actual $\%CO_2$ and $\%CO_2$ associated with low molecular weight hydrocarbons for $Co/Cu/Al_2O_3$ hybrids.

	$Co/Cu/SiO_2$40Å;10:1:100		$Co/Cu/SiO_2$40Å;10:5:100		$Co/Cu/SiO_2$40Å;10:10:100	
T(°C)	actual $\%CO_2$	% CO_2 associated with C1s+C2s+C3s	actual $\%CO_2$	$\%CO_2$ associated with C1s+C2s+C3s	actual $\%CO_2$	% CO_2 associated with C1s+C2s+C3s
250	3.0	0.069	1.5	0.084	3.6	0.33
275	3.5	0.091	2.8	0.16	3.8	0.38
300	8.2	0.12	6.9	0.24	12	0.35
325	14	0.16	15	0.30	27	0.35

Table 4.4.5b Actual % CO_2 and % CO_2 associated with low molecular weight hydrocarbons for $Co/Cu/SiO_2$40Å hybrids.

production *via* the KE synthesis. Metallic Co^o is known to be a superior FT catalyst to Cu^o (Vannice, 1975). The $Co/Cu/Al_2O_3$;10:10:100 catalyst would therefore be anticipated to have possessed less than double the activity of Co/Al_2O_3;10:100. However there was a six-fold difference in total hydrocarbon production at 325°C, for example, between these two catalysts (0.05% against 0.29% CO_2 equivalent - compare tables 4.4.2 and 4.4.5a).

The Co/Al_2O_3;10:100 + Cu/Al_2O_3 physical mixes all produced methane as the major product, with trace amounts of C2 and C3 hydrocarbons. The Cu species were responsible for the methane formation (see sections 4.4.3 and 4.4.4). Over the $Co/Cu/Al_2O_3$ hybrids methane production was always less than for the corresponding intimate mixes (compare figs. 4.4.4a and 4.4.5a). This suppression of methane shows that when Cu was doped into Co, the activity of the Cu was modified. It seems that Cu^o was altered from being active towards methanation on the single metal catalysts and physical mixes to being active towards the WGSR on the hybrids.

From the TPR results (see sections 4.2.5 and 4.3.5) it was inferred that a Co^o/Cu^o metallic species, derived from the mixed Co/Cu oxide, was present on the active catalysts. The modification of Cu^o activity is probably a consequence of the resultant interaction of Co^o and Cu^o.

Co/Cu/$SiO_2$40Å Catalysts

The $Co/Cu/SiO_2$40Å catalysts produced approximately double the concentration of hydrocarbon products as did their $Co/Cu/Al_2O_3$ counterparts (refer to fig. 4.4.5b). This may well be a result of the greater post activation availability of active metals (see section 4.3.5).

At 325°C the CO_2 levels measured far exceeded the levels calculated to be associated with hydrocarbon production (refer to table 4.4.5). The WGSR was probably not the source of the difference. A marked increase in hydrocarbon production while moving from 250°C to 325°C would accompany a marked rise in H_2 availability, as occurred for the $Co/SiO_2$40Å;10:100 + $Cu/SiO_2$40Å physical mixes (see section 4.4.4). Such behaviour was not observed. The majority of the CO_2 probably instead originated

from coking, *via* the Boudouard reaction. The comparative effluent levels of CO_2 were higher than for the Al_2O_3 catalysts which suggests coking proceeded to a greater extent on the $SiO_2$40Å supported hybrids.

The yield of hydrocarbons increased with temperature, according to the Arrhenius equation, and Cu loading. The Al_2O_3 supported hybrids gave similar hydrocarbon distributions as a function of these variables. The trend of increased activity with Cu loading can be explained by the arguments as rationalised the behaviour of the $Co/Cu/Al_2O_3$ catalysts - a mixed Co^o/Cu^o metal species formed, the Cu^o content of which limited the H_2 available of CO hydrogenation by Co^o. The nature of the mixed Co^o/Cu^o species was probably similar on both $SiO_2$40Å and Al_2O_3 supports since the activities of the two hybrid sets, particularly with respect to hydrocarbon distributions, were much the same.

The screening data from the $Co/Cu/SiO_2$40Å catalysts provide less obvious evidence for the formation of mixed Co^o/Cu^o species than did the $Co/Cu/Al_2O_3$ results. No modification in the behaviour of Cu was observed for the $SiO_2$40Å systems. The $Cu/SiO_2$40Å catalysts were active towards the WGSR (see sections 4.4.3 and 4.4.4) just as the Cu^o species on the hybrids appear to have been. Nevertheless there were some key differences between the behaviour of the $SiO_2$40Å supported hybrid catalysts and the corresponding physical mixes which suggest that interaction between Co^o and Cu^o again occurred.

The patterns of CO_2 production with temperature differed markedly. Over $Co/Cu/SiO_2$40Å;10:10:100, for example, CO_2 production increased exponentially to 27% at 325°C. The increase was not as dramatic over the $Co/SiO_2$40Å;10:100 + $Cu/SiO_2$40Å;10:100 intimate mix (compare tables 4.4.4b and 4.4.5b). Coking therefore appears to have proceeded to a lesser extent on the physical mix.

Another difference occurred in the degree of hydrocarbon production at 325°C. There was a jump of hydrocarbon concentrations in moving from 300°C to 325°C over the physical mixes (see section 4.4.4). The same did not occur over the hybrid catalysts. Consequently the overall extent of hydrocarbon synthesis was, at 325°C, lower on $Co/Cu/SiO_2$40Å catalysts.

4.5 Summary

The TPR results suggested that mixed Co/Cu oxides formed on the hybrid $Co/Cu/SiO_2$40Å and $Co/Cu/Al_2O_3$ systems. It was postulated that these species formed a mixed Co^0/Cu^0 "alloy" when reduced. Screening data implied that no such direct interaction occurred on the physical mixes. The KE activities of the hybrid catalysts contrasted with the behaviour of the corresponding intimate mixes, reflecting the differences in the sets of TPR profiles.

Several oxidic species occurred on the Al_2O_3 supported hybrids. They were the mixed Co/Cu oxide, tetrahedral Co^{2+} and aluminates. The Co/Cu oxide was partially converted to aluminates as well as reduced to Co^0 and Cu^0 during activation whereas the other oxidic species remained intact. The $Co/Cu/SiO_2$40Å catalyst systems were simpler than the $Co/Cu/Al_2O_3$ analogues in terms of the distribution of the active metals. Just one oxidic species, the mixed Co/Cu oxide, seemed to be present on the calcined $SiO_2$40Å supported samples (see section 4.2.5). It was totally reduced during activation (see section 4.3.5).

The hybrid systems showed considerable promise as KE catalysts. All were more active than the benchmark catalyst, $Co/SiO_2$40Å;10:100. The $SiO_2$40Å supported hybrids produced twice the hydrocarbon concentration of the Al_2O_3 supported systems. The greatest activities for each set were obtained at high temperature (325°C) when the weight loadings of Co and Cu were both around 10%.

Not only were the activities relatively high, the product distributions of $Co/Cu/SiO_2$40Å;10:10:100 and $Co/Cu/Al_2O_3$; 10:10:100 were desirable. Methane production was suppressed, and both catalysts synthesised a high proportion of aromatic products compared to other longer chain (>C4) products. Aromatic compounds are valuable to the pretrochemical industry. They have a higher octane rating than the straight chain aliphatic analogues and are therefore used as boosters in transport fuels (Larkins, 1985). The desirable activity was unique to the hybrid catalysts, and was probably associated with the mixed Co/Cu species present on these systems.

5 THE CATALYTIC PERFORMANCE OF $Co/Cu/SiO_2$ 40Å;10:10:100

5.1 Introduction

In Chapter 4 it was established that $Co/Cu/SiO_2$ 40Å;10:10:100 was an active KE catalyst and that the hydrocarbon distributions it gave were favourable, particularly in terms of the concentration of aromatics produced. After consideration of these factors, it was decided to investigate the effect of feed composition on catalytic performance.

The screening method used in this section of the work was more thorough than for preliminary screening (see section 3.3.2). Concentrations of H_2 were measured in addition to CO, CO_2 and C1 to C3 hydrocarbons. Detailed hydrocarbon analysis was carried out as a matter of course. Such complete product analysis was necessary to obtain information regarding the relative rates of the WGSR, the FTR and the Boudouard reaction. Thereby it was hoped to gain some insight into the KE mechanism.

The investigation was also warranted on applied chemistry grounds. By adjustment of the conditions it was hoped to maximise selectivity towards aromatics while minimising the formation of undesirable products such as coke and methane. A catalyst which selectively synthesises aromatic hydrocarbons using a CO/H_2O feed would be commercially viable. High selectivity is more important than high conversions. Separation of products on an industrial scale incurs much expense. Increasing conversion, by recycling the feed or lifting the pressure for example, is not such an expensive proposition.

A similar study has been carried out by Chaffee and Loeh (1986) using a Ni/SiO_2 catalyst. The main body of the work was a detailed analysis of C8 hydrocarbon distributions and how these changed as a function of reaction conditions. Comments were also made regarding variations in the extent of H_2 production *via* the WGSR. These comments were not backed up by direct measurement of H_2 concentrations, and in quantifying the ideas the Boudouard reaction was ignored. In the current study the roles of the WGSR and the Boudouard reaction were more carefully evaluated.

5.2 Experimental Variables

The $Co/Cu/SiO_2$;10:10:100 catalyst was screened at 250°C, 275°C, 300°C and 325°C with $CO:H_2O$ ratios in the feed gas of 3:1, 2:1, 1:1, 1:2 and 1:3. Five separate experiments were performed. For each experiment the $CO:H_2O$ ratio was fixed and the reactor temperature adjusted (see section 3.3.1).

The desired $CO:H_2O$ ratios were obtained by setting the water bath (refer to fig. 3.3.1) to appropriate temperatures. When the $CO:H_2O$ ratio was 3:1, for example, the bath temperature was adjusted to 65.3°C. The vapour pressure of H_2O was, therefore, 190 mm Hg (CRC Handbook, 1974-1975). Since the apparatus operated at atmospheric pressure, the partial pressure of CO in the feed was 570 mm Hg (760 mm Hg less 190 mm Hg), three times the partial pressure of H_2O. When the bath temperature was 92.2°C, the $CO:H_2O$ ratio was 1:3 using the same rationale. In this situation the relative CO and H_2O partial pressures were 190 mm Hg and 570 mm Hg respectively.

The CO flow was held constant for all the experiments at 5.00 ml/min (see section 3.3). Consequently, the overall flow rate of the CO/H_2O feed changed with varying $CO:H_2O$ ratio. At a ratio of 3:1, for example, the overall flow was 6.67 ml/min (5 ml/min plus a third of 5 ml/min). Similarly, at a $CO:H_2O$ ratio of 1:3, the overall flow was 20 ml/min.

Thus inherent to the change in $CO:H_2O$ ratio was alteration in three other variables; CO partial pressure, H_2O partial pressure and overall flow rate.

5.3 Presentation of Data

The hydrocarbon distributions and overall mole % CO conversion figures are given in figs. 5.3.1 - 5.3.5 and tables 5.3.1 - 5.3.5. The overall conversion figs. are represented graphically in figures 5.3.6 - 5.3.9. The % CO conversion figures are plotted cumulatively as a function of feed composition. The difference between the baseline and % CO conversion to H_2 line represents the extent of the WGSR. The difference between the % CO conversion to H_2 line and the % CO conversion to hydrocarbons (HCs) + H_2 represents the extent of the KE synthesis. Finally, the difference between the % CO conversion to HCs + H_2 line and the % CO conversion to carbon + HCs + H_2 represents the extent of the Boudouard reaction. The % CO conversion to carbon + HCs + H_2 was the overall conversion.

Values of % CO conversion to hydrocarbons (*via* the KE synthesis), hydrogen (*via* the WGSR) and coke (*via* the Boudouard reaction) were calculated from the absolute product concentrations measured (see Appendix 2). The effluent H_2 was H_2 produced in excess of that consumed by the FTR. These effluent levels may not necessarily correlate with H_2 concentrations within the catalyst bed.

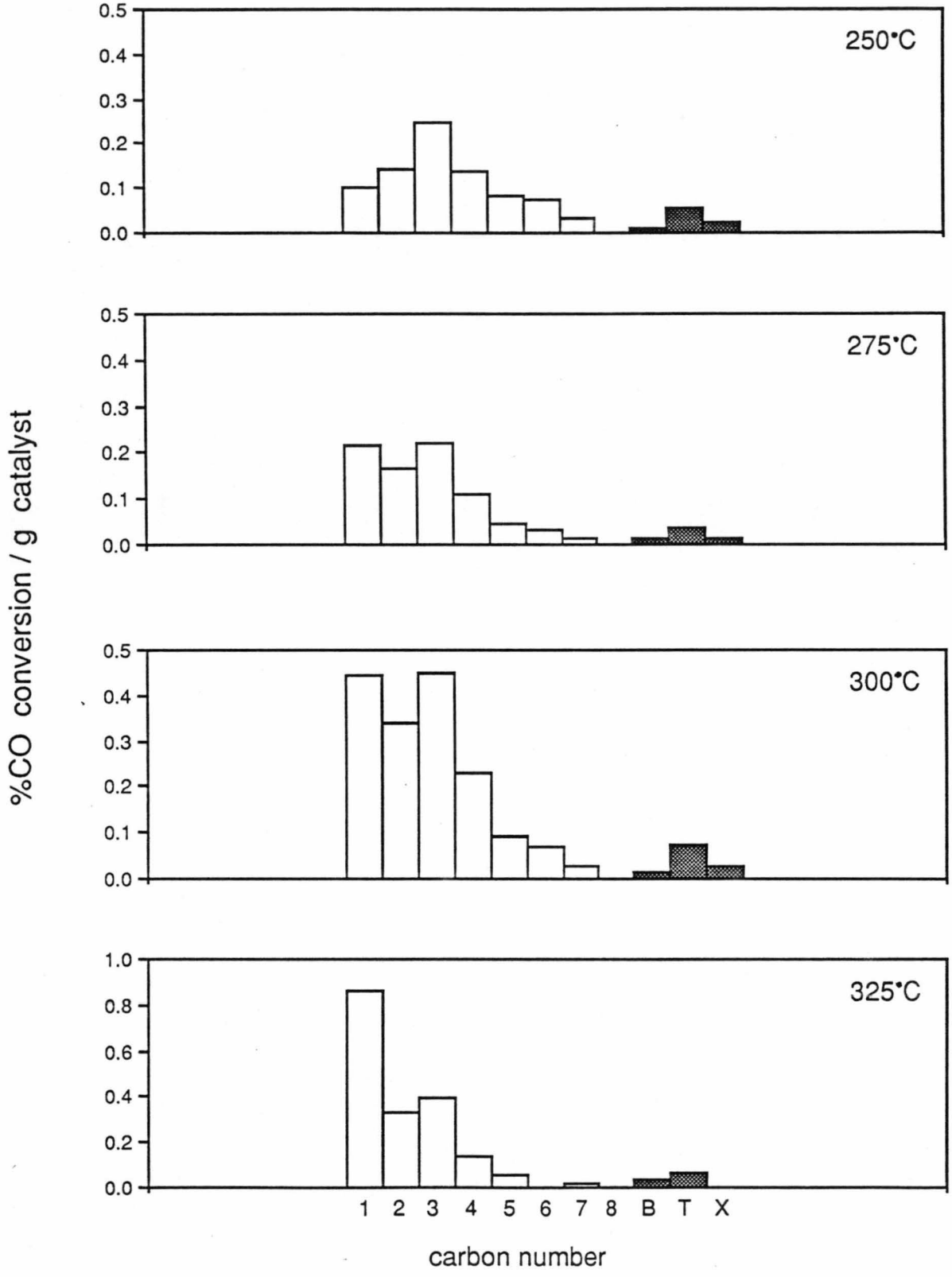

fig. 5.3.1 %CO conversions to hydrocarbons at a CO:H_2O ratio of 3:1.

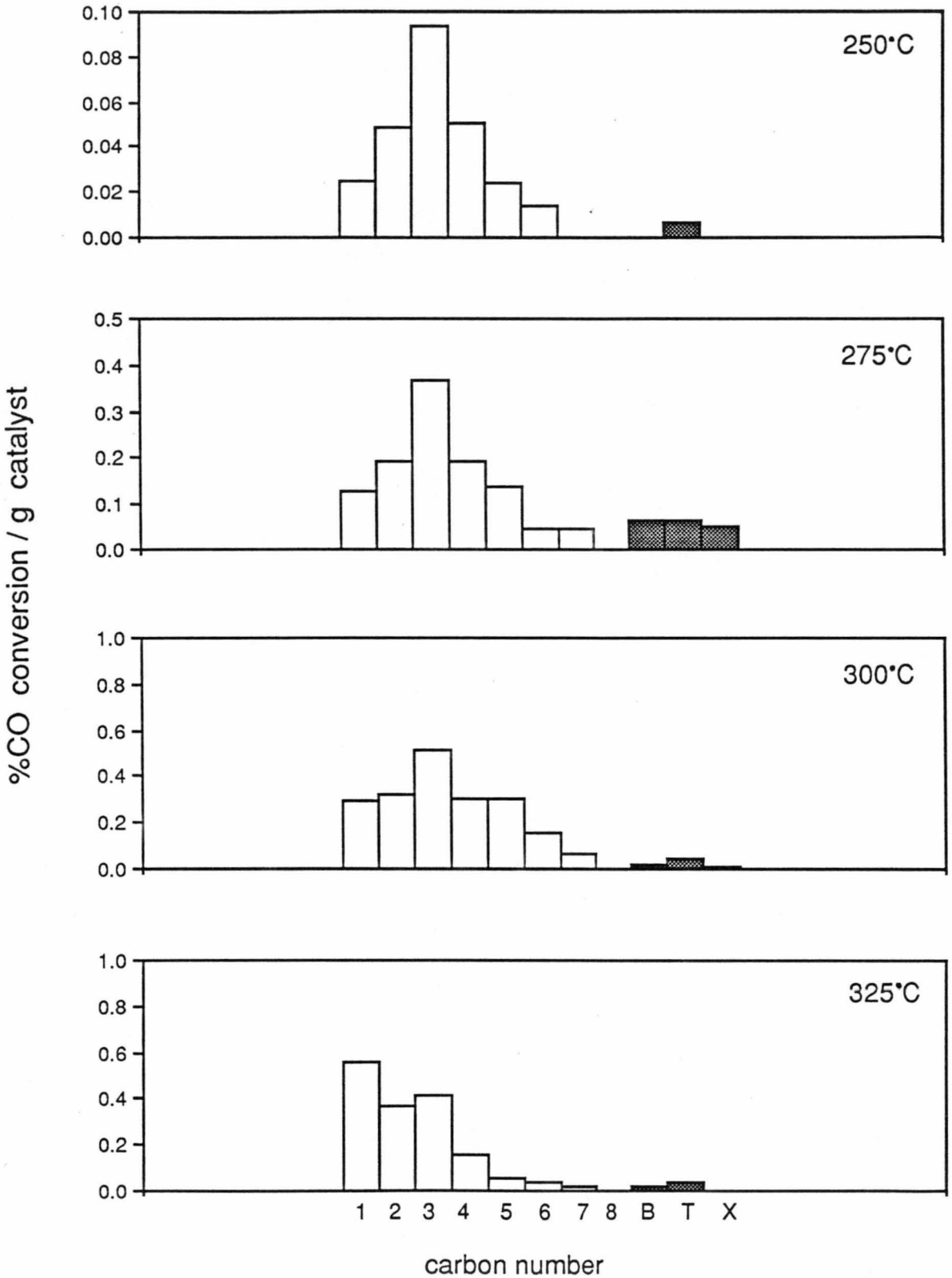

fig. 5.3.2 %CO conversions to hydrocarbons at a CO:H_2O ratio of 2:1.

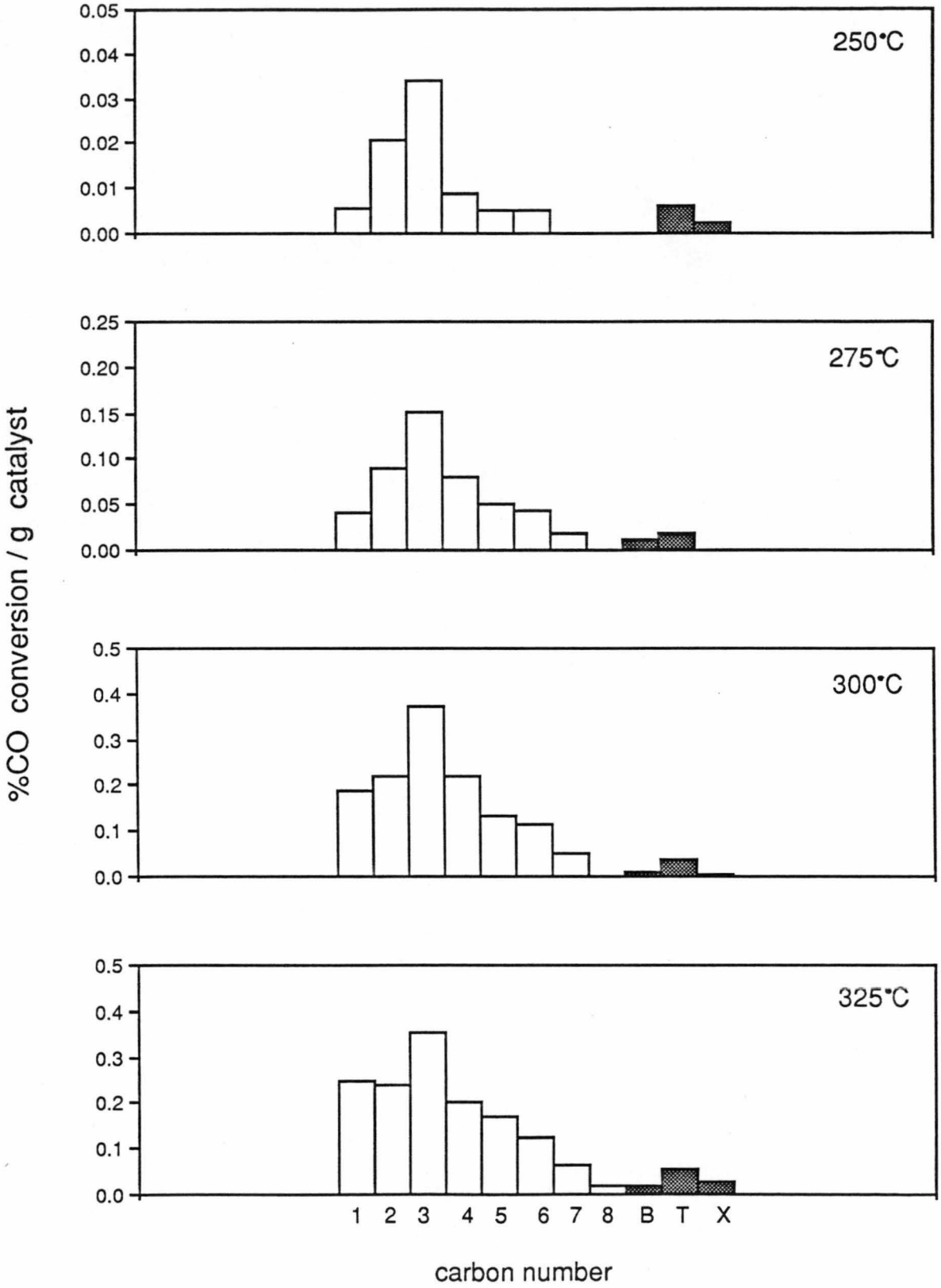

fig. 5.3.3 %CO conversions to hydrocarbons at a CO:H_2O ratio of 1:1.

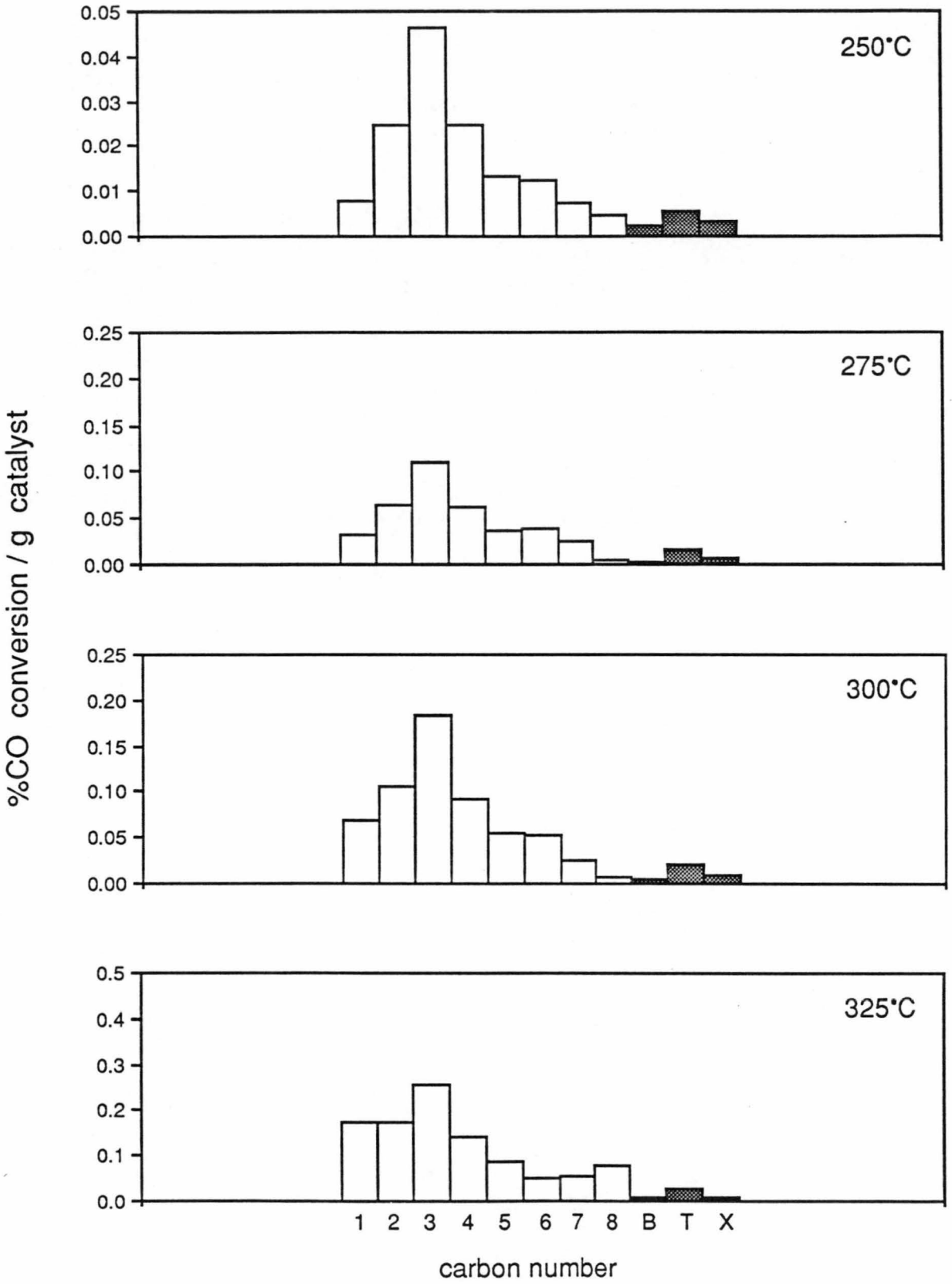

fig. 5.3.4 %CO conversions to hydrocarbons at a CO:H_2O ratio of 1:2.

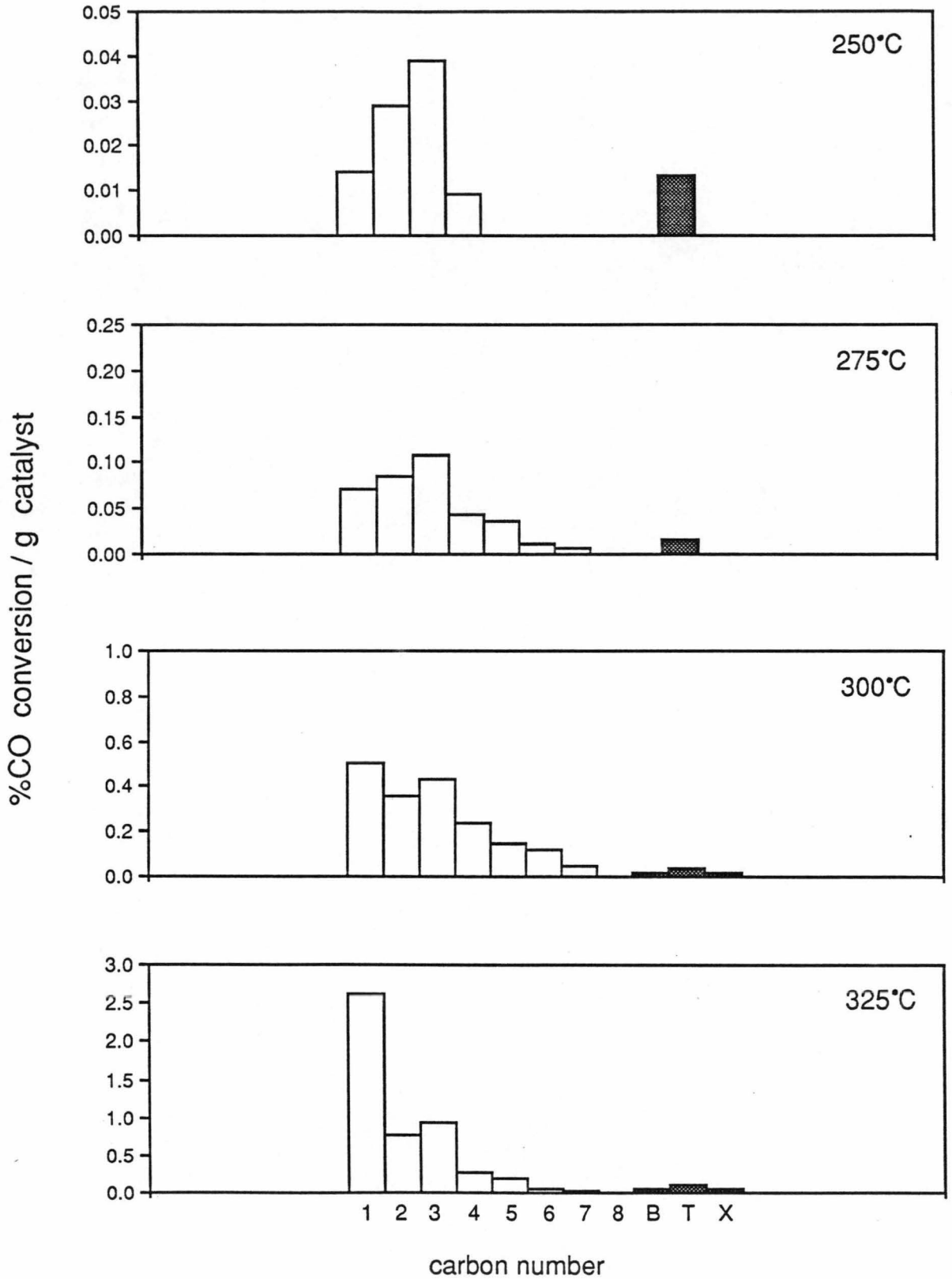

fig. 5.3.5 %CO conversions to hydrocarbons at a CO:H_2O ratio of 1:3.

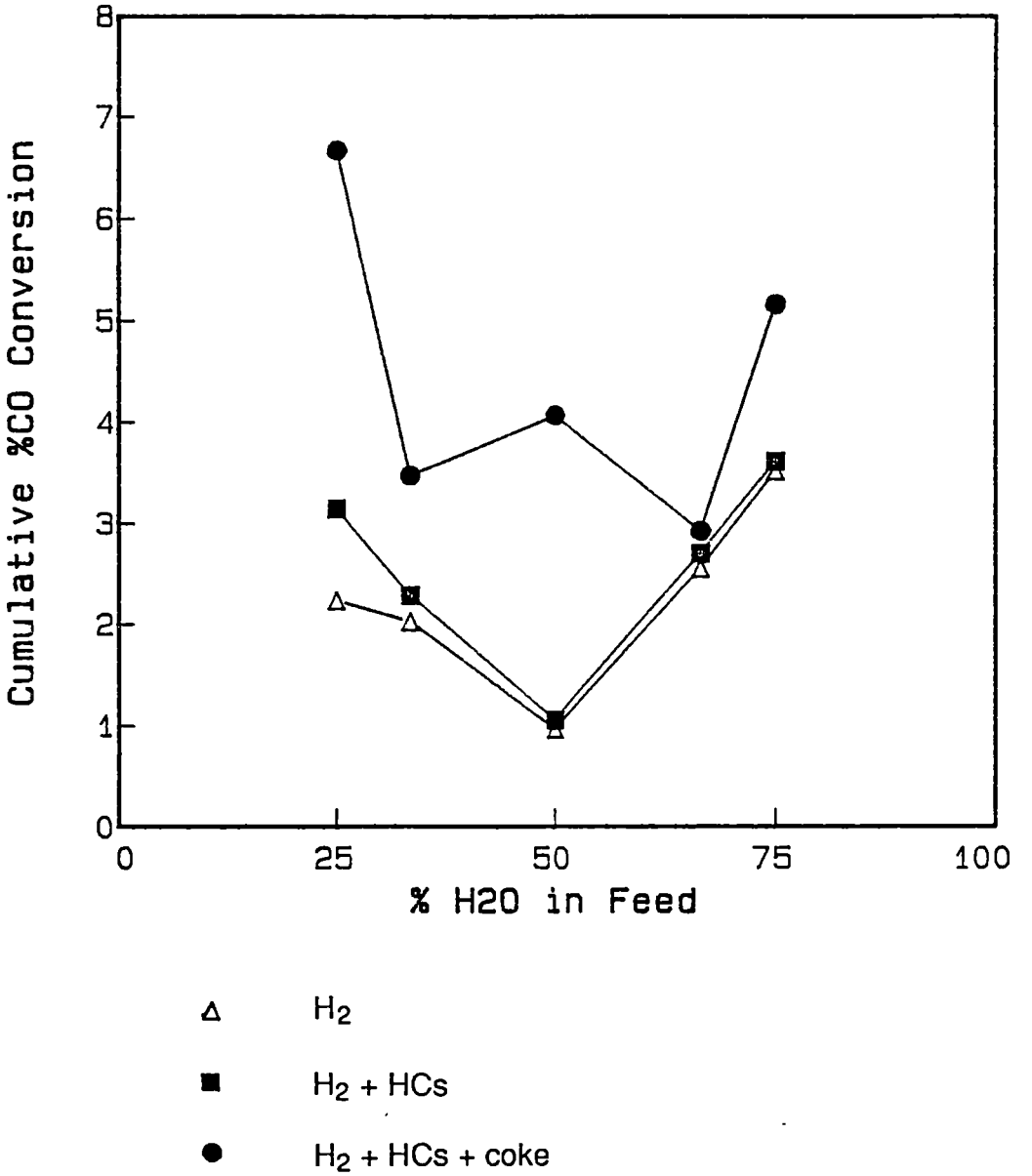

fig. 5.3.6 Cumulative %CO conversions as a function of feed composition at 250°C.

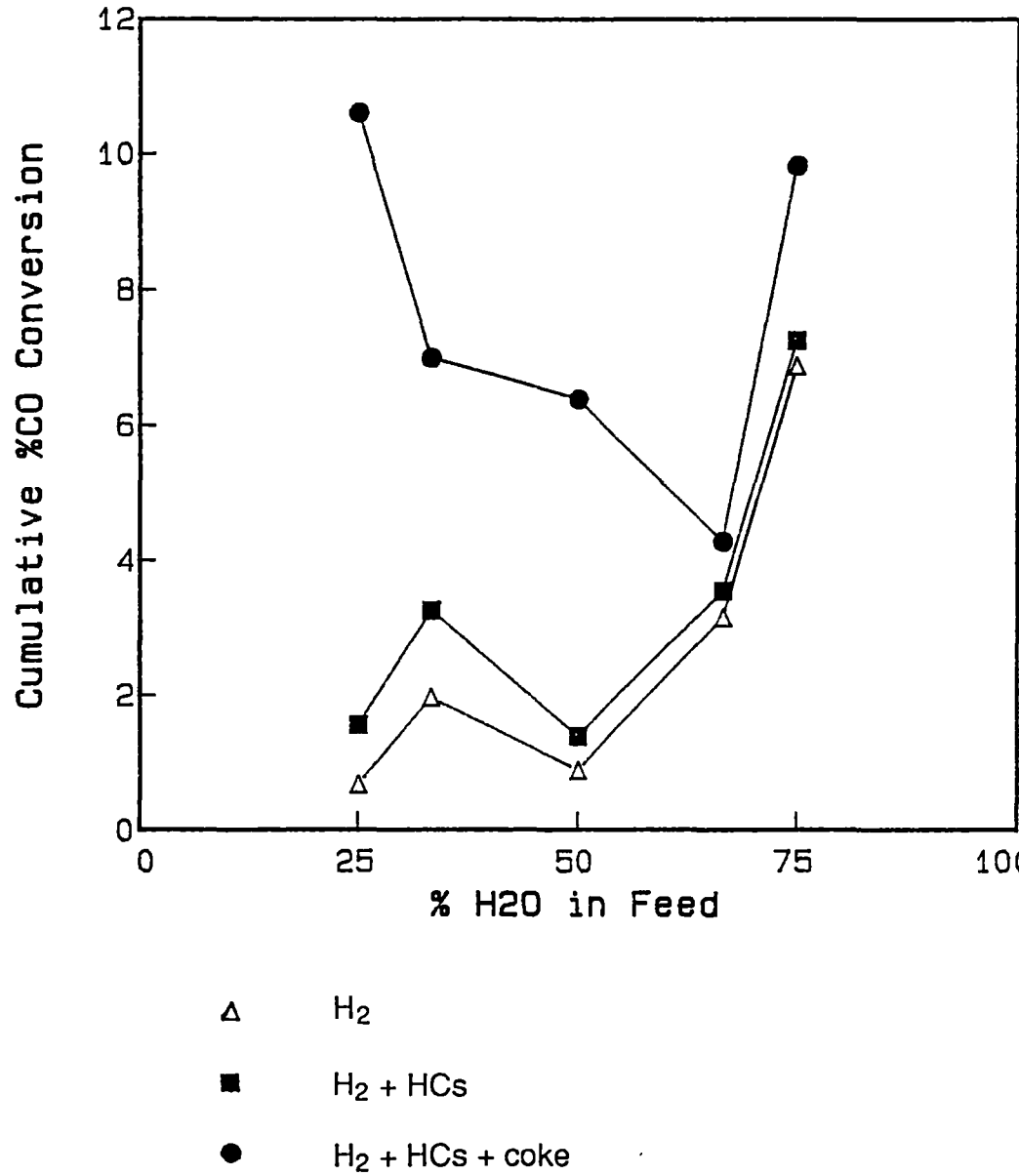

fig. 5.3.7 Cumulative %CO conversions as a function of feed composition at 275°C.

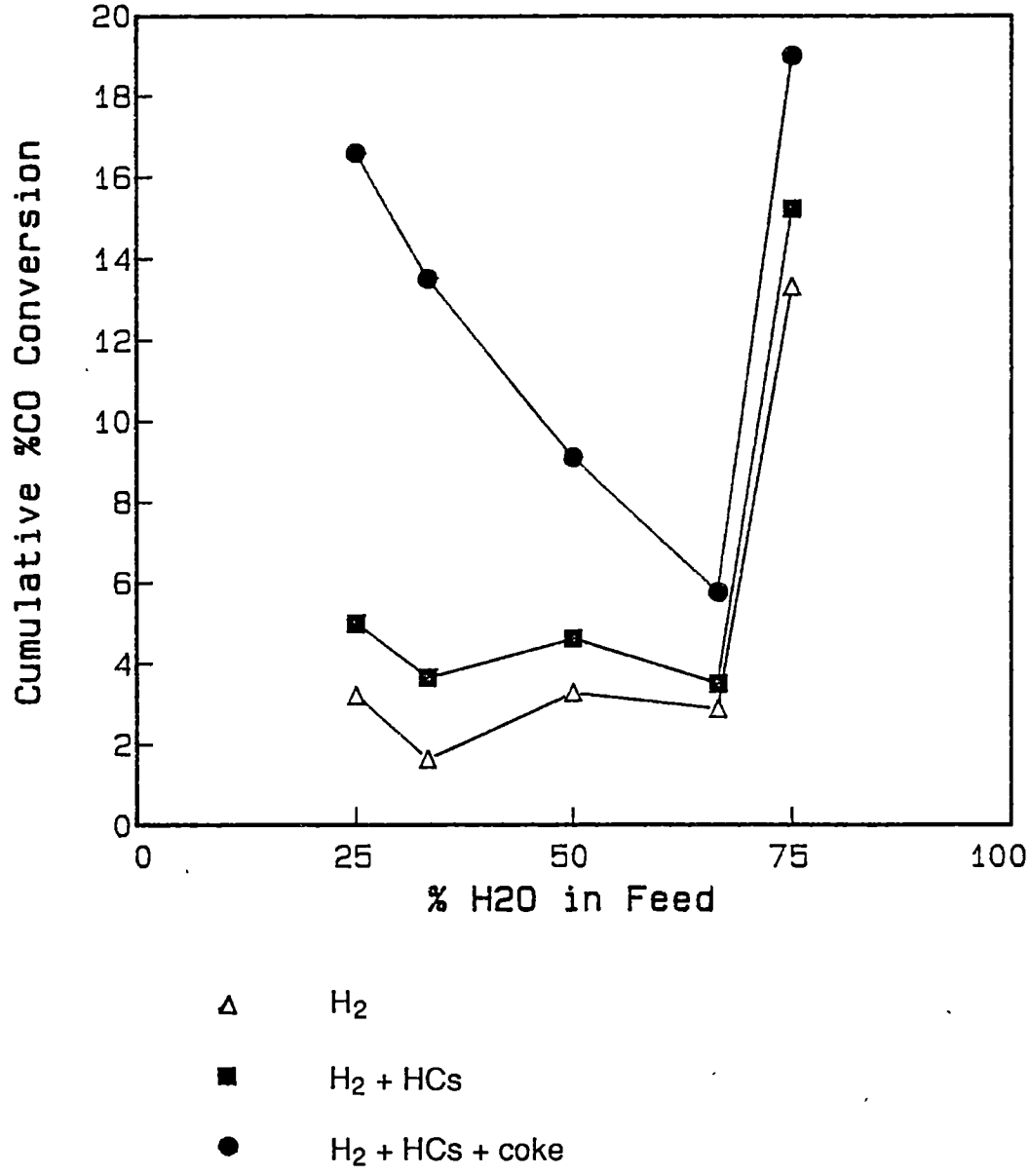

fig. 5.3.8 Cumulative %CO conversions as a function of feed composition at 300°C.

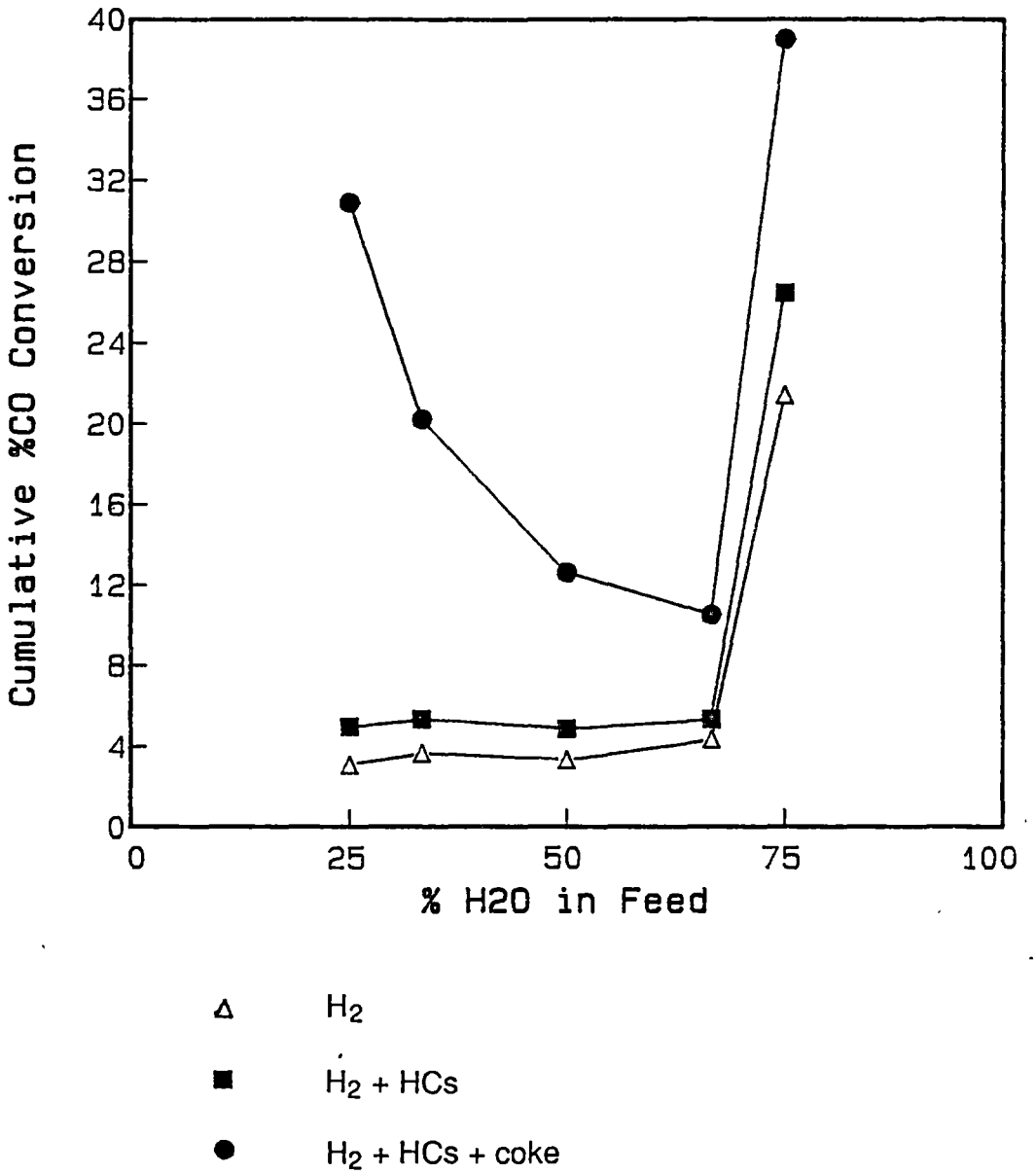

fig. 5.3.9 Cumulative %CO conversions as a function of feed composition at 325°C.

% conversion/g	250°C	275°C	300°C	325°C
hydrocarbons	0.906	0.874	1.77	1.88
H_2	2.23	0.674	3.20	3.06
carbon	3.53	9.10	11.6	26.0

Table 5.3.1 % CO conversions at a CO:H_2O feed ratio of 3:1.

% conversion/g	250°C	275°C	300°C	325°C
hydrocarbons	0.262	1.29	2.02	1.68
H_2	2.02	1.96	1.62	3.64
carbon	1.19	4.46	9.85	14.9

Table 5.3.2 % CO conversions at a CO:H_2O feed ratio of 2:1.

% conversion/g	250°C	275°C	300°C	325°C
hydrocarbons	0.0873	0.504	1.34	1.54
H_2	0.959	0.878	3.27	3.31
carbon	3.02	5.00	4.49	7.78

Table 5.3.3 % CO conversions at a CO:H_2O feed ratio of 1:1.

% conversion/g	250°C	275°C	300°C	325°C
hydrocarbons	0.152	0.399	0.622	0.998
H_2	2.55	3.14	2.87	4.33
carbon	0.220	0.727	2.26	5.17

Table 5.3.4 % CO conversions at a CO:H_2O feed ratio of 1:2.

% conversion/g	250°C	275°C	300°C	325°C
hydrocarbons	0.102	0.377	1.91	5.04
H_2	3.51	6.87	13.3	21.4
carbon	1.55	2.57	3.78	14.4

Table 5.3.5 % CO conversions at a CO:H_2O feed ratio of 1:3.

5.4 Activity as a Function of Feed Composition

5.4.1 The "Regime" Interpretation

Similar changes in product distributions occurred with variation of the $CO:H_2O$ ratio at each of the four temperatures (250^oC, 275^oC, 300^oC, 325^oC) studied. The changes in behaviour of the $Co/Cu/SiO_2$40Å;10:10:100 catalyst which occurred as a function of feed composition thus applied, and are discussed, generally.

The levels of effluent H_2 did not significantly alter in moving from a $CO:H_2O$ ratio of 3:1 to 1:2 (refer to figs 5.3.6 - 5.3.9, tables 5.3.1-5.3.5). A jump in H_2 concentrations occurred once the $CO:H_2O$ ratio reached 1:3.

Overall hydrocarbon yields decreased gradually in moving from a $CO:H_2O$ ratio of 3:1 to 1:2. The decrease in % CO conversion to hydrocarbons at 325^oC for example, was never greater than 50% between successive $CO:H_2O$ ratios. Once the $CO:H_2O$ ratio reached 1:3 a marked increase in overall % CO conversion to hydrocarbons occurred, accompanying the lift in H_2 levels (refer to tables 5.3.1 - 5.3.5, figs 5.3.6 - 5.3.9). At 325^oC there was a 5-fold increase in hydrocarbon levels on moving from a $CO:H_2O$ ratio of 1:2 to 1:3. The increase was due to raised levels of light products, particularly methane (refer to figs. 5.3.1 - 5.3.5).

The overall % CO conversions also decreased in the $CO:H_2O$ range of 3:1 to 1:2 (refer to figs. 5.3.6 - 5.3.9). The jump in activity occasioned by changing the $CO:H_2O$ ratio to 1:3 meant that the overall conversions at 3:1 and 1:3 were similar. In the water rich ($CO:H_2O$ 1:3) conditions most of the CO conversion was associated with H_2 and HC production. However in the CO rich conditions ($CO:H_2O$ 3:1) most conversion was associated with coke production. There appear to have been distinct regimes at the extremes of the $CO:H_2O$ water ratio range.

The behaviour of the $Co/Cu/SiO_2$40Å;10:10:100 catalyst at the intermediate $CO:H_2O$ ratios was similar to that at a ratio of 3:1, particularly with respect to H_2 levels and hydrocarbon distributions (refer to figs 5.3. 1-5.3.5, tables 5.3.1 - 5.3.5). This group of conditions ($CO:H_2O$ = 3:1, 2:1, 1:1, 1:2) can be classified together as the "CO rich regime". The behaviour at a $CO:H_2O$ ratio of 1:3, the "H_2O rich regime", was

exceptional. The regimes must be regarded as separate since catalytic activity within each was altogether different. Such an interpretation has not previously been put forward in the literature and correspondingly a jump in activity at high H_2O partial pressures has not been observed.

5.4.2 The CO Rich Regime ($CO:H_2O$ = 3:1 - 1:2)

Conversion to H_2

The constancy of H_2 levels suggesting that H_2 concentration reached a lower limit, below which its incorporation into hydrocarbons did not occur. The levels of H_2 in the effluent, and consequently % CO conversion to H_2 values, were a measure of this lower limit rather than the actual degree of H_2 production. In this case, the WGSR can be regarded as the rate determining step of the KE synthesis despite the presence of slight excess H_2.

The concentration of H_2 within the bed is known to determine the extent of hydrocarbon synthesis (Kolbel and Ralek, 1984). Thus the hydrocarbon levels indirectly reflect the internal quantities of H_2. The % CO conversion to HCs values are therefore a more valid measure of internal H_2 production than the %CO conversion to H_2 values derived from effluent H_2 concentrations (see section 5.3).

Conversion to Hydrocarbons

The decrease in hydrocarbon yields can partly be attributed to the concomitant increase in flow rates (see section 5.2). A change in flow rate by some factor typically sees a change in residence time, and thus conversion, by the reciprocal of that factor. This general rule applies when conversion is not maximal, which was certainly the case in the CO rich regime. The maximum %CO conversion observed was just 30.9% which occurred in the $CO:H_2O$ 3:1 feed at a temperature of 325°C.

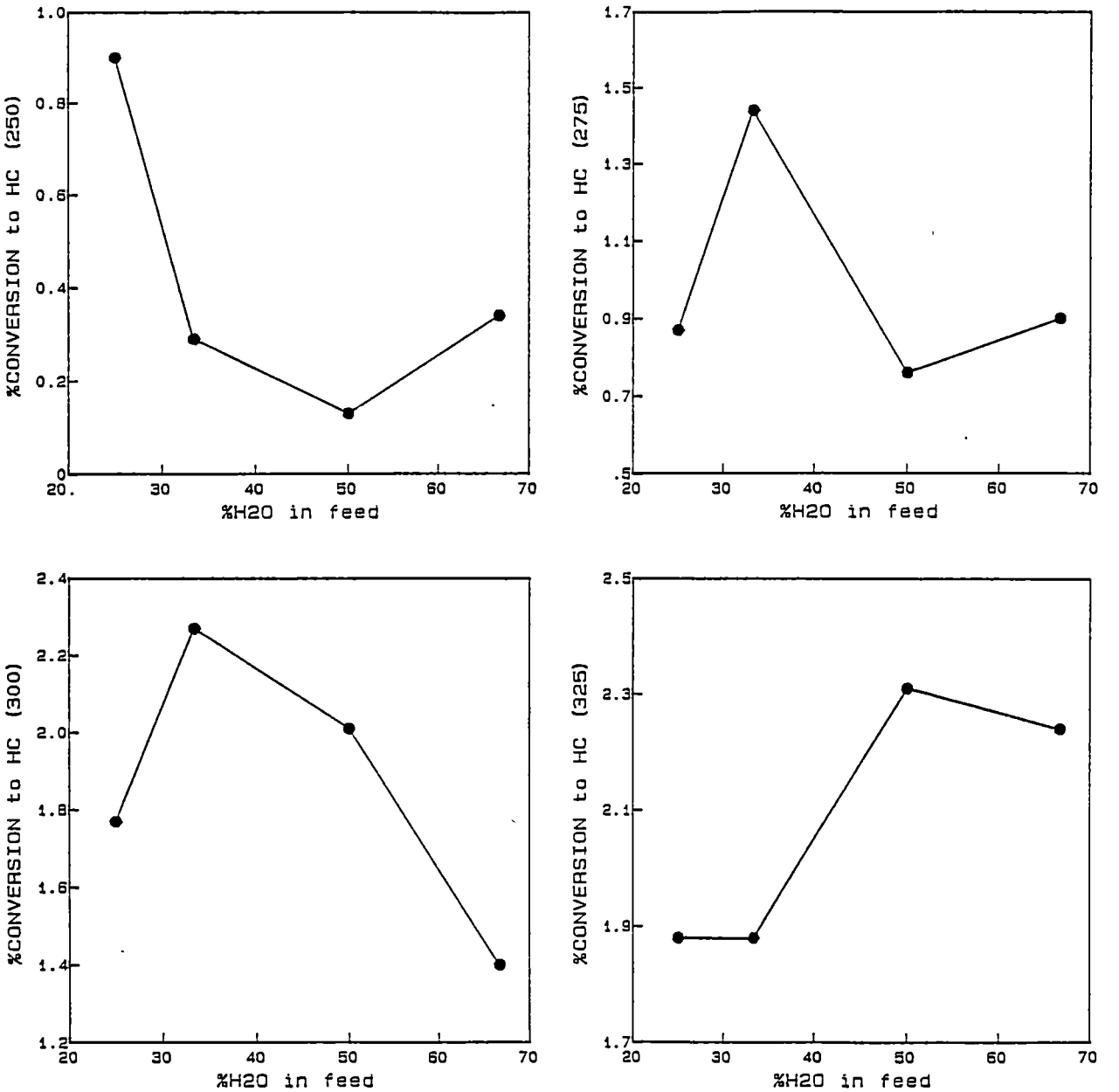

fig. 5.4.2a %CO conversions to hydrocarbons corrected for flow rates.

A correction for this consideration was applied and the modified %CO conversion to hydrocarbon are plotted in fig. 5.4.2a. The % CO conversion to HCs figures were scaled relative to the flow rate at a CO:H_2O ratio of 3:1 (*i.e.* 6.67 ml/min). At each of the CO:H_2O ratios, the conversion values were multiplied by the feed flow at that ratio, and divided by 6.67 ml/min. An increase in conversion with the relative proportion of water shows up. No consistent trends emerge. At 250°C conversions declined as the partial pressure of H_2O increased. At 325°C, conversions increased with the partial pressure of H_2O. At 275°C and 300°C corrected to %CO conversion to HCs values were maximal at a CO:H_2O ratio of 2:1.

At any instant the rate law for the KE synthesis is of the form:

$$R = k_1[CO]^a[H_2O]^b + k_2[CO]^c[H_2]^d \qquad \text{eqn. 5.4.2}$$

(Kolbel and Ralek, 1984). This expression requires integration to find the average rate. The %CO conversions to HCs effectively represent the average rate. The absence of consistent trends in normalised conversions shows that the values of the rate constants (k_1, k_2) and the concentration exponents (a, b, c, d) varied incongruously as a function of temperature. The precise values of these parameters, together with feed composition and flow rate, fix the precise hydrocarbon yield for a particular set of conditions.

Chaffee and Loeh (1986) quoted similar trends pertaining to hydrocarbon yields as occurred within the CO rich regime. In moving from a CO:H_2O ratio of 4.3:1 to 1:1, CO conversion to hydrocarbons decreased. Also as space velocity (and hence flow rates, assuming a constant sample size) decreased, hydrocarbon yields increased. The flow rate of CO did not appear to be held constant in the study and thus flow rates and CO:H_2O ratios were treated as independent variables rather than dependent as in the current work (see section 5.2). This difference complicates direct comparison of results.

Conversion to Coke

Coking is represented by the difference between the % CO conversion to carbon + HCs +H_2 and the % CO conversion to HCs +H_2 lines in figs. 5.3.6 - 5.3.9. Clearly coking decreased in moving from a CO:H_2O ratio of 3:1 to 1:2.

The decline can, to an extent, be rationalised by increased flow rates. Normalised % CO conversion to carbon figures are plotted in fig 5.4.2b. Despite this correction, downward trends are still exhibited at each temperature. Factors other than altered flow rates must also have contributed to the decline.

Kinetic considerations dictate that the rate of the Boudouard reaction would have declined as the partial pressure of CO was lowered. This was probably the major reason for the decline in coking rates. Other factors which may have contributed were the competition with CO by H_2O for catalyst sites, and the removal by H_2O of coke precursors and/or adsorbed carbon. As the partial pressure of H_2O was increased (see section 5.2) these processes would have proceeded more rapidly. Such reasons have been postulated to rationalise the inhibition of coking on supported Co (Kolbel and Ralek, 1984; Tottrup, 1976) and Ni (Gardner and Bartholomew, 1981; Anderson, 1984) systems.

Overall Conversions

In the CO rich regime (CO:H_2O 3:1 to 1:2), the overall %CO conversions (as expressed by the %CO conversion to coke + HCs+H_2 in figs. 5.3.6 - 5.3.9) declined as the CO:H_2O ratio was lowered. After correction for the flow rate considerations, the same trend still emerged (refer to fig. 5.4.2a). The only reaction which was slowed when the flow rates were taken into account was the Boudouard reaction. The decrease in the rate of this reaction was, therefore, entirely responsible for the decrease in normalised overall % CO conversions. The increase in flow rates caused by lowering the CO:H_2O ratio (see section 5.2) was partly responsible, along with the decrease in the rate of the Boudouard reaction, for the decrease in absolute overall % CO conversions.

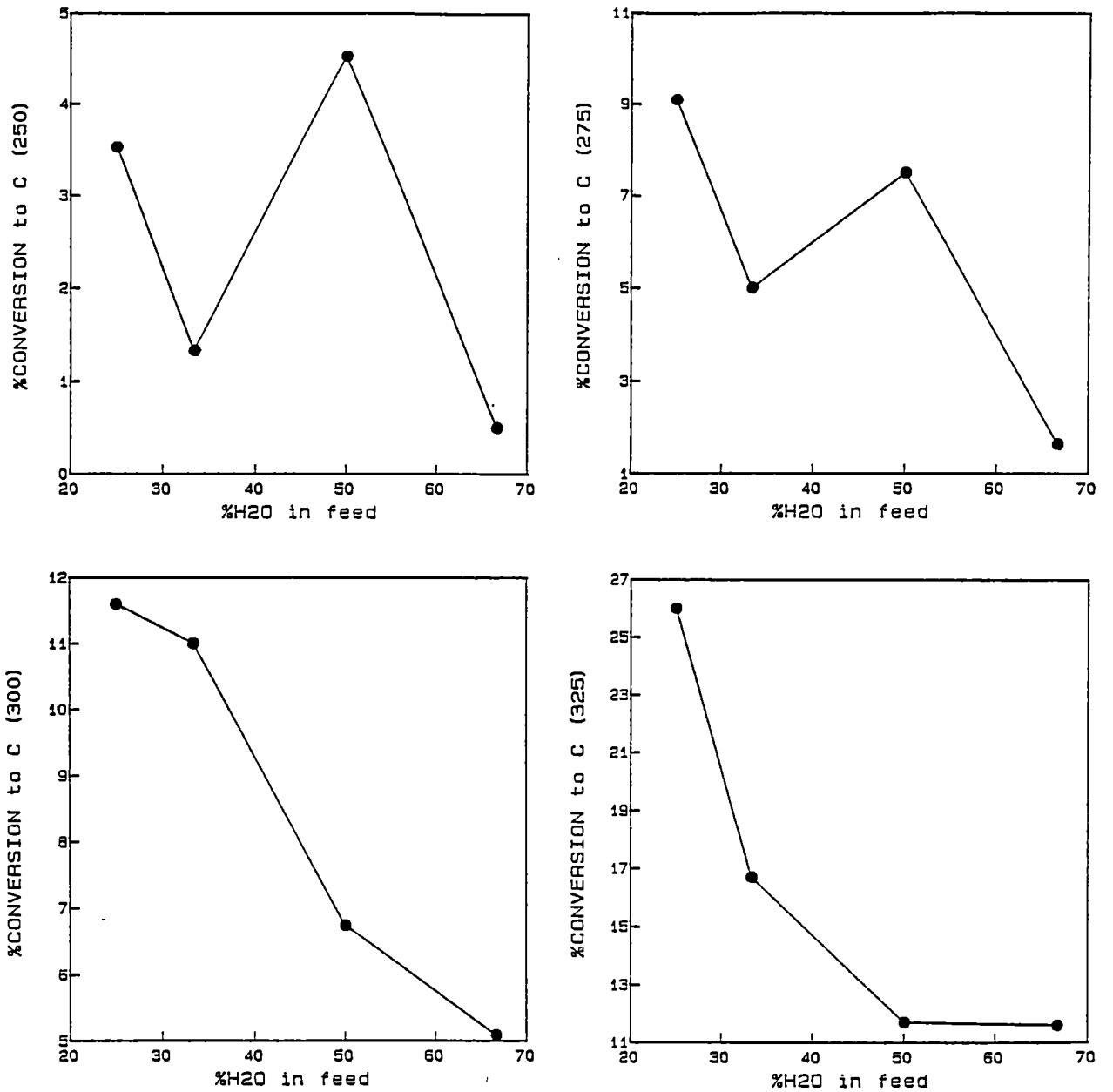

fig. 5.4.2b %CO conversions to coke corrected for flow rates.

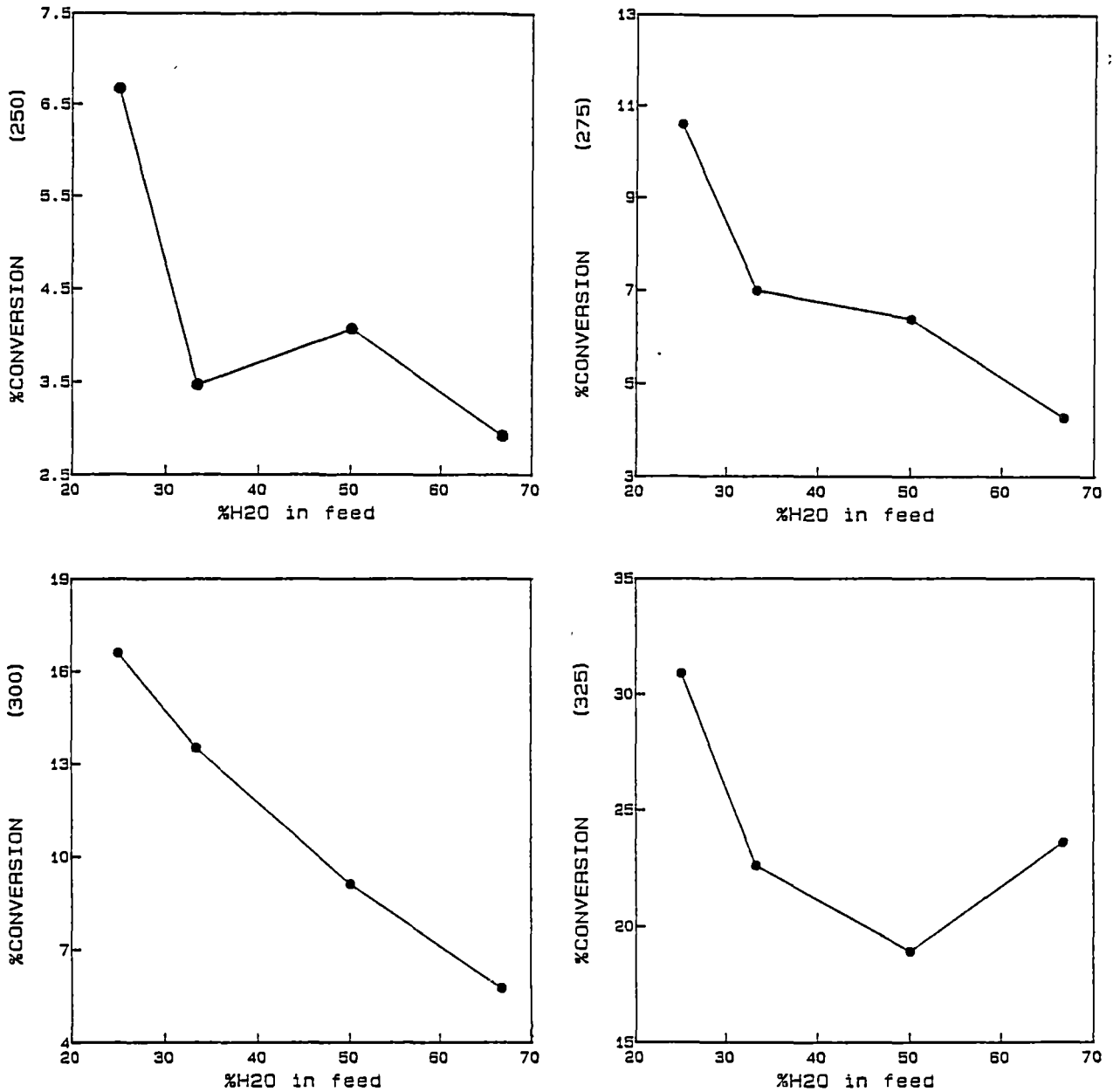

fig. 5.4.2c Overall %CO conversions corrected for flow rates.

5.4.3 The H_2O Rich Regime ($CO:H_2O$ = 1:3)

The change of CO and H_2O partial pressures in moving from a $CO:H_2O$ ratio of 1:2 to 1:3 was no more significant, in absolute numerical terms, than the changes caused by the other adjustments of the feed make-up. The magnitude of the deviation in product distributions (see section 5.4.1) shows that significant changes did occur in the relative rates of the reactions constituting the KE synthesis.

In particular, the rate of the WGSR must have increased dramatically in the H_2O rich environment. The higher levels of effluent H_2 directly manifest this fact. The production of such levels of excess H_2 indicates that the FTR, rather than the WGSR, was the rate determining step of the water rich KE synthesis. In the CO rich regime, the reverse applied. The WGSR still did not closely approach equilibrium conversions. The value of K_p ([P CO_2] [P H_2]/[P CO] [P H_2O]) at 325°C, the temperature at which the WGSR was closest to equilibrium, equalled 4.17×10^{-2} (see Appendix 3). The equilibrium value is 48 (Gustafson, 1981).

The higher hydrocarbon levels (refer to figs. 5.3.1 - 5.3.5) demonstrate that an increase in H_2 levels within the catalyst bed also occurred. The product distribution is consistent with high partial pressures of H_2. Such conditions are comparable to a FT environment and the synthesis of low molecular weight hydrocarbons is known to be favoured under these circumstances (Dry, 1984).

The extent of coking was comparable to that which occurred at $CO:H_2O$ ratios of 1:1 and 1:2 (compare tables 5.3.3, 5.3.4 and 5.3.5). The same factors which may have contributed to the decreased coking rates as H_2O levels were raised in the CO rich regime (low CO partial pressure, H_2O competition with CO for catalyst sites and reaction with coke - see section 5.4.2), rationalise, in part, this behaviour. The high H_2, levels unique to the H_2O rich regime, may also have decreased carbon deposition. Hydrogenation of coke in such conditions is known to proceed, and methane is the major product (Araki and Ponec, 1976; Wentreck *et al.*, 1976; Rabo *et al.*, 1978; Sachtler *et al.*, 1979; Biloen *et al.*, 1979). Some of the methane observed may well have been produced in this way.

The major change in activity in moving from the CO rich to H_2O rich regimes was probably associated with an alteration in the structure of Co/Cu/$SiO_2$40Å;10:10:100. Increased H_2 levels can be used to rationalise such an alteration. The number of sites active towards the WGSR may have been proportional, beyond some critical concentration, to the ambient levels of H_2. Were this critical concentration exceeded, the production of H_2 would result in the evolution of more active sites which, in turn, would result in the formation of more H_2 and so on. An increase in H_2 levels would thus become a self-perpetuating process up to some limiting value. The critical concentration idea explains why the small perturbation in conditions occasioned by changing the CO:H_2O ratio from 1:2 to 1:3 was accompanied by a significant change in activity. Whether or not the critical H_2 concentration was exceeded may have been sensitive to the CO:H_2O ratio, or any other parameter.

The same reasoning can be applied to explain the activity jump observed in moving from a temperature of 300°C to 325°C when the $SiO_2$40Å supported physical mixes were screened (see section 4..4.4). An increase in H_2 levels as the result of an increase in the rate of the WGSR was probably related to the behaviour observed. However this was not confirmed by direct H_2 measurement.

5.5 The Effect of Temperature

The general effects of temperature on product yields were the same whatever the CO:H_2O ratio. Conversion figures respond to increased temperature according to the Arrhenius equation - higher temperatures resulted in higher effluent levels of total hydrocarbon products, CO_2 and H_2.

Product distributions, as well as overall yields, were influenced by temperature. The proportion of coking as a fraction of overall % CO conversion increased with temperature. Graphically this is represented in figs. 5.3.6 - 5.3.9 by the greater comparative magnitude of the difference between the % CO conversion to carbon + HCs + H_2 and the % CO conversion to HCs + H_2 lines relative to the modulus of the % CO conversion to carbon + HCs + H_2 values at varying temperatures and a fixed CO : H_2O ratio. This shows that the rate of Boudouard reaction increased more rapidly as a function

of temperature than did the rates of the WGSR and hydrocarbon producing reactions. This feature is generally accepted to apply for the KE synthesis (Kolbel and Ralek, 1984).

The increase in relative coking rates was accompanied by increased yields of aromatic hydrocarbons, particularly toluene. Methane and C2 and C3 hydrocarbon yields were raised simultaneously. In contrast, the levels of aliphatic C4 to C8 molecules dropped (refer to figs. 5.3.1 - 5.3.5).

An increase with temperature in the proportion of low molecular weight hydrocarbons relative to longer chain linear products has frequently been reported (Kolbel and Ralek, 1984). An equivalent relationship is that the probability of chain growth decreases with temperature. A categorical assertion of increased aromatic yields with temperature has not previously been made.

The temperatures at which Co/Cu/$SiO_2$40Å;10:10:100 was systematically investigated (250°C through 325°C) are high compared to those used in previous work on the screening of KE catalysts. Most of these studies have focussed on the 200°C to 240°C region. The lack of high temperature studies is symptomatic of the general lack of interest in the KE synthesis. In the better researched field of FT catalysis, screening temperatures have ranged from 180°C to greater than 450°C (Anderson, 1984).

5.6 Hydrocarbon Distributions

5.6.1 Relative Patterns

Within the CO rich regime (see section 5.4.2) the relative % conversions to the various hydrocarbon fractions were similar at each individual temperature and feed ratio. In the H_2O rich regime the Co/Cu/$SiO_2$40Å;10:10:100 catalyst gave markedly different overall product and hydrocarbon distributions (see sections 5.4.1 and 5.4.3) . The patterns of hydrocarbon distribution within the CO and H_2O rich regimes are discussed in this section of the work and the mechanistic ramifications are evaluated.

5.6.2 The Suppression of Methane

In the CO rich regime, the production of methane was generally suppressed, probably as a result of low ambient H_2 partial pressures. The rate of the methanation reaction is directly proportional to the partial pressure of H_2 (Kolbel and Ralek, 1984). The % CO conversions to H_2 and overall hydrocarbons were only approximately 3% and 1% respectively (refer to tables 5.3.1 - 5.3.4), results which also suggest that internal H_2 concentrations were low. Methanation, as would be expected (Kolbel and Ralek, 1984), increased with temperature.

In the H_2O rich regime, methane suppression did not occur. The maximum % CO conversion to methane was 2.61%, obtained at a temperature of 325°C. The WGSR was producing a lot of excess H_2 under these conditions (see section 5.4.3) which explains the high methane yields.

5.6.3 The Suppression of C2 Formation

At temperatures above 250°C in the CO rich regime, the levels of C2 hydrocarbons were less than both methane and C3 hydrocarbons. Furthermore, GCMS analysis at 250°C and a CO:H_2O ratio of 1:1 showed that the C2 fraction was predominantly ethane (80%) whereas approximately equal amounts of propene and propane constituted the C3 fraction. Similar distributions may be expected throughout the CO rich regime.

The carbon number product distribution typically passes through a minimum at C2 for both the KE (Kolbel and Ralek, 1984) and FT syntheses (Dry, 1981). Using ^{14}C labelled olefins Pichler and Schulz (1970) showed that over standard FT catalysts ethene was incorporated into hydrocarbon chains. Propene and heavier olefins were not so reactive. These differing reactivities can be used to account for the suppression of ethene and hence C2 formation. The polymerisation of ethene may also have contributed.

5.6.4 The Formation of Aromatics

The % CO conversions to benzene and toluene were the main parameters used in the analysis of data pertaining to aromatic formation. The % CO conversions to xylene could not sensibly be included because the concentrations of each isomer (1,2 - dimethylbenzene, 1,3 - dimethylbenzene, 1,4 - dimethylbenzene) were close to the low detectable limit. Thus quantification of % CO conversions to aromatic C8s was prone to error.

The rates of synthesis of aromatic products did not, in general, parallel the rates of formation of the appropriate aliphatic analogues. As the temperature was raised from 250°C to 325°C at a $CO:H_2O$ ratio of 3:1, for example, % CO conversion to benzene plus toluene increased by a factor of 1.5, whereas the % CO conversion to aliphatic C6 and C7 molecules decreased by a factor of 6.8.

The disparity between aliphatic and aromatic concentrations is highlighted by Schulz Florey treatment of the data. The Schulz Florey plot obtained by analysis of the aliphatic hydrocarbon distribution given at a temperature of 325°C and a $CO:H_2O$ ratio of 3:1 is shown in fig 5.6.4a. The correlation coefficient for the line of best fit is high (> 0.9). This shows that the production of aliphatic hydrocarbons obeyed Schulz Florey kinetics. Aliphatics must therefore have been produced by the insertion of single carbon atom species (see section 2.2.2). When aromatic hydrocarbons were involved in calculations involving C6 and C7 fractions, the relevant points lie above the line of best fit. The same pattern emerged throughout the screening runs. Calculation of logarithmic values are not required to demonstrate this effect. Departures from a monotonic decrease in %CO conversion with carbon number (refer to figs. 5.3.1 - 5.3.5) characterise departures from Schulz Florey kinetics. A major implication of such product distributions is that aromatic hydrocarbons were formed by a different mechanism than were aliphatic hydrocarbons.

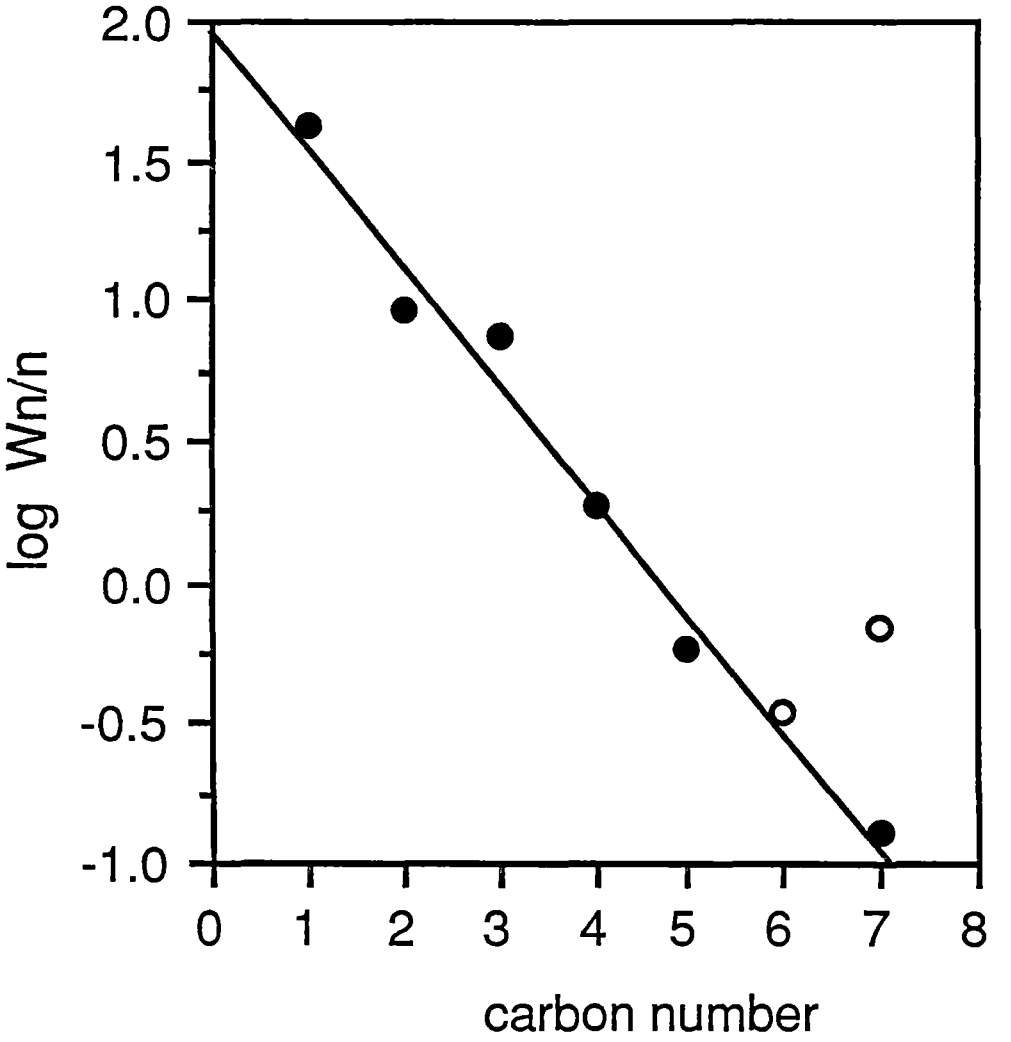

fig. 5.6.4a Schulz Florey plot of hydrocarbon distributions at 325°C using a 3:1 $CO:H_2O$ feed ratio.

The FID analysis (see sections 3.3.2 and 4.4.1) discriminated only between aliphatic and aromatic products. Aliphatic C6 and C7 fractions may well have contained compounds closely related to benzene and toluene (*e.g.* cyclohexadiene, methyl cyclohexane) in addition to linear aliphatic compounds. The aromatic derivatives, if present, were thus grouped with linear aliphatics for the purposes of calculation. Such grouping may be viewed as contradictory since aromatic derivatives would have been synthesised by the same mechanism as aromatics proper rather than by the mechanism which produced linear aliphatics.

Although this grouping may engender small quantitative errors, it would not affect the argument that aromatics and linear aliphatics were synthesised *via* different pathways. Correction for the consideration would lower the values of log (Wn/n) for the aliphatic fractions and raise the aromatic values (refer to fig. 5.6.4a). The term Wn represents the weight percentage of the hydrocarbon fraction with carbon number n, a figure which can be read directly from the integrated FID trace (see Appendix 1). The differences between the two sets of values would be highlighted not obscured.

A plot of % CO conversion to coke versus % CO conversion to benzene and toluene shown in fig. 5.6.4b reveals a positive correlation between the two parameters. The inference is that aromatic formation was linked with coke formation. Such a relationship has not previously been suggested.

Coke is generally considered to be graphitic carbon (Unmuth *et al.*, 1980). The skeletal structures of graphite and aromatic hydrocarbons are similar. Reaction of graphite with H_2 or H_2O during synthesis could conceivably have produced planar, cyclic organic molecules. An alternative relationship is that coke and aromatic molecules were formed from a common intermediate.

At each $CO:H_2O$ feed ratio, there was, with the exception of a couple of points ($CO:H_2O$ = 2:1, 250°C and 275°C), a positive correlation between the two parameters cited. Hence the scatter on the graph is a consequence of variations in the feed composition. Basically the plot consists of points lying on five separate lines, corresponding to each feed ratio. All these lines have positive gradients, except in the case of the 2:1 feed. The data would not be expected to lie on a common line because the changes in CO and H_2O partial pressures inherent to a feed alteration (see section 5.2) undoubtedly have complex ramifications on the rates of aromatic and coke production.

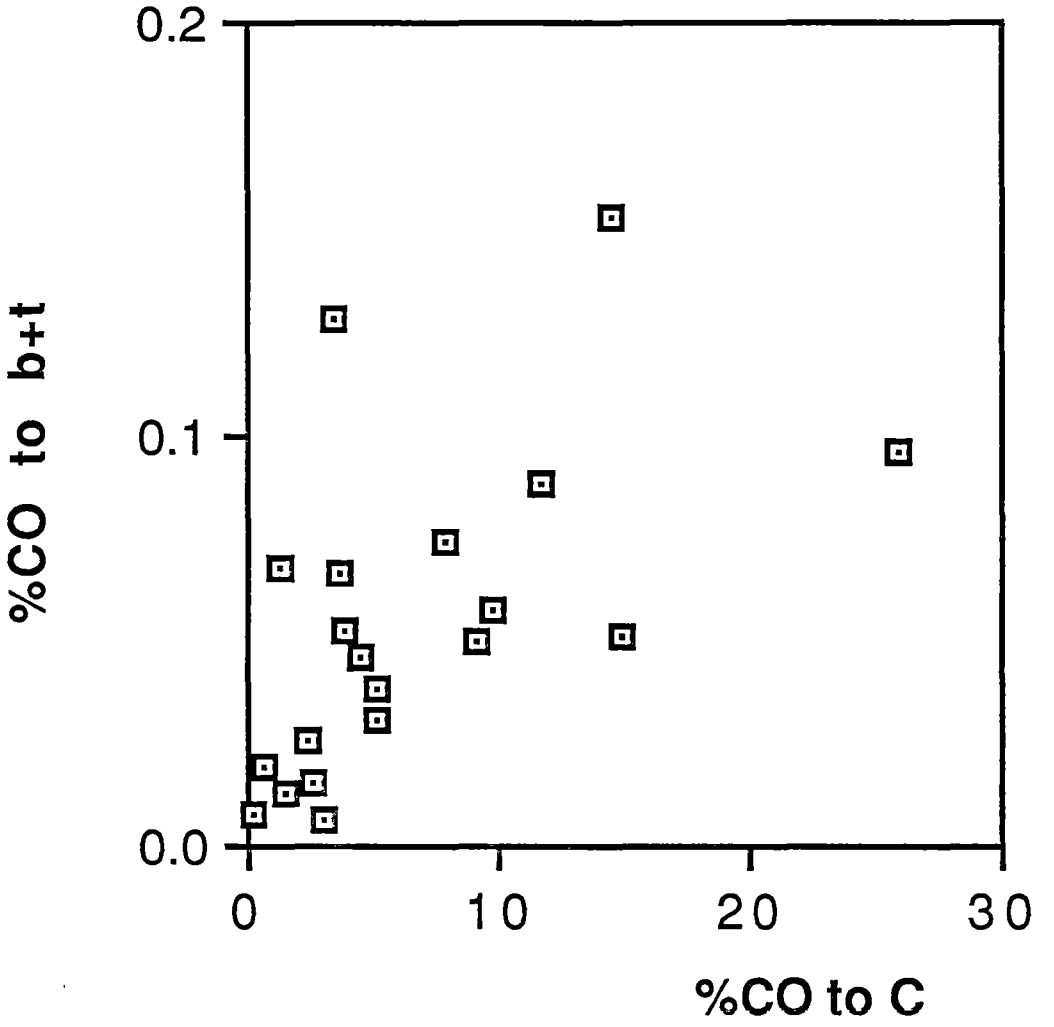

fig. 5.6.4b %CO conversion to benzene plus toluene versus % CO conversion to coke.

5.7 Evaluation of Conditions

5.7.1 The Ideal Conditions

Ideally, a catalyst for any process should give high conversions and high selectivities to desired products. As mentioned in section 5.1, high selectivity takes precedence over high conversions. The rate of undesired side reactions should also be minimised.

The desired products of the KE synthesis are hydrocarbons, particularly long chain products. The performance of $Co/Cu/SiO_2$40Å;10:10:100 was therefore evaluated in terms of selectivity to hydrocarbons relative to overall % CO conversions.

By expressing hydrocarbon selectivity as a fraction of overall conversion, H_2 and coke are effectively regarded as undesired products. Coke is known to poison FT catalysts (Hofer *et al.*, 1955), and similarly affects KE catalysts (Kolbel and Ralek, 1984). Classification of coke as an unwanted product is beyond dispute. Unlike coke, H_2 is advantageous as well as disadvantageous and thus is classified as undesirable in a more limited context. Clearly the presence of H_2 in any amount is a disadvantage because it lowers the concentration of hydrocarbon products, so complicating their separation. The production of substantial excess H_2, as observed at a $CO:H_2O$ ration of 1:3 (see sections 5.4.1 and 5.4.3), is further deleterious in that methane synthesis becomes predominant. Methane is not a useful product - it requires upgrading before conversion to synthetic fuels and is available as natural gas in vast supplies. (Larkins, 1985). A possible benefit of H_2 is that it may enhance the performance of KE catalysts by preventing oxidation. Another positive feature of H_2 production is that H_2 has potential use in other processes including the FT synthesis and coal liquefaction (Larkins, 1985). The preparation of an active WGSR catalyst was not, however, an aim of this project.

Aromatics were potentially the most useful products synthesised by Co/Cu/$SiO_2$40Å;10:10:100 (see section 4.5). The selectivity to aromatics as a function of % CO conversion to hydrocarbons was therefore considered another important criterion for the choice of optimal conditions. The absence of a complete listing of CO conversions to aromatic products has precluded such analysis in the past literature.

5.7.2 Hydrocarbon Selectivity

The % selectivity to hydrocarbons, expressed as a fraction of overall % CO conversions, are plotted against overall % CO conversions in fig. 5.7.2. All combinations of CO:H_2O ratios (3:1, 2:1, 1:1, 1:2, 1:3) and temperatures (250°C, 275°C, 300°C, 325°C) are represented. The conversions given in section 5.3 were used in all the calculations.

At low conversions (between 0% and 5%), selectivities to hydrocarbons were less than 10%. The low selectivities were a result of the low (<0.4%) %CO conversions to hydrocarbons (refer to tables 5.3.1 - 5.3.5). The conversions at a CO:H_2O ratio of 1:2 and temperatures of 250°C and 275°C were in this region of the graph.

When the % CO conversions exceeded 20%, selectivities were again below 10%. At CO:H_2O ratios of 3:1 and 2:1, this was a result of high coking rates (≥15% - refer to tables 5.3.1-5.3.5). At a CO:H_2O ratio of 1:3 the low selectivity was a result of excess H_2 production (see section 5.4.2).

The best catalyst performance was given in the % CO conversion range of 5% to 20%. Hydrocarbon selectivities reached up to 18.5% and were generally in the range of 10% to 15%. The conversions at temperatures of 275°C, 300°C and 325°C and a 1:1 CO:H_2O ratio were in this region. That the selectivity did not vary regularly as a function of temperature and CO:H_2O feed composition reflects a complex interplay between coking, hydrocarbon synthesis and hydrogen production.

fig. 5.7.2 %Selectivity to hydrocarbons versus overall %CO conversions.

key-

black	250°C
blue	275°C
green	300°C
red	325°C

upright triangle	$CO:H_2O$ 3:1
square	$CO:H_2O$ 2:1
circle	$CO:H_2O$ 1:1
diamond	$CO:H_2O$ 1:2
inverted triangle	$CO:H_2O$ 1:3

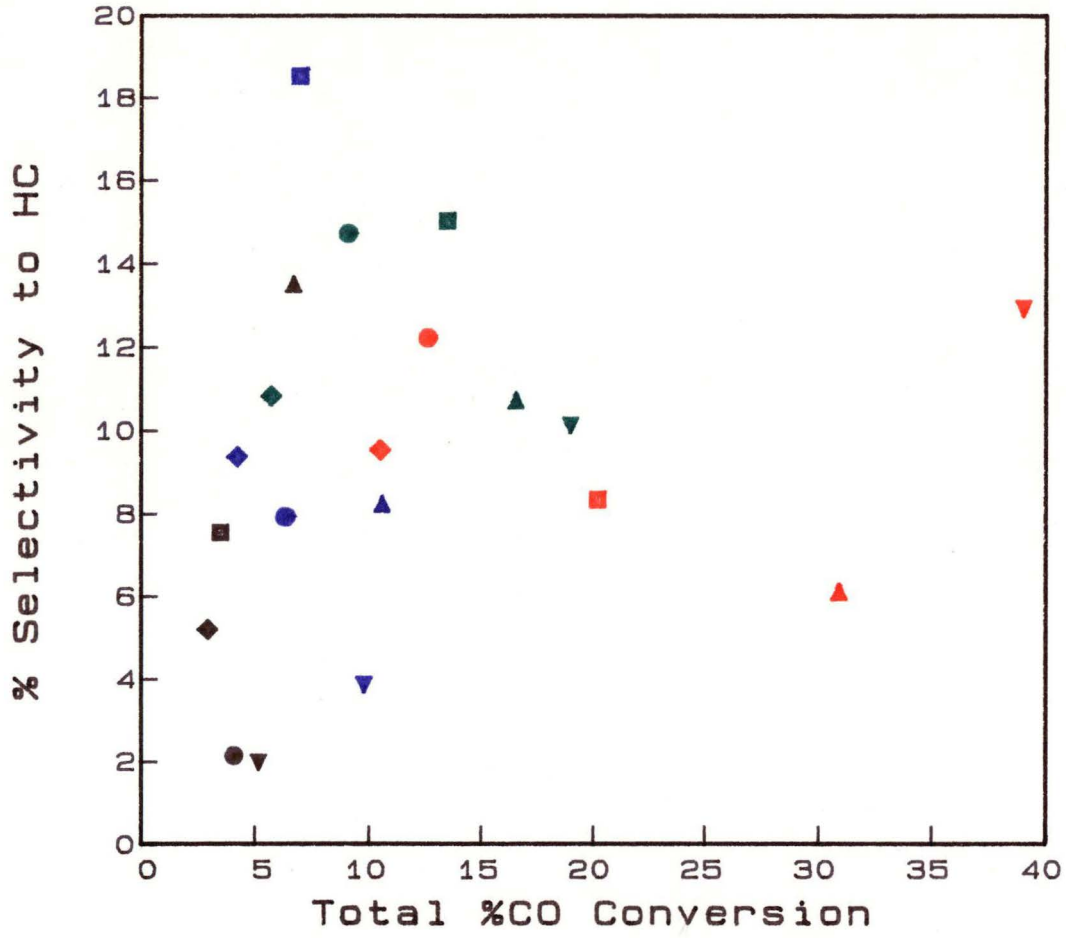
% Selectivity to HC
Total %CO Conversion
0
2
4
6
8
10
12
14
16
18
20
0
5
10
15
20
25
30
35
40

It is difficult to compare the absolute hydrocarbon yields obtained in this study with those cited in previous works (Kolbel and Ralek, 1984; Chaffee *et al.*, 1984; Chaffee and Loeh, 1985, 1986; Ekstrom and Lapscewicz, 1985; Tominaga *et al.*, 1984, 1986). The complication arises because of the various ways in which CO conversions to hydrocarbons and other products are expressed. Selectivity is a relative expression and thus simple to collate. The hydrocarbon selectivities which apply in the current work emerge as typical.

5.7.3 Aromatic Selectivity

The % selectivity to aromatics, benzene plus toluene, as a proportion of % CO conversion to hydrocarbons, is plotted against % CO conversion to hydrocarbons in fig. 5.7.3. No clear trends in selectivity as a function of conversion show up. The average selectivity was approximately 4.7%.

In the absence of a variation in selectivity, maximum conversions should be sought. The % CO conversions to aromatics tended to increase with temperature and $CO:H_2O$ ratio. The increase was associated with increased coking rates (see section 5.6.3). The relationship between the reactions is unfortunate, because the synthesis of aromatics in high yields would be associated with eventual catalyst poisoning by coke (see section 5.7.1).

5.7.4 Optimal Conditions

None of the results reported in the previous sections are outstanding with respect to selectivity and conversion. Conversions of CO to hydrocarbons never exceeded 5%, with highest conversions occurring simultaneously with poor selectivities. Another problem was that the highest aromatic yields were associated with coking. The choice of optimal conditions therefore involves a compromise. The intermediate $CO:H_2O$ ratio of 1:1 can logically be described as the optimal feed conditions on this basis.

fig. 5.7.3 %Selectivity to benzene plus toluene versus %CO conversions to hydrocarbons.

key-

black	250°C
blue	275°C
green	300°C
red	325°C

upright triangle	$CO:H_2O$ 3:1
square	$CO:H_2O$ 2:1
circle	$CO:H_2O$ 1:1
diamond	$CO:H_2O$ 1:2
inverted triangle	$CO:H_2O$ 1:3

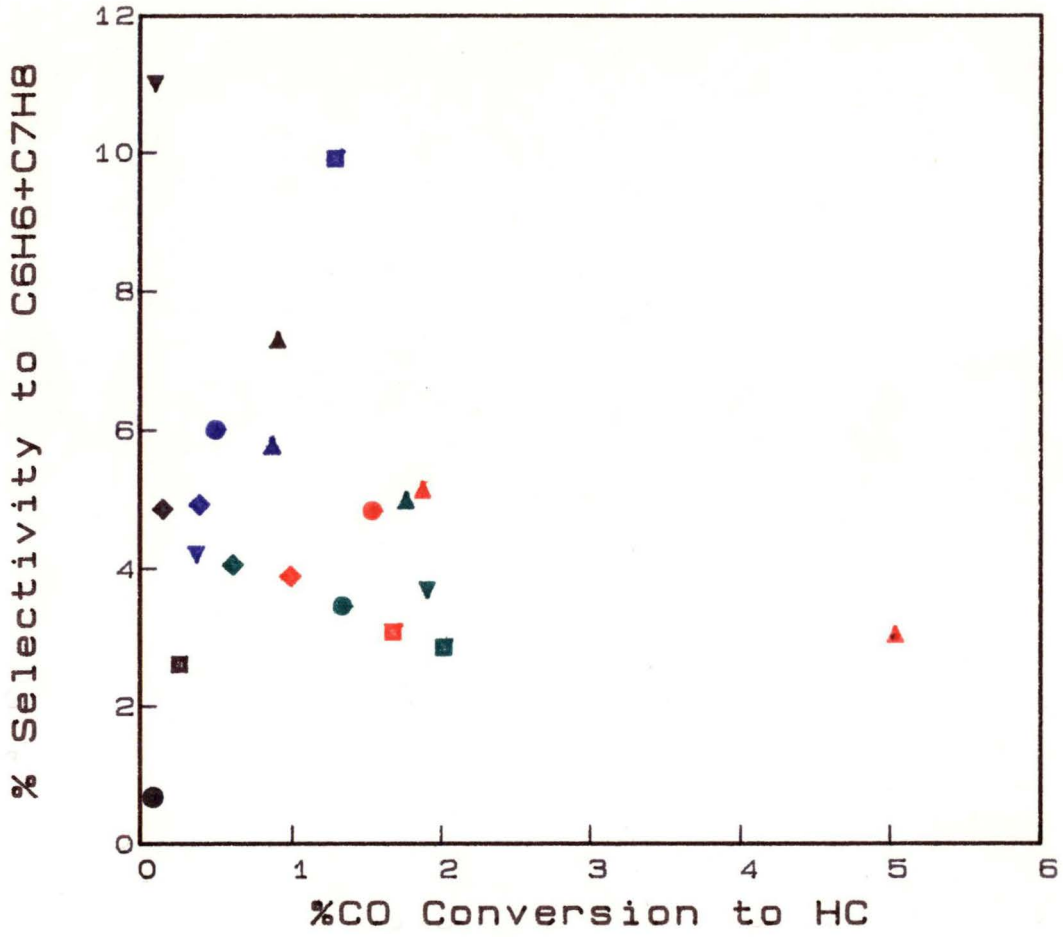
% Selectivity to C6H6+C7H8
12
10
8
6
4
2
0
0
1
2
3
4
5
6
%CO Conversion to HC

The main reason for this choice is that coking and the excess WGSR (see sections 5.3 and 5.7.1) proceeded to a relatively minor extent under these conditions. Coking was problematical at the higher $CO:H_2O$ ratios of 3:1 and 2:1. At most 26.0% of CO was converted to coke ($CO:H_2O$ 3:1, 325°C). Excess H_2 production was characteristic of the water rich regime ($CO:H_2O$ 1:3) and the maximum appropriate conversion was 21.4% at 325°C (see sections 5.3 and 5.4). The performance of $Co/Cu/SiO_2$40Å;10:10:100 at the 1:1 $CO:H_2O$ ratio clearly compares favourably with its performance at the more extreme feed compositions.

The hydrocarbon selectivities were also favourable. They ranged between 10% and 15% at a $CO:H_2O$ ratio of 1:1. The maximum value occurred at 300°C. The % CO conversions to hydrocarbons varied from 0.1% at 250°C to 1.5% at 325°C (refer to table 5.3.3). Higher temperatures (300°C, 325°C) are therefore beneficial at this particular $CO:H_2O$ ratio.

The magnitude of these hydrocarbon parameters provides the reason for judging the $CO:H_2O$ ratio of 1:1 superior to 1:2. The rates of the unwanted side reactions (coking, excess H_2 production - see section 5.7.1) stayed relatively slow in both the feeds at temperatures below 325°C. At a $CO:H_2O$ ratio of 1:2 the production of hydrocarbons was also suppressed to such an extent that %CO conversions were less than 1% at all temperatures. The hydrocarbon selectivities were less at a $CO:H_2O$ ratio of 1:2 than 1:1 as a consequence of these overly low conversions.

The selectivity to aromatics at a $CO:H_2O$ ratio of 1:1 was average (*circa* 6%). The maximum % CO conversions to aromatics were only marginally less than the maximum % CO conversions given throughout the $CO:H_2O$ range (refer to figs. 5.3.1 - 5.3.5). For example, the maximum % CO conversion to toluene in the 1:1 $CO:H_2O$ feed was 0.056% (325°C) compared with the maximum values throughout the feed composition range of 0.063 % (325°C, $CO:H_2O$ 3:1).

Further features of hydrocarbon distribution which were favourable at the $CO:H_2O$ ratio of 1:1 included the suppression of methane (see section 5.7.1). The suppression was typical of the CO rich regime (see sections 5.4.2 and 5.6.2). A drawback of the FT synthesis is the high levels of methane produced. The KE synthesis is accepted to be superior in this aspect (Kolbel and Ralek, 1984). Analysis by GCMS showed that the aliphatic hydrocarbons were predominantly (>50%) unsaturated. Again this is a general feature of the KE synthesis (Kolbel and Ralek, 1984). Unsaturated hydrocarbons are preferable to saturated analogues because of their higher reactivities, especially susceptibilities to polymerisation, and octane ratings (Larkins, 1985).

For completeness, the activity of $Co/Cu/SiO_2$40Å;10:10:100 was assessed outside the 250°C to 325°C temperature range at the optimal $CO:H_2O$ feed ratio. Below 250°C hydrocarbon production was so low as to be non-quantifiable. At 350°C, coking and methanation became predominant. The %CO conversions to methane, coke and H_2 were 5.23%, 77.1% and 4.80% respectively. Coking accounted for greater than 90% of CO conversion at 375°C and 400°C. These results show that 250°C and 325°C were approaching the practical temperature limits for synthesis at a $CO:H_2O$ ratio of 1:1. The same limits probably applied at the other $CO:H_2O$ ratios in the CO rich regime (3:1, 2:1, 1:2).

5.8 Summary

The screening results showed that there were two distinct regimes related to feed composition, the CO rich regime and the H_2O rich regime. Within each the performance of $Co/Cu/SiO_2$40Å;10:10:100 was entirely different. In the CO rich regime, coking was the main cause of CO conversion at high temperatures. Substantial excess H_2 production occurred in the H_2O rich regime, probably associated with structural modification of the catalyst.

In the CO rich regime, suppression of methane and C2 production occurred. The yields of lighter hydrocarbon products, especially methane and C2s, were relatively high in the H_2O rich regime because of high internal H_2 concentrations. Coke and aromatics appeared to form by related pathways at all feed compositions

The optimal conditions occurred within the CO rich regime at an intermediate $CO:H_2O$ feed ratio of 1:1. Coking and excess H_2 production were minimal under these circumstances. The most favourable activities and selectivities were given at high temperatures using this feed composition. At 325°C, for example, the overall % CO conversion was 12.6%, the selectivity to hydrocarbons 12.2%, and selectivity to aromatics relative to hydrocarbon yields 6.67%.

6 DETAILED CHARACTERISATION OF Co/Cu/$SiO_2$40Å;10:10:100

6.1 Introduction

To understand precisely how a catalyst works, accurate characterisation is essential. In particular the nature of active species should be determined.

The results of TPR and screening experiments suggest mixed Co/Cu species occurred on the Co/Cu/Al_2O_3 and Co/Cu/$SiO_2$40Å hybrids. The catalysts behaved in an interesting, and in terms of hydrocarbon distributions, favourable way because of these moieties (see Chapter 4).

A detailed characterisation of Co/Cu/$SiO_2$40Å; 10:10:100 was carried out. This catalyst had proved to be the most active hybrid, and simpler in terms of active metal distributions than Co/Cu/Al_2O_3;10:10:100 (see section 4.5). The properties of a Co/$SiO_2$40Å;10:100 + Cu/$SiO_2$40Å;10:100 physical mix, and the single metal catalysts themselves, were also assessed Comparison of the results was an important aspect of the characterisation strategy. The catalysts were examined at three key stages - post calcination (400°C in air, 24 hours) post activation (400°C in H_2, 2 hours), and post reaction.

The catalysts were spent by reacting them, after activation, at 250°C with the optimal feed (CO:H_20 1:1 - see section 5.7.1) until steady state % CO conversions were achieved. The performance of Co/Cu/$SiO_2$40Å;10:10:100 under these conditions was similar to its performance throughout the CO rich regime (see section 5.4.1). This similarity suggests that the active species formed under these circumstances were typical of those present throughout the CO rich regime.

The main aim of this section of the work was to determine the nature of active Co/Cu species on the Co/Cu/$SiO_2$40Å; 10:10:100 hybrid. In doing so, the reasons why interaction between Co and Cu occurred on the hybrid catalyst but not the appropriate physical mix (see section 4.5), were established. The characterisation techniques employed included elemental analysis, X-ray diffraction electron probe microanalysis, surface area measurement, thermogravimetry and temperature programmed reduction.

6.2 Characterisation of Calcined Samples

6.2.1 Elemental Analysis

The analysis results for Co/$SiO_2$40Å; 10:100, Cu/$SiO_2$40Å;10:100, a physical mix of the two single metal catalysts and Co/Cu/$SiO_2$40Å; 10:10:100 are given in table 6.2.1.

Subtraction of the weight percent metal loadings from 100 gave the relative combined weights of the $SiO_2$40Å support and oxygen associated with Co and Cu. The contributions of associated oxygen to this value were deduced by consideration of the oxidation states of the various metal species present on each sample as determined by TPR (see section 4.2). The metal to support weight ratios were calculated by relating the weights of metals and support (see Appendix 4).

The results show that the preparation procedures (see section 3.2) gave, within experimental error, quantitative transfer of metal ions from solution to support. The desired loadings were therefore obtained. The loadings of Co and Cu were, as predicted in section 4.2.4, halved by physically mixing Co/$SiO_2$40Å;10:100 and Cu/$SiO_2$40Å, 10:100.

catalyst	wt % Co	wt % Cu	Co : Cu : $SiO_2$40Å weight loading ratios
Co/$SiO_2$40Å;10:100	8.12	-	9.08 : 0 : 100
Cu/$SiO_2$40Å;10:100	-	8.39	0 : 9.37 : 100
Co/$SiO_2$40Å;10:100 +Cu/$SiO_2$40Å;10:100	3.84	4.39	4.29 : 4.91 : 100
Co/Cu/$SiO_2$40Å;10:10:100	6.93	7.68	8.57 : 9.49 : 100

Table 6.2.1 Atomic absorption analysis.

6.2.2 X-ray Diffraction

The Method

Since X-rays are electromagnetic waves, they can be diffracted. Crystals are suitable X-ray gratings because the spacings between adjacent atomic planes often have the same order of magnitude as X-ray wavelength (Ewing, 1985).

No two chemical substances form crystals in which the spacing of the planes is identical in all analogous directions. The distances between various adjacent planes therefore compose a unique set for any one crystalline substance (Ewing, 1985).

This set is acquired in the X-ray diffraction experiment. A sample is orientated at all possible angular positions in the path of an X-ray beam. Where constructive interference of the beam occurs, the angle of diffraction (2θ), integral X-ray wavelengths ($n\lambda$) and the distance between adjancent planes (d) are related by eqn. 6.2.2, known as Bragg's equation.

$$n\lambda = 2d \sin\theta \qquad \text{eqn. 6.2.2}$$

Constructive interference can be readily detected (Anderson and Pratt, 1985).

Some information can be obtained from the size and shape of the diffractions. The intensity of diffraction peaks is proportional to the amount of diffracting material. From line widths an estimate of the average crystallite size can be obtained while from the line shape the distribution of crystallite sizes can be determined (Anderson and Pratt, 1985).

A rigorous analysis of the X-ray diffraction patterns was not performed. Rather, the "fingerprint" aspect of the technique was exploited.

Standard Samples

The standard d values for a collection of standard oxide species containing Co and/or Cu are given in table 6.2.2a. The data were taken from the Inorganic Index to the Powder Diffraction File (1972), not acquired in house. The x designates the peak of highest intensity for each sample. The strongest diffraction is assigned an intensity of 100, and the other peaks are scaled relative to this.

sample	d values(Å) and relative intensities		
Co_3O_4	2.44_x	1.43_{50}	2.86_{40}
Co_2O_3	2.87_x	2.33_x	1.78_x
CoO	2.13_x	2.46_{80}	1.51_{50}
CuO	2.52_x	2.32_2	2.53_{50}
$6CuO.Cu_2O$	2.50_x	1.58_{80}	1.25_{80}
Cu_2O	2.47_x	2.14_{40}	1.51_{30}
Co_2CuO_4	2.43_x	1.42_{40}	1.55_{30}
$CoCuO_2$	2.35_x	2.80_{80}	2.13_{80}
$CoCu_2O_3$	2.23	2.50_{40}	2.45_{40}

Table 6.2.2a Diffractions of standard oxides.

Co/Cu/oxide Reference

A mixed Co/Cu/oxide was prepared (see section 3.4.3) as a reference for the catalysts. The set of d values for the mixed oxide was determined from its X-ray diffraction pattern by using Bragg's equation (eqn. 6.2.2). The intensities of the diffractions were measured by estimation of the diffraction peak areas. These were normalised to the largest peak. The values cannot be compared, in absolute terms, to the peak intensities of the standard samples. The peak positions and relative peak sizes can be collated however. The results are given in table 6.2.2b.

The mixed oxide clearly consisted of Co_3O_4 and CuO. Bulk Co_3O_4 was associated with the d values 2.45Å, 1.43Å and 2.87Å and bulk CuO with 2.52Å, 2.32Å and 2.55Å. The relative intensities of the Co_3O_4 diffractions were 100, 38 and 38, and for CuO 51, 56 and 25. The maximum difference between standard and reference d values was 0.01Å. The diffraction with d value 1.43Å was 38% as intense as the diffraction with d value 2.45Å. The standard values (see table 6.2.2a) list this factor as 50%. This was the maximum intensity discrepancy. The variance between the standard and experimental figures can be considered insignificant.

The weights of Cu and Co were equivalent in the Co/Cu/oxide. Thus the weight percentages of Co_3O_4 and CuO were 50.22% and 49.78% respectively.

X-ray Diffraction Patterns of Calcined Samples

The results for the catalysts are given in table 6.2.2b. Diffraction intensities were normalised to the largest peak given by the mixed Co/Cu/oxide, due to Co_3O_4. No peaks were given by the $SiO_2$40Å blank. This shows that the support was amorphous.

Co/$SiO_2$40Å;10:100

Diffractions appropriate to Co_3O_4 appeared (compare tables 6.2.2a and 6.2.2b). This result concurs with TPR evidence (see section 4.2), and further justifies the reduction peak assignments made. The concentration of Co_3O_4 on the catalyst was

sample	d values (Å) and relative intensities		
Co/Cu/oxide	2.45_{x}	1.43_{38}	2.87_{38}
	2.52_{51}	2.32_{56}	2.53_{25}
$Co/SiO_2$40Å;10:100	2.45_{15}	$1.43_{5.1}$	$2.87_{5.1}$
$Cu/SiO_2$40Å;10:100	-	-	-
$Co/SiO_2$40Å;10:100 + $Cu/SiO_2$40Å;10:100	$2.45_{9.0}$	$1.43_{3.8}$	$2.87_{3.8}$
$Co/Cu/SiO_2$40Å;10:10:100	2.45_{18}	$1.43_{5.1}$	$2.87_{5.1}$

Table 6.2.2b Diffractions of calcined catalysts and Co/Cu/oxide standard.

less than in the Co/Cu oxide mix, and so the diffraction intensities were comparatively lower.

The line widths given by $Co/SiO_2$40Å;10:100 were broader than the Co_3O_4 line widths given by the standard oxide. This suggests that the supported Co_3O_4 particles were smaller than the unsupported particles (Anderson and Pratt, 1985).

$Cu/SiO_2$40Å;10:100

No crystalline material occurred on this catalyst. This demonstrates that the Cu^{2+} surface networks (see section 4.2.3) were not well ordered structurally.

$Co/SiO_2$40Å;10:100 + $Cu/SiO_2$40Å;10:100

The Co_3O_4 supported on $Co/SiO_2$40Å; 10:100 was the only crystalline material in this sample (refer to table 6.2.2b). The diluent effect of mixing caused the diffraction peaks to be less intense than for $Co/SiO_2$40Å; 10:100.

$Co/Cu/SiO_2$40Å;10:10:100

The only crystalline species evident was Co_3O_4. Oxidic Cu species were known to occur (see section 4.2.5), but they were not bonded in a well defined crystalline lattice. The mixed Co/Cu/oxide species proposed to exist on this catalyst was clearly not one of the stoichiometric crystalline mixed metal oxides, since none of the appropriate diffractions occurred (compare tables 6.2.2a and 6.2.2b). The results are entirely consistent with TPR data (see section 4.2).

The Co/Cu oxide was prepared in the same was as the hybrid catalyst except in the absence of the support. The mixed metal oxide can therefore be viewed as a control. The bonding of Co was not affected by the support. Bulk Co_3O_4 occurred on both samples. In contrast Cu preferentially interacted with $SiO_2$40Å and did not form bulk CuO. The preparation procedure did not result in the formation of stoichiometric mixed metal oxides in either situation.

6.2.3 Electron Probe Microanalysis

The Method

Several different phenomena can result from the bombardment of a substance by energetic particles or photons. The primary process is the ejection of electrons from the target atoms, which leaves vacancies. Following that, relaxation may follow by either of two competing paths; X-rays may be emitted or secondary (Auger) electrons ejected (Ewing, 1985).

A sample subjected to electron probe microanalysis is scanned with a beam of electrons. The instrument incorporates a secondary electron image processor or an optical microscope to enable the location of desired sample regions (Ewing, 1985).

Each element emits X-rays of characteristic energies. The intensities and energies of the various X-rays released from the targeted region are monitored by an X-ray spectrometer (Ewing, 1985). These data can then be manipulated to find elemental concentrations.

The detector and the electron probe are synchronised. Thus the intensity of a particular energy X-ray can be recorded as a function of probe position. Maps can be constructed which show the positions of a chosen element in a 2-dimensional plane.

Macroscopic Analysis

Maps of Co, Cu, and Si were acquired at low magnification (140 to 700 times). The Si map defined the outline of the catalyst particles. The results are shown in figs. 6.2.3a - 6.2.3e.

Distributions

The Cu and Co maps of the two single metal samples reveal that the two metals occurred on all of the respective catalyst particles (refer to figs. 6.2.3a and 6.2.3b). Elemental microanalysis demonstrated that the metals were distributed evenly from particle to particle. The metal loadings obtained were consistent with atomic absorption results (see section 6.2.1).

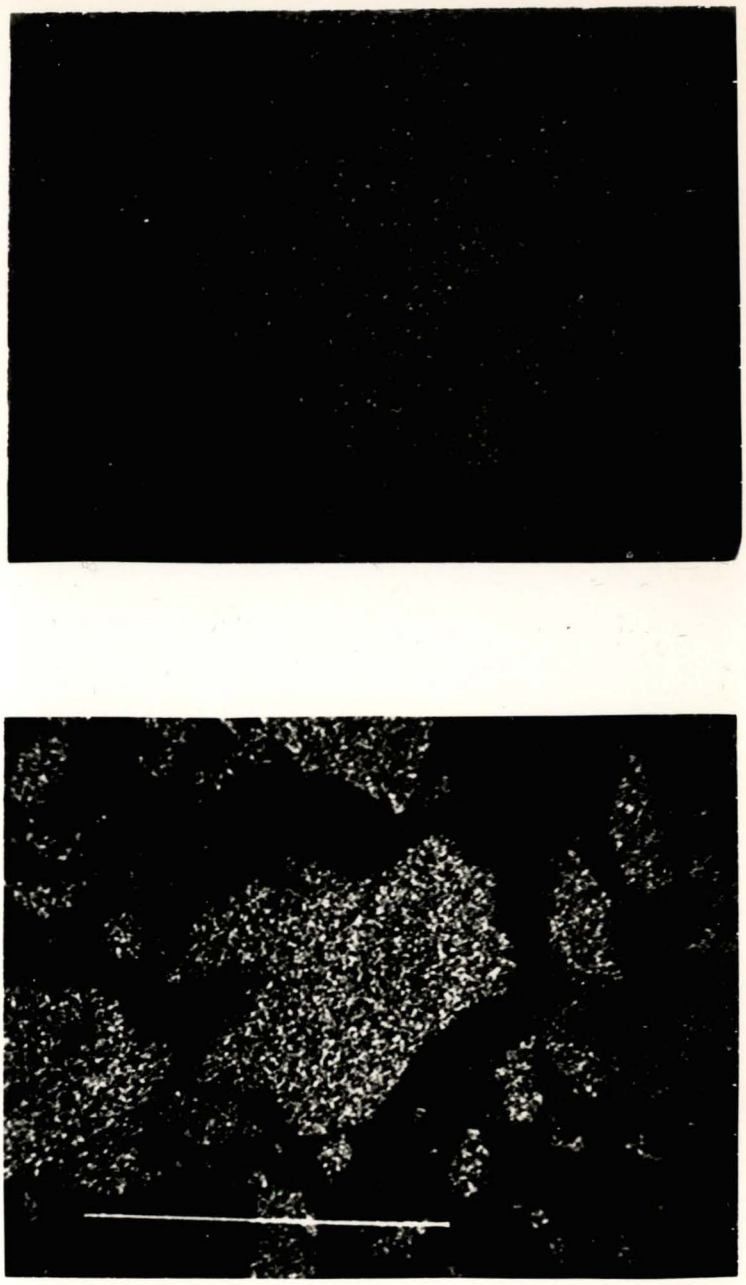

fig. 6.2.3a Co (top) and Si (bottom) maps for calcined $Co/SiO_2$40Å;10:100 (200x).

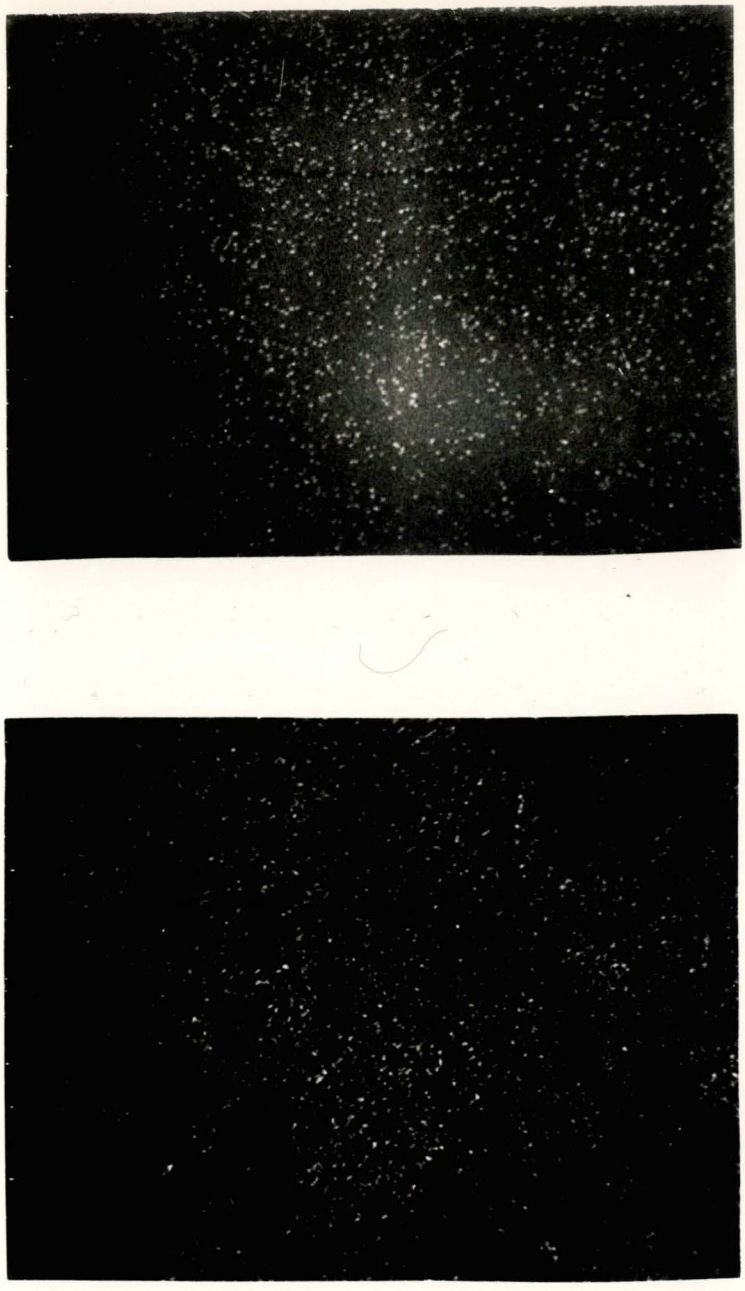

fig. 6.2.3b Cu (top) and Si (bottom) maps for calcined $Cu/SiO_2$40Å;10:100 (200x).

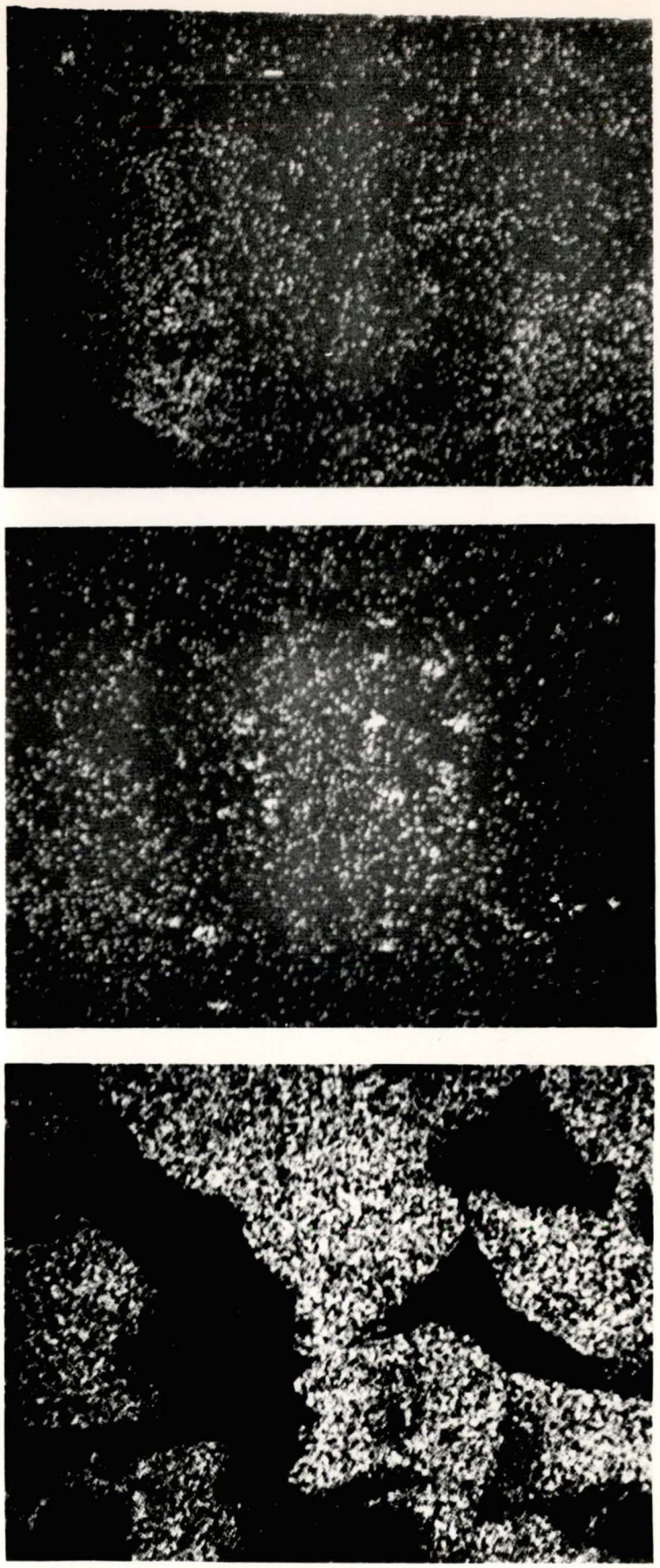

fig. 6.2.3c Co (top), Cu (middle), and Si(bottom) maps for calcined $Co/SiO_2$40Å;10:100 + $Cu/SiO_2$40Å;10:100 physical mix (200x).

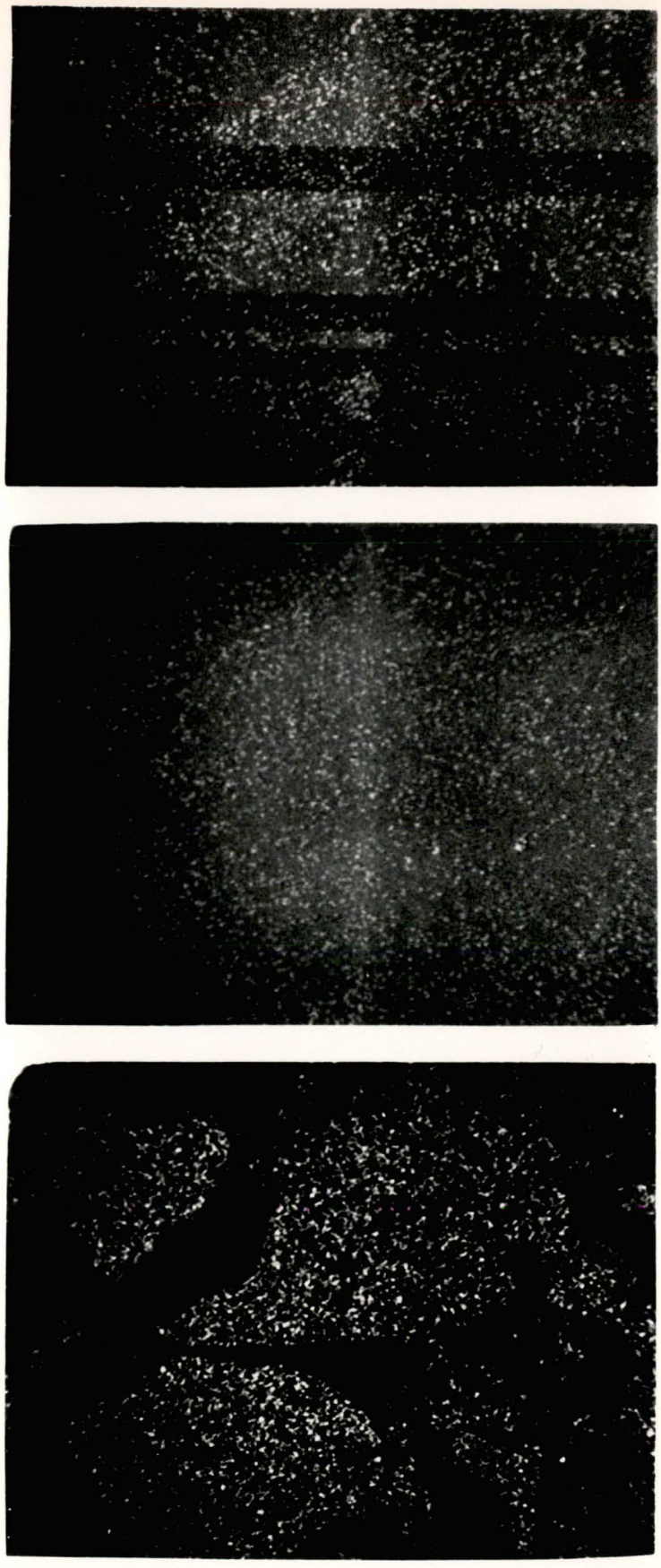

fig. 6.2.3d Co (top), Cu (middle), and Si (bottom) maps for calcined Co/Cu/$SiO_2$40Å;10:10:100 (220x).

fig. 6.2.3e Si map for blank calcined $SiO_2$40Å (300x).

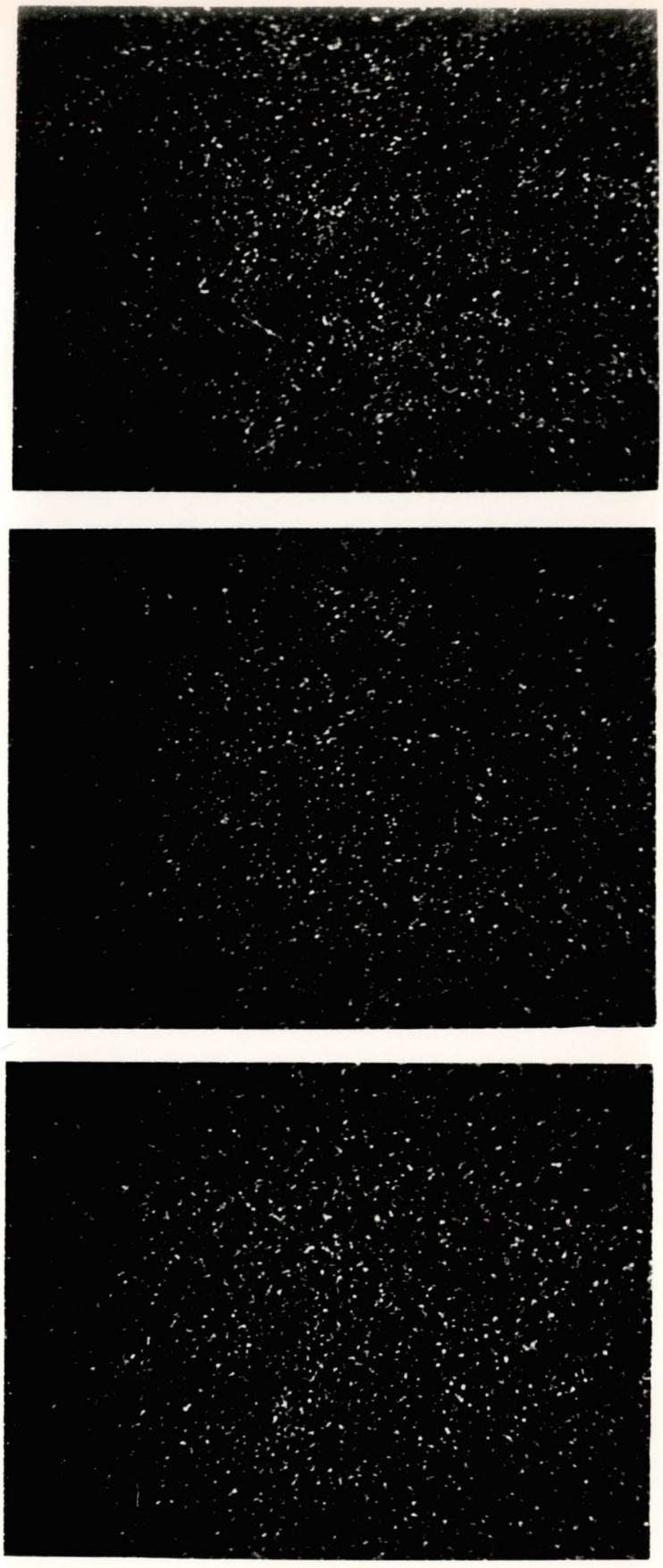

fig. 6.2.3f Co (top), Cu (middle), and Si (bottom) maps for calcined Co/Cu/$SiO_2$40Å;10:10:100 (3000x).

The Co and Cu maps of the physical mix exhibit mutually exclusive regions of high metal concentration (refer to fig. 6.2.3c). These regions correspond to the position of catalyst particles as defined by the Si map. Background counts, which were observed across both the metal maps, are not indicative of significant metal concentrations. The obvious interpretation of these results is that the physical mix simply consisted of Co and Cu supported on different particles.

The particles of the hybrid catalyst, in contrast, contained both Co and Cu species (refer to fig. 6.2.3d). The proximity of the two metals would have facilitated interaction between them.

Morphology

The average particle sizes of the $SiO_2$40Å blank (refer to fig. 6.2.3e) and the Co containing catalysts, Co/$SiO_2$40Å;10:100 and Co/Cu/$SiO_2$40Å;10:10:100 (refer to figs. 6.2.3a and 6.2.3d) were roughly equivalent. The largest $SiO_2$40Å particle shown had a maximum dimension of 233 μm, the largest Co/$SiO_2$40Å; 10:100 particle a maximum dimension of 200 μm and the largest Co/Cu/$SiO_2$40Å; 10:10:100 a maximum dimension of 250 μm. Well defined edges were characteristic of all these particles.

The Cu/$SiO_2$40Å; 10:100 sample differed in shape from the other samples (see fig. 6.2.3b). The particles had rounded edges, and grain boundaries were not as well defined as for the Co containing particles and the $SiO_2$40Å blank. This made the measurement of particle size difficult. Nevertheless, the Cu containing grains did appear to have roughly equivalent maximum dimensions (*circa* 250 μm) as other samples.

The morphology of a particle may well be affected by the nature of the species present on the particle. The bulk Co_3O_4 which occurred on the Co containing particles (see sections 4.2.1 and 6.2.2) may have acted as a "binder", maintaining the cohesion of the $SiO_2$40Å within each particle. The isolated interactive Cu^{2+} species, which exclusively occurred on Cu/$SiO_2$40Å;10:100 (see section 4.2), seemingly had an opposite effect.

Microscopic Analysis of Co/Cu/$SiO_2$40Å;10:10:100

The Si, Co and Cu maps for Co/Cu/$SiO_2$40Å;10:10:100 acquired at a magnification of 3000 are shown in fig. 6.2.3f. The pattern which emerges shows that Cu was evenly distributed whereas Co clustered to an extent. The Cu surrounds the Co clusters. Such a pattern is consistent with the description that oxidic Cu occurred as surface Cu^{2+} networks and oxidic Co as Co_3O_4 crystallites on the hybrid catalyst.

The results are less than definitive however. The severe grinding involved in the preparation of the sample disk (see section 3.4.4) may have violated the integrity of species present.

6.2.4 Surface Areas

The BET surface areas of the various catalysts and the $SiO_2$40Å blank are given in table 6.2.4. They are all more than 500 m^2/g, which is generally regarded as high (Anderson and Pratt, 1984).

The Co containing catalysts, Co/$SiO_2$40Å; 10:100 and Co/Cu/$SiO_2$40Å ; 10:10:100, had surface areas approximately 65 m^2/g less than the $SiO_2$40Å blank. Lower surface areas of oxidic Co species compared to $SiO_2$40Å itself may have caused this drop.

The Cu/$SiO_2$40Å;10:10:100 had a surface area greater than the $SiO_2$40Å blank. The increase was probably a result of the differing morphologies of the two particle types (see section 6.1.3). The rounded Cu/$SiO_2$40Å;10:100 particles would have exhibited higher surface areas than particles of equivalent volume with well defined grain boundaries.

The surface area of the physical mix of Co/$SiO_2$40Å;10:100 10 + Cu/$SiO_2$40Å;10:100 was the average (within 3.4%) of Co/$SiO_2$40Å;10:100 and Cu/$SiO_2$40Å; 10:100 surface areas. The result was predictable because equivalent weights of the two catalysts were contained in the mix and there was no interaction between the particles occasioned by physical mixing (see sections 4.2.4 and 6.2.3).

sample	surface area (m^2/g)
$SiO_2$40Å	617.0
Co/$SiO_2$40Å;10:100	552.2
Cu/$SiO_2$40Å;10:100	642.0
Co/$SiO_2$40Å;10:100 + Cu/$SiO_2$40Å;10:100	617.5
Co/Cu/$SiO_2$40Å;10:10:100	551.0

Table 6.2.4 Surface areas of $SiO_2$40Å. and supported catalysts.

6.2.5 The Nature of the Oxidic Species on Co/Cu/$SiO_2$40Å;10:10:100

The TPR (see section 4.2), X-ray diffraction (see section 6.2.2) and electron probe results (see section 6.2.3), consistently suggest that Cu on calcined Co/Cu/$SiO_2$40Å; 10:10:100 occurred as surface Cu^{2+} networks and Co as Co_3O_4.

It follows that the Cu^{2+} species were interspersed through and integrated in the $SiO_2$40Å support. Bulk Co_3O_4 crystallites, which by definition did not interact with the support, must have been distributed amongst the Cu^{2+} species.

The species on the hybrid catalyst were only different from those on the single metal catalysts and the Co/$SiO_2$40Å; 10:100 + Cu/$SiO_2$40Å;10:100 intimate mix in that oxidic Co and Cu were in intimate contact. In terms of their nature they were no different - interactive Cu^{2+} occurred on Cu/$SiO_2$40Å; 10:100 (see section 4.2 and 6.2.2) and bulk Co_3O_4 occurred on Co/$SiO_2$40Å;10:100 (see sections 4.2 and 6.2.2).

6.3 Characterisation of Activated Catalysts

6.3.1 Temperature Programmed Reduction

The activation procedure (2 hours, 400°C, 5 ml/min H_2 flow - see section 3.3.1) reduced the oxidic metal species on calcined catalysts to potentially active Co^o and Cu^o. In section 4.3, TPR was used to establish the extents of reduction of metal species occasioned by activation of Co/$SiO_2$40Å;10:100, Cu/$SiO_2$40Å; 10:100, the physical mix of these single metal catalysts, and Co/Cu/$SiO_2$40Å; 10:10:100. In this section of the work the Co^o and Cu^o species were characterised.

When X-ray diffraction experiments and electron probe microanalyses were performed, the activated samples were air exposed. Although air exposure would not be expected to result in gross changes of species distribution (*e.g.* species migration from one particle to another), the oxidation states of metals may well alter (*e.g.* oxidation of Cu^o to CuO). The TPR profiles of activated and air exposed samples were acquired in order to assess the extent of re-oxidation during air exposure. The results are shown in fig. 6.3.1.

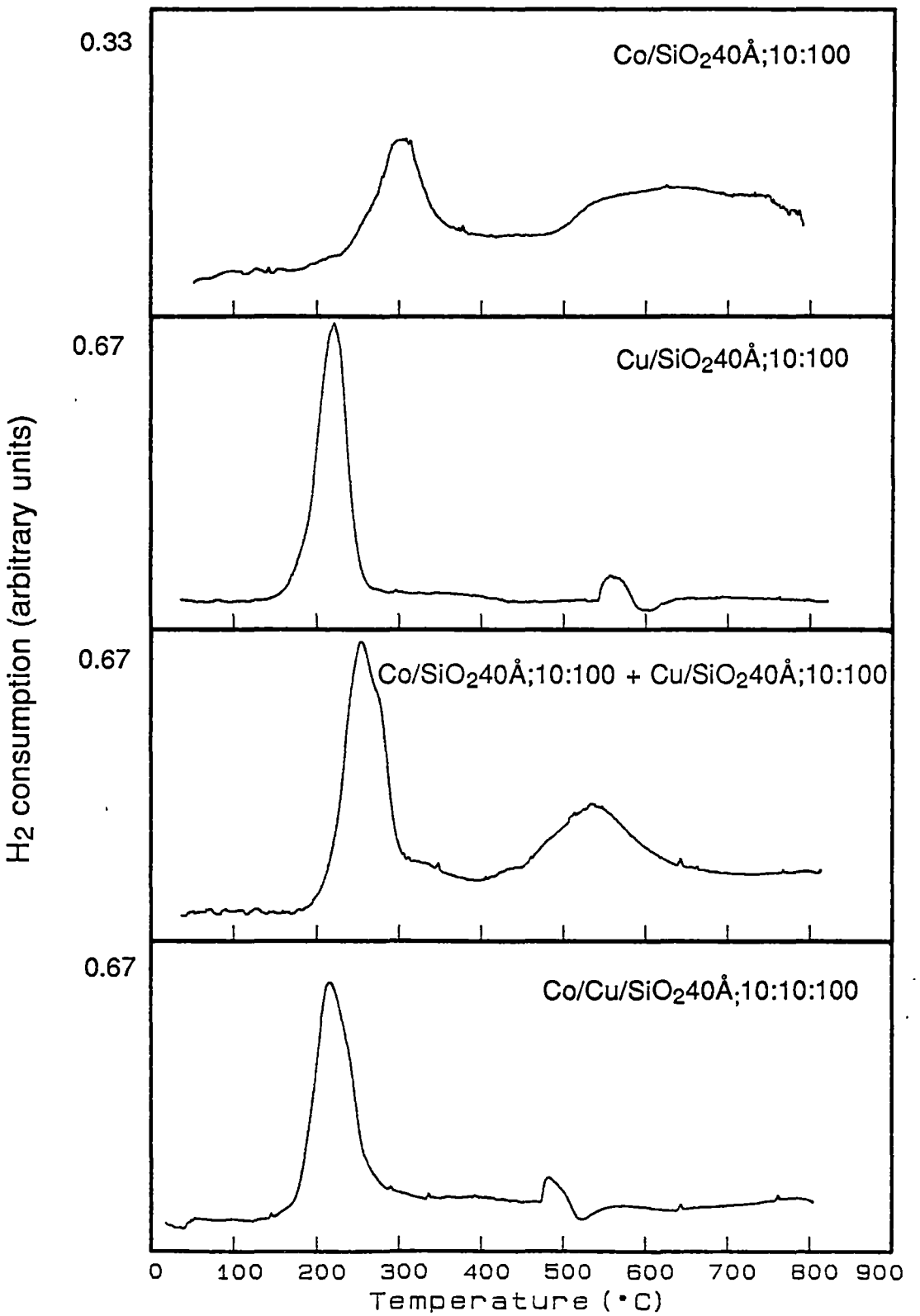

fig. 6.3.1 TPR profiles of activated, air exposed catalysts.

Co/$SiO_2$40Å;10:100

Consumption of H_2 occurred from temperatures of 300°C upwards. Reduction commenced at 600°C when the catalyst was activated *in situ* and not air exposed (see section 4.3.2).

The profile shows a peak at 300°C, which is 70°C less than the temperature at which Co_3O_4 reduced on the calcined sample (see section 4.2.2). This peak can be assigned to the reduction of Co_3O_4 covering Co^0 particles. The lower reduction temperature was probably a result of metal assisted (or autocatalytic) reduction. This process is known to decrease the reduction temperatures of metal oxides (Jones and McNicol, 1986).

The reduction from 400°C to 600°C occurred in a similar temperature region to the reduction of octahedral Co^{2+} on calcined Co/$SiO_2$40Å;10:100 and may therefore be similarly assigned (see section 4.2.2). This assignment requires that air exposure resulted in the re-integration of Co^{2+} into the support. Alternatively reduction may be attributed to CoO or Co_2O_3 formed, as was Co_3O_4, by the reaction of Co^0 and O_2. The peak was possibly caused by a combination of these reduction processes. The H_2 consumption at high temperature (600°C to 800°C) was probably due to the reduction of intact octahedral Co^{2+} (see sections 4.2.2 and 4.3.2).

Measurement of the area under the TPR peak suggests that 40% of the Co^0 present immediately post activation was re-oxidised by air exposure. Approximately 75% of the total Co loading was reduced by activation (see section 4.3.2). Thus approximately 30% of the total Co loading occurred as Co^0 after activation and air exposure.

Cu/$SiO_2$40Å;10:100

A peak at 230°C occurred on the TPR profile of activated and air exposed Cu/$SiO_2$40Å; 10:100. The peak assigned to interactive Cu^{2+} species on the calcined sample occurred at 300°C (see section 4.3.3). Therefore the logical assignment of the 230°C peak is to autocatalysed reduction of oxidic Cu^{2+} which re-integrated with the

support during air exposure. This assignment is supported by the colour change of the sample. Initially the sample was copper coloured, but turned the same shade of green as the calcined sample (see section 4.3.2) after air exposure. The re-integration of Cu^{2+} into the support must have been a facile process to have occurred under such mild conditions.

The area of the peak represents approximately 80% of the metal Cu loading, assuming a valency of +2 for the oxidic Cu species. All of the Cu on the $Cu/SiO_2$40Å,10:100 catalyst was reduced by activation (see section 4.3.3). The 20% of the total Cu loading present as Cu^0 after activation and air exposure can be adjudged typical of the metallic Cu which was present immediately post-activation. The rate of re-oxidation would have decreased exponentially, leaving the small amounts of residual and representative Cu^0.

$Co/SiO_2$40Å;10:100 + $Cu/SiO_2$40Å;10:100

The activated and air exposed physical mix behaved as an additive of the two single metal catalysts (refer to fig. 6.3.1). The H_2 consumption due to the autocatalysed reduction of interactive Cu^{2+} and Co_3O_4 appeared respectively as a peak at 230°C and a 300°C shoulder. Consumption at 400°C and above was caused by the reduction of oxidic Co.

$Co/Cu/SiO_2$40Å; 10:10:100

The TPR profile of the hybrid catalyst was similar to the profiles of $Cu/SiO_2$40Å;10:100 and the $Co/SiO_2$40Å; 10:100 + $Cu/SiO_2$40Å;10:100 physical mix in that a sharp peak appeared at 230°C. The peak was probably caused again by the reduction of interactive Cu^{2+}, autocatalysed by Cu^0 and Co^0. The area of the peak suggests that 80% of the total Cu loading, and thus the Cu^0 present after activation (see section 4.3.5), was re-oxidised during air exposure. There were no peaks indicating the presence of oxidic Co.

6.3.2 X-ray Diffraction

The d values and relative peak intensities given by Cu and Co metals are given in table 6.3.2a (Inorganic Index to the Powder Diffraction File, 1972). The same information for the activated and air exposed samples is given in table 6.3.2b. The intensities in tables 6.3.2a and 6.3.2b again cannot be directly compared (see section 6.2.2). The diffraction angle (2θ) was not scanned above 70° in the current experiments (see section 3.4.3). Thus the diffractions for Co^0 and Cu^0, with d values 1.25 and 1.28 (see table 6.3.2a) respectively were not observed. These correspond to diffraction angles of 76.2° and 74.1°. The intensities in table 6.3.2b are scaled relative to the largest peak given by the mixed Co/Cu/oxide (see section 6.2.2).

$Co/SiO_2$40Å;10:100

No obvious diffractions were observed for the activated and air exposed sample. This suggests that the Co^0 present (see section 6.3.2) was dilute and/or non-crystalline. Small metal particles are effectively non-crystalline, since line broadening (see section 6.2.2) occurs to such an extent that diffractions become obscured.

It has been suggested (Roe, 1986; Roe *et al.*, 1988) that the Co^0 on activated $Co/SiO_2$40Å; 10:100 occurred as large metal particles originating from Co_3O_4 reduction and small metal particles from octahedral Co^{2+} reduction. Assuming that the large metal particles were predominantly re-oxidised during air exposure (see section 6.3.4), the Co^0 would have mainly occurred as small particles. The X-ray diffraction technique would have failed to detect these particles.

No obvious diffractions were observed which could be associated with Co_3O_4. Bulk oxide coating Co^0 particles, which seemed present according to TPR evidence (see section 6.3.2), may not have been well defined crystallographically. Detection of such a phase would thus have been difficult.

substance	d values (Å) and relative intensities		
Co^o (cubic)	2.05_x	1.77_{40}	1.25_{30}
Cu^o	2.09_x	1.81_{50}	1.28_{20}

Table 6.3.2a Diffractions of Co and Cu metals.

sample	d values (Å) and relative intensities	
$Co/SiO_2$40Å;10:10	-	-
$Cu/SiO_2$40Å;10:100	2.09_{20}	$1.81_{9.6}$
$Co/SiO_2$40Å;10:100 + $Cu/SiO_2$40Å;10:100	2.09_{12}	$1.81_{3.8}$
$Co/Cu/SiO_2$40Å;10:100	2.05_{13}	2.09_{12}

Table 6.3.2b Diffractions of activated catalysts.

Cu/$SiO_2$40Å;10:100

Diffractions due to Cu^o were apparent, despite the extent of re-oxidation (80% - see section 6.3.2). No diffractions from oxidic Cu species were observed. This is consistent with the idea that Cu^{2+} species were re-integrated with the support (see section 6.3.1). Surface networks of Cu^{2+} gave no diffractions (see section 6.2.2).

Co/$SiO_2$40Å; 10:100 + Cu/$SiO_2$40Å; 10:100

Diffractions due to Cu^o were clearly observed. They were weaker than for Cu/$SiO_2$40Å; 10:100 because of the dilution occasioned by mixing (see sections 4.2.4, 5.2.1 and 6.2.2). The diffraction pattern was an additive of those given by the single metal catalysts.

Co/Cu/$SiO_2$40Å;10:10:100

A doublet diffraction was given by this sample. It was composed of Co^o and Cu^o diffractions. The diffractions were broad and had therefore merged. The Co^o diffraction was the more intense of the two. The weak Co^o and Cu^o diffractions (see table 6.3.2a) were not clearly observed.

The appearance of a Co^o diffraction for the hybrid catalyst sample shows that the crystalline Co^o phase was more concentrated on Co/Cu/$SiO_2$40Å; 10:10:100 compared to Co/$SiO_2$40Å; 10:100 and the physical mix. The higher concentration of Co^o matches the higher concentration of Co_3O_4, as opposed to interactive Co^{2+}, present on calcined Co/Cu/$SiO_2$40Å; 10:10:100 (see sections 4.2.2 and 4.2.5). This parallel suggests that only bulk oxide reduced to well defined Co^o crystallites, as mentioned in the discussion of Co/$SiO_2$40Å; 10:100 results.

6.3.3 Electron Probe Microanalysis

Macroscopic Analysis

The Co, Cu and Si maps of the activated and air exposed samples are given in figs. 6.3.3a - 6.3.3d.

Distributions

The Co map of the typical Co/$SiO_2$40Å; 10:100 particle shown demonstrates that the metal was distributed evenly. The distribution of Cu on Cu/$SiO_2$40Å;10:100 was similar by enlarge, although some clustering occurred. The two clusters observed (top right hand corner of Cu map - refer to fig. 6.3.3b) were 10 μm across. The clusters represented a minor proportion of the total Cu loading on the sample.

The maps of the activated air exposed physical mix reveal that Cu and Co essentially remained on separate particles even after activation. Migration occurred only to a minor extent. Microanalysis of individual Co/$SiO_2$40Å;10:100 and Cu/$SiO_2$40Å;10:100 particles showed that less than 0.30% (on a weight percent basis) of Cu and Co respectively occurred on the two particle types. The concentrations of dominant metals associated with the individual particles accorded with atomic absorption analysis (*i.e. circa* 9% on a weight percent basis).

These results establish categorically why the physical mixes behaved as additives of the single metal catalysts in TPR (see sections 4.2 and 4.3), and screening (see section 4.4) experiments. Interaction between Co^o and Cu^o, which necessarily required their migration, did not occur to any significant degree.

The Co/Cu/$Si0_2$40Å;10:10:100 particles were covered with both Co and Cu as for the calcined sample. The close spatial proximity would have enabled interaction (see sections 4.3, 4.4 and 4.5).

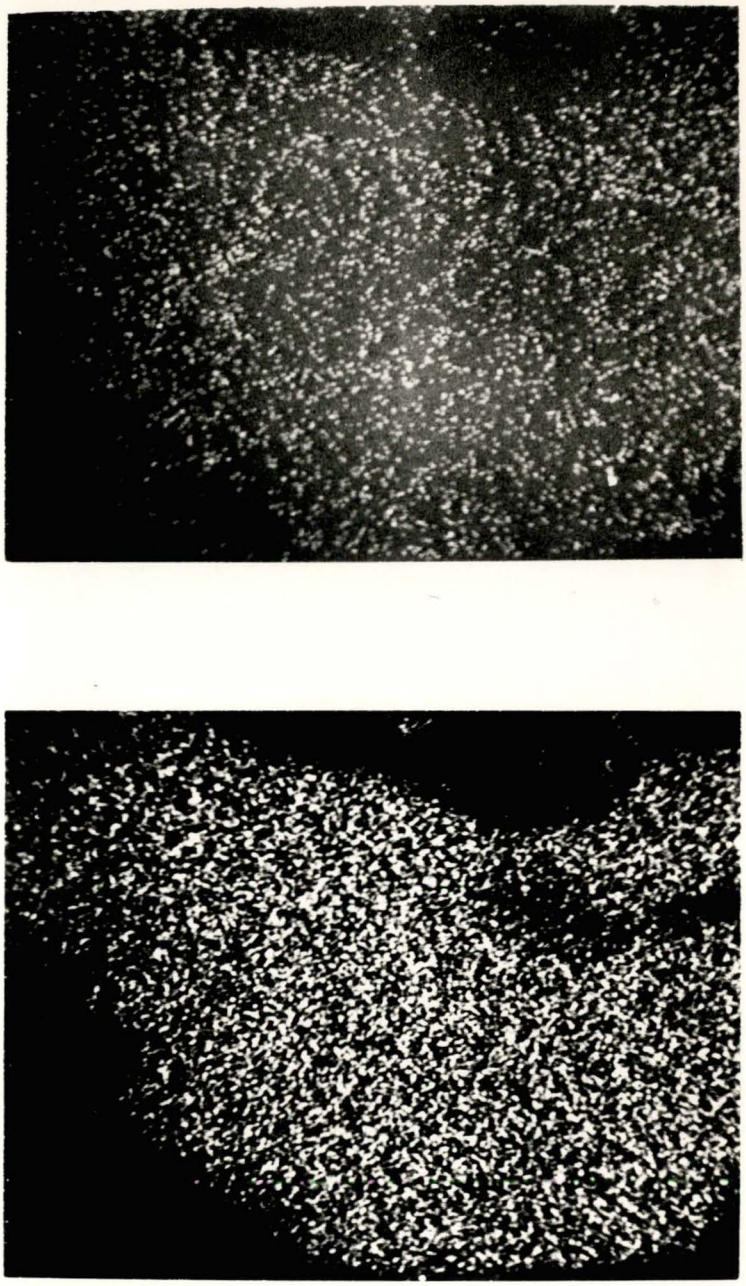

fig. 6.3.3a Co (top) and Si (bottom) maps for activated Co/$SiO_2$40Å;10:100 (700x).

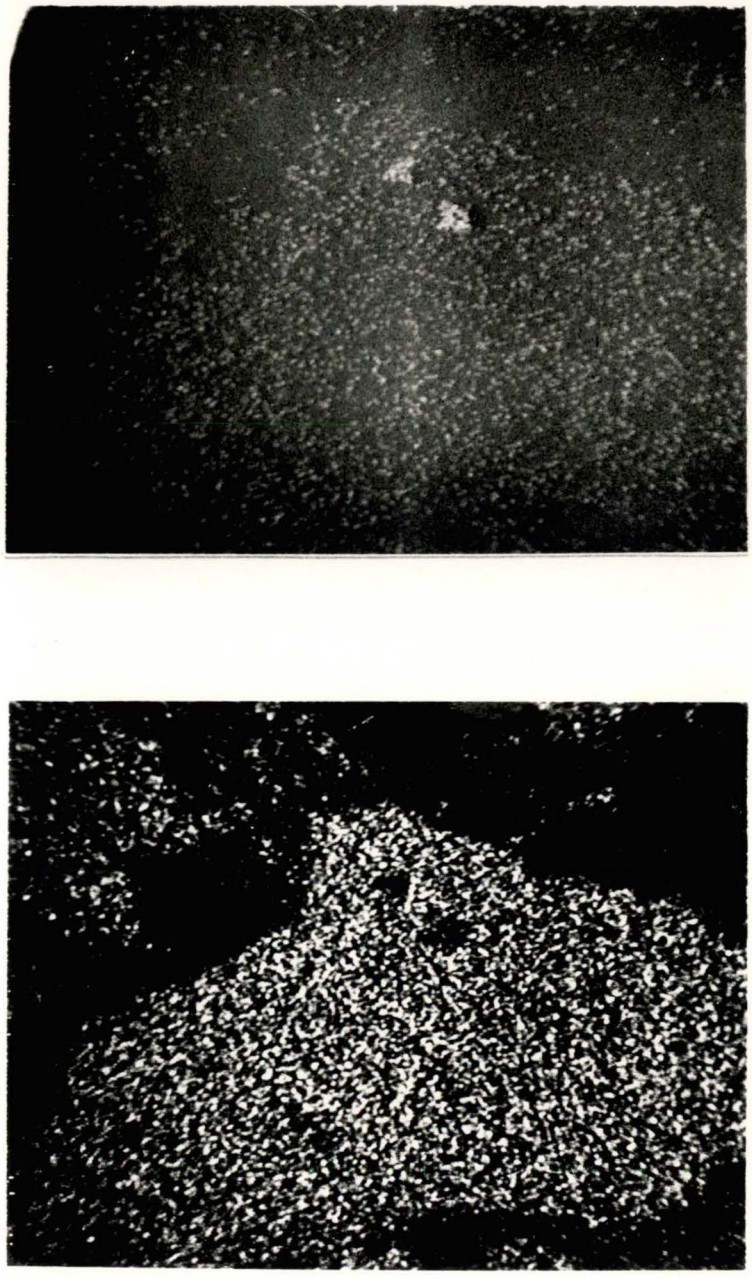

fig. 6.3.3b Cu (top) and Si (bottom) maps for activated Cu/$SiO_2$40Å;10:100 (300x).

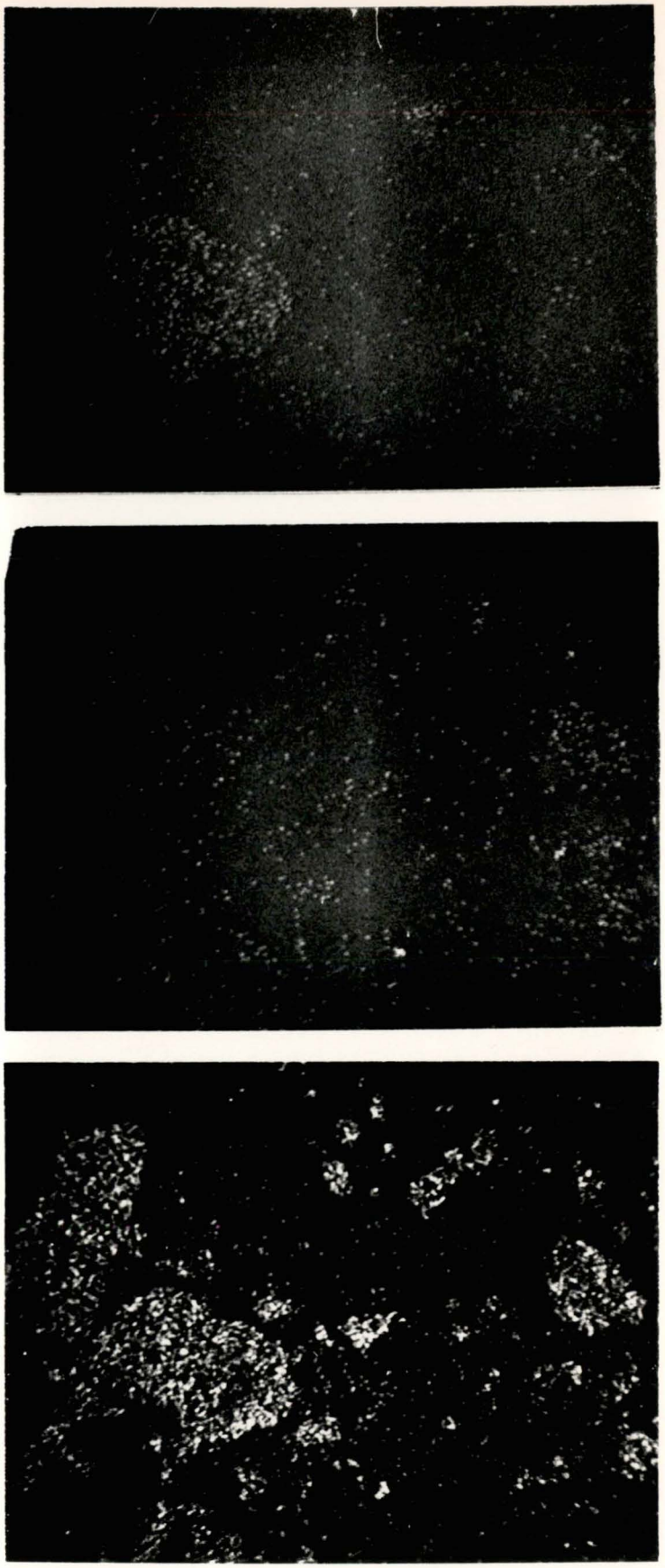

fig. 6.3.3c Co (top), Cu (middle), and Si (bottom) maps for activated $Co/SiO_2$40Å;10:100 + $Cu/SiO_2$40Å;10:100 physical mix (140x).

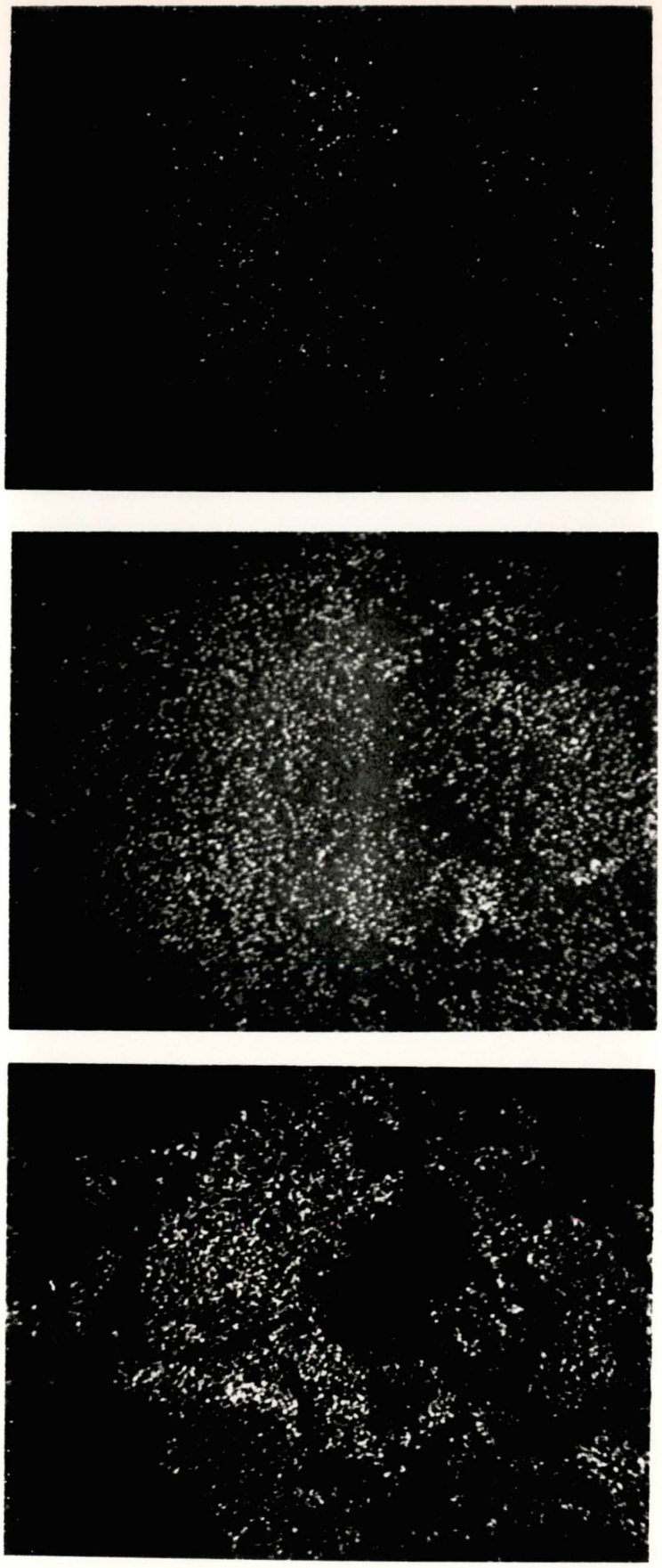

fig. 6.3.3d Co (top), Cu (middle) and Si (bottom) maps for activated Co/Cu/$SiO_2$40Å;10:10:100 (140x).

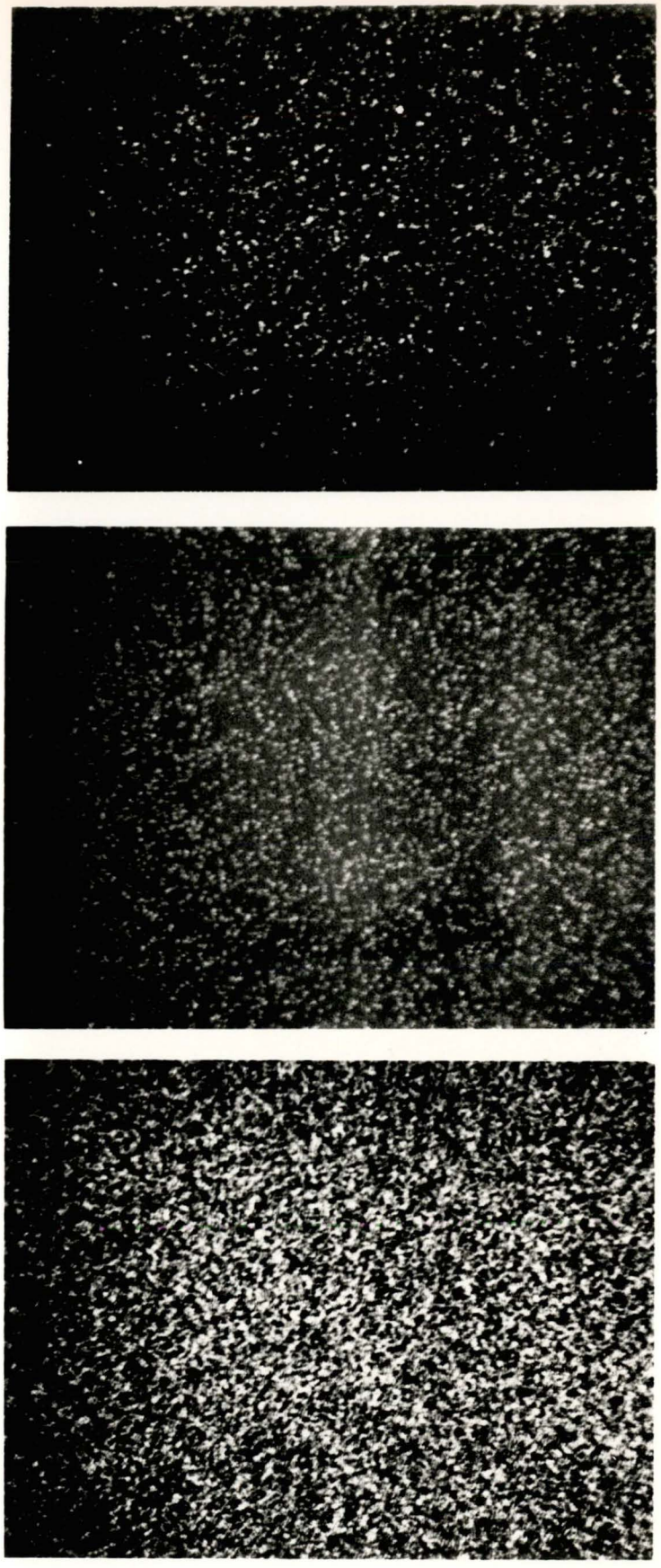

fig. 6.3.3e Co (top), Cu (middle), and Si (bottom) maps for activated Co/Cu/$SiO_2$40Å;10:10:100 (3000x).

Morphology

The average size of Co containing catalyst particles (200 μm to 250 μm - see section 6.2.3) did not change during the activation process. The boundaries of $Cu/SiO_2$40Å;10:100 particles became more sharply defined. The maximum dimension of the representative particle shown (see fig 6.3.3b) was 270 μm, which is of the same order as for particles of the other catalysts. The formation of Cu^o crystallites possibly led to the better definition of particle edges. The Cu^o crystallites may have bound the support in some way, as was suggested for Co_3O_4 crystallites (see section 6.2.3).

Microscopic Analysis of $Co/Cu/SiO_2$40Å;10:10:100

The maps of Co, Cu and Si acquired at a magnification of 3000 are given in fig. 6.3.3e. The even distribution of Co and Cu over the sample suggests that the metallic species remained in close proximity at a microscopic level during activation.

The comments regarding the violation of structural integrity through grinding of the sample (see section 6.2.3) again apply here. Significant re-oxidation of Cu^o (see section 6.3.1) during preparation of the sample may have affected the distribution of the metallic species which were present immediately after activation. These complications qualify interpretation of the data.

6.3.4 Gravimetric Uptake of CO

Presentation of the Data

The CO uptake results are given in table 6.3.4. The $SiO_2$40Å blank did not adsorb any CO and hence adsorption on catalyst samples was associated with metallic Co^o and Cu^o species.

In order to arrive at a value for dispersion, the number of moles corresponding to the weight of CO adsorbed were calculated. The assumption was then made that one molecule of CO associated with one atom of reduced surface metal. The weight of associated metal was deduced using effective atomic weights in the cases of the Co/$SiO_2$40Å; 10:100 + Cu/$SiO_2$40Å; 10:100 physical mix and the Co/Cu/$SiO_2$40Å; 10:10:100 hybrid (see Appendix 5). The weight of exposed metal was finally expressed as a fraction of the total metal loading.

The dispersion results are a useful measure of the number of active sites for each catalyst. However the values are not directly comparable because particles of Co^o and Cu^o are unlikely to adsorb CO with precisely the same stoichiometrics. Equivalent stoichiometries were assumed in calculating the dispersions of the physical mix and the hybrid catalyst. The absolute uptakes of CO, not being so manipulated, can be validly compared.

In the thermogravimetric experiments the samples were reduced under a static H_2 atmosphere (see section 3.4.6). It is reasonable to assume that the same changes in species distribution occurred during this activation process as it did during reduction at the same temperature (*i.e.* 400°C) in flowing H_2, the conditions used for screening and in other characterisation experiments (see sections 3.3.1 and 3.4). Excess H_2 was present in both static and flowing situations.

sample	CO uptake (mg/g catalyst)	% dispersion
$Co/SiO_2$40Å;10:100	1.85	4.80
$Cu/SiO_2$40Å;10:100	1.54	4.17
$Co/SiO_2$40Å;10:100 + $Cu/SiO_2$40Å;10:100	1.96	5.18
$Co/Cu/SiO_2$40Å;10:10:100	2.06	3.08

Table 6.3.4 CO uptake and dispersion values.

Comparison of the Catalysts

The $Co/SiO_2$40Å; 10:100 and $Cu/SiO_2$40Å; 10:100 catalysts both had dispersions of more than 4.0%. The reduction of the well dispersed interactive surface networks of Co^{2+} and Cu^{2+} which occurred on the calcined samples (see sections 4.2.2 and 4.2.3) would logically have given rise to well dispersed Co^o and Cu^o.

The gravimetric uptake of CO by the physical mix can be considered the average of the uptakes by $Co/SiO_2$40Å; 10:100 and $Cu/SiO_2$40Å; 10:100. The value was within 15% of the mathematical mean (1.70 mg/g). The dispersion of the physical mix was also an average of the dispersions of the single metal catalysts consequently. The sample weight was not halved (see section 4.2.4) in the calculation of the CO adsorption per gram of catalyst.

The gravimetric uptake for the physical mix should be doubled in order to make a valid comparison with the hybrid catalyst uptake (see section 4.2.4). The appropriate values are 3.92 mg/g and 2.06 mg/g respectively. The lesser uptake by $Co/Cu/SiO_2$40Å;10:10:100 probably resulted because of the reduction properties of bulk Co_3O_4. It has been shown that the bulk oxide reduces to give poorly dispersed (<0.05%) Co^o (Roe, 1986; Roe *et al.*, 1988). The entire Co loading on the hybrid catalyst was constituted by Co_3O_4 (see sections 4.2.4 and 6.2), and its reduction would not be anticipated to give rise to Co^o capable of significant CO adsorption. On the $Co/SiO_2$40Å;10:100 + $Cu/SiO_2$40Å;10:100 physical mix, a fraction (35%) of the total Co loading was constituted by octahedral Co^{2+}, associated with the single metal Co catalyst, which was reduced to well dispersed Co^o (Roe, 1986; Roe *et al.*, 1988; refer to table 6.4.2). The difference in Co distributions was apparently reflected by the differing CO uptakes of the hybrid catalyst and the physical mix.

A further implication of the low dispersion of Co^o derived from Co_3O_4 is that, in the absence of Co/Cu interactions, any CO adsorption on $Co/Cu/SiO_2$ 40Å;10:10:100 would effectively have been associated entirely with Cu^o. Since the Cu^o on both $Cu/SiO_2$40Å; 10:100 and the hybrid catalyst originated from equivalent amounts of identically interactive Cu^{2+} (see sections 4.2.3, 4.2.5, 4.3.3, 4.3.5 and 6.2), this approach suggests that the CO uptakes of the two samples should have been approximately equal. However the uptake by the hybrid catalyst was 34% higher than by $Cu/SiO_2$40Å; 10:100.

The difference between the two uptake values probably represents adsorption at Co^o and Cu^o crystallite interfaces. Distinct Co^o and Cu^o species were present on the activated hybrid sample (see section 6.3.2) in close proximity (see section 6.3.3). Furthermore Co^o and Cu^o are known to be not highly miscible (Huckel, 1951). Crystallite interfaces would therefore have readily formed. Adsorption of CO at Cu^o/ZnO interfaces has been previously reported (Parris and Klier, 1986).

Although the hybrid $Co/Cu/SiO_2$40Å;10:10:100 catalyst had the lowest dispersion, it gave the highest CO uptake. The net uptake is a more important gauge of activity since it is usually the number of active sites per gram of catalyst rather than their proportion relative to metal loading which determines catalytic performance.

6.3.5 The Nature of Co^0 and Cu^0 Species on Activated $Co/Cu/SiO_2$40Å;10:10:100.

Results from TPR showed that Cu^0 and Co^0 were present on activated $Co/Cu/SiO_2$40Å;10:10:100 (see section 4.3.5). The X-ray diffraction results (see section 6.3.2) suggest that Co^0 and Cu^0 occurred as distinct crystallites as opposed to true Co/Cu alloys, consistent with previous work (Huckel, 1951). Electron probe microanalysis (see section 6.3.3) showed that these crystallites were closely proximal. Interfaces where contact between crystallites occurred provided potential active sites for CO adsorption (see section 6.3.4).

The interaction between Co^0 and Cu^0 which was suggested by preliminary screening experiments (see sections 4.4.5 and 4.5) probably resulted from the intimate contact of crystallites. The Cu^0 particles can be regarded as supported by Co^0 (and *vice versa*) rather than by the $SiO_2$40Å.

On calcined Co/Cu/SiO40Å;10:10:100 interactive Cu^{2+} networks were seemingly interspersed with Co_3O_4 crystallites (see sections 4.3.5 and 6.2). These species may be anticipated to have reduced to well dispersed Cu^0 particles and larger Co^0 crystallites (see section 6.3.4). A feasible description of the activated hybrid catalyst is that small Cu^0 particles in contact with the $SiO_2$40Å support were surrounded by Co^0 clusters. The facile re-integration of Cu^{2+} into the support (see section 6.3.1) and the larger Co^0 particle size on activated and air exposed $Co/Cu/SiO_2$40Å; 10:100 compared to identically treated $Co/SiO_2$40Å; 10:100 (see section 6.3.2) are consistent with this model. Certainly no results contradict the description but none definitively confirm it.

6.4 Characterisation of Spent Catalysts

6.4.1 Temperature Programmed Reduction

The metal species present immediately after activation may have been altered by exposure to a CO/H_2O feed. They could have been oxidised by water, or converted to carbides for example. The characterisation of the active Co^o, Cu^o and Co^o/Cu^o species accomplished in section 6.3 can be considered to apply for the ultimate active species only if no substantial modification occurred.

The profiles of spent catalysts were acquired without air exposure (see section 3.4.1). If the samples had been exposed, it would not have been possible to tell whether re-oxidation was caused by oxygen in air or by the CO/H_2O feed. The profiles are shown in fig. 6.4.1.

$Co/SiO_2$40Å; 10:100

The TPR profile was very similar to that given by the activated sample (compare figs. 6.3.1 and 6.4.1) which shows that the same reduced and oxidic Co species were present in both situations (see section 6.3.1). Re-oxidation of Co^o was probably caused by H_2O in the feed and/or impurity O_2.

$Cu/SiO_2$40Å; 10:100

A peak appeared at 230°C, the same position as the peaks given by activated and air exposed Cu containing catalysts. It can therefore be assigned to the same species - surface networks of interactive Cu^{2+} re-integrated with the support (see sections 6.3.1 and 6.3.2).

This catalyst was the only spent sample re-oxidised to any major extent. The peak size was still less than for activated and air exposed $Cu/SiO_2$40Å; 10:100 (compare figs. 6.3.1 and 6.4.1). Quantitative analysis suggests that 30% of the Cu^o present immediately after activation was re-oxidised, most likely by H_2O in the feed, leaving 70% intact. This represented 70% of the total Cu loading, since all was reduced to Cu^o by the activation process (see section 4.3.3).

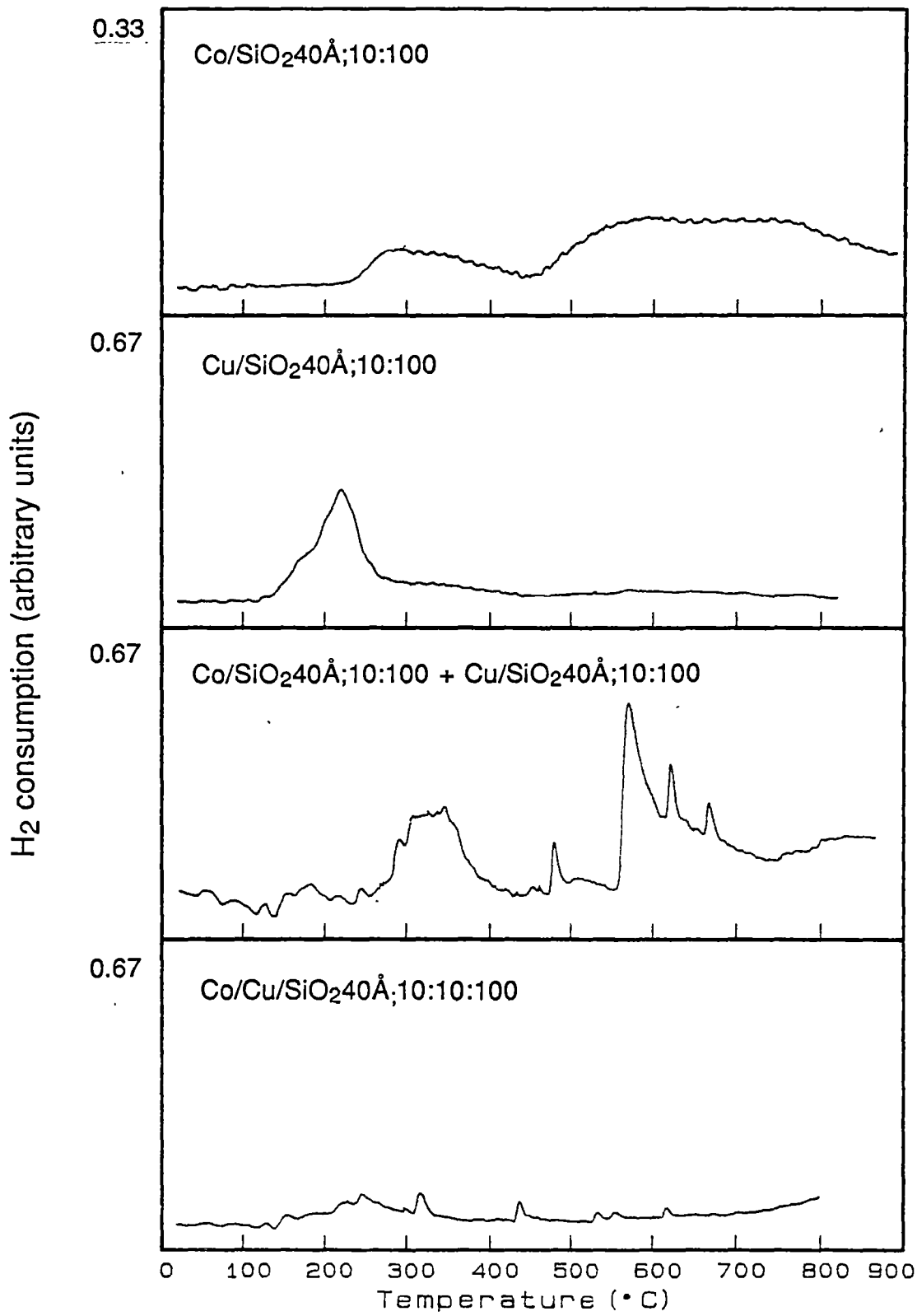

fig. 6.4.1 TPR profiles of spent catalysts.

Co/$SiO_2$40Å;10:100 + Cu/$SiO_2$40Å;10:100

Small peaks were given at 200°C, 300°C and 620°C by this sample. These can be assigned to re-integrated interactive Cu^{2+}, Co_3O_4 coating Co^o and intact tetrahedral Co^{2+} species respectively (see section 6.3.1).

In addition several H_2 consumption spikes were observed at temperatures above 400°C, the largest of which was positioned at 570°C. These can be tentatively assigned to the progressive "burning off" of discrete carbonaceous phases. Various long chain hydrocarbons were probably adsorbed to the KE active catalyst mix (see sections 4.4.1 and 4.4.3) which may well have reacted progressively.

The probable product of the burning off of carbonaceous deposits was methane (see section 2.2.2). Such a process is described by eqn. 6.4.1.

$$-CH_2\text{-ads} + H_2 \rightarrow CH_4 \qquad \text{eqn. 6.4.1}$$

The response of the TCD (see section 3.4.1) as this reaction proceeded would have been of the same sign as when reduction occurred because methane has a lower thermal conductivity than H_2 (see section 4.2.1). The response would not have been directly comparable to the reduction signal in quantitative terms because methane replaced H_2 in the gas stream. The water which replaced H_2 during reduction was trapped from the effluent gas stream. The response of the TCD would nevertheless have been of the same order in both cases.

The TPR profile of the physical mix was not an exact additive of the profiles given by the single metal catalysts. The physical interactions between Co/SiO_2Å;10:100 and Cu/$SiO_2$40Å;10:100 occasioned by their mixing (see section 4.4.4) can be used to explain these differences.

Spikes did not occur on the profiles of the single metal catalysts, as they did on the profile of the mixture. Hydrocarbon production did not proceed significantly on the single metal catalysts (see sections 4.4.2 and 4.4.3). This inactivity explains the absence of spikes given that spikes were due to the "burning off" of adsorbed hydrocarbons.

The peak due to re-oxidised Cu^{2+} observed at 230°C on the spent $Cu/SiO_2$40Å;10:100 profile did not appear on the mix profile. The 300°C peak, due to Co_3O_4 formed by re-oxidation of Co^o, occurred on single metal and mix profiles, but the 500°C peak occurred on the single metal profile alone. Higher H_2 production by the physical mix compared with the single metal catalysts, resulting from the synergism between the supported Co and Cu catalysts (see section 4.4.4), may have slowed the rate of metal re-oxidation in the physical mix. Smaller peaks at 300°C and 500°C, caused by re-oxidised Cu and Co respectively, would thus be expected.

The feed gas used in preliminary screening experiments had a different composition to that in which the current samples were spent (see section 3.3.1). The main difference was that Ar was used as a diluent in preliminary experiments. The absence of Ar would not logically have altered the modes of physical interaction between $Co/SiO_2$40Å;10:100 and $Cu/SiO_2$40Å;10:100.

The key aspect of the TPR profile is that the area beneath it is small. This implies that any changes to the species present immediately after activation (see section 6.3) were minor.

$Co/Cu/SiO_2$40Å; 10:10:100

The H_2 consumption between 200°C and 350°C was due to the reduction of both re-integrated interactive Cu^{2+} and Co_3O_4 coating Co^o. The intermittent spikes probably resulted from the reaction of adsorbed hydrocarbons. The high temperature reduction (>600°C) was associated with octahedral Co^{2+} (see section 4.3.5).

Nett H_2 consumption again was small, suggesting that any changes which occurred during synthesis to the species present immediately after activation were insignificant. The species present immediately after activation (see section 6.3) seemingly retained their integrity during synthesis.

6.4.2 X-ray diffraction

The X-ray diffraction results given by the spent catalysts are given in table 6.4.2. Diffraction intensities are scaled relative to the largest peak in the Co/Cu oxide standard. The spent samples were air exposed in the acquisition of diffraction patterns.

The results were much the same as given by the activated and air exposed samples. The TPR results suggested that the species present immediately after the catalyst were activated or spent were very similar (see section 6.4.1). The similarity of the diffraction patterns was therefore predictable. Differences which did occur only involved diffractions of low intensity and thus species in low concentrations.

Co/$SiO_2$40Å;10:100

The spent Co/$SiO_2$40Å;10:100 sample gave weak diffractions which coincided with the d values given by CoO (compare tables 6.2.2 and 6.4.2). This suggests that CoO may substantially have caused the 500°C reduction on the TPR profile of Co/$SiO_2$40Å; 10:100 (see sections 6.3.1 and 6.4.1). The same diffractions were not observed for activated and air exposed Co/$SiO_2$40Å; 10:100, which demonstrates that CoO was more concentrated on the spent sample.

Cu/$SiO_2$40Å; 10:100

The Cu^o diffractions on Cu/$SiO_2$40Å; 10:100 were 25% less intense than the diffractions on the activated and air exposed sample. The result shows that the re-oxidation of Cu^o after the catalyst was spent and air exposed was more than for when the catalyst was activated and air exposed. More importantly, the remaining Cu^o can be considered representative (see section 6.3.2) of the Cu^o present during synthesis.

sample	d values (Å) and relative intensities		
$Co/SiO_2$40Å;10:100	$2.13_{6.4}$	$2.46_{3.8}$	$1.51_{3.8}$
$Cu/SiO_2$40Å;10:100	2.09_{15}	$1.81_{7.7}$	
$Co/SiO_2$40Å;10:100 + $Cu/SiO_2$40Å;10:100	2.09_{14}	$1.81_{3.8}$	
$Co/Cu/SiO_2$40Å;10:10:100	2.09_{15}	2.05_{12}	$1.81_{3.8}$

Table 6.4.2 Diffractions of spent samples.

Co/$SiO_2$40Å; 10:100 + Cu/$SiO_2$40Å; 10:100

Diffractions due to CoO, as observed for spent Co/$SiO_2$40Å;10:100, were not given by the spent physical mix. This result is consistent with the absence of 500°C reduction on its TPR profile (see section 6.4.1). Thus the physical mix did not behave precisely as an additive of the single metal catalysts with respect to X-ray diffraction as well as TPR results. The Cu^0 diffractions were less intense than for spent Cu/$SiO_2$40Å; 10:100 probably because of the dilution incurred by mixing (see sections 4.2.4, 6.2.1 and 6.2.2).

Co/Cu/$SiO_2$40Å;10:10:100

The two strongest diffractions given by the spent and air exposed hybrid had the same d values as the diffractions due to Co^0 and Cu^0 which were observed for the activated and air exposed catalyst. The intensity of the Cu^0 diffraction with d value 2.09Å was 25% higher for the spent sample. Associated with the stronger intensity was the appearance of the Cu^0 diffraction with d value 1.81Å. The Co^0 diffraction (d value 2.05Å) was 10% weaker on the spent sample. The slight intensity changes are again insignificant. That no new diffractions have appeared is of more note. This indicates that no new species were formed during synthesis.

6.4.3 Electron Probe Microanalysis

The Co, Cu and Si maps of the spent and air exposed samples are given in figs. 6.4.3a - 6.4.3d. A microscopic analysis of spent Co/Cu/$SiO_2$40Å;10:10:100 is shown in fig. 6.4.3e.

No apparent changes occurred in either the morphologies of catalyst particles or the distributions of metal species compared to the activated samples (see section 6.3.3). These results, in conjunction with TPR data (see section 6.4.1), demonstrate the key point that Co^o and Cu^o were in close proximity during synthesis over Co/Cu/$SiO_2$40Å;10:10:100. Over the analogous physical mix, in contrast, the active metal species remained on separate catalyst particles.

6.4.4 The Nature of Co^o/Cu^o Species on Spent Co/Cu/$SiO_2$40Å; 10:10:100

The characterisation results showed that metallic Co^o and Cu^o species present on the catalysts immediately after activation were not much affected by synthesis. The only changes which occurred seemed to be carbon deposition and slight (<30%) re-oxidation. The ultimate active species on Co/Cu/$SiO_2$40Å; 10:10:100 within the CO rich regime (see section 6.1) was thus as described in section 6.3.5 - Co^o and Cu^o crystallites in close spatial proximity.

Co and Cu species present on Co/Cu/$SiO_2$40Å; 10:10:100 were fully reduced in the CO rich regime and would presumably have been in the same oxidation state in the H_2 rich environment characteristic of the H_2O rich regime (see section 5.4). The change in the nature of active species which seemingly occurred in moving from a CO:H_2O feed ratio of 1:2 to 1:3 could not therefore have involved the reduction of detectable amounts of oxidised metal. The removal of trace surface oxides and/or carbides may have accounted for the jump in activity which marked the transition from the CO rich to H_2O rich regime. Bulk structural modifications which may have been involved include surface enrichment with, or clustering of, WGSR active Cu^o.

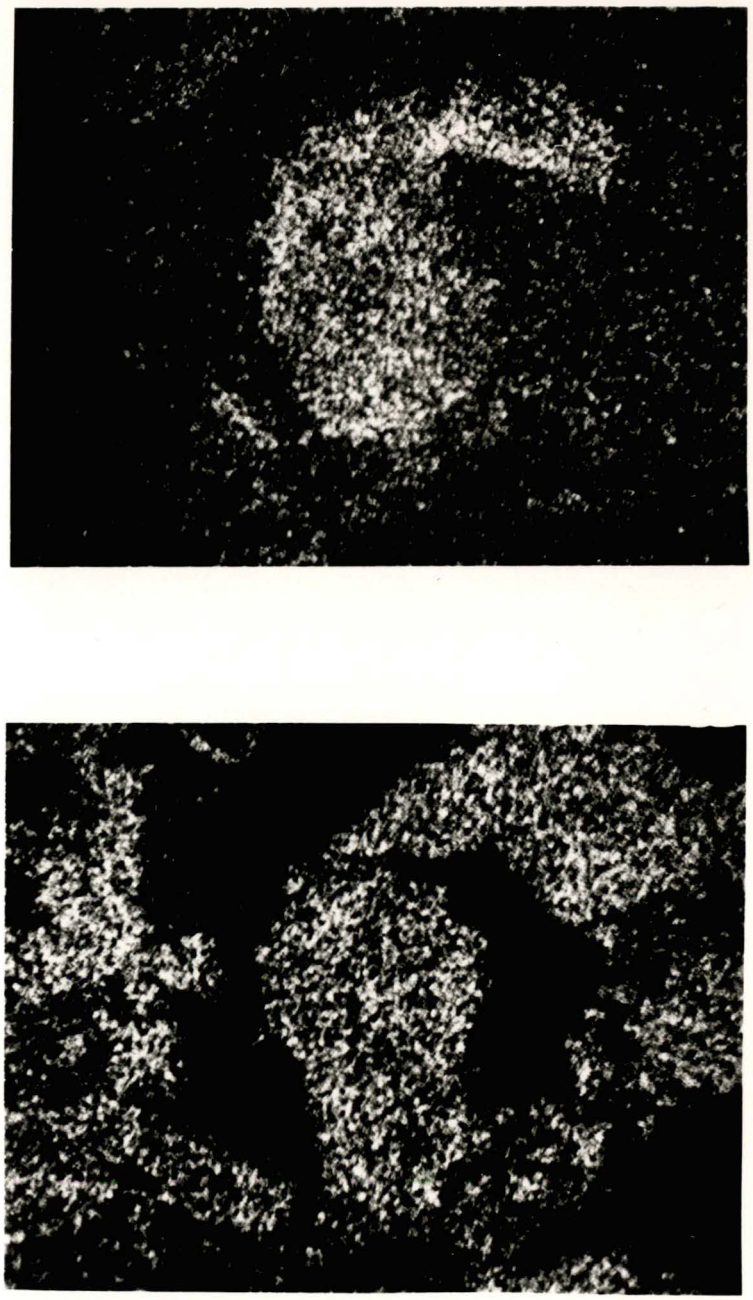

fig. 6.4.3a Co (top) and Si (bottom) maps for spent $Co/SiO_2$40Å;10:100 (200x).

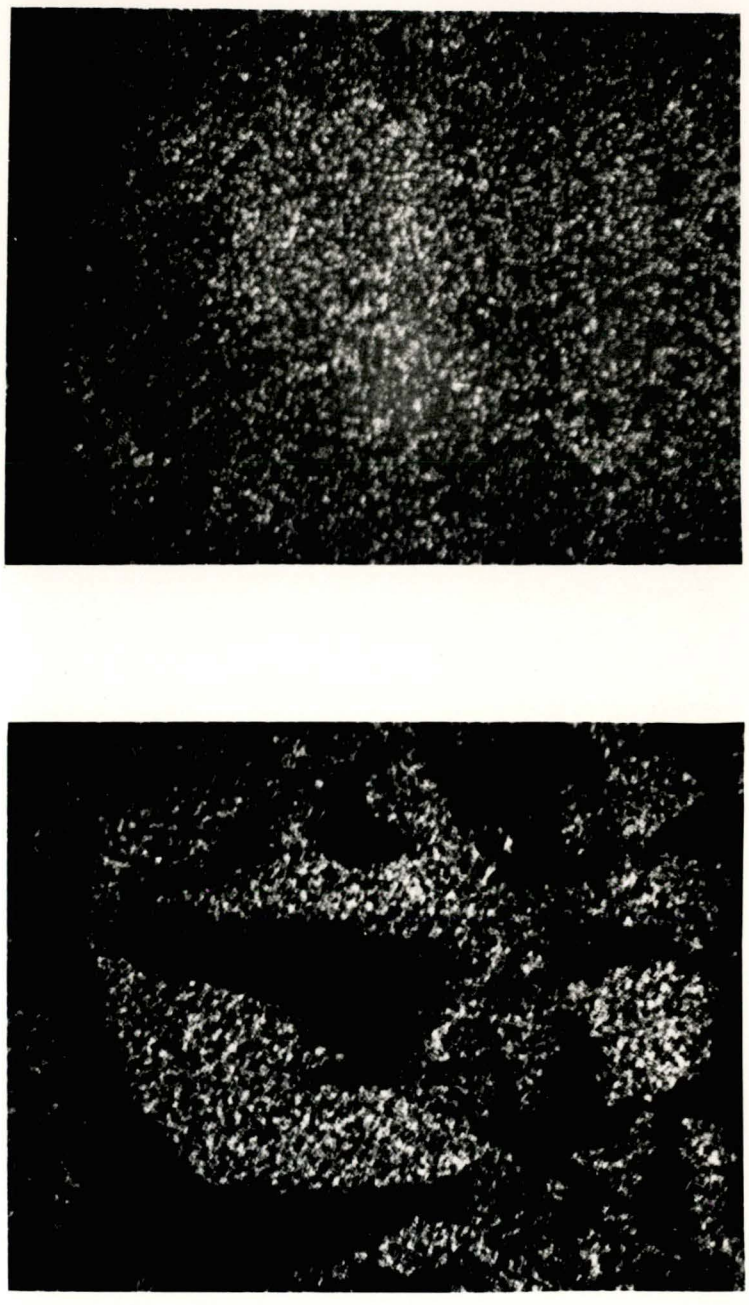

fig. 6.4.3b Cu (top) and Si (bottom) maps for spent $Cu/SiO_2$40Å;10:100 (200x).

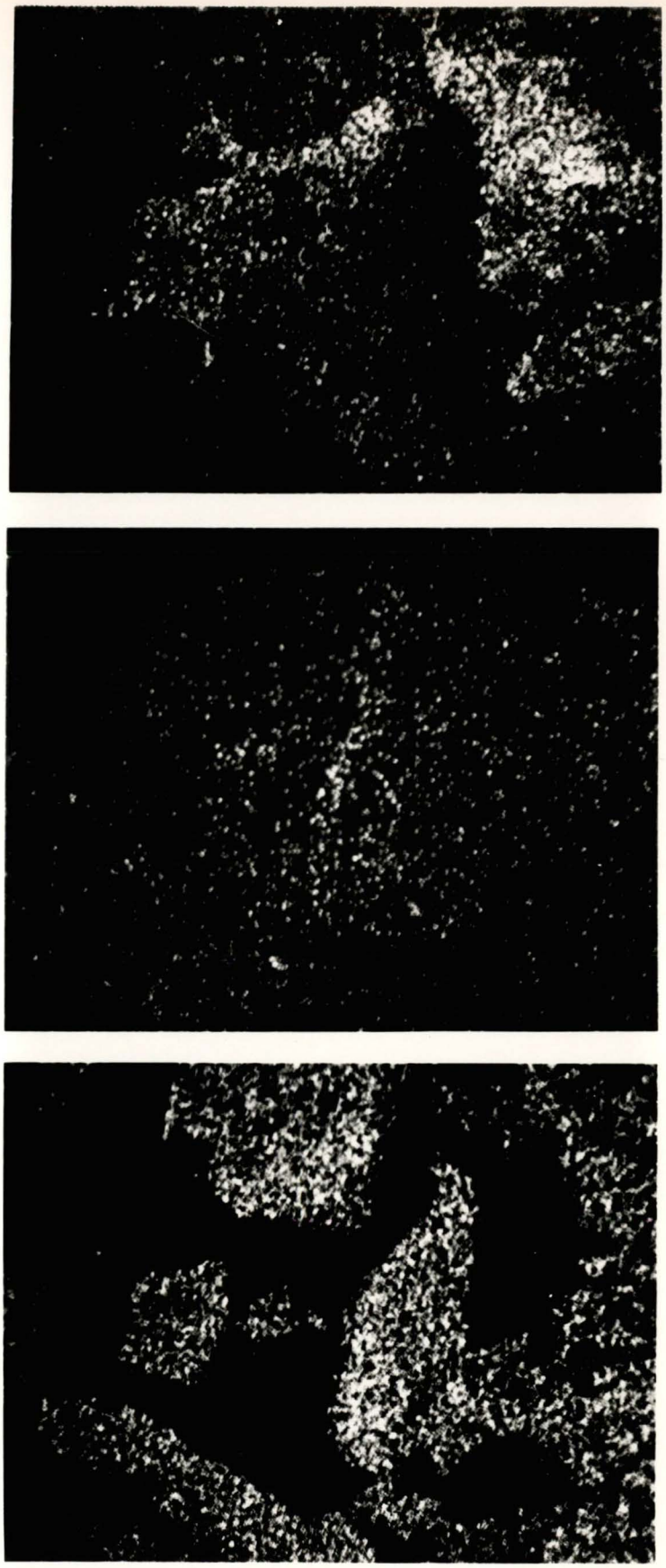

fig. 6.4.3c Co (top), Cu (middle), and Si (bottom) maps for spent $Co/SiO_2$40Å;10:100 + $Cu/SiO_2$40Å;10:100 physical mix (200x).

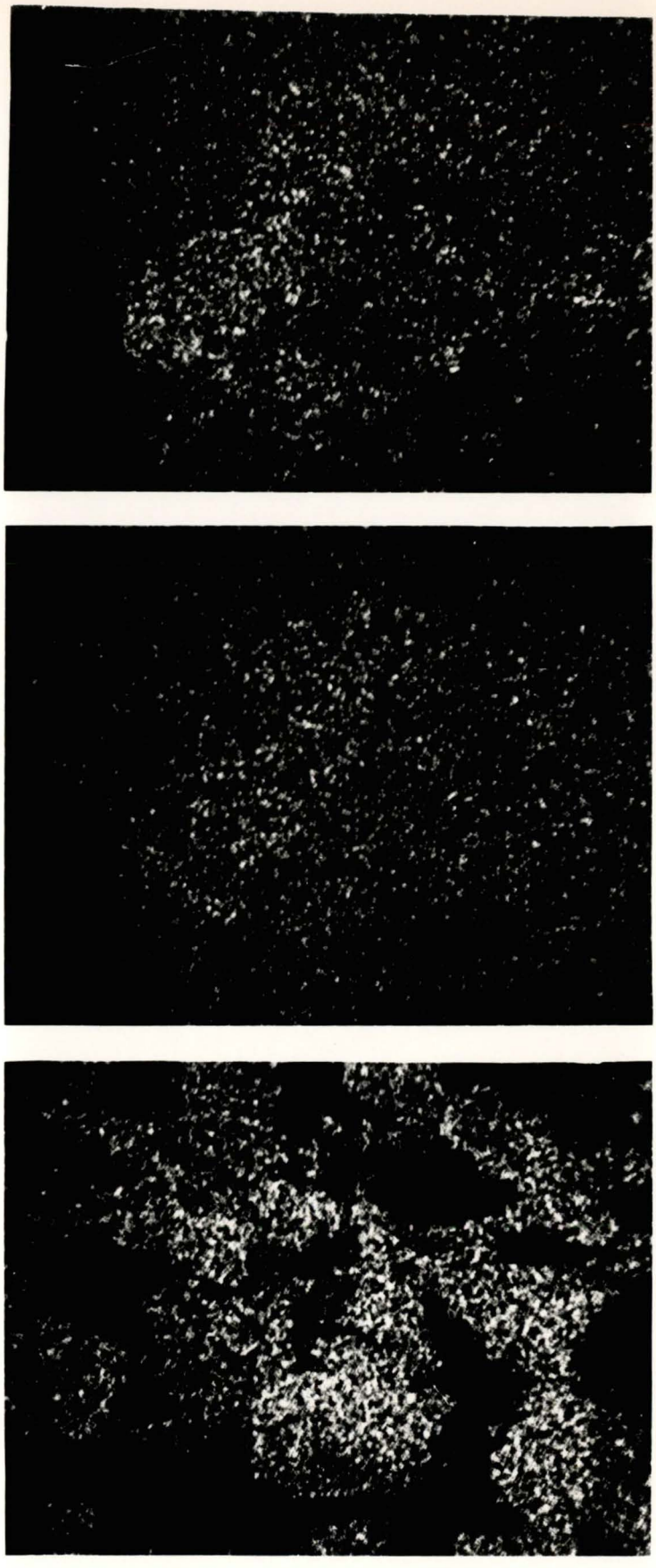

fig. 6.4.3d Co (top), Cu (middle), and Si (bottom) maps for spent $Co/Cu/SiO_2$40Å;10:10:100 (200x).

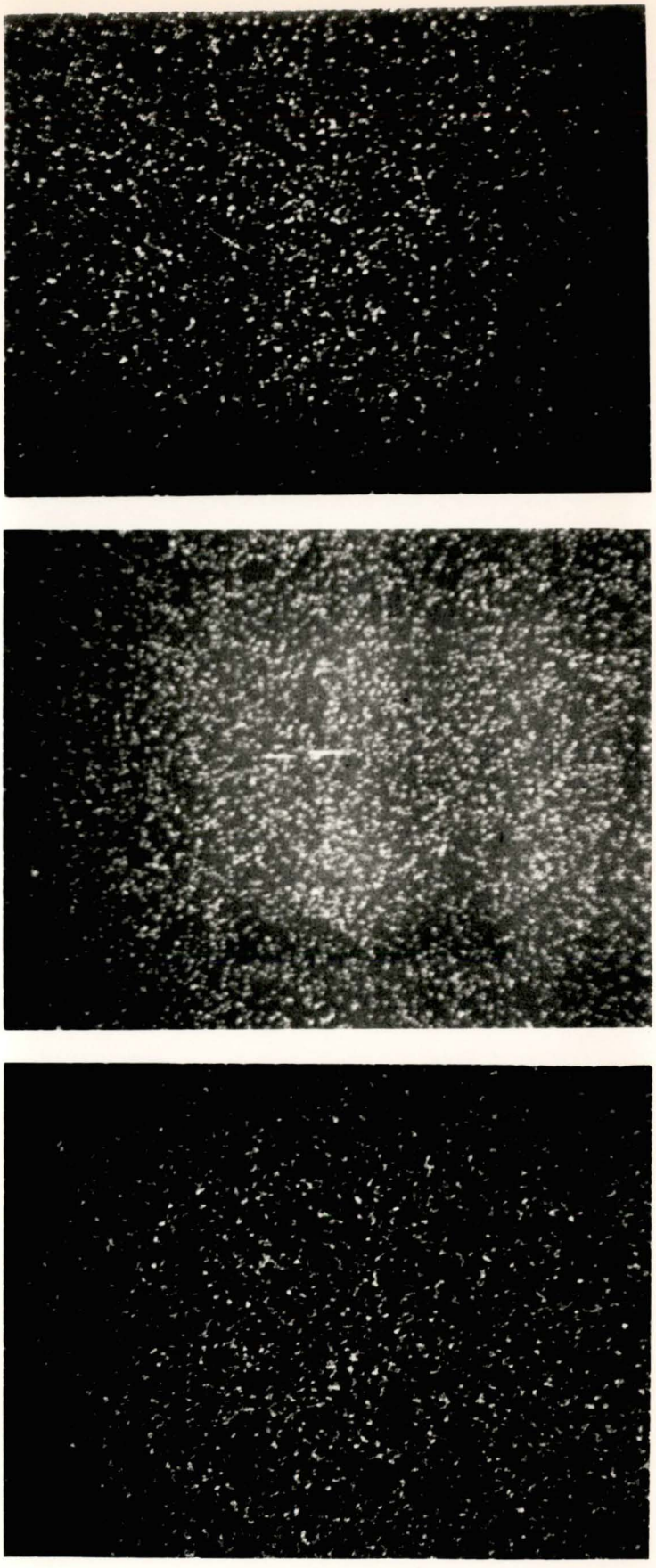

fig. 6.4.3e Co (top), Cu (middle), and Si (bottom) maps for spent $Co/Cu/SiO_2$40Å;10:10:100 (3000x).

6.5 Summary and Extrapolation of Results to Other Systems

The mixed oxide species on calcined Co/Cu/$SiO_2$40Å; 10:10:100 seemed to be interactive Cu^{2+} networks interspersed with Co_3O_4 crystallites. These were reduced during the activation process to Cu^o and Co^o crystallites in intimate contact. Possibly the Co^o crystallites supported smaller Cu^o particles. No alloying, in the true chemical sense, occurred. The interfaces between Cu^o and Co^o crystallites provided sites for CO adsorption. The species present immediately after activation were carburised and slightly re-oxidised during synthesis within the CO rich regime.

The similarity of the TPR profiles from 300°C to 500°C given by the variously loaded Al_2O_3 and $SiO_2$40Å supported hybrids suggested that the similar oxidic species occurred on all these catalysts (see section 4.2). Their similar activities suggested that similar Co^o/Cu^o moieties catalysed hydrocarbon synthesis (see sections 4.3 and 4.4). The description of the Co/Cu species on Co/Cu/$SiO_2$40Å; 10:10:100 can thus be extended to all the related catalysts. The relative and absolute proportions of Co and Cu would have differed for each catalyst (see sections 4.2 and 4.3). However the nature of Co/Cu species probably did not vary.

Interaction between Co and Cu on Co/Cu/$SiO_2$40Å; 10:10:100, and the other hybrid catalysts by extrapolation, resulted because of the intimate contact between the species associated with the two metals. In the case of the activated Al_2O_3 systems such interaction caused Cu^o to be modified from methanation active, on the single metal and physical mix samples, to WGSR active on the hybrids (see section 4.4). This result suggests that the influence of Al_2O_3 on the properties of the Cu^o particles it supported was attenuated by interaction between Cu^o and Co^o.

Insignificant migration of metal species between individual Co/$SiO_2$40Å; 10:100 and Cu/$SiO_2$40Å; 10:100 particles of the physical mix occurred. Interaction was therefore impossible. It seems reasonable that no significant migration occurred between supported Co and Cu particles in any of the physical mixes. All the Al_2O_3 and $SiO_2$40Å supported physical mixes thus behaved as additives of the appropriate single metal catalysts (see sections 4.4.2 and 4.4.4).

7 MECHANISTIC STUDIES

7.1 Introduction

The overwhelming concensus in the literature (see section 2.2) is that the KE synthesis proceeds by a sequential coupling of the WGSR (eqn. 1.1.7) and the FTR (eqn. 1.1.1). This hypothesis is supported further by results in the current study (see section 4.4).

The main aim of this section of the work was to identify reactive intermediates involved. No reports have appeared in the literature which have attempted to address this question. The hybrid Co/Cu/$SiO_2$40Å; 10:10:100 catalyst, shown to be active towards the KE synthesis (see section 4.4 and Chapter 5), was the sample used for the series of experiments reported here.

The first key step in the KE synthesis must necessarily have been the adsorption and activation of CO. This process was studied using IR spectroscopy (see section 3.5.3). Thermogravimetry was used earlier (see section 6.3.4) to assess CO adsorption, but the method is limited compared to the IR technique because direct evidence of the CO molecule cannot be obtained. The CO molecule is ideally suited to IR study because of its strong absorption. Much work has been published in this field, including reports regarding the chemisorption of CO on supported Co and Cu catalysts (Sheppard and Nguyen, 1978). However hybrid Co/Cu catalysts have not been previously investigated.

A further *in situ* IR experiment was performed in an attempt to detect KE synthesis intermediates directly. The mechanisms of the FT synthesis and the WGSR have often been probed by this method (see section 2.2). Given that the KE synthesis proceeds by sequential coupling of these reactions, this work provides a basis for the interpretation of spectra obtained during KE synthesis.

Interesting aspects of the hydrocarbon distributions given by $Co/Cu/SiO_2$40Å; 10:10:100, namely the suppression of C2 formation (see section 5.6.3) and the production of aromatics (see section 5.6.4), were also investigated. A possible relationship between the two features is that ethene polymerisation may have led to aromatic formation. The reactivity of ethene was assessed partly in order to probe this possible link, but primarily to see whether ethene polymerisation accounted for C2 suppression. The possibility that coke was an intermediate to aromatic production (see section 5.6.2) was pursued in a separate experiment by stripping pre-deposited coke with H_2O and H_2.

7.2 Infrared (IR) Studies

7.2.1 The Nature of the $Co/Cu/SiO_2$40Å; 10:10:100 Sample

The pre-treatment of $Co/Cu/SiO_2$40Å; 10:10:100 for the IR experiments differed from that used in microreactor and characterisation experiments. The key difference was that activated and air exposed samples were re-reduced at 300°C within the IR cell (see section 3.3.3).

Total reduction of the activated and air exposed catalyst was shown to occur at 230°C in TPR studies (see section 6.3.1). The reducing conditions used to activate the IR samples (300°C, 3 ml/min H_2, 12 hours - see section 3.5.1) were more severe than those which caused reduction in the TPR runs. The H_2 was more concentrated and the sample was reduced for an effectively longer time in the former case. Since the reduction temperature (300°C) was still mild, significant temperature induced alterations of structure, such as sintering, would not have been probable. The reduction cycle used to activate the hybrid catalyst IR sample would thus be expected to have left Co^0 and Cu^0 as the only metal species present, as was the case immediately after activation and prior to air exposure (see section 4.2.5).

No major structural alteration of the activated Co/Cu/$SiO_2$40Å; 10:10:100 catalyst occurred upon the introduction of Ar (see section 4.2.5), CO or H_2O (see section 6.4.1) in previous experiments. No modifications would be expected to occur during the IR investigations when the activated sample was exposed to the same gases (see section 3.5.1). The characterisation of Co/Cu/$SiO_2$40Å; 10:10:100 described in sections 6.3, 6.4 and 6.5 can thus be regarded as applicable to the IR samples.

7.2.2 The Spectrum of Blank Co/Cu/$SiO_2$40Å;10:10:100

The IR spectrum given by Co/Cu/$SiO_2$40Å; 10:10:100 immediately after activation, but prior to the introduction of CO (see section 3.5.1) is shown in fig. 7.2.2. The spectrum was acquired at room temperature in a H_2 atmosphere, and was ratioed against air. Four clear peaks were observed in the region of 4000 cm^{-1} to 1500 cm^{-1}; a sharp peak at 2350 cm^{-1}, broad peaks centred at 1980 cm^{-1} and 1860 cm^{-1} and another sharp peak at 1620 cm^{-1}. Below 1500 cm^{-1}, the $SiO_2$40Å support began to "black out" the IR radiation (Primet *et al.* 1977).

The 2350 cm^{-1} can be assigned to gaseous CO_2, specifically the antisymmetric C=O stretch (Davies, 1963). The CO_2 was probably a contaminant of the H_2 used. The peaks at 1980 cm^{-1} and 1860 cm^{-1} were probably due to overtones of Si-O stretches. Such peaks have been observed for SiO_2 supported catalysts and SiO_2 itself (Sheppard and Nguyen, 1978), but their assignment is often overlooked. The 1620 cm^{-1} is typical of adsorbed H_2O, and was caused by the H-O-H bending vibration (Little, 1966).

Spectra acquired subsequent to the adsorption of CO (see section 3.3.3) were referenced to this spectrum of the blank catalyst. This procedure simplifies interpretation of spectra in the energy region in which adsorbed CO vibrations occur (*i.e.* 2200 - 1650 cm^{-1}). The Si-O stretch overtones, which appeared in this energy band, were effectively subtracted out.

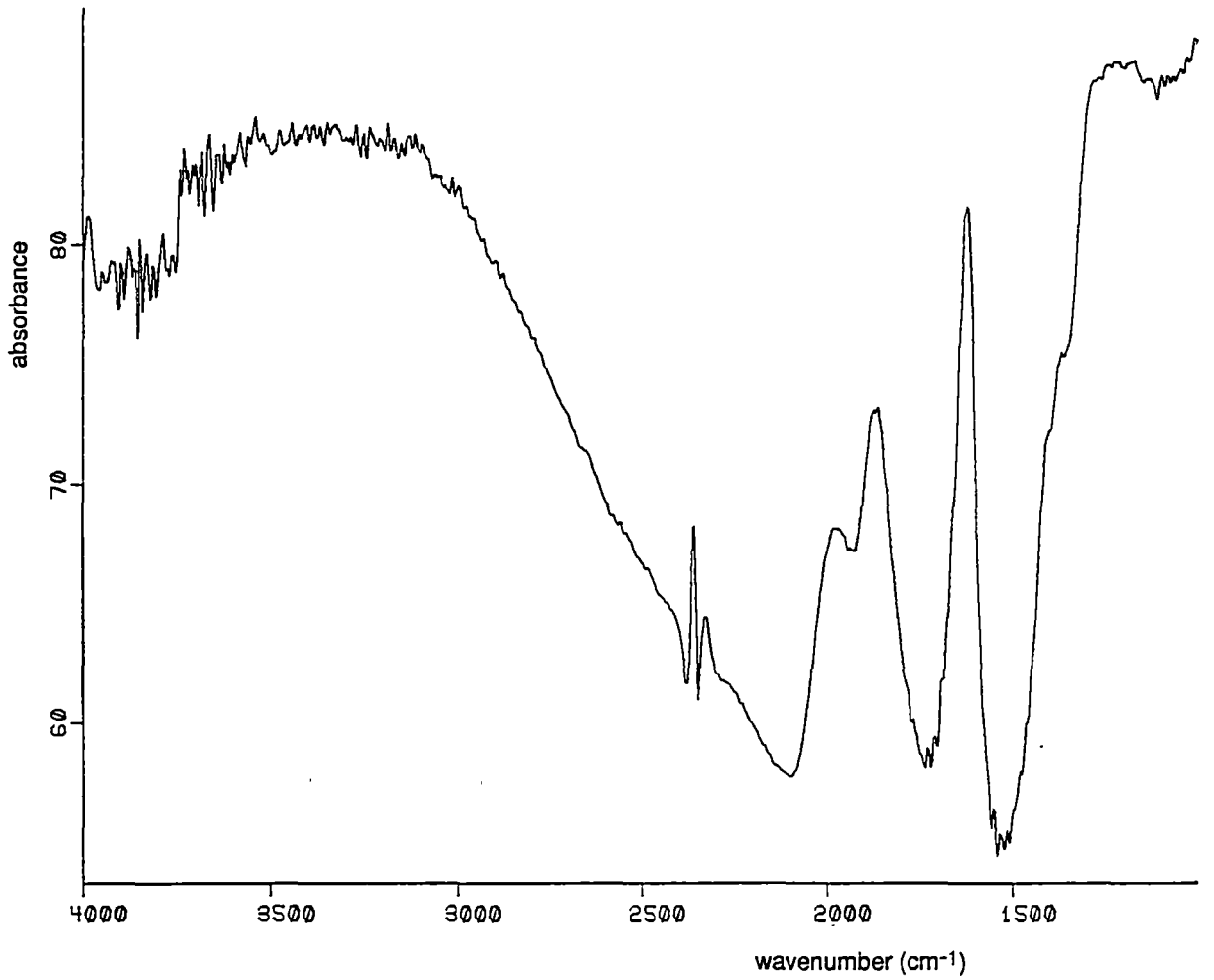

fig. 7.2.2 IR spectrum given by Co/Cu/$SiO_2$40Å;10:10:100 prior to CO exposure.

7.2.3 The Spectrum of Adsorbed CO

The spectrum given by Co/Cu/$SiO_2$40Å; 10:10:100 following exposure of the catalyst to CO at room temperature is shown in fig. 7.2.3a. A sharp peak at 2122 cm^{-1} and a broad peak spanning the energy range of 2020 cm^{-1} to 1970 cm^{-1} were observed.

The $SiO_2$40Å support did not adsorb CO as shown by gravimetric measurement (see section 6.3.4). The CO uptake must therefore have been associated with the Co^o and/or Cu^o species present on the catalyst (see section 7.2.1).

To further assist in the assignment of the peaks, the spectra of similarly treated Cu/$SiO_2$40Å; 10:100 and Co/$SiO_2$40Å; 10:100 were obtained (see section 3.3.3). These spectra are shown in figs. 7.2.3b and 7.2.3c respectively.

The spectrum given by Cu/$SiO_2$40Å; 10:100 exhibits a sharp peak at 2118 cm^{-1}. This peak can be assigned to linearly bonded CO molecules (Little, 1966; Sheppard and Nguyen, 1978). Differences between the Cu/$SiO_2$40Å; 10:100 spectrum after CO adsorption and the reference spectrum acquired immediately prior to CO exposure also caused the appearance of negative peaks at 2350 cm^{-1} and 2002 cm^{-1} and positive peaks at 1714 cm^{-1}, 1651 cm^{-1}, 1607 cm^{-1} and 1458 cm^{-1}. These peaks had at most 30% of the 2118 cm^{-1} peak intensity. The 2350 cm^{-1} absorption was due to atmospheric CO_2 and the 1714 cm^{-1}, 1651 cm^{-1} and 1607 cm^{-1} peaks were caused by adsorbed water (see section 7.2.2). The 2002 cm^{-1} and 1458 cm^{-1} were associated with Si-O vibrations. An imbalance in the ambient pressures of H_2O vapour when the reference and sample spectra were acquired probably accounted for the noisy baseline, particularly from 4000 cm^{-1} to 3000 cm^{-1}.

Similar arguments as were used to justify the total reduction of air exposed Co/Cu/$SiO_2$40Å; 10:10:100 (see section 7.2.1) suggest that Cu^o was the only metal species present on the IR sample. The Cu/$SiO_2$40Å; 10:100 catalyst was shown to reduce totally at 300°C in TPR studies (see section 4.2.3) and the more severe reducing conditions used in the IR experiments (see sections 3.5.1 and 7.2.1), would be anticipated to have caused the same extent of reduction. The colour of the wafer

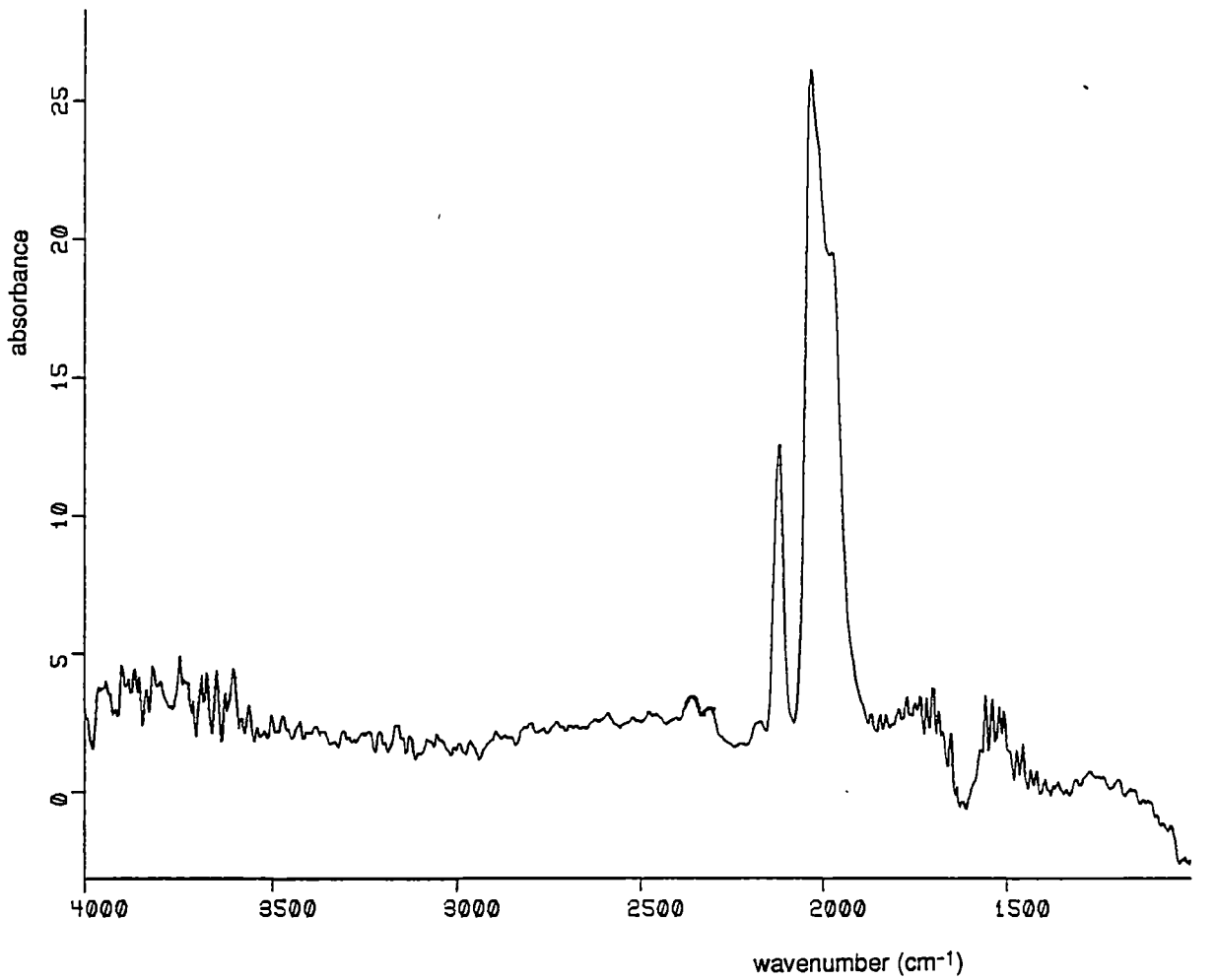

fig. 7.2.3a IR spectrum of adsorbed CO on Co/Cu/$SiO_2$40Å;10:10:100.

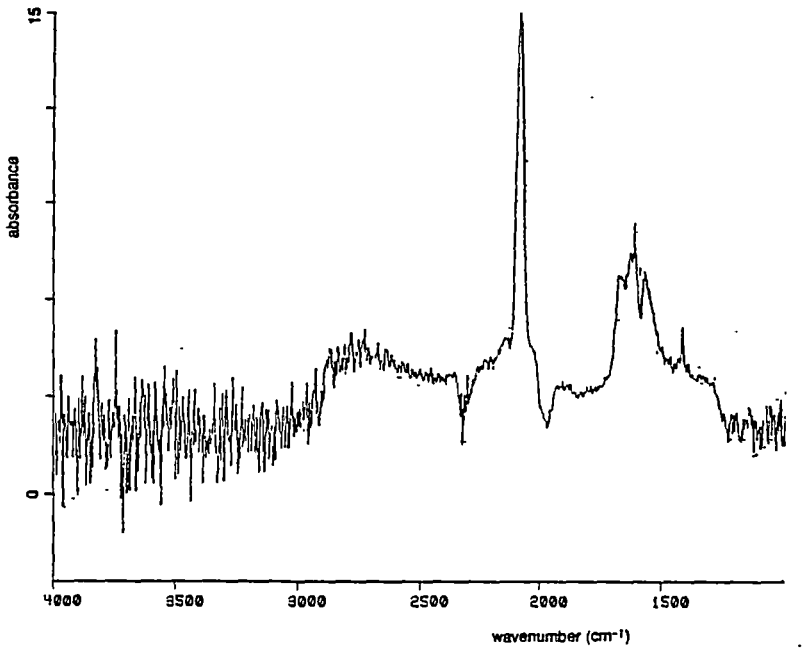

fig. 7.2.3b IR spectrum of adsorbed CO on $Cu/SiO_2$40Å;10:100.

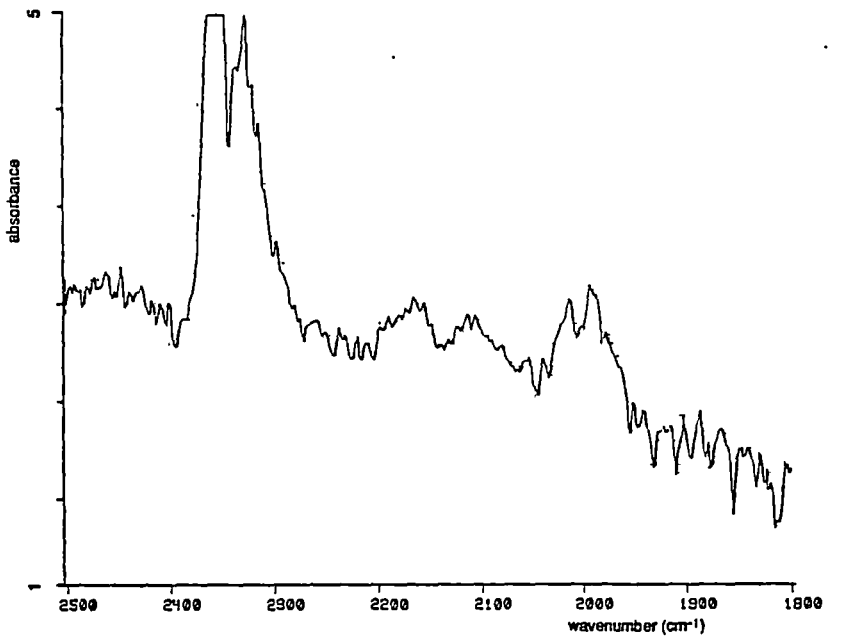

fig. 7.2.3c IR spectrum of adsorbed CO on $Co/SiO_2$40Å;10:100.

changed from green to copper, which supports the assertion of complete reduction. The linearly adsorbed CO which gave the 2118 cm^{-1} peak on the $Cu/SiO_2$40Å; 10:100 catalyst particles, must therefore have been associated with Cu^o .

The peak at 2122 cm^{-1} on the hybrid catalyst spectrum can be assigned identically since it is similar both in position and in shape to 2118 cm^{-1} peak in the $Cu/SiO_2$40Å; 10:100 spectrum. The slight difference in position (4 cm^{-1}) of the two peaks possibly reflects the interaction between Cu^o and Co^o an activated $Co/Cu/SiO_2$40Å; 10:10:100 (see sections 6.3.5 and 6.5).

Both peaks were at higher energy (by 15 cm^{-1}) than is usually observed for CO adsorbed on Cu metal (Sheppard and Nguyen, 1978). The shift shows that the properties of the Cu^o on the hybrid Co/Cu and single metal Cu catalysts were affected by the interplay with the other catalyst constituents present in each situation.

The spectrum of $Co/SiO_2$40Å; 10:100 (refer to fig. 7.2.3c) exhibited four peaks due to adsorbed CO positioned at 2170 cm^{-1}, 2122 cm^{-1}, 2021 cm^{-1} and 2002 cm^{-1}. A gaseous CO_2 peak appeared at 2350 cm^{-1}.

Using the same rationale as in section 7.2.1, it can be deduced that the same Co species occurred on the activated $Co/SiO_2$40Å; 10:100 IR sample as on the samples used in other experiments - Co^o, derived from both Co_3O_4 and octahedral Co^{2+}, as well as tetrahedral Co^{2+} (see section 4.3.2). In addition, slight re-oxidation of Co^o clusters may have occurred to give surface coatings of Co_3O_4. Thus four different Co species may well have occurred on the IR sample which could have given rise to an equal number of sites for CO adsorption. Four IR peaks would be expected on this basis. A possible assignment of peaks, consistent with the literature, is that the two higher energy peaks were due to CO linearly adsorbed on the oxidic Co species while the lower energy peaks were due to CO bonded with the same geometry on the two Co^o types of different origin.

The peaks indicative of adsorbed CO in the spectrum of $Co/SiO_2$40Å; 10:100 were less intense by an order of magnitude than the peaks in the appropriate spectra of $Co/Cu/SiO_2$40Å;10:10:100 and $Cu/SiO_2$40Å; 10:100 (compare figs. 7.2.3a, b and c).

The maximum peak height was just a single absorbance unit as opposed to approximately 15 in the other cases. The low intensities suggest that substantially less CO adsorbed to the $Co/SiO_2$40Å; 10:100 sample compared to the other systems investigated. Some caution must be exercised in precisely quantifying the IR data because of the complications presented by extinction coefficients, and wafer thickness for example. The results are nevertheless surprising in the light of thermogravimetric data (see section 6.3.4) which showed that under a static CO atmosphere $Co/SiO_2$40Å; 10:100, $Cu/SiO_2$40Å; 10:100 and $Co/Cu/SiO_2$40Å; 10:10:100 all absorbed approximately the same weight of CO.

The same Co species were present on the activated thermogravimetric and IR samples (see section 6.4.3). Since there were no significant structural differences in the samples used in the two separate experiments other factors must have caused the varying extents of CO uptake by the supported Co catalyst.

Contrasting experimental conditions may have been responsible. An obvious difference between the two experiments was that Ar was flowed over the sample subsequent to CO adsorption in IR experiments whereas a constant pressure of CO was maintained in the gravimetric procedure (see sections 3.4.6 and 3.5.3). Thus only strongly adsorbed CO would have remained on the IR samples. The low peak intensities may indicate comparatively weak Co-CO bond strengths. Alternatively CO may have dissociated on the Co^o particles to form an "oxycarbide" species. Such a species would be detectable by thermogravimetric but not IR techniques.

Regardless of the reasons for the low CO adsorption uptake on $Co/SiO_2$40Å; 10:100, the results show that adsorption to Co^o could not have significantly contributed to the intensities of peaks in the $Co/Cu/SiO_2$40Å; 10:10:100 spectrum. The broad peak which was centred at 2000 cm^{-1} could not therefore have been associated with Co^o only. It was previously shown not to be associated with Cu^o. Sites for CO adsorption must therefore have been created by interaction between the two metals, as was previously suggested in discussion of thermogravimetric results (see section 6.3.4).

Close inspection of the broad adsorption reveals that it is a triplet composed of peak at 2025 cm^{-1}, 2018 cm^{-1} and 1975 cm^{-1} (refer to fig. 7.2.3a). The last peak is in the energy region generally accepted to be indicative of adsorbed CO with a bridged geometry. The positions of the higher energy peaks are typical of linearly adsorbed CO (Sheppard and Nguyen, 1978; Little, 1966). A multiplicity of sites capable of bonding CO in any configuration can be envisaged to occur at the Co^o/Cu^o crystallite interfaces proposed to occur on $Co/Cu/SiO_2$40Å; 10:10:100 (see sections 6.3.4 and 6.5).

7.2.4 The Effect of Temperature on CO Adsorption

A stacked plot of the spectra given by $Co/Cu/SiO_2$40Å; 10:10:100 as it was heated in flowing Ar subsequent to CO adsorption is given in fig 7.2.4. The temperature range was 25°C to 200°C.

A negative peak at 1620 cm^{-1} due to H_2O adsorbed to the catalyst (see section 7.2.2) appeared as H_2O was released. The peak was negative because there was less H_2O on the catalyst at higher temperatures than there was when the reference spectrum was acquired at room temperature (see section 7.2.1).

The triplet centred at 2000 cm^{-1} which was associated with CO adsorbed at Co^o/Cu^o crystalline interfaces (see section 7.2.3) disappeared in moving from 45°C to 60°C. This shows that the CO was removed from the various adsorption sites.

There are two possible pathways by which removal could have occurred. The CO molecule may have dissociated to C and O according to eqn. 1.1.3

$$CO_{ads} \rightarrow C_{ads} + O_{ads} \qquad \text{eqn. 1.1.3}$$

A carbidic species may well have been produced from the adsorbed C atoms (see section 1.1). Alternatively CO may desorb non-dissociatively according to eqn. 7.2.4.

$$CO_{ads} \rightarrow CO\ (g) \qquad \text{eqn. 7.2.4}$$

It is difficult to differentiate between the two possibilities by analysis of the IR spectra alone. An increase in background absorption in the 4000 cm^{-1} to 3200 cm^{-1} and 1500 cm^{-1} to 1000 cm^{-1} regions occurred simultaneously with the disappearance of the

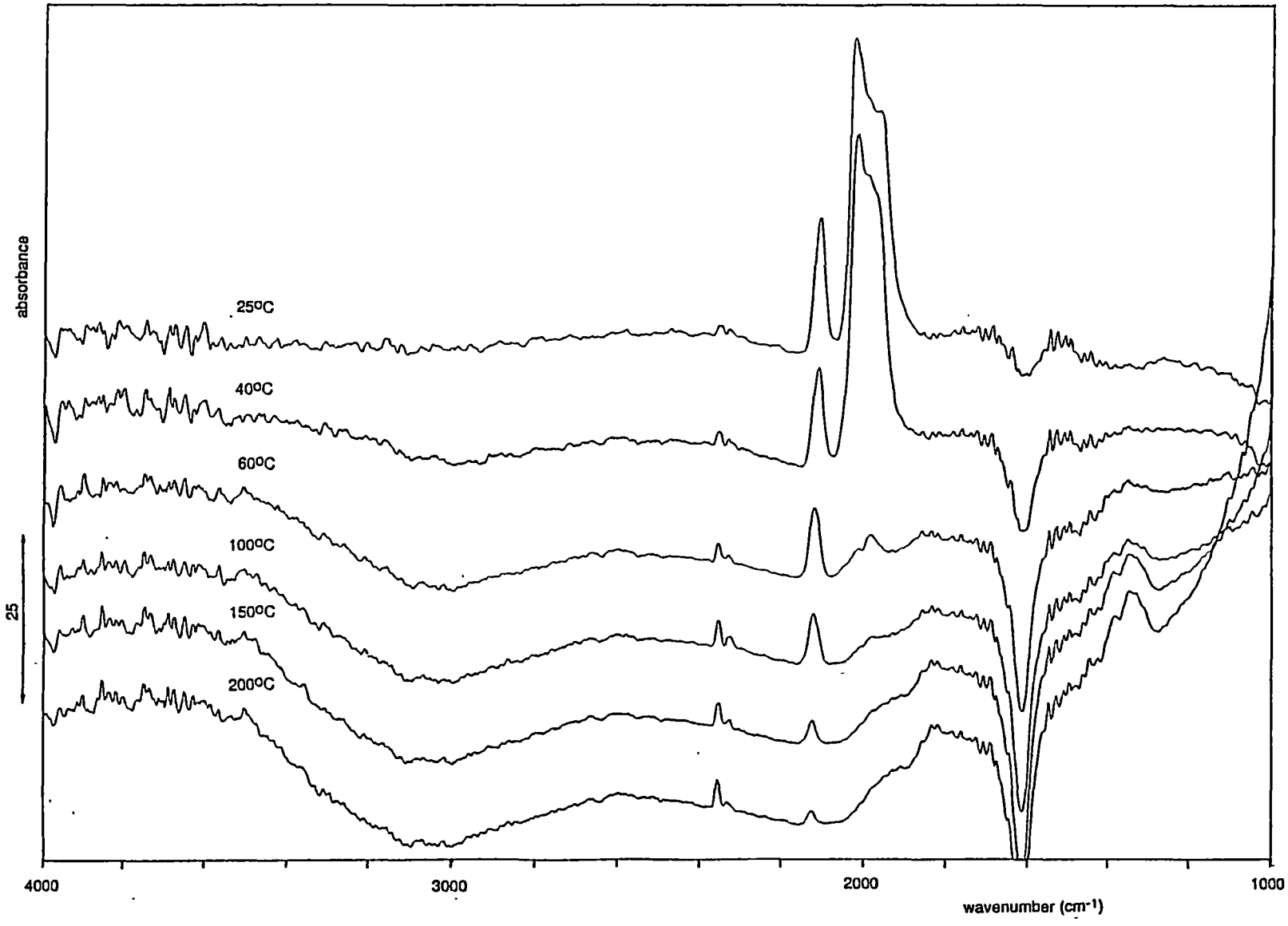

fig. 7.2.4 IR spectra of adsorbed CO on Co/Cu/$SiO_2$40Å;10:10:100 at various temperatures.

triplet CO peak. This shows that catalyst structure was modified in the 45°C to 60°C temperature region. The decomposition of CO would be expected to have such an effect. However an increase in the temperature of the catalyst may also alter structural features. The increase in CO_2 level in moving from 45°C to 60°C, shown by an increase in the intensity of the 2350 cm^{-1} peak, tends to suggest that some carbon was deposited according to the Boudouard reaction (eqn. 1.1.6) by the dissociation of CO adsorbed at crystallite interfaces.

The CO associated with Cu^0 particles desorbed gradually as the sample temperature was raised. The appropriate 2122 cm^{-1} peak was still apparent at 200°C which demonstrates that CO was still bonded intact to Cu^0 particles at this temperature. It was again difficult to discriminate whether CO was removed by dissociation and/or desorption.

7.2.5 Identification of KE Intermediates

The spectrum given by the Co/Cu/$SiO_2$40Å; 10:10:100 sample after activation and exposure to a CO:H_2O gas mix at 250°C is shown in fig 7.2.5. The reference spectrum was that of the hybrid catalyst at 250°C after CO adsorption and heating (see section 7.2.4). The peaks observed must therefore have been caused by the reactant gases or species produced by the catalyst, either in the gas phase or adsorbed to the catalyst surface.

The doublet due to the fundamental vibration of CO was observed at 2143 cm^{-1}, and the C=O stretch of gaseous CO_2 at 2350 cm^{-1}. The intensity of the CO_2 peak indicates that substantial quantities of the gas were present. Hence significant CO conversion must have occurred during the time in which reaction was allowed to proceed (0.5 hours - see section 3.5.3).

At 250°C in the presence of CO and H_2O, Co/Cu/$SiO_2$40Å; 10:10:100 was known to produce hydrocarbons as well as surface carbon and gaseous H_2 (see section 5.4). However no obvious peaks were observed in the IR spectrum which could be

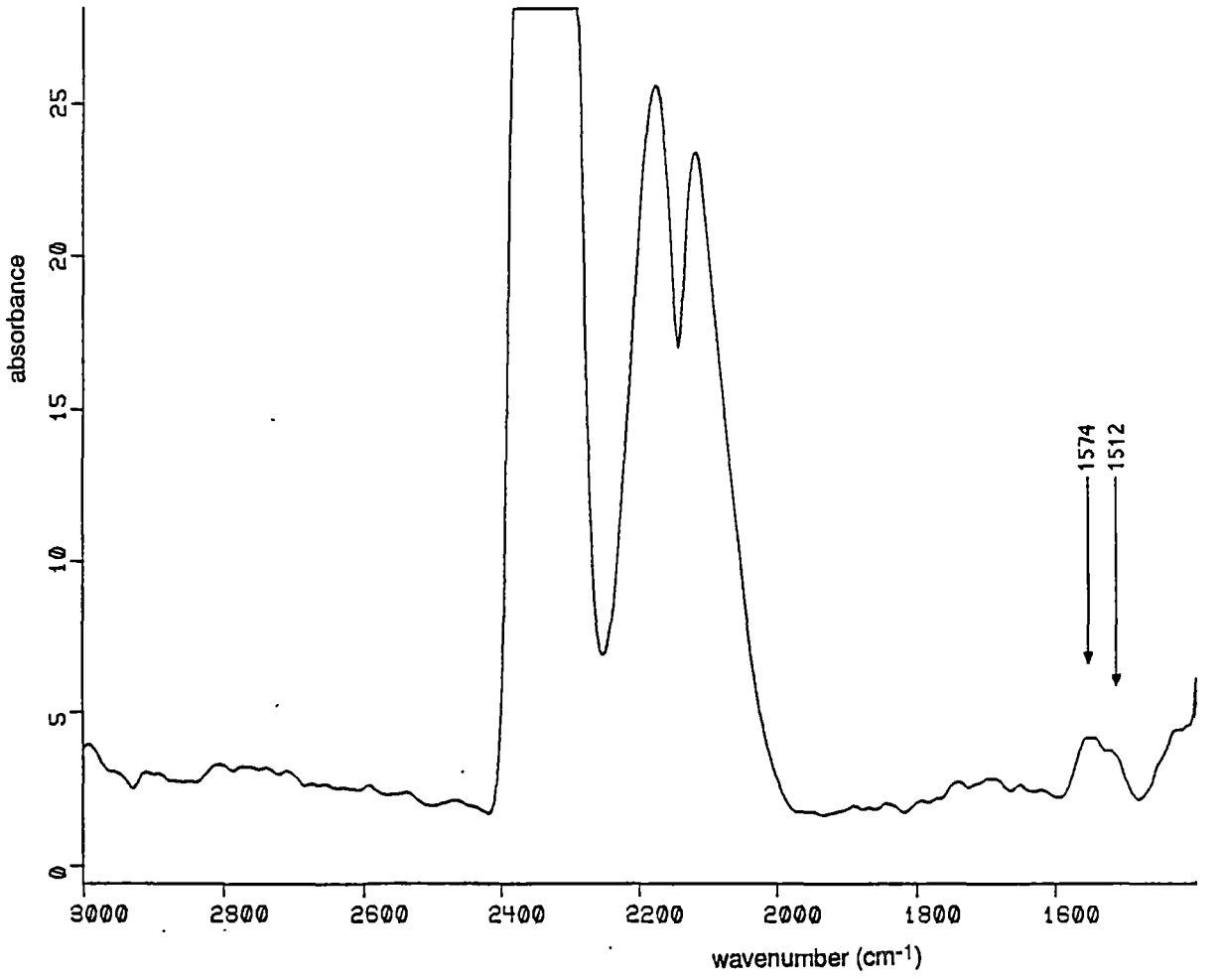

fig. 7.2.5 IR spectrum of species present under synthesis conditions over $Co/Cu/SiO_2$40Å;10:10:100 at 250°C.

assigned to these product molecules suggesting that their concentrations were below the limits of detection.

Peaks due to adsorption of CO at the sites described in section 7.2.4 were also absent. This absence does not imply that the sites no longer existed. Rather it suggests that the steady state occupancy of these sites by CO was low. Upon adsorption of CO, activation and reaction to give intermediates probably occurred rapidly. Such kinetics probably explain the low concentrations of adsorbed CO molecules.

The small peak at 1574 cm^{-1} can be assigned to adsorbed formate by comparison with the work of Edwards and Schrader (1984) and Amenomiya (1979). The vibration was an antisymmetric O-C- O stretch which, of all the possible formate vibrations, is known to give the most intense peak.

Formate type species are generally accepted to be the key WGSR intermediates (see section 2.1.3). Such species must logically form by the direct reaction of CO adsorbed intact, as opposed to dissociated CO, with H_2O. Such a process is described by eqn. 7.2.5

$$CO_{ads} + H_2O \rightarrow [H_2CO_2]_{ads} \qquad \text{eqn. 7.2.5}$$

Intact CO species were definitely observed at high temperature (200°C) only on the Cu^o component of the hybrid catalyst (see section 7.2.4). The results therefore suggest that Cu^o was involved in the production of H_2 *via* a formate type WGSR intermediate. This assertion is consistent with the idea that Cu^o was the active WGSR species (see section 4.4.5).

Another small peak at 1512 cm^{-1} can be assigned to the C=C stretch of polyene (Bhasin *et al.*, 1970; Heaviside de *et al.*, 1978; Larkins *et al.*, 1987). The C=C stretch has been shown to give the most intense peak in the polyene spectrum and so the absence of obvious C-H stretches at around 3000 cm^{-1} (Nakanishi, 1964) is not inconsistent with this assignment.

Polyene is commonly regarded as being a polymeric, conjugated and straight chain species. However it can more accurately be described as hydrogenated coke.

The position of the C=C stretch (1512 cm^{-1}) is within the energy range over which polycyclic aromatics absorb, that being 1600 cm^{-1} to 1500 cm^{-1} (Nakanishi, 1962). The structure of such compounds can be considered closely related to that of polyene. Long straight chain hydrocarbons absorb at significantly higher energies, 1640 cm^{-1} to 1580 cm^{-1} (Nakanishi, 1964). Energetic considerations further suggest that adsorbed conjugated hydrocarbon systems should exist as stable aromatic like structures rather than straight chain moieties.

Polyene, so described, may well have been the proposed common intermediate to coke and aromatic formation (see section 5.6.4). Dehydrogenation of polyene would yield coke, whereas fragmentation and subsequent desorption would yield aromatic compounds.

The formation of polyene would have been facilitated by the structure of the hybrid catalyst. Nascent H_2, presumably produced on Cu^o, would have been distributed amongst carbidic species deposited on the catalyst. In section 4.4 it was demonstrated that Cu^o components derived from interactive Cu^{2+} did not catalyse the Boudouard reaction. Hence they did not tend to accumulate carbon deposits. The carbidic deposits probably formed therefore on Co^o components of $Co/Cu/SiO_2$40Å; 10:10:100. Consistent with this idea is that $Co/SiO_2$40Å; 10:100 is known to be carburise (Roe, 1986; Roe *et al.*, 1988). The CO molecules adsorbed at Co^o/Cu^o interfaces and on Cu^o particles may have spilled over carbon to Co^o particles.

Polyene production would not have been so favoured for the physical mixes (see section 4.4) where nascent H_2, formed on $Cu/SiO_2$40Å; catalysts, could not have been in such close proximity to carbide deposits on Co^o moieties. This may explain the lower extent of aromatic production observed for the $Co/SiO_2$40Å;10:10:100 + $Cu/SiO_2$40Å; 10:10:100 physical mix compared to $Co/Cu/SiO_2$40Å; 10:10:100, the hybrid analogue.

It is unlikely that polyene was also involved in the production of linear hydrocarbons *via* the FTR (eqn. 1.1.1). Fragmentation of such a surface carbon species would probably not have yielded straight chain products (see section 2.2.2).

The assertion of non-involvement is also consistent with the idea that linear hydrocarbons and aromatics were synthesised by different pathways (see section 5.6.4). Dissociatively adsorbed CO, most likely present on Co^0 particles, may well have been involved in FT hydrocarbon formation according to the CH_x polymerisation mechanism (see section 2.2.1).

The observation of possible intermediates of the KE synthesis without observation of products probably resulted because of apparatus limitations. Gaseous products once desorbed would have occupied the full volume of the IR cell (see section 3.5.3). Adsorbed intermediates would necessarily have been localised on the IR wafer. The IR beam only sampled through middle 1 cm^2 of the cell. The sampled concentrations of gaseous products could therefore have been less than the sampled concentrations of intermediates even though absolute product molar levels were possibly higher.

7.3 Reactivity of Ethene

7.3.1 Presentation of the Data

The four main reactions of ethene which presumably occurred over $Co/Cu/SiO_2$40Å; 10:10:100 were

$$nH_2C = CH_2 \rightarrow (-CH_2 - CH_2-)_n \qquad \text{eqn. 7.3.1a}$$

$$nH_2C = CH_2 \rightarrow (-CH = CH-)_n + nH_2 \qquad \text{eqn. 7.3.1b}$$

$$nH_2C = CH_2 \rightarrow 2\,(CH)_n + nH2 \qquad \text{eqn. 7.3.1c}$$

$$nH_2C = CH_2 \rightarrow 2(C)_n + 2nH_2 \qquad \text{eqn. 7.3.1d}$$

No oxygen containing products were observed which suggests that H_2O was inert and played no important role in the current experiment.

The production of saturated hydrocarbons of odd and even carbon number, including methane, is represented by eqn. 7.3.1a. The production of unsaturated hydrocarbons, including acetylene and aromatics, is represented by eqn. 7.3.1b.

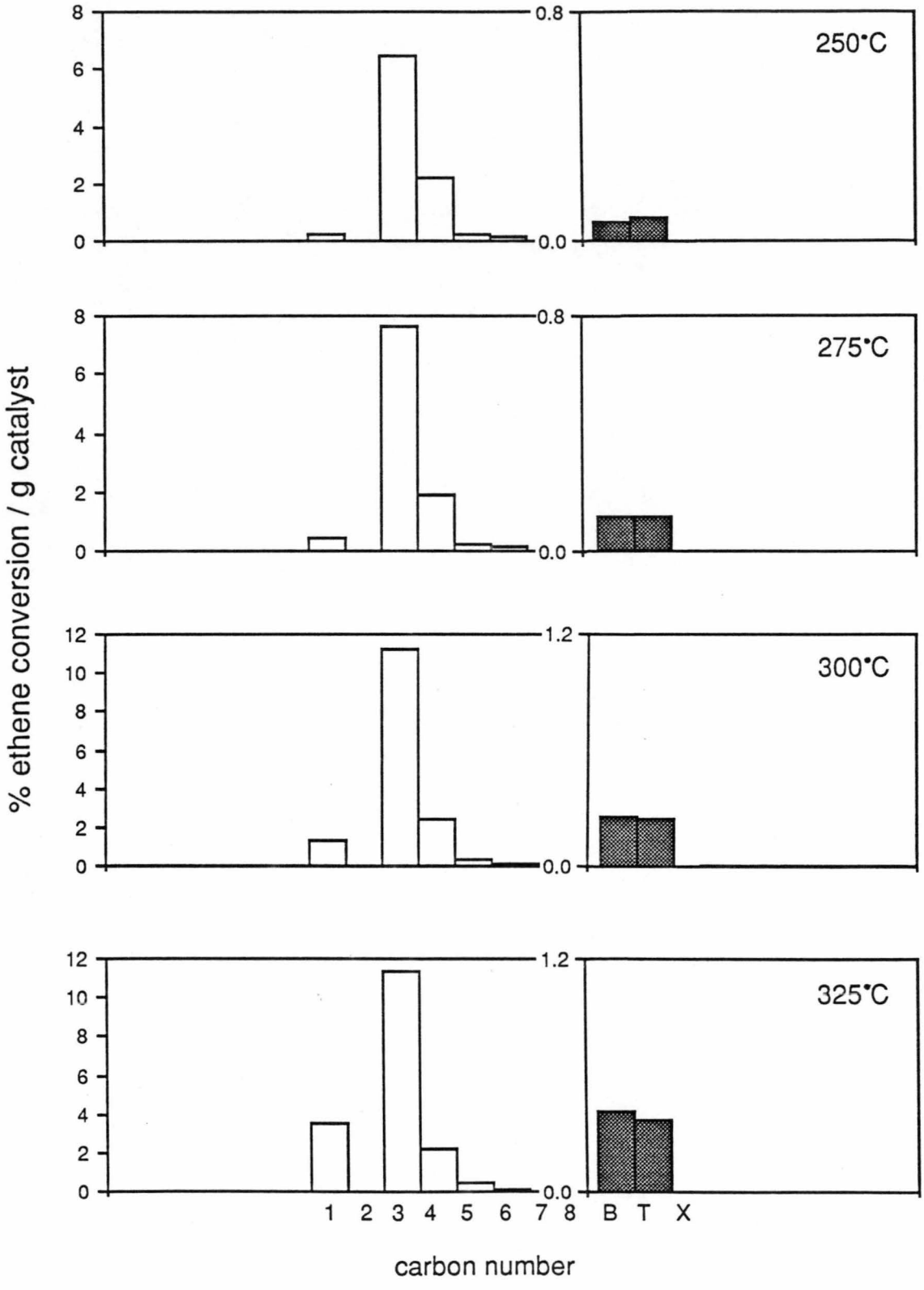

fig. 7.3.1 %ethene conversions to hydrocarbons.

% conversion/g to	250°C	275°C	300°C	325°C
hydrocarbons (excluding C2s)	9.39	10.6	15.9	18.3
coke	0.974	7.58	15.9	40.9
total	10.4	18.2	31.8	59.2

Table 7.3.1 Ethene conversions.

Combinations of equations 7.3.1a and 7.3.1b describe the formation of hydrocarbons with varying degrees of unsaturation.

Volatile hydrocarbon (see section 4.4.1) of all the types mentioned were detected. The % conversions of ethene to C1 and C3 through C8 fractions at all temperatures studied (250°C, 275°C, 300°C, 325°C - see section 3.5.1) are given in fig 7.3.1. The % conversion of ethene to C2s represented unpolymerised ethene, and these values are not plotted.

The product of eqn. 7.3.1c is [illegible]hydrogenated coke known as polyene (see section 7.2.5). Coke containing no H is formed according to eqn. 7.3.1d. Combinations of equations 7.3.1c and 7.3.1d represent formation of polyene with varying H content.

The treatment of data outlined in Appendix 6 allowed the estimation of combined % ethene conversions to polyene and coke. The values are given in table 7.3.1. The relative proportions of two carbonaceous species could not be evaluated.

7.3.2 Ethene Conversions

The results certainly show that ethene was reactive. The conversions to hydrocarbons plus coke at 250°C and 275°C were low (<20%). The overall conversions increased with temperature to 59.2% at 325°C.

The reaction of ethene over Co/Cu/$SiO_2$40Å; 10:10:100 gave the same order of product yields as did the reaction of CO over the same catalyst using the 1:1 CO:H_2O feed (see section 5.3). However the feed concentration of ethene was only 5% compared to 50% for CO. The results therefore demonstrate that ethene is a more reactive molecule than CO.

The results do not account for the suppression of C2 formation over Co/Cu/$SiO_2$40Å; 10:10:100 during KE synthesis (see sections 5.6.3 and 7.2.1). At 250°C and 275°C the percentage CO conversion to C2s was virtually zero using a KE feed with a CO:H_2O ratio of 1:1 (refer to fig. 5.3.3). In the current experiment ethene conversions at these temperatures were also minimal. The concurrence of these low

conversion figures suggests that C2s, once synthesised, were not substantially polymerised under KE conditions.

The relative hydrocarbon distributions resulting from ethene polymerisation over Co/Cu/$SiO_2$40Å; 10:10:100 were similar to those during KE synthesis. Cleavage of ethene must have occurred to produce odd carbon numbers and hydrocarbons. The most predominant hydrocarbon fraction at all temperatures was the set of C3 products. Increasing the temperature from 250°C to 325°C favoured the formation of low molecular weight products as well as benzene and toluene.

Even at the highest temperature studied (325°C) the selectivity to benzene and toluene as a fraction of overall hydrocarbon production was only 4.32%. The values were less at the lower temperatures. The small magnitude of the aromatic selectivity value suggests that ethene polymerisation was not exclusively associated with aromatic formation. If this was the case, a selectivity value approaching 100% would be expected.

The assertions that ethene polymerisation neither caused the suppression of C2 concentrations nor accounted for aromatic formation are not unequivocal. An inherent assumption is that the reactivity of ethene under synthesis conditions was identical to that in the reactivity experiment. This may not necessarily be true.

Every effort was made to control the reactivity experiment. The Co/Cu/$SiO_2$40Å; 10:10:100 sample was allowed to reach steady state in the optimal KE feed (CO:H_2O 1:1 - see section 5.7.4) before the ethene based feed was introduced. In addition, the partial pressure of H_2O in this feed was held at 380 mm Hg, the same pressure as during synthesis (see section 5.2). Despite these efforts, the following differences in experimental variables still remained.

The maximum average hydrocarbon concentration using a 1:1 CO:H_2O feed was *circa* 0.02% at 325°C. The concentrations of ethene would have been of the same order. The concentrations of ethene in the current feed was 10% initially and 5% after dilution with H_2O vapour (see sections 3.5.1 and 7.1). Ethene concentrations during synthesis were thus at least two orders of magnitude lower than the ethene

concentration in the current experiment. The small amounts of ethene present during synthesis may be polymerised more completely and to a different range of products than the higher concentrations used in the assessment of ethene reactivity.

Another possible disparity of variables is that ethene formed on the active catalytic particles during synthesis may have differed in reactivity to ethene adsorbed from the current feed. However the adsorption of ethene was probably a reversible process in which case the two types of adsorbed species can be regarded as equivalent.

The current experiment was also restricted in the sense that the reactivity of ethene was assessed only in terms of polymerisation. This restriction applied because the feed contained just ethene, Ar and H_2O (see section 3.5.2). No CO was present. Another pathway by which ethene may react during synthesis is by insertion into growing hydrocarbon chains originating from CO. The propensity of ethene for such incorporation was not assessed. This reaction rather than polymerisation may account for the suppression of C2 formation (see section 5.6.3).

7.3.3 Polyene and Aromatic Formation

The rise in aromatic yields with temperature coincided with the increase in formation of polyene and/or coke (refer to fig. 7.3.1 and table 7.3.1). The same trend emerged during synthesis (see section 5.6.4).

The selectivities towards aromatics (benzene plus toluene) as a function of overall hydrocarbon yields were approximately equal during ethene reaction and synthesis in a 1:1 $CO:H_2O$ feed. At 325°C, for example, the values were 4.32% and 4.84% respectively.

The proportion of benzene relative to toluene produced by ethene polymerisation was greater than for synthesis. The quotient of % ethene conversion to benzene divided by % conversion to toluene was 1.11. The appropriate quotient involving % CO conversions under the analogous synthesis conditions (325°C, $CO:H_2O$ 1:1) was 0.328. The formation of even carbon number products would be kinetically and energetically favoured during the reaction of ethene. Only one step,

polymerisation, would have been involved. The production of odd carbon numbered products must have entailed two steps, cleavage and polymerisation.

The quantitative similarity between aromatic selectivities in both synthesis and ethene polymerisation situations, and the positive correlation between coke deposition and aromatic yield in both cases, suggests that the same precursor was involved in the production of aromatics by the two processes. This precursor may well have been polyene (see section 7.2.5).

Polyene, or hydrogenated coke, would be expected to have formed readily from ethene. Atomic of H would necessarily have been adjacent to carbon species during polyene deposition. During synthesis, similar proximity of H and C resulted because of the structure of Co/Cu/$SiO_2$40Å; 10:10:100 (see section 7.2.5).

The idea that the common intermediate to aromatic production was polyene is supported by the comparison of ethene polymerisation results *per se* with synthesis conversions. Such comparison simplifies the interpretation of results. Complications from the assumption that ethene reactivities during synthesis and polymerisation were similar (see section 7.2.2) do not arise.

7.4 Reactivity of Coke

7.4.1 Coke + H_2O

Only trace amounts of hydrocarbon products were detected when predeposited coke was stripped with H_2O vapour. This negative result shows that no hydrocarbons, aromatic products included, were synthesised by the direct reaction of H_2O with coke.

7.4.2 Coke +H_2

Methane and C2 hydrocarbons were produced when a H_2/H_2O/Ar feed was passed over coked Co/Cu/$SiO_2$40Å; 10:10:100. Only trace amounts of other hydrocarbons were detected. Since Ar and H_2O did not react with the predeposited

% conversion/g to	250°C	275°C	300°C	325°C
CH_4	0.273	0.297	0.499	0.678
C_2H_6	0.0788	0.0650	0.0583	0.0523
total	0.352	0.362	0.557	0.730

Table 7.4.1 Hydrogen conversions.

carbon layer (see section 7.4.1), the reactive component of the feed must have been H_2. The % H_2 conversions are given in table 7.4.2. These values were calculated as outlined in Appendix 7.

At all temperatures studied, the absolute concentrations of methane corresponding to % H_2 conversion values listed in table 7.3.2, were of the same order of magnitude, though slightly more, than the concentrations produced during synthesis. The concentrations of ethane were less by approximately one order of magnitude. In the stripping experiment at 325°C, for example, the methane and C2 hydrocarbon concentrations were measured to be *circa* 0.04% and 0.003% respectively. Under analogous conditions during screening (CO:H_2O 1:1, 325°C), the comparable concentrations were *circa* 0.01% and 0.02%.

The coincidence of the two methane concentrations suggests that hydrogenation of coke may have yielded methane during synthesis, particularly at higher temperatures (300°C, 325°C). The H_2 would have formed *via* the WGSR (see sections 1.1, 5.2 and 5.4.2). The low concentrations of C2 and heavier products measured in the stripping experiment imply that no higher hydrocarbons were synthesised directly from the reaction of coke. The results do not preclude the formation of aromatics from polyene (see section 7.2).

The concentrations of H_2 were closer during synthesis and the stripping experiments than when ethene was used as the reactant gas (see section 7.2.2). The concentrations of H_2 used for stripping, 10% after dilution with H_2O vapour (see sections 3.5.2 and 5.2), were greater by a maximum factor of 20 than the effluent H_2 concentrations measured during synthesis. The maximum difference occurred at 275°C. The minimum factor was 6 at 325°C. The average H_2 concentrations within the catalyst bed must have been of the same order, though slightly more, than the effluent levels. The comparative closeness of the H_2 concentrations validates direct comparison between the behaviour of Co/Cu/$SiO_2$40Å; 10:10:100 during synthesis and under stripping conditions.

7.5 Summary

Various sites for CO adsorption were identified on Co/Cu/$SiO_2$40Å; 10:10:100 by IR spectroscopy. Molecular CO adsorbed linearly on Cu^o particles and in linear and bridged geometries at Co^o/Cu^o interfaces. Upon heating, these species tended to desorb and/or dissociate, although CO remained intact on Cu^o particles up to 200°C.

Under KE synthesis conditions a formate type species associated with the WGSR and hence H_2 production, was observed. Polyene, which is a potential precursor to aromatic and coke formation, was also detected. The formate type intermediate may well have been produced by the reaction of molecular CO on Cu^o particles. Polyene production was facilitated by the structure of the hybrid catalyst, since nascent H_2 formed within carbidic deposits. Carbide probably occurred on Co^o components of the sample. No FTR intermediates were observed.

The reactivity results were negative in the sense that they disproved the hypotheses they were designed to test. Ethene polymerisation was shown not to account for the suppression of C2 hydrocarbons observed during synthesis. It was also demonstrated that the direct reaction of coke with H_2O produced no hydrocarbon products, while only methane and ethane were produced from reactions with H_2. Aromatic products were not therefore formed from the direct reaction of coke. The two sets of results were positive in that they supported the idea that polyene was a key intermediate for aromatic hydrocarbon production.

8 CONCLUSIONS

8.1 The Current Study

A suite of Co and Cu catalysts, physical mixes of the single metal samples and hybrid Co/Cu systems were prepared using Al_2O_3 and $SiO_2$40Å supports. Each catalyst was investigated by TPR and assessed in terms of KE activity. The results suggested that Co and Cu interacted on the hybrid samples only. A mixed Co/Cu oxide was formed during calcination, similar in nature on both supports, which reduced to a mixed Co^0/Cu^0 species upon activation. The mixed metal species were associated with favourable KE activity, both in terms of net hydrocarbon synthesis and especially aromatic production.

The most promising catalyst, activity and species distribution wise, proved to be Co/Cu/$SiO_2$40Å; 10:10:100. Three different aspects of this hybrid catalyst were studied. Its performance in CO/H_2O feeds of differing compositions was assessed, it was characterised in detail and the KE mechanism which applied during synthesis over the sample was investigated. The conclusions which were drawn can be considered generally applicable to the hybrid systems since the mixed Co/Cu species which occurred on Co/Cu/$SiO_2$40Å; 10:10:100 were representative.

The performance of Co/Cu/$SiO_2$40Å; 10:10:100 at either extreme of the feed composition range investigated was markedly different. At a CO:H_2O ratio of 3:1 a high fraction of CO conversion was caused by coking *via* the Boudouard reaction. At a ratio of 1:3 most conversion was associated with excess H_2 production *via* the WGSR. Two different regimes of feed composition were defined accordingly, the CO rich and the H_2O rich regimes. It was proposed that an alteration in the structure of the catalyst accompanied the change in activity observed in switching regimes. The most favourable product distributions, with respect to both hydrocarbon and aromatic selectivities, were given within the CO rich regime at a CO:H_2O ratio of 1:1. Even under these conditions hydrocarbon yields were low. A problem with optimising aromatic selectivity was that aromatic production and coking increased simultaneously.

The detailed characterisation of the Co/Cu/$SiO_2$40Å; 10:10:100 catalyst showed that the mixed Co/Cu oxide on the calcined sample consisted of Cu^{2+} networks and Co_3O_4, as was suggested by TPR evidence. The same species occurred on the calcined physical mix of Co/$SiO_2$40Å; 10:100 + Cu/$SiO_2$40Å; 10:100. The interaction indicated by TPR was a result of the proximity of oxidic Co and Cu rather than any chemical interaction such as the formation of stoichiometric Co/Cu oxides. The same finding applied for the activated sample. The mixed Co/Cu oxide was reduced to Co^0 and Cu^0, but not a Co^0/Cu^0 alloy. The interaction which occurred on the activated hybrid catalyst, as shown by activity studies, was caused by contact between Co^0 and Cu^0 particles. The interaction between Co^0 and Cu^0 appeared to weaken the influence of metal support effects. The species present immediately after activation were not obviously modified during synthesis within the CO rich regime.

The screening results were all consistent with the sequential KE mechanism. Mechanistic studies using IR spectroscopy identified a possible route between CO adsorption and intermediate formation. It was shown that CO adsorbed on Cu^0 particles and at Co^0/Cu^0 crystallite interfaces. The CO associated with Cu^0 was converted to a formate type intermediate by reaction with H_2O. This formate species was probably the key WGSR intermediate. The CO adsorbed at Co^0/Cu^0 interfaces may have been dissociatively chemisorbed, and subsequently involved in the production of linear FT type hydrocarbons as well as carbon deposition. The close proximity of H_2 and adsorbed carbon facilitated the formation of polyene, potentially a common intermediate to aromatic and coke formation. The existence of a common intermediate explained the link between aromatic and coke production established in screening experiments. Ethene and coke reactivity studies confirmed the role of polyene as an intermediate species.

In the current work a reasonable understanding of a particular Co/Cu catalyst, and by extrapolation Co/Cu systems in general, was gained. This knowledge provides a foundation which may enable the tailoring of catalyst composition and operational conditions to produce an industrially viable catalyst.

8.2 Proposals for Further Work

There are two areas in which the current work could be developed. The first involves refinement of the ideas presented. Further characterisation of Co/Cu systems using techniques such as X.P.S. and nuclear magnetic resonance spectroscopy would be useful. The mode by which Co^0 and Cu^0 interact may be established using such techniques. The proposed transition in structure in moving from the CO rich to H_2O rich regime could also be investigated. Further development of particularly the IR mechanistic studies seems worthwhile. Temperature programmed desorption would reveal whether CO dissociated or was removed intact upon heating (see section 7.2.4). Methods in which experimental geometry allows higher intermediate concentrations would be advantageous. A recently acquired diffuse reflectance IR cell may assist in providing such a method.

The second area in which research could proceed is in further screening and assessment of catalyst performance. Such work would be more interesting than refinement from the view of optimising KE synthesis conditions. Since either excess H_2 or excess coke was produced by the Co/Cu systems investigated, the maximisation of hydrocarbon yields should be kinetically rather than thermodynamically limited. For example, the product distributions given by a low Cu loading hybrid catalyst in the H_2O rich regime may be more favourable than those given by high Cu loading analogues. The production of H_2 would probably be relatively suppressed, thus giving hydrocarbon distributions as observed in the CO rich regime, but in a different environment. The effect of variation in pressure could also be assessed. Catalyst performance as a function of time on stream and activation procedures are other details of interest.

The suggestions aforementioned must be regarded as developmental work rather than new. The preparation of novel Co/Cu catalysts and evaluation of their behaviour falls into the latter category. By preparing catalysts at a controlled pH, or using pellets rather than powder, a catalyst superior in activity to those already made could be discovered. The addition of promoters could also prove beneficial. Potassium, for example, may reduce coking rates but not aromatic production.

Profitable work could also be performed on related, though not identical, bimetallic systems. The Fe/Co system is being investigated at the moment. Comparisons of the behaviour of various related systems may assist in further elucidation of the KE process. Such work could be extended to trimetallic catalysts.

The KE synthesis certainly requires more study before it can be accepted or discounted as a viable industrial process. That the FT synthesis operates cost effectively indicates that eventually the KE synthesis, or at least hydrocarbon production in H_2 deficient feeds should be able to do the same. Furthermore the KE synthesis may prove superior in that a CO/H_2O feed is used rather than a CO/H_2 mix, and because hydrocarbon distributions are more favourable.

APPENDICES

1) QUANTIFICATION OF EXTENSIVE FID ANALYSES

In quantifying such data it was assumed that all aliphatic hydrocarbons, except methane, had the molecular formula $(CH_2)n$ where n was the carbon number. The equations of formation of aliphatics and aromatics were therefore

$4CO$	+	$2H_2O$	$\rightarrow$	CH_4	+	$3CO_2$	C1
$6CO$	+	$2H_2O$	$\rightarrow$	C_2H_4	+	$4CO_2$	C2
$9CO$	+	$3H_2O$	$\rightarrow$	C_3H_6	+	$6CO_2$	C3
$12CO$	+	$4H_2O$	$\rightarrow$	C_4H_8	+	$8CO_2$	C4
$15CO$	+	$5H_2O$	$\rightarrow$	C_5H_{10}	+	$10CO_2$	C5
$18CO$	+	$6H_2O$	$\rightarrow$	C_6H_{12}	+	$12CO_2$	C6
$21CO$	+	$7H_2O$	$\rightarrow$	C_7H_{14}	+	$14CO_2$	C7
$24CO$	+	$8H_2O$	$\rightarrow$	C_8H_{16}	+	$11CO_2$	C8
$15CO$	+	$3H_2O$	$\rightarrow$	C_6H_6	+	$9CO_2$	benzene
$18CO$	+	$4H_2O$	$\rightarrow$	C_7H_8	+	$11CO_2$	toluene
$21CO$	+	$5H_2O$	$\rightarrow$	C_8H_{10}	+	$13CO_2$	xylene

The molecular weights (MWs) of hydrocarbon products were

CH_4	16
C2	28
C3	42
C4	56
C5	70
C6	84
C7	98
C8	112
benzene	78
toluene	92
xylene	106

The key assumption that the FID signal given by some molecule is proportional to its molecular weight implies that an FID trace represents a weight percent distribution of hydrocarbon fractions. This consideration allows the following expression to be derived.

$$\%\ CO_2 \text{ associated with Cn} = [CH_4] \times \frac{\text{integrated area of Cn peaks}}{\text{integrated area of } CH_4 \text{ peak}} \times \frac{\text{MW } CH_4}{\text{MW Cn}} \times \frac{\text{moles } CO_2}{\text{moles Cn}}$$

where

n = carbon number.

$[CH_4]$ was measured by an on line GC.

$\frac{\text{integrated area of } CH_4 \text{ peak}}{\text{integrated area of Cn peaks}}$ was computed from integrated extensive FID analyses.

$\frac{\text{MW } CH_4}{\text{MW Cn}}$ came from the list of MWs given.

$\frac{\text{moles } CO_2}{\text{moles Cn}}$ came from the equations given.

Normalisations for weight and flow were then carried out on the associated % CO_2 values. In section 4.4 the flow was normalised for 5 ml of CO entering the reaction per unit time. This involved multiplication of $\%CO_2$ values by 1.2.

The above equation involves calculating the $\%CO_2$ concentrations associated with each hydrocarbon fraction relative to CH_4. Analogous equations can be deduced in which concentrations are expressed relative to C2 or C3 levels.

2) CALCULATION OF %CO CONVERSIONS

Using the following calculations, CO conversions to hydrocarbon, carbon (or coke) and excess H_2 were found. The problems of pressure gradients, exact outlet flows *etc.* are dealt with internally. Concentrations are expressed relative to unity. For percentage calculations, the appropriate figures must be multiplied by 100.

Consider the three key reactions which may proceed in a CO/H_2O feed at steady state; the Boudouard reaction, the WGSR and the KE synthesis.

$$2CO \rightarrow C + CO_2 \qquad \text{eqn. 1.1.6}$$

$$CO + H_2O \rightarrow CO_2 + H_2 \qquad \text{eqn. 1.1.7}$$

$$3CO + H_2O \rightarrow -CH_2 - +2CO_2 \qquad \text{eqn. 1.1.8}$$

Let the conversion of CO to the processes be 2C, H and 3HC respectively.

If a 1 ml "plug" of CO enters the reactor over some period of time and a fraction 2C is converted to coke then C ml of gaseous CO_2 are evolved compared to the 2C ml of gaseous CO consumed. The change in gas volume caused by such conversion is -C ml. The change in volume caused by CO conversion *via* the WGSR is +H ml, taking into account removal of H_2O from the effluent. The change caused by conversion *via* the KE synthesis must lie between O and HC ml.. The range applies because numerous CO molecules are incorporated into just one long chain hydrocarbon. For ease of calculation this difference can be approximated to zero. The approximation is justified because HC was always much less than one, as shown by the low hydrocarbon concentrations measured. Thus every 1 ml of gaseous CO which enters the reaction is converted to 1 + H - C ml of gaseous products.

The actual concentration of each product is the volume of that product divided by total effluent volume. In the case of H_2 for example, where H ml of H_2 is produced, the actual H_2 concentration (x) is given by eqn. A2.1.

$$x = \frac{H}{1 + H - C} \qquad \text{eqn. A2.1}$$

Similarly

$$y = \frac{HC}{1 + H - C} \qquad \text{eqn. A2.2}$$

$$z = \frac{H + C - 2HC}{1 + H - C} \qquad \text{eqn. A2.3}$$

where y is the "equivalent hydrocarbon concentration" and z is the actual CO_2 concentration. The equivalent hydrocarbon concentration is effectively the concentration of CO molecules contained in hydrocarbon products as opposed to the absolute concentration of hydrocarbon products themselves. The necessity of using this modified concentration is explained by the following approach.

By multiplying the effluent volume by the concentration of any one hydrocarbon fraction, the volume of that hydrocarbon fraction can be found. The volume of CO associated with the formation of each fraction, the parameter of interest, can be deduced from the equations listed in Appendix 1. The total volume of CO involved in hydrocarbon formation is given by the following expression:

$$(1+H-C)\ (4[CH_4] + 6[C2] + ...+27[C9] + 15\ [C_6H_6] + ...+ 21[C_8H_{10}])$$

Dividing this number by the volume of CO entering the reactor (*i.e.* 1) gives the total conversion of CO to hydrocarbon products (*i.e.* 3HC). Therefore, by comparison with eqn. A2.2, y equals one third of the bracketed hydrocarbon concentration term.

Algebraic expression of eqns.. A2.1, A2.2 and A2.3 allows C,H and HC to be expressed in terms of the measurable values x, y and z. First let

$$P = 1 + H - C \qquad \text{eqn. A2.4}$$

Therefore

$$H = xP \qquad \text{eqn. A2.5}$$

$$HC = yP \qquad \text{eqn. A2.6}$$

$$H + C + 2HC = zP \qquad \text{eqn. A2.7}$$

Substitute eqn. A2.5 into eqn. A2.4

$$1 + xP - C = P$$

Hence

$$C = 1 + (x - 1)\,P \qquad \text{eqn. A2.8}$$

Substitute eqns. A2.5, A2.6 and A2.8 into eqn. A2.7

$$xP + 1 + (x - 1)P + 2yP = zP$$

Therefore

$$P = \frac{1}{1 - 2x - 2y + z} \qquad \text{eqn. A2.9}$$

Thus

$$H = \frac{x}{1 - 2x - 2y + z} \qquad \text{eqn. A2.10}$$

$$C = 1 + \frac{x - 1}{1 - 2x - 2y + z} \qquad \text{eqn. A2.11}$$

The conversions are obtained by multiplying H, HC and C by 1, 3 and 2 respectively. To obtain the CO conversion to each hydrocarbon fraction, 3HC is apportioned according to the contribution made by each fraction to y. Normalisation for weight, flow *etc.* can then be carried out.

3) CALCULATION OF K_p

The partial pressure of CO was initially 190 mm Hg. The amount of CO consumed was

$$\frac{(\%CO \text{ converted to carbon} + HCs + H_2)}{100} \times 190$$

$= 0.408 \times 190$

$= 77.6$ mm Hg.

Therefore the final partial pressure was 112.4 mm Hg.

The initial concentration of water was 570 mm Hg. The amount of H_2O consumed was, by stoichiometry,

$$\frac{(\%CO \text{ converted to } HCs/3 + H_2)}{100} \times 190$$

$= 0.231 \times 190$

$= 43.9$ mm Hg.

Therefore the final partial pressure was 526.1 mm Hg.

The amount of H_2 produced was

$$\frac{(\%CO \text{ converted to } H_2)}{100} \times 190$$

$= 0.214 \times 190$

$= 40.7$ mm Hg.

The amount of CO_2 produced was

$$\frac{(\%CO \text{ converted to carbon}/2 + HCs \times 2/3 + H_2)}{100} \times 190$$

$= 0.320 \times 190$

$= 60.7$ mm Hg.

The sum of the total pressures was 739.9 mm Hg according to this approach. Equilibration to atmospheric pressure (760 mm Hg) would have involved alterations in the pressures of all the gases by the same factor because the WGSR equilibrium is not pressure dependent (equal moles of reactant and product gases). Since $K_p = [PCO_2][PH_2]/[PCO][PH_2O]$ these factors cancel. The K_p value obtained is thus 4.17×10^{-2}.

4) CALCULATION OF METAL TO SUPPORT RATIOS

Co/$SiO_2$40Å;10:100

Consider the O associated with Co on 100g of the sample. Its weight is

$$\frac{40}{100} \times \frac{8.12}{58.9} \times \frac{4}{3} \times 16.0 + \frac{60}{100} \times \frac{8.12}{58.9} \times 1 \times 16 = 2.50g$$

The 40/100 term is the percentage of Co present as Co_3O_4 and the 60/100 the percentage associated with interactive Co^{2+} (Roe *et al.*, 1988). The total weight of Co on the sample is 8.12 g (as determined by elemental analysis). Division of this weight by the molecular weight of Co (58.9) gives the moles of Co. Multiplication by the stoichiometric terms 4/3 and 1 gives the moles of O associated with Co. Moles are converted to weight by using the atomic weight of O (16.0). The weight of support proper is therefore

100 - 8.12 - 2.50 = 89.38g.

The ratio of metal to support proper is then

8.12 : 89.38

i.e. 9.08 : 100.

Cu/$SiO_2$40Å;10:100

O associated with Cu

$$\frac{100}{100} \times \frac{8.39}{63.6} \times 1 \times 16.0 = 2.11g$$

weight of support proper

100 - 8.39 - 2.11 = 89.5g

metal to support ratio.

8.39 : 89.5

i.e. 9.37 : 100

Co/$SiO_2$40Å;10:100 + Cu/$SiO_2$40Å;10:100

O associated with Co

$$\frac{40}{100} \times \frac{4.39}{58.9} \times \frac{4}{3} \times 16.0 + \frac{60}{100} \times \frac{3.84}{58.9} \times 16.0 = 1.18g$$

O associated with Cu

$$\frac{100}{100} \times \frac{4.39}{63.6} \times 1 \times 16.0 = 1.10g$$

Weight of support proper

100 - 3.84 - 4.39 - 1.10 - 1.18 = 89.4g

Co to Cu to support ratio

3.84 : 4.39 : 89.4

i.e. 4.29 : 4.91 : 100

Co/Cu/$SiO_2$40Å;10:10:100

O associated with Co

$$\frac{100}{100} \times \frac{6.93}{58.9} \times \frac{4}{3} \times 16.0 = 2.51g$$

O associated with Cu

$$\frac{100}{100} \times \frac{7.68}{63.6} \times 1 \times 16.0 = 1.93\ g$$

Weight of support proper

100 - 6.93 - 7.68 - 2.51 - 1.93 = 81.0g

Co to Cu to support ratio

6.93 : 7.68 : 81.0

i.e. 8.57 : 9.49 : 100

5) CALCULATION OF DISPERSIONS

$Co/SiO_2$40Å;10:100

The weight of CO adsorbed was 1.85 mg/g catalyst. This corresponds to 1.85 x 10^{-3} / 28.0 moles of CO. From elemental analysis the total metal weight on 1g of catalyst was 8.12 / 100g, equivalent to 0.0812 / 58.9 moles. Assuming one mole of CO was associated with one mole of Co during adsorption, the percentage of metal involved was

$$\frac{1.85 \times 10^{-3} / 28.0}{0.0812 / 58.9} \times 100 = 4.80\%.$$

This value is defined as the dispersion.

$Cu/SiO_2$40Å;10:100

moles of CO adsorbed/g catalyst

$1.54 \times 10^{-3} / 28.0 = 5.50 \times 10^{-5}$

moles of Cu on catalyst

$0.0839 / 63.6 = 1.32 \times 10^{-3}$

% dispersion

$$\frac{5.50 \times 10^{-5}}{1.32 \times 10^{-3}} \times 100 = 4.17\%$$

$Co/SiO_2$40Å;10:100 + $Cu/SiO_2$40Å;10:100

moles of CO adsorbed/g catalyst

$1.96 \times 10^{-3} / 28.0 = 7.00 \times 10^{-5}$

moles of Co + Cu on catalyst

$0.5\ (0.0812 / 58.9 + 0.0839 / 63.6) = 1.35 \times 10^{-3}$

The factor 0.5 appears because the physical mix contained equal amounts of the Co and Cu supported catalysts. The elemental analyses of the single metal samples, rather than the physical mix analysis, were used for internal consistency.

% dispersion

$$\frac{7.00 \times 10^{-5}}{1.35 \times 10^{-3}} \times 100 = 5.18\%$$

Co/Cu/$SiO_2$40Å;10:10:100

moles CO adsorbed/g catalyst

$2.06 \times 10^{-3} / 28.0 = 7.36 \times 10^{-5}$

moles Co + Cu on catalyst

$0.0693 / 58.9 + 0.0768 / 63.6 = 2.39 \times 10^{-3}$

% dispersion

$$\frac{7.36 \times 10^{-5}}{2.39 \times 10^{-3}} \times 100 = 3.08\%$$

6) CALCULATION OF ETHENE CONVERSIONS

Consider a 1 ml plug of the feed entering the reactor over some period of time. It is composed by 0.1 ml of ethene and 0.9 ml of Ar. Thus regardless of ethene reacted the associated outlet volume can be approximated to 1 ml. The maximum error caused by this approximation is 10%.

The ethene conversion to hydrocarbons (HC) is then given by

$$x = 0.1\ HC / 1 \qquad \text{eqn. A6.1}$$

where x is an equivalent hydrocarbon concentration derived in an analogous way to y in the CO conversion calculation (see Appendices 1 and 2). The value HC includes ethene conversion to C2s, that is unreacted ethene.

The ethene conversion to coke (C) added to HC must be one, given that the two relevant product types are the only species formed. Thus

$$C = 1 - HC \qquad \text{eqn. A6.2}$$

The ethene conversion to hydrocarbons (HC) was apportioned according to the contribution made by each fraction to x. The conversion figures to all products other than C2s were normalised for sample weight.

7) CALCULATION OF H_2 CONVERSIONS IN COKE STRIPPING

The two reactions involved were

$C + 2H_2 \rightarrow CH_4$ eqn. A7.1

$2C + 3H_2 \rightarrow C_2H_6$ eqn. A7.2

Let conversion to CH_4 be 2C1 and to C_2H_6 3C2.

Consider a 1 ml plug of feed gas, composed of 0.2 ml of H_2 and 0.8 ml of Ar, entering the reactor over some period of time. The associated effluent gas volume is

$0.8 + 0.2 (1-2\,C1 + C1 - 3C2 + C2)$

i.e. $1 - 0.2 (C1 - 2C2)$

Thus

$$x = \frac{0.2C1}{1 - 0.2 (C1-2C2)}$$ eqn. A7.3

$$y = \frac{0.2C2}{1 - 0.2 (C1-2C2)}$$ eqn. A7.4

Let

$P = 1 - 0.2 (C1-2C2)$ eqn. A7.5

Then

$0.2C1 = xP$ eqn. A7.6

$0.2C2 = yP$ eqn. A7.7

Substitute eqns. A7.6 and A7.7 in eqn. A7.5

$P = 1 - xP - 2yP$

Hence

$P + xP + 2yP = 1$

$P (1 + x + 2y) = 1$

$$P = \frac{1}{1 + x + 2y}$$ eqn. A7.8

Substitute eqn. A7.8 in eqns. A7.6 and A7.7

$$0.2C1 = \frac{x}{1 + x + 2y}$$

$$\textit{i.e.}\ C1 = \frac{5x}{1 + x + 2y} \qquad \text{eqn. A7.9}$$

$$0.2C2 = \frac{y}{1 + x + 2y}$$

$$\textit{i.e.}\ C2 = \frac{5y}{1 + x + 2y} \qquad \text{eqn. A7.10}$$

Conversions of H_2 are found by multiplication of C1 and C2 by 2 and 3 respectively. Normalisations for weight can then be carried out.

REFERENCES

ANDERSON, J.R., and PRATT, K.L., "Introduction to Characterization and Testing of Catalysts", Academic Press, North Ryde, 1985.

ANDERSON, R.B., Catalysis, 1956, 4, 257.

ANDERSON, R.B., Chapter 4 in "The Fischer Tropsch synthesis", Anderson, R.B., (ed.), Academic Press, San Diego, 1984.

ANDREW, S.P.S., Post Congress Symposium 7th International Congress on Catalysis (Osaka, 1980), paper 12.

AMENOMIYA, Y., J. Catal., 1979, 57, 64.

AMENOMIYA, Y., and PLEIZIER, A., J. Catal., 1981, 67, 90.

ARAKI, M., and PONEC, V., J. Catal., 1976, 44, 439.

ARNOLDY, P., and MOULJIN, J.A., J. Catal., 1985, 93, 38.

BHASIN, M.M., CURRAN, C., and JOHN, G.S., J. Phys. Chem., 1970, 74, 3973.

BILOEN, P., MELLE, J.N., and SACHTLER, W.M.M., J. Catal., 1979, 58, 95.

BLYHOLDER, G., J. Phys. Chem., 1966, 70, 893.

BLYHOLDER, G., and NEFF, L.D., J. Phys. Chem., 1962, 66, 1664.

BLYHOLDER, G., and NEFF, L.D., J. Catal., 1963, 2, 138.

BLYHOLDER, G., SHIBABI, D., WHYATT, W.V., and BARTLETT, R., J. Catal., 1976, 43, 122.

BONZEL, H.B., and KREBS, H.J., Surf. Sci., 1980, 91, 499.

CASTNER, D. G., and SANTILLI, D.S., Catalytic Materials: Relationship between Structure and Reactivity, A.C.S., Symposium Series No. 248, Whyte, T.E., Dalla Betta, R.A., Derovane, E.G., and Baker, R.T.K., (eds.), Washington, 1984.

CHAFFEE, A.L., EKSTROM, A., LAPSZEWICZ, J., and LOEH, H.J., Proceedings of the Australian Coal Science Conference, 1984, 223.

CHAFFEE, A.L., and LOEH, H.J., Applied Catalysis, 1985, 19, 419.

CHAFFEE, A.L., and LOEH, H.J., Applied Catalysis, 1986, 26, 123.

CHIN, R.L., and HERCULES, D.H., J. Phys. Chem., 1982, 86, 360.

CHIN, R.L., and HERCULES, D.H., J. Phys. Chem., 1982, 86, 3079.

CRAXFORD, S.R., and RIDEAL, E.K., J. Chem. Soc., 1939, 1604.

CRC HANDBOOK OF CHEMISTRY AND PHYSICS, Weast, R.C., (ed.), CRC Press, Cleveland, Ohio, 1974-1975.

CRESSLEY, J., RIEGERT-KAMEL, S., KIENNEMANN, A., and DELUZARCHE, A., Bull. Soc. Chim. Fr., 1982, 5-6, Part II, 171.

DAVIES, M., (ed.), "Infra Red Spectroscopy and Molecular Structure", Elsevier Publishing Company, 1963.

DAVYDOV, A.A., BORESKOV, G.K., YUREVA, T.M., and RUBENE, N.A., Doklady Akademi Navk SSSR, 1977, 236, 1402.

DELK, F.S., and VAVERE, A., J. Catal., 1984, 85, 380.

DRY, M.E., Catalysis Science and Technology, Anderson, J.R., and Boudard, M., (eds.), Springer Verlag, New York, 1981, 160.

EDWARDS, J.F., and SCHRADER, G.L., J. Phys. Chem., 1984, 88, 5620.

EKSTROM, A., and LAPSZEWICZ, J., Applied Catalysis, 1986, 21, 111.

EWING, G.W. "Instrumental Methods of Chemical Analysis", McGraw Hill, U.S.A., 1985.

FISCHER, F., and KOCH, M., Gesammelte Abh. Kennt. Kohle, 1930, 10, 575.

FLOREY, P.J., J. Am. Chem. Soc., 1936, 58, 1877.

GALWAY, A.K., "Chemistry of Solids", Chapman and Hall Ltd., London, 1967.

GARDNER, D.C. and BARTHOLOMEW, C.H., Ind. Eng. Chem. Prod. Res. Dev., 1981, 20, 80.

GENTRY, S.J., and WALSH, P.T., J. Chem. Soc., Faraday Trans. 1, 1982, 78, 1515.

GHOSH, P.K., TIWARI, J.S., SINHA, S.L., ROY, N., and SDARKER, A., Proceedings of the Symposium of Chemicals and Oils from Coal, Dahnobad, India, Rao, R.N., Sen, S., and Rao, S.R., (eds.), 1969 (published 1972), paper 24.

GRENOBLE, D.C., ESTADT, M.M., and OLLIS, D.F., J. Catal., 1981, 67, 90.

GUSTAFSON, B.L., Ph.D. Dissertation, Texas A and M University, 1981.

GUSTAFSON, B.L., and LUNSFORD, J.H., J. Catal., 1982, 74, 393.

HEAVISIDE, J., HENDRA, P.J., TSAI, P., and COONEY, R.P., J. Chem. Soc., Faraday Trans. 1, 1978, 74, 2542.

HOFER, L.J.E., STERLING, E., and McCARTNEY, J.T., J. Phys. Chem., 1959, 59, 1153.

HUCKEL, W., "Structural Chemistry of Inorganic Compounds", Elsevier, Netherlands, 1951.

HURST, N.W., GENTRY, S.J., and JONES, A., Catal. Rev. Sci., Eng., 1982, 24(2), 233.

INORGANIC INDEX TO THE POWDER DIFFRACTION FILE, Joint Committee on Powder Diffraction Standards, Swarthmore, Pennsylvania, 1972.

JENKING, J.W., McNICOL, B.D., and ROBERTSON, S.D., Chem. Tech., 1977, 316.

JONES, A., and McNICOL, B.D., "Temperature Programmed Reduction for Solid Materials Characterisation", Marcel Decker, New York, 1984.

KAKUTA, N., KAZUSAKA, A., and MIYAHARA, K., Bull. Chem. Soc. Jpn., 1986, 59, 3267.

KING, D.L., J. Catal., 1980, 61, 77.

KOLBEL, H., and BHATTACHARYYA, K.K., Liebigs Ann. Chem., 1958, 67, 618.

KOLBEL, H., and ENGELHARDT, F., Chem. - Ing. - Tech., 1950, 22, 97.

KOLBEL, H., and ENGELHARDT, F., Erdoel Kohle, 1950, 3, 529.

KOLBEL, H., and ENGELHARDT, F., Erdoel Kohle, 1951, 5, 1.

KOLBEL, H., and ENGELHARDT, F., Chem. - Ing. - Tech., 1951, 23, 153.

KOLBEL, H., and ENGELHARDT, F., Brennst. - Chem., 1951, 32, 150.

KOLBEL, H., and ENGELHARDT, F., Brennst. - Chem., 1952, 33, 13.

KOLBEL, H., and GAUBE, J., Brennst. - Chem., 1961, 42, 149.

KOLBEL, H., and HAMMER, H., Z. Elektrochem., 1960, 64, 224.

KOLBEL, H., and RALEK, M., Chapter 7 in "The Fischer Tropsch Synthesis", R.B. Anderson, (ed.), Academic Press, San Diego, 1984.

KOLBEL, H., RALEK, M., and JIRU, P., Erdoel Kohle Erdgas Petrochem., Brennst. - Chem., 1970, 9, 580.

KOLBEL, H., and VORWERK, E., Brennst. - Chem., 1957, 38, 2.

KOTANIGAWA, T., CHAKRABARTTY, S., and BERKOWITZ, N., Fuel Processing Technology, 1981, 5, 79.

KUIJPERS, E.G.M., TJEPKEMA, R.B., and GEVS, J.W., J. Molecular Catalysis, 1984, 45, 241.

KUMMER, J.T., DE WITT, T.W., and EMMETT, P.H., J. Am. Chem. Soc., 1948, 70, 3632.

LARKINS, F.P., Catalysis: Principles and Applications, 3rd Year Notes, University of Tasmania, 1985.

LARKINS, F.P., PANG, L.S.K., CHELKOWSKA, E.Z., and SEDDON, D., in preparation.

LEHERTE, G., DERIE, R., and DUVIGNEAUD, P.H., "Preparation of Catalysts", Delmon, B., Jacobs, P.A., and Poncelet, G., (eds.), Elsevier Scientific Publishing Co., Amsterdam, 1976, 303.

LEMMAITRE, J., Chapter 2 in "Characterization of Heterogeneous Catalysts", Delanney, F., (ed.), Marcel Decker, New York, 1984.

LITTLE, L.H., "Infrared Spectra of Adsorbed Species", Academic Press, 1966.

LUNSFORD, J.H., and NIWA, M., A.C.S. Div. Pet. Chem. Preprints, 1982, 27, 429.

MARTENS, J.M.A., VAN'T BLIK, H.F.J., and PRINS, R., J. Catal., 1986, 97, 200.

MINDERMAN, J.P., DELUZARCHE, A., KIEFFER, R., and KIENNEMAN, A., Prepr. Can. Symp. Catal. 8th, 1982.

MIYATA, Y., AKIMOTO, M., DOBA, N., and ECHIGUYA, E., Bull. Chem. Soc. Jpn., 1984, 57, 667.

NAKANISHI, K., "Infrared Absorption Spectroscopy - Practical", Holden Day Inc., San Francisco and Nankodo Cpy. Ltd., Tokyo, 1964.

NEWSON, D.S., Catal. Rev. Sci. Eng., 1980, 21, 275.

PARRIS, G.E., and KLIER, K., J. Catal., 1986, 97(2), 374.

PARYJCZAK, T., RYNKOWSKI, J., and KARSKI, S., J. Chromatogr., 1980, 188, 254.

PASCAL, P., "Nouveau Traite de Chimie Minerale", Masson et cie, Paris, 1963.

PETTIT, R., and BRADY, R.C., J. Am. Chem. Soc., 1981, 103, 1287.

PICHLER, N., and SCHULZ, H., Chem. Ing. Tech., 1976, 42, 1162.

PONEC, V., Coal Science, 1984, 3,2.

PONEC, V., and VAN BARNEWELD, W.A., Ind. Eng. Chem. Prod. Res. Dev., 1979, 18, 268.

PRIMET, M., DALMON, J.A., and MARTIN, G.A., J. Catal., 1977, 46, 25.

RABO, J.A., and ELEK, L.F., Preprints 7th Int. Cong. Catal., Tokyo, 1980, 190.

RABO, J.A., RISCH, A.P., and POUTSMA, M.L., J. Catal., 1978, 53, 295.

RAUTAVUOMA, A.O.I., Thesis, Technical University of Eindhoven, The Netherlands, 1979.

ROBERTS, M.W., Advances in Catalysis, 1980, 29, 55.

ROBERTSON, S.D., McNICOL, B.D., DE BAAS, J.H., KLOET, S.L., and JENKINS, J.W., J. Catal., 1975, 7, 424.

ROE, G.M., Honours Thesis, University of Tasmania, 1986.

ROE, G.M., RIDD, M.J., CAVELL, K., and LARKINS, F.P., Stud. Surf. Sci. Catal., 1988, 36, 509.

SACHTLER, J.W., KOOL, J.M., and PONEC, V., J. Catal., 1979, 56, 284.

SCHULZ, G.V., Z. Phys. Chem., 1935, Abt. B29, 299.

SERMON, P.A., ROLLINS, K., REYES, P.N., LAWRENCE, S.A., LUENGO, M.A.M., and DAVIES, M.J., J. Chem. Soc., Faraday Trans. 1, 1987, 83, 1347.

SEXTON, A.E., HUGHES, A.E. and TURNEY, T.W., J. Catal., 1986, 97(2), 390.

SHEPPARD, N., and NGUYEN, T.T., Adv. Infrared and Raman Spectroscopy, 1978, 5, 67.

SHIMOKAWABE, M., TAKEZAWA, N., and KOBAYASHI, H., Bull. Chem. Soc. Jpn., 1985, 56, 1337.

STRANICK, M.A., HOUALLA, M., and HERCULES, D.H., J. Catal., 1987, 103, 151.

TAMARU, K., Pure Appl. Chem., 1980, 52, 2067.

TOMINAGA, H., FUJIMOTO, K., and TATSUMI, T., Reports of special project research on energy under grants in aid of sceintific research of the Ministry of Education, Science and Culture, Japan, 1984, 289.

TOMINAGA, H., MIYAUCHI, M., and FUJIMOTO, K., Bull. Chem. Soc. Jpn., 1987, 60, 2310.

TOTTRUP, P.B., J. Catal., 1976, 42, 29.

UNMUTH, E.E., SCHWARTZ, L.H., and BUTT, J.B., J. Catal., 1980, 63, 404.

VAN HERWIJNEN, T., and DE JONG, W.A., J. Catal., 1980, 63, 83.

VAN HERWIJNEN, T., GUCZLASKI, R.T., and DE JONG, W.A., J. Catal., 1980, 63, 94.

VANNICE, M.A. J. Catal., 1975, 37, 449.

VAN'T BLIK, H.F.J., KONNINGSBERGER, D.C., and PRINS, R., J. Catal., 1986, 97, 200.

VAN'T BLIK, H.F.J., and PRINS, R., J. Catal., 1986, 97, 188.

WENTRECK, P.R., WOOD, P.J., and WISE, M., J. Catal., 1976, 53, 363.

YATES, J.T. Jr., and HALLER, G.L., J. Phys. Chem., 1984, 88, 4660.

YOUNG, P.W., and CLARK, G.B., Chem. Eng. Progress, 1973, 69, 69.